MAFIC-FELSIC INTERACTION IN A HIGH LEVEL MAGMA CHAMBER – THE HALFMOON PLUTON, STEWART ISLAND, NEW ZEALAND: IMPLICATIONS FOR UNDERSTANDING ARC MAGMATISM

A thesis submitted in fulfilment
of the requirements for the degree of

Doctor of Philosophy in Geology

at the
University of Canterbury

by

Rose E. Turnbull

University of Canterbury
2009

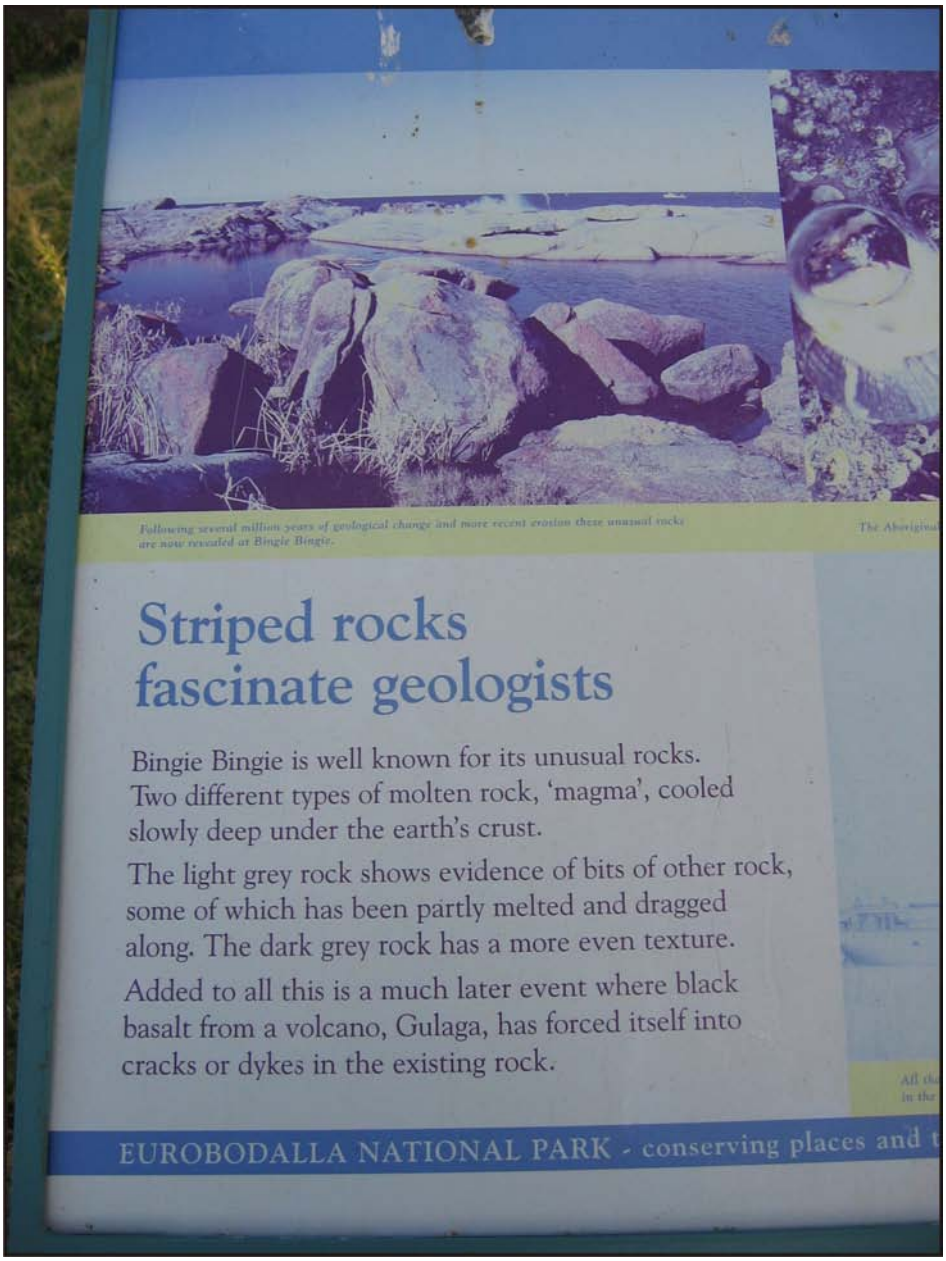

Helpful sign at Bingie Bingie Point, New South Wales, Australia

ABSTRACT

Field evidence from exposed plutonic rocks indicates that mafic-felsic magma interaction is an important process during the construction and evolution of magma chambers. The exhumed, ~140 Ma, Halfmoon Pluton of Stewart Island, New Zealand is characterized by a sequence of mingled mafic sheets and enclaves preserved within an intermediate-felsic host, and provides a unique opportunity to directly investigate the physico-chemical processes that operate within an arc setting. Interpretation of mingling structures and textures in the field, in combination with extensive petrographic, geochemical and geochronological data, allow for conclusions to be reached regarding the nature of the mafic-felsic magma interactions, and the physical, chemical and thermal processes responsible for the generation and evolution of the calc-alkaline magmas. Detailed documentation and interpretation of mafic-felsic magma mingling structures and textures reveal that the Halfmoon Pluton formed incrementally as the result of episodic replenishments of mafic magma emplaced onto the floor of an aggrading intermediate-felsic magma chamber. Physico-chemical processes identified include fractional crystallization and accumulation of a plagioclase – hornblende – apatite – zircon mineral assemblage, episodic replenishment by hot, wet basaltic magmas, magmatic flow and compaction. Early amphibole and apatite crystallization played an important role in the compositional diversity within the Halfmoon Pluton. Variations in the style of magma mingling preserved within the magmatic "stratigraphy" indicate that processes operating within the chamber varied in space and time. Variations in mineral zoning and composition within hornblende indicate that the Halfmoon Pluton crystallized within a magma in which melt composition fluctuated in response to repeated mafic magma replenishments, fractionation, crystal settling and convection. Mineral assemblages, chemical characteristics, isotopic data and geochronological evidence indicate that the amphibole-rich calc-alkaline Halfmoon Pluton was emplaced into a juvenile arc setting, most probably an island-arc. Data are consistent with a model whereby 'wet' amphibole-rich basaltic magmas pond at the crust-mantle interface and episodically rise, inject and mingle with an overlying intermediate-felsic magma chamber that itself represents the fractionated product of the mantle melts.

ACKNOWLEDGEMENTS

There are a large number of people without whom this project would never have been able to have been completed. First and foremost I would like to thank my cohort of excellent supervisors for all their assistance and guidance. Firstly thanks to Professor Steve Weaver who initially got me interested in granites and geochemistry way back in undergrad, and for your unwavering support, advice and subtle digs at my swede and oyster consumption. You have been an excellent supervisor, mentor and friend over the last few years despite your desertion to the upper echelons of the Registry. Thanks to Professor Bob Wiebe for suggesting Stewart Island as a potential project, the several trips down to Stewart Island to explain the rocks and sample the local produce, and the general expertise and enthusiasm you displayed towards answering many of my questions. Also, thanks to you and Dave Hawkins for a great week of fieldwork in Maine. Thanks to Dr Andy Tulloch for generously sharing your knowledge of Stewart Island geology, and also for field logistics, and brilliant chapter reviews. Thanks to Professor Jim Cole for your constant support, never ending enthusiasm for receiving chapter drafts for review, and for generous funding through the Marsden Fund.

I am extremely grateful for funding from a TEC Bright Futures Top Achiever Doctoral Scholarship, The Royal Society of NZ Marsden Fund, The Department of Geological Sciences, the Mason Trust Fund and a Westpac Southland Scholarship. I am also grateful for conference funding from the NZ Federation of Graduate Women, the AGU Student Travel Grant, and a Royal Society of NZ Canterbury Branch travel grant.

This project could not have been undertaken without access to several private properties/wildlife sanctuaries around Stewart Island. Thanks must firstly go to Rex Bradshaw for allowing me unlimted access and free accommodation on The Neck, an endless supply of fresh kaimoana, and for the quality conversations and whiskey ‘tastings’ in the evening. Other landowners on The Neck and the Rakiura Maori Land Trust are also thanked for allowing access to their land. Thanks to Stewart Island DOC who permitted sampling within Rakiura National Park and on Ulva Island.

Field assistance from friends and family was also very much appreciated. Thanks to Annie Turnbull for being the most complying and longest serving (or suffering?) helper, Mel Hollis for braving 4 weeks of mid-winter field work and the strange vampire dude, William Turnbull for the creation of kelp man which subsequently frightened away several tourists in the process, Edward Turnbull for the game of golf on the most challenging of courses, and finally to Trigger the dog for great company and being a mobile garbage disposal, although was the only field assistant to steal my rock samples and almost lose my fieldbook in the pond!

Several people within the Department of Geological Sciences at the University of Canterbury have also greatly assisted me throughout this study. Thanks to Rob Spiers for cutting hundreds of thin and probe sections and always with a grin; to Stephen Brown for XRF analysis; John Southward for all my computer woes; Kerry Swanson for thin section imaging; Cathy Higgins and Vanessa Tappenden for fieldwork gear; and to Anekant Wandres for advice, abuse, support and general banter, you're a great mate. Thanks also to DHB for Friday evening wine and cheese – long may the tradition continue! Also, help from Professor Joel Baker, Dr Monica Handler and Dr Richard Wyscosanki at VUW and Trevor Ireland at ANU is also greatly appreciated. To fellow PhDers within the department who kept the place lively and have made the last 3 and a bit years the best of my life; in particular Tom, Sam and Chad (founding member of the amphibole club) it's been a blast and I can't think of a better group of people to have gone though the highs and lows of a PhD with. Also thanks to the fellow Friday footballers (Persian Prince, Beard Faće, Bavarian Butcher in particular).

And finally and most importantly, thanks to my family for supporting me 110% in life and in all my university endeavours over the last 8 years. To Grandma and Grandad for always being so interested in what I am doing and for all the dinners out and financial support. Thanks to my siblings Eddie, Willy and Annie for just being awesome. It's been great having you all up here to share this experience with me, and your support, encouragement and weekly Turnbull get-togethers mean more to me than you can know. And lastly, to my parents, I can't express in words how much your support has meant to me, especially during the hard times when I needed you the most. This thesis is for you.

TABLE OF CONTENTS

LIST OF FIGURES

LIST OF TABLES

CHAPTER ONE

SCOPE AND PURPOSE OF THESIS

1.1 INTRODUCTION

The processes by which magma chambers are constructed and evolve are fundamental to understanding the formation and evolution of the Earth's crust, and the processes that lead to the generation and eruption of large volume silicic caldera forming magmatic systems. Developing an understanding of the origin and evolution of large felsic systems in arc settings invariably focuses on that which has erupted, however a significant volume never actually reaches the surface (volcanic/plutonic ratio is on average 1:5; White *et al*., 2006). Plutonic bodies have long been overlooked in favour of studying volcanic deposits because of a long-held view that plutonic bodies are monotonously homogeneous, and that magmatic processes that operated within them are no longer preserved having been eliminated by near-solidus processes. Work by several authors (Frost & Mahood, 1987; Blundy & Sparks, 1992; Wiebe 1993a, 1993b, 1994; Coleman *et al*. 1995; Wiebe & Collins, 1998; Bachl *et al*., 2001; Miller & Miller, 2002; Harper *et al*., 2004; Perugini *et al*., 2005; Collins *et al*., 2006; Kamiyama *et al*., 2007; Walker *et al*., 2007) over the last two decades has shown however that plutonic bodies are often internally highly varied and complex, and contain structures and textures that formed through the complex interplay between several petrogenetic processes. Field evidence from these exposed plutons indicates that felsic magma chambers often trap basaltic magmas as they rise through the crust. This process commonly results in the formation of spectacular mingling structures and textures in which quenched mafic material is enclosed within a more felsic host. Mingling structures and textures have previously been ascribed to processes occurring during pluton emplacement but detailed field observations of the authors mentioned above indicate that these textures represent processes operating within an active magma chamber during the process of pluton construction, and provide insight into physical processes that were operating within the active chamber, including magma mixing and mingling, crystal accumulation, magmatic flow and compaction.

Through understanding the magmatic history of such plutons, insights can be gained on the physical, chemical and thermal processes responsible for the formation of plutons within arc settings, and conclusions drawn on the origin of magma source regions, rates of pluton construction and the size and longevity of these magmatic systems.

The overall aim of this thesis is to provide a better understanding of both the physical and chemical processes that operate within such compositionally diverse plutons, which will be addressed through investigation of the Halfmoon Pluton on Stewart Island. The Halfmoon Pluton displays spectacular field relationships characteristic of magma mingling between compositionally diverse but coeval magmas. Research incorporates detailed documentation and interpretation of magma mingling structures and textures in the field, coupled with petrography, geochemistry and geochronology, with the aim of elucidating the magmatic processes responsible for the generation and evolution of the composite Halfmoon Pluton. Comparisons are also drawn with similar and contrasting composite plutons overseas. Conclusions reached regarding the magmatic history of the subduction-related Halfmoon Pluton have the potential to provide unique insights into the magmatic processes that take place in arc-settings, which is currently a topic of renewed debate and controversy.

1.2 QUESTIONS TO BE ANSWERED

The main goal of this thesis is to identify the processes that operate within high-level composite mafic/felsic magma chambers using the Halfmoon Pluton on Stewart Island as an example. Processes that are thought to operate within active magma chambers, include replenishment, magma mixing and mingling, crustal assimilation, convection, crystallization, fractionation, crystal accumulation and compaction. The identification and quantification of such processes will be achieved chiefly through the study of macro- and microscopic structures and textures within the mingled rocks of the Halfmoon Pluton, coupled with detailed geochemical and geochronological analyses. Identification of these processes will aid understanding of active arc systems.

Specific objectives to be addressed within this thesis are:

- Establishment of the magmatic "stratigraphy" and the sequence of mafic replenishment events within the Halfmoon Pluton. Was the chamber emplaced as one large molten body or constructed incrementally from multiple replenishments of both mafic and felsic magma?
- Categorization of the different degrees/styles of mafic-felsic magma interaction within the Halfmoon Pluton and of the parameters that controlled the style of interaction preserved.
- Documentation of changes in the style of magma mingling within the magmatic sequence and identification of the processes that govern the style of mingling.
- Determination of the physical and chemical processes that operated within the Halfmoon Pluton, and of which processes are responsible for the chemical and isotopic evolution and diversity of the pluton.
- Determination of the degree of thermal, mechanical and chemical transfer between the mafic and felsic rocks.
- Constraining the timescale of magmatism through documentation and interpretation of field structures and textures coupled with precise U-Pb dating of key samples throughout the magma chamber. Was the plutonic body part of a long-lived magmatic system or was it short-lived?
- Discussion of the implications of the processes identified within the Halfmoon Pluton for understanding the mechanisms of emplacement and evolution of mid- to upper-crustal arc plutons.

1.3 THESIS STRUCTURE

An evaluation of magmatic processes and mafic-felsic magma interactions is presented in **Chapter 2**. This includes a review of geological literature pertaining to magma chamber emplacement, processes responsible for the chemical diversification of magmas, timescales of magmatic differentiation/crystallization, and the dynamics of mafic-felsic magma interaction. Implications of the research outcomes for understanding the dynamics of arc magmatism are also discussed briefly. **Chapter 3** presents field and petrographic data for the Halfmoon Pluton, from which a

"stratigraphic" sequence through the magma chamber is reconstructed. This magmatic sequence serves as the model for which interpretations based on geochemical and geochronological data could be applied in order for interpretations to be made regarding chemical evolution of the magma chamber from the base towards the top. **Chapter 4** presents interpretations of the whole-rock geochemical evolution of the Halfmoon Pluton, and makes inferences on source characteristics based on REE and isotopic characteristics. The majority of results presented in Chapters 3 and 4, plus some zircon U-Pb results (see Chapter 6) have been included in a manuscript that is currently under review with the *Journal of Petrology*. **Chapter 5** presents mineral chemistry data for biotite, plagioclase and hornblende. Evaluation of the chemical history and evolution of the magma chamber is achieved by the application of the Al-in-hornblende geobarometer and the plagioclase-hornblende and Ti-in-hornblende geothermometers to determine intensive parameters (i.e. P-T-fO_2, PH_2O). Results from this chapter will be re-drafted into a manuscript once additional EMPA analyses of hornblende and plagioclase have been obtained, and well as O- and H-isotopes on hornblende separates to further constrain magma source(s). This manuscript is intended for submission to *Contributions to Mineralogy and Petrology*. **Chapter 6** presents geochronological (U-Pb SHRIMP) and geochemical (LA-ICP-MS) data from zircon crystals from six intermediate-felsic host rock samples within the Halfmoon Pluton. The aim of this chapter is to constrain the timescales of magmatism, and any thermal perturbations to the system by application of the Ti-in-zircon geothermometer. Zircon results and interpretations will be incorporated into a manuscript intended for submission to *American Mineralogist* once O-isotope data have been obtained. **Chapter 7** summarizes results and conclusions reached for the origin and magmatic evolution of the Halfmoon Pluton from Chapters 3 to 6. A model of magma chamber construction and evolution is presented, and implications of the processes identified within the Halfmoon Pluton discussed with respect to understanding the origin and evolution of arc magmas. **Chapter 8** compares the results from this research with those from other composite plutons from different tectonic settings. **Chapter 9** summarizes the important conclusions reached from this research and contributions to knowledge.

A sample catalogue describing all hand specimens and sample treatment with respect to location, petrography, geochemistry and geochronology is presented in

Appendix 1. Thin sections descriptions are presented in **Appendix 2**. Results and methodology of whole rock XRF analyses are outlined in electronic **Appendix 3**. Isotopic analyses (MC-ICPMS) and methodology are outlined in electronic **Appendix 4**. Electron microprobe results are presented in **Appendix 5**. U/Pb SHRIMP dating techniques and results are outlined in electronic **Appendix 6**. LA-ICPMS zircon analyses are presented in electronic **Appendix 7**.

1.4 REFERENCES

Bachl, C.A., Miller, C.F., Miller, J.S. and Faulds, J.E. 2001 'Construction of a pluton: Evidence from an exposed cross section of the Searchlight pluton, Eldorado Mountains, Nevada' *GSA Bulletin* 113(9): 1213-1228

Blundy, J.D. and Sparks, R.S.J. 1992 'Petrogenesis of mafic inclusions in granitoids of the Adamello Massif, Italy' *Journal of Petrology* 33: 1039-1104

Coleman, D.S., Glazner, A.F., Miller, J.S., Bradford, K.J., Frost, T.P., Joye, J.L. and Bachl, C.A. 1995 'Exposure of a Late Cretaceous layered mafic-felsic magma system in the central Sierra Nevada batholith, California' *Contributions to Mineralogy and Petrology* 120: 129-136

Collins, W.J., Wiebe, R.A., Healy, B. and Richards, S.W. 2006 'Replenishment, crystal accumulation and floor aggradation in the megacrystic Kameruka Suite, Australia' *Journal of Petrology* 47: 2073-2104

Frost, T.P. and Mahood, G.A. 1987 'Field, chemical, and physical constraints on mafic-felsic magma interaction in the Lamarck Granodiorite, Sierra Nevada, California' *Geological Society of America Bulletin* 99: 272-291

Harper, B.E., Miller, F., Miller, G., Koteas, C., Cates, N.L., Wiebe, R.A., Lazzareschi, D.S. and Cribb, J.W. 2004 'Granites, dynamic magma chamber processes and pluton construction: the Aztec Wash pluton, Eldorado Mountains, Nevada, USA' *Transactions of the Royal Society of Edinburgh: Earth Sciences* 95: 277-295

Kamiyama, H., Nakajima, T. and Kamioka, H. 2007 'Magmatic stratigraphy of the tilted Tottabetsu Plutonic Complex, Hokkaido, North Japan: Magma chamber dynamics and pluton construction' *The Journal of Geology* 115: 296-314

Miller, C.F. and Miller, J.S. 2002 'Contrasting stratified plutons exposed in tilt blocks, Eldorado Mountains, Colorado River Rift, NV, USA' *Lithos* 61: 209-224

Perugini, D., Poli, G. and Rocchi, S. 2005 'Development of viscous fingering between mafic and felsic magmas: evidence from the Terra Nova Intrusive Complex (Antarctica)' *Mineralogy and Petrology* 83: 151-166

Walker, B.A., Miller, C.F., Claiborne, L.L., Wooden, J.L. and Miller, J.S. 2007 'Geology and geochronology of the Spirit Mountain batholith, southern Nevada: implications for timescales and physical processes of batholith construction' *Journal of Volcanological and Geothermal Research* 167: 239-262

White, S.M., Crisp, J.A. and Spera, F.A. 2006 'Long-term volumetric eruption rates and magma budgets' *Geochemistry Geophysics Geosystem* 7: Q03010, doi:10.1029/2005GC001002

Wiebe, R.A. 1993a 'The Pleasant Bay layered gabbro-diorite, Coastal Maine: ponding and crystallization of basaltic injections into a silicic magma chamber' *Journal of Petrology* 34:3 461-489

Wiebe, R.A. 1993b 'Basaltic injections into floored silicic magma chambers' *Eos* 74(1): 1-4

Wiebe, R.A. 1994 'Silicic magma chambers as traps for basaltic magmas: the Cadillac Mountain intrusive complex, Mount Desert Island, Maine' *The Journal of Geology* 102: 423-437

Wiebe, R.A. and Collins, W.J. 1998 'Depositional features and stratigraphic sections in granitic plutons: implications for the emplacement and crystallization of granitic magma' *Journal of Structural Geology* 20(9/10): 1273-1289

CHAPTER TWO

AN EVALUATION OF MAGMATIC PROCESSES AND MAFIC-FELSIC MAGMA INTERACTIONS

2.1 INTRODUCTION

Granitoids represent the most abundant igneous rocks in the upper continental crust, and provide one of the most important records of magmatic processes. Study of structures, textures and minerals within plutonic bodies offers insights into the processes responsible for the construction and evolution of the continental crust, and provides information regarding the processes that operate beneath active volcanic settings. The formation of granitic plutons involves four main stages; (1) generation of melt; (2) segregation of melt from the source; (3) magma ascent; and (4) magma emplacement and solidification (Petford *et al*., 2000). The timescales over which each of these stages operates are controversial, however a growing body of evidence indicates that plutonic bodies are long-lived and form through multiple injections of both mafic and felsic magma. Mingling between mafic and felsic magmas results in structures and textures that can be interpreted with respect to the magmatic processes involved.

This chapter will review the last two stages of pluton formation; ascent and emplacement, discussing the different models of pluton construction, and the mechanics of magmatic differentiation. An overview of the different types of mafic-felsic magma interaction will also be outlined, with emphasis on how magmatic processes can be inferred from the identification of magma mingling structures and textures and used to answer fundamental questions regarding the emplacement and crystallization of plutonic bodies within the upper crust.

2.2 A REVIEW OF MAGMA CHAMBERS AND THEIR PROCESSES

Plutonic bodies often preserve a detailed history of the physical, chemical and temporal magmatic processes responsible for their construction and evolution within the crust, however interpretation of these processes and the mechanics of magma ascent and emplacement within the mid-upper crust are long-standing subjects of controversy. The long-established view that plutons ascend and are emplaced as large diapiric liquid-rich bodies of magma (2.1(A)) (Pitcher & Berger 1972; Sylvester *et al*., 1978; Marsh, 1982; Hutton, 1988; Paterson & Vernon, 1995; Miller & Paterson, 1999) has been challenged in recent years. The magnitude of large magma pulses, and the difficulty of accommodating space requirements have seen a shift in opinion towards a model of incremental magma chamber assembly within the upper crust (Figure 2.1(B)). Whereas evidence exists in the field to support the diapiric rise of magma (Weinburg & Pedladchikov, 1994; Miller & Paterson, 1999), a growing body of evidence indicates that plutonic bodies are more commonly characterized by the incremental emplacement of mafic and felsic magmas of contrasting compositions (Coleman *et al*., 1995; Wiebe, 1996; Wiebe & Collins, 1998; Glazner *et al*., 2004; Lipman, 2007). This is compatible with geophysical observations that indicate that active magma chambers imaged beneath volcanic regions are large in volume (<10, 000km^3) but contain less than 10% melt (Iyer *et al*., 1990; Glazner *et al*., 2004).

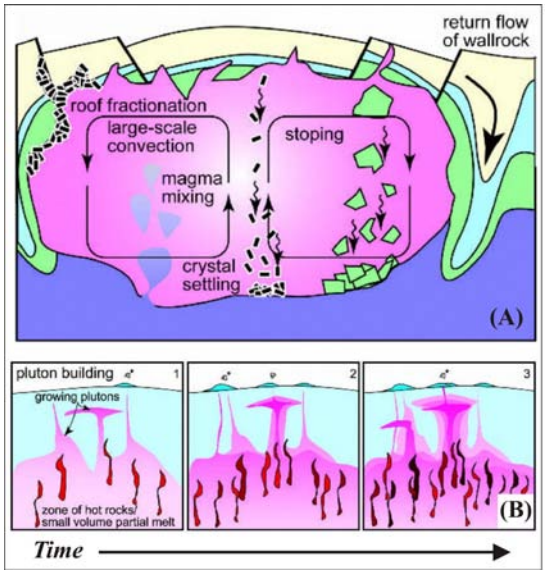

Figure 2.1. Diagrams illustrating (A) Diapirically emplaced liquid-rich magma chamber, and (B) Incrementally emplaced pluton. Liquid-rich areas are dark pink, new basalt intrusions are red, cooling to darker reds. From Glazner *et al*. (2004).

2.2.1 PROCESSES OF MAGMATIC DIFFERENTIATION

The processes responsible for magmatic differentiation are also contentious. Many geochemical and petrological studies (Bacon & Druitt, 1988; Mahood & Halliday, 1988; Hildreth *et al*., 1991; Graham *et al*., 1995; Tamura & Tatsumi, 2002) have concluded that silicic magmas in arc-settings (both volcanic and plutonic) are generated and diversify through a complex interplay of several key processes including but not limited to;

- fractional crystallization (crystal-liquid separation)
- volatile mass transfer
- assimilation
- magma mixing

Fractional crystallization has long been considered to be the main process driving magmatic differentiation (Bowen, 1928; Bachmann *et al*. 2007). Chemical fractionation induced by crystal-liquid separation can be achieved by at least three physical mechanisms, depending on the crystallinity of the magma. The most common form of crystal-liquid separation is gravitational settling by way of crystals being removed from the melt, forming cumulates. This process can only be sustained in magmas containing <40% crystals, as magma containing >40% crystals will be too crystalline to permit the downward or upward movement of solid particles (Bachmann *et al*., 2007). When the crystal content of a magma is >60%, crystal-liquid separation is achieved by compaction of the crystal mush, which results in filter pressing and extraction of more evolved interstitial liquid (Bachmann *et al*., 2007). Compaction of the crystal mush is caused by the weight of the overlying accumulated material. Between crystal contents of 40-60%, either of the above mechanisms can occur, depending on the properties of the magma. These include density and viscosity of the melt, presence of convective movements, plus open-system processes such as magma mixing and wall-rock assimilation (Bachmann *et al*., 2007). Flow segregation is a minor mechanism that can induce crystal-liquid separation. This process is most commonly observed in dikes which exhibit fine-grained margins, with phenocryst-rich centres. Flow segregation results from crystal-rich flow along the walls of a magma body which creates shearing around the edges of crystals nucleating at the margin. Phenocrysts migrate into the centre of the intrusion where flow

is more channelised, resulting in concentrations of coarser phenocrysts in the centre of dikes (Winter, 2001). This mechanism of crystal-liquid separation is however localized and is not responsible for the large-scale magmatic differentiation observed within large compositionally diverse plutonic bodies. Local conditions within magma chambers exist that limit whether crystal-liquid separation occurs, including the density and viscosity of the melt, and the presence of convective currents (Bachmann *et al*., 2007).

Volatile mass transfer occurs when a separate vapour phase co-exists with the magma, allowing liquid-vapour fractionation to occur. This form of chemical differentiation does not have a large effect on most magmatic systems as a whole, either resulting in the formation of aplite or pegmatite dikes, or resulting in rare plutonic bodies with unusual compositions (Winter, 2001).

Chemical differentiation of magmas by the closed-system processes outlined above cannot alone account for the diversity of magma compositions present within the crust. Almost all crustal magmas have been affected by the open-system processes of assimilation of country rock and/or magma replenishment and subsequent mixing.

The geochemical evolution of a batch of magma is closely linked to interactions with its environment (Spera & Bohrson, 2001). Compositional and isotopic signatures of many granitoid bodies provide unequivocal evidence for the assimilation of recycled crustal rocks, either from the direct incorporation of country rock material to the magma chamber, or the more fundamental process of partial melting of crustal material at depth (Pitcher, 1997). Crustal contamination of magmas can be identified through geochemical and isotopic signatures. Large ion lithophile elements (LILE) such as K, Rb, Ba, Pb and Sr are mobile, and are typically controlled by aqueous fluids and melts that concentrate them in continental crust (Rollinson, 1993). Concentrations of LILEs within magma can therefore indicate crustal contamination. The isotopic signature of magmas is however a more precise method of determining the effects of assimilation as several other processes may be responsible for the concentration of LILEs within magma. Most Phanerozoic continental crust is enriched in $^{87}Sr/^{86}Sr$ and depleted in $^{143}Nd/^{144}Nd$ whereas primitive

magmas are depleted in $^{87}Sr/^{86}Sr$ and have high values of $^{143}Nd/^{144}Nd$. Therefore, in a general sense, crustal contamination of primitive magmas can be inferred if they have high $^{87}Sr/^{86}Sr$ and low $^{143}Nd/^{144}Nd$ values (Rollinson, 1993; Winter, 2001).

Composite plutons that document the interaction between coeval mafic and felsic magmas provide clear evidence that felsic magma chambers are periodically replenished by more mafic magmas. Mineral chemistry and isotopic signatures also indicate that even homogenous granitic plutons may represent hybrid magmas formed by thorough mixing of two or more interacting magmas of contrasting composition and/or mantle source. Replenishment of crustal magma chambers with mafic magma has been identified as an important process for several reasons, including triggering volcanic eruptions (Sparks *et al*., 1977), and the longevity of silicic magmas, allowing them to rise to shallow levels within the crust (Hildreth *et al*., 1991; Wiebe, 1996). The efficiency of these processes is dependent on how rapidly heat flows from the mafic magma to the felsic magma (Snyder, 2000).

2.2.2 TIMESCALES OF MAGMA DIFFERENTIATION/CRYSTALLIZATION

The timescales over which magmas separate, ascend and crystallize within the crust are also a topic of considerable debate. There are two contrasting views on the timescales over which magmatic systems are active; those based on thermal modeling which indicate that granite magmatism is a rapid, dynamic process operating over periods of $<10^4$ years regardless of tectonic setting (Petford *et al*., 2000), and those based on geochronological and field evidence that indicate magmatic systems are active over timescales of $>10^6$ years (Walker *et al*., 2007). The thermal modeling approach may be limited in that any one magmatic system is unique, evolving through the combination of several different processes. In recent years, a growing body of evidence suggests that many large plutonic bodies have formed incrementally over millions of years as a result of multiple injections of both mafic and felsic magma (Davies *et al*., 1994; Bachl *et al*., 2001; Jellinek & DePaolo, 2003; Coleman *et al*., 2004; Glazner *et al*., 2004; Harper *et al*., 2004; Hawkins & Wiebe, 2004; Walker *et al*., 2007). These plutons consist of melt-rich,

melt-poor and entirely crystalline zones during their active life (Walker *et al*. 2007), and are never wholly molten at any one time.

2.3 Dynamics of Mafic-Felsic Magma Interaction

Plutonic bodies commonly preserve evidence for the interaction between mafic and felsic magmas. The interaction between two or more magmas of contrasting composition and physical properties can generate a number of structures and textures that may be preserved within plutonic bodies that can be interpreted with respect to magmatic processes that were operating at the time the magma chamber was active. A number of key factors control the style of the mafic-felsic magma interaction that occurs, and include;

- temperature contrasts between the two magmas
- degree of crystallization of the felsic host magma
- compositional contrasts
- relative volumes of the two magmas
- rate of replenishment of the intruding magma
- water contents of the magmas
- amount of time available for mixing to occur

The main factor controlling the style of magma interaction is the rheological contrast between the two interacting magmas, which is related largely to the temperature contrast between the two interacting magmas, and therefore the degree of crystallization. Fluid dynamic studies carried out by several authors (e.g. Sparks & Marshall, 1986; Frost & Mahood, 1987; Snyder & Tait, 1995) show that temperature, which is the primary determinant of magma viscosity and hence viscosity contrast is the main parameter controlling whether magmas mix or mingle. These studies showed that in almost all situations where a hotter more mafic magma injects into a cooler, more felsic magma chamber, the mafic magma quenches, resulting in a large viscosity contrast between the two interacting magmas. At this point, magma mixing and homogenization is only possible if cooling rates are slow, and if turbulent convection, chemical diffusion or other

diffusive processes are operating (Frost & Mahood, 1987). Magma mixing is only likely if there is a <10% SiO_2 difference between the host and injected magma, or if the injected magma is large in volume (>50%) (Frost & Mahood, 1987).

The composition of any given magma influences its temperature and viscosity – the key parameters influencing the type of interaction preserved. Interacting magmas with a difference of <10% SiO_2 are more likely to mix than mingle as their temperatures and viscosities are likely to be similar when they interact (Frost & Mahood, 1987). This of course depends on the rheological evolution of the felsic host magma, as once it meets its liquidus and begins to cool and crystallize, the relative rheological contrast with the replenishing hot, liquid mafic magma will be far greater. Compositional contrast between interacting magmas therefore plays a minor role in the style of interaction preserved. This is also evident from the number of studies on composite plutons that exhibit the same or similar mingling structures and textures, yet have varied compositional contrasts.

In any magma interaction relationship, the relative volumes of the two interacting materials play an important role. If there is a large influx of mafic magma there may be an insufficient quantity of cooler felsic host magma to chill against, and therefore mixing occurs. Frost and Mahood (1987) conclude that injected mafic magma mass fractions of >50% are required before mixing is favoured. Alternatively, when very small amounts of mafic magma are injected into large quantities of felsic magma, mingling more readily occurs and mafic enclave formation may be favoured.

The initial water content of the two interacting magmas may also have an effect on the style of mafic-felsic magma interaction. Increasing the water content of magma lowers its initial viscosity. If water contents are increased in the felsic host magma, progressively larger amounts of mafic magma are required if hybridization between the two magmas is to occur (Frost & Mahood, 1987). Increasing the water content of mafic magma lowers its liquidus temperature, making it cooler and less likely to quench within the felsic host (Frost & Mahood, 1987), therefore, increasing the water content of the felsic host magma favours mingling, and increasing the water content of the mafic magmas favours mixing.

The rate at which mafic magmas intrude into the felsic host magma is also an important parameter controlling the mingling style. Faster rates of mafic magma replenishment may promote disaggregation of the mafic magma into the chamber to form mafic enclaves, whereas slower rates favour mafic sheet formation. Mafic enclave formation may also form at the edges of thick flows that form mafic sheets. Snyder and Tait (1995) showed using fluid mechanics studies that a flow-front instability develops at the edge of mafic sheets that favours the formation of enclaves as the sheet breaks apart from upwelling less dense liquid below (Figure 2.2).

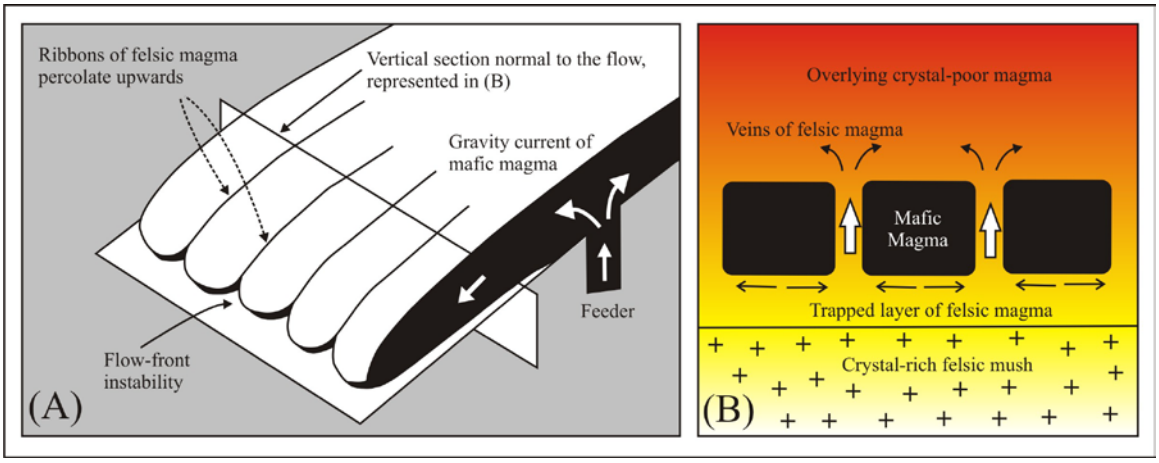

Figure 2.2. (A) Perspective view of the fingered morphology of a basaltic injection into a silicic magma chamber. (B) Cross-sectional view perpendicular to the flow direction of the basalt fingers (after Snyder & Tait, 1998a).

2.4 MAGMA MINGLING

Mingling between interacting mafic and felsic magmas occurs when there is a sufficient temperature and density contrast between the two magmas. Recent work by Wiebe and Collins (1998) has shed new light on the interpretation of magmatic processes within composite plutons, largely based on the interpretation of structures and textures of mingled and mixed magmas in the field. Rather than reflecting emplacement, Wiebe and Collins (1998) believe that many structures and textures in granitic plutons reflect processes that operated in an active magma chamber during solidification; processes such as replenishment, convection, mixing, crystallization, deposition and compaction. They proposed that many mingling structures and textures have formed as a result of mafic

magma injection between an aggrading crystal-rich chamber base, and an overlying crystal-poor magma above. Figures 2.3-2.5 display how these mafic magmas are emplaced, and the resulting mingling structures formed.

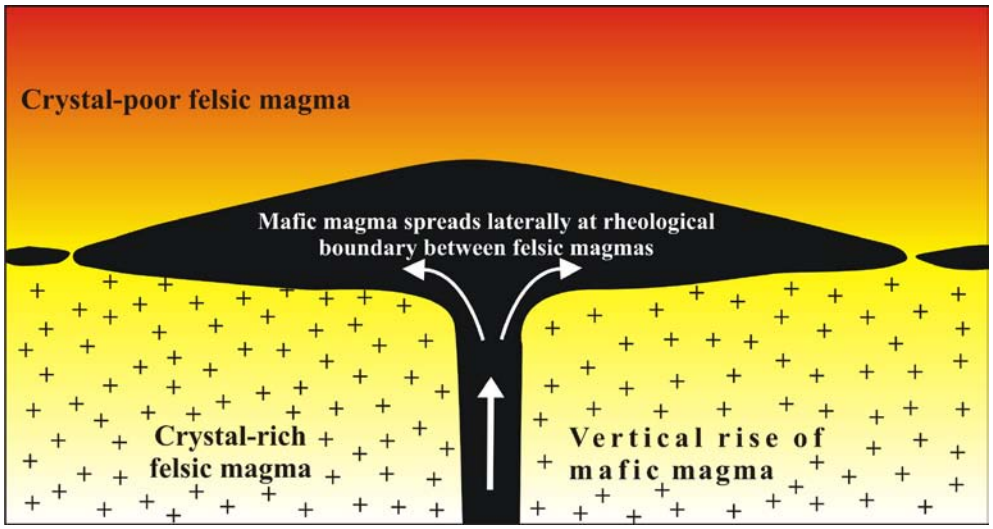

Figure 2.3. Initial vertical emplacement of mafic magma within a more felsic host magma before mafic magma spreads laterally at rheological boundary between the crystal-rich mush and the overlying crystal-poor magma (after Wiebe & Collins, 1998)

Figure 2.3 shows how the injected mafic magma initially rises vertically through the crystal-rich mush at the base of the chamber, before spreading laterally at the rheological boundary with the overlying crystal-poor liquid magma. Disruption at the thin edge of mafic sheets as a result of upwelling of trapped felsic liquid below results in mafic enclave formation.

The mafic sheet is much hotter than the adjacent felsic host magma, and chills rapidly against it. The mafic sheet is also much denser than the surrounding felsic magma, and therefore will begin to sink as it chills. A gravitational instability arises in which more buoyant felsic magma is trapped underneath the sinking mafic sheet. The felsic liquid tries to escape upwards, forming flame-structures in the base of the mafic sheet (Figure 2.4). Convective currents generated by the cooling and crystallizing mafic sheet can tear off chunks of the still mushy mafic sheet to form mafic enclaves. These mafic enclaves sink within the liquid-rich felsic magma to accumulate above the top of

the mafic sheet. Crystallinities of ~30% are required in order to prevent sinking of mafic enclaves in a granitoid magma, which implies that crystal contents within the overlying magma from which mafic enclaves have sunk would have been less than 30% (Soo, 1967; Vigneresse *et al*., 1996). This process determines the typical morphology of a mafic sheet characterized by a fine-grained chilled basal contact punctuated by flame structures and load casts, a coarser-grained centre as a result of prolonged cooling, and a gradational upper contact with a rubbly enclave-rich layer above.

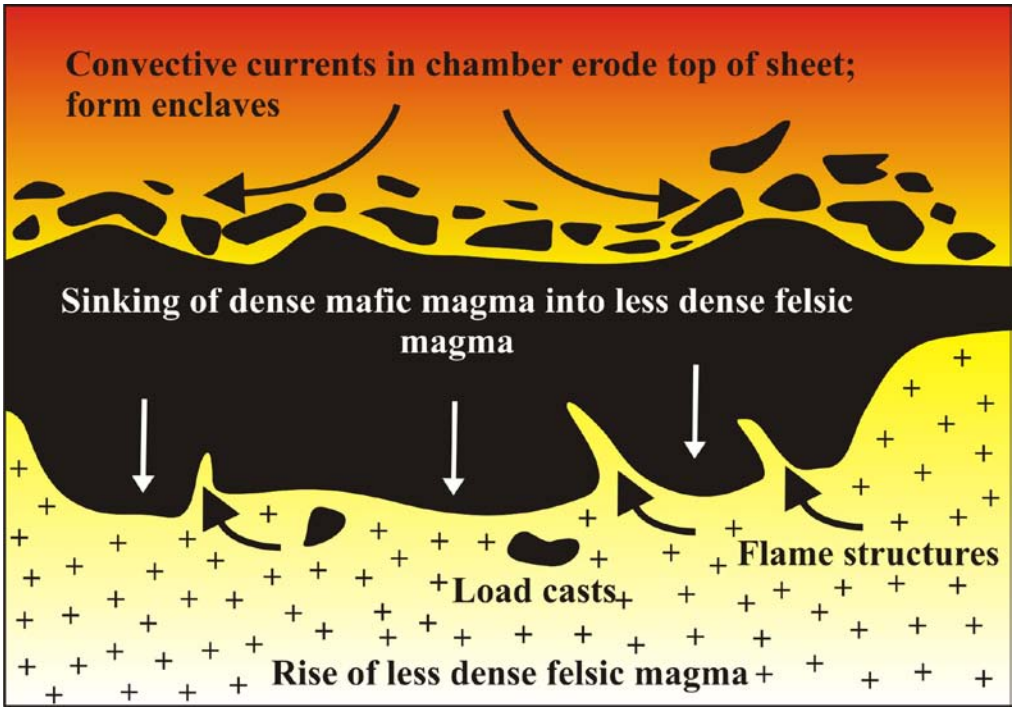

Figure 2.4. Cooling and sinking of the mafic sheet. Upwelling of buoyant felsic magma forms flame structures and load casts at the base of the sheet. Enclaves accumulate along the top of the sheet (after Wiebe & Collins, 1998).

Mafic enclaves become highly stretched defining a magmatic foliation as a result of convective flow within the overlying magma. Injection of an overlying mafic sheet causes compaction of the material below as a result of loading. This is evidenced by cuspate margins on mafic sheets and enclaves that lie perpendicular to the degree of shortening (Figure 2.5). Continued injection of mafic magma results in a sequence of mafic sheets and enclaves being preserved, providing a stratigraphic record of the history of events within the pluton.

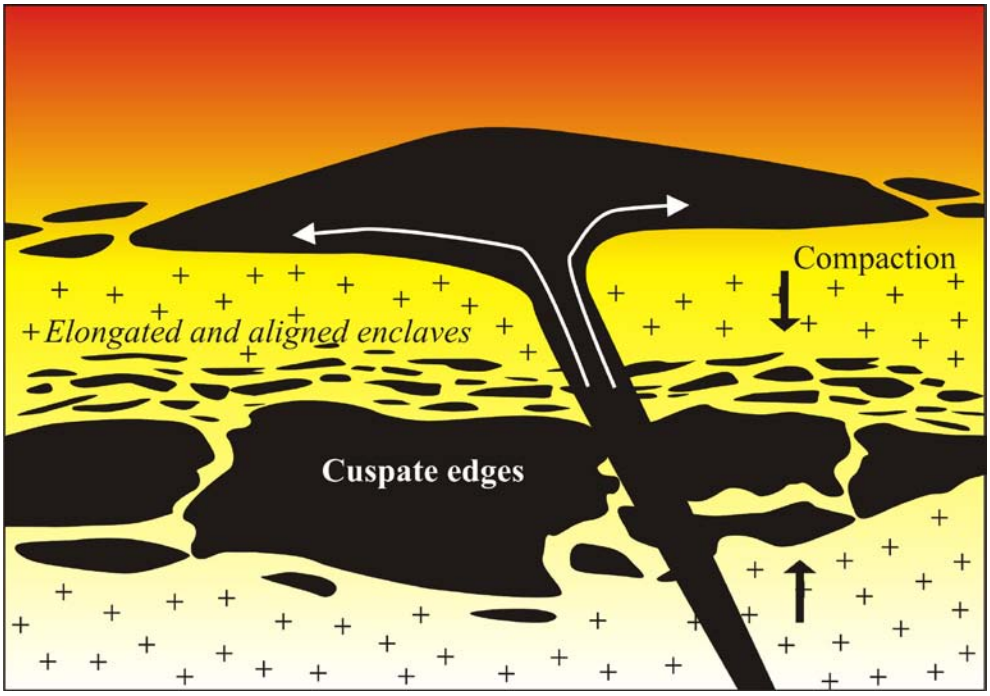

Figure 2.5. Continued replenishment of the felsic magma chamber results in a series of overlapping mafic sheets (after Wiebe & Collins, 1998).

Studies of composite plutons from around the world in which magma mingling structures and textures are providing a growing body of evidence that indicate that the above process of mafic sheet and enclave formation is a characteristic feature of several plutonic complexes from diverse tectonic settings (Bachl *et al*., 2001; Miller & Miller, 2002; Harper et al., 2004; Wada *et al*., 2004; Collins *et al*., 2006; Kamiyama et al., 2007).

Changes in the parameters that control the mingling of magmas (viscosity, temperature, rate of replenishment, relative volumes, etc) can result in the disaggregation of mafic sheets within felsic magma chambers to form mafic enclave swarms. Formation of mafic enclaves may also occur as a result of exsolving of volatiles during second boiling prior to rapid cooling of the wet mafic magma in contact with the cooler felsic magma. Volatiles may then allow the mafic enclaves to float or be remobilized by magmatic flow throughout the magma chambers (Eichelburger, 1980). Mafic enclaves have previously been interpreted as xenoliths of crystalline rock that have been broken off and incorporated into the felsic host, however their characteristic rounded shape and the common presence of fine-grained chilled margins indicates that they are magmatic in

origin, and were injected into the felsic host magma when it was liquid enough to permit mingling.

Many of the structures and textures within the mingled magmas are analogous to those found in sedimentary rocks that have experienced interaction between two materials of contrasting densities. Just as these structures can be used to infer younging direction in sedimentary sequences, they can be used within plutonic bodies to infer way-up, and include such features as flame structures and load casts. Other distinctive field relationships that can be used to infer way-up include; veins of filter-pressed felsic material that extend vertically into mafic sheets above, sinking of denser material towards the base, cross-cutting mafic feeder dikes that then spread laterally and mingle with the felsic host, accumulations of amphibole beneath chilled mafic sheets due to the vertical escape of volatiles, felsic layers with laminated feldspars and faint modal layering indicative of cumulates (Wiebe, 1993; Wiebe & Collins, 1998). All of these structures further support the hypothesis that magma chambers are constructed incrementally from the base up. The type, size and shape of mingling structures preserve information of the style and dynamics of the mingling of magmas, and lead to interpretations regarding the processes responsible for their formation.

2.5 EXCHANGE BETWEEN THE TWO INTERACTING MAGMAS

Thermal, mechanical and chemical interactions are the principal types of exchange between co-exisiting magmas. As discussed in the previous sections, the style and nature of interactions between coexisting magmas is controlled by their initial temperatures, degree of crystallization, compositions, relative volumes, rate of replenishment, and water content. As these intensive and interacting parameters do not change simultaneously during the evolution of the systems, the various interactions may appear sequentially (Barbarin & Didier, 1992).

2.5.1 Thermal Exchange

Thermal exchange is the most rapid of the three exchanges, typically being several orders of magnitude faster than chemical diffusion in silicate melts (Sparks and Marshall 1986).

The initially high thermal contrast between the two contrasting magmas leads to thermal exchange. Textures preserved in mingled magmas such as their fine grain size and chilled margins indicate the rapid crystallization and local quenching of the mafic magma after rapid loss of heat to the enclosing felsic host magma. The relative volumes of the interacting magmas play an important role in how fast thermal exchange is achieved (Sparks & Marshall, 1986; Frost & Mahood, 1987; Snyder, 2000). Large volumes of mafic magma injected into a felsic magma chamber take a relatively long time to cool and attain thermal equilibrium with the surrounding felsic host magma. This has an affect on how much chemical exchange can occur between the two magmas, with smaller mafic magma volumes reaching thermal equilibrium relatively quickly, becoming solid enough to limit and even inhibit chemical exchange (Barbarin & Didier, 1992). Large volumes of mafic magma that take a longer time to reach thermal equilibrium allow for a longer period over which extensive chemical exchange can occur.

The style of magma mingling preserved is strongly controlled by the rate at which thermal equilibrium is reached. As displayed in Figure 4, granitic and basaltic magmas display different crystallization histories. When coeval mafic and felsic magmas follow a common cooling history, the temperature at which each magma reaches a given rheological threshold is strongly dependant on its composition (Fernandez & Gasquet, 1994). Once thermal equilibrium is attained, regardless of the temperature, crystallization is much more advanced in the quenched mafic magmas than in the surrounding felsic magma. An inversion temperature therefore exists where the felsic magma becomes less viscous than the mafic magma (Fernandez & Gasquet, 1994). Once this inversion temperature is reached, different mingling structures may result, in particular, brecciation of the more solid mafic magma into angular inclusions within the more mobile felsic magma.

The rate at which thermal equilibration is achieved has a strong bearing on the degree of mechanical and chemical exchange that occurs between the two interacting magmas. When thermal equilibration is rapid and mafic magmas quench and chill rapidly within the felsic magma, mechanical and chemical exchange is inhibited by the solid

fine-grained chilled margin that forms at the edge of the mafic inclusions. Once thermal equilibrium is reached, the final viscosities of the two magmas are the main physical parameter controlling the degree of mechanical and chemical exchange that will occur (Poli *et al*., 1996).

2.5.2 *Mechanical Exchange*

Mechanical exchange between coexisting magmas occurs as either exchange of blobs of viscous magma to form enclaves, or exchange of individual crystals to form xenocrysts (Barbarin & Didier, 1992; Waight *et al*., 2001). Mechanical exchange between coexisting magmas can occur at four different locations; prior to emplacement at depth, during emplacement as a result of flow-front instabilities or within the conduit, interactions at the base of mafic sheets, and interactions at the top of mafic sheets at the contact with the overlying felsic host (Wiebe *et al*., 2002). At all of these locations, mechanical exchange can only occur when the magmas are still mobile enough to permit stirring. Stirring within magma chambers can be generated in a number of ways, including;

- thermal gradients which induce double-diffusive convection
- injection of mafic magma into felsic magma as a fountain can form a double-diffusive convective layer and possible overturning
- turbulent stirring due to the relative ascent of two magmas with different physical properties
- magmatic flow
- viscous fingering (Barbarin & Didier, 1992; Snyder & Tait 1998a)

The extent of mixing between magmas of contrasting composition (i.e. localized mixing vs. complete hybridization of a magma chamber) is controlled largely by the compositional contrasts of the two interacting magmas, and therefore their relative density and viscosity contrasts. Complete hybridization of magma chambers is considered a rare occurrence as the large density and viscosity contrasts between coeval mafic and felsic magmas typically impedes large-scale mixing.

2.5.3 Chemical Exchange

Chemical exchange occurs across the entire time-span during which two interacting magmas are in contact, however it generally occurs after thermal equilibration of the coexisting magmas is attained. The rate at which chemical exchange occurs relies heavily on the chemical contrast and physical state of both magmas, and also the water content of the magmas (Barbarin & Didier, 1992). Chemical exchange can occur between both the mafic and felsic magmas.

Chemical exchange within the mafic magmas is generally enhanced by vigorous stirring of the magma chamber which promotes continuous felsic magma replenishment, maintaining the chemical contrast between the interacting magmas (Barbarin & Didier, 1992). Disaggregation of large volumes of mafic magma into smaller blobs also promotes chemical exchange by increasing the surface area over which felsic magma is in contact with the mafic inclusion and across which chemical diffusion occurs (Barbarin & Didier, 1992; Snyder & Tait, 1998b). Fluid dynamic studies by Snyder and Tait (1998b) have shown that multiple mafic magma injections can also cause significant diffusive exchange between the two magmas, affecting the trace element and isotopic character of the overlying chamber of felsic magma.

The ability of elements and isotopes to diffuse between the magmas is variable, with field and experimental data indicating that alkalis and H_2O diffuse at rates much faster than other elements (Blundy & Sparks, 1992; Waight *et al*., 2001). Isotopic diffusion is much faster than chemical diffusion (Snyder & Tait, 1998b), with many enclaves within composite plutons displaying identical isotopic signatures to their enclosing felsic host (Snyder & Tait, 1998b). Because isotopes diffuse faster than chemicals, isotopic equilibrium is commonly attained across the entire pluton, whereas chemical equilibration is localized (Barbarin & Didier, 1992). Isotopic and chemical diffusion may also occur after emplacement once both magmas are crystalline. Both chemical and isotopic diffusion are also enhanced by the presence of fluid phases, especially water (Barbarin & Didier, 1992). Chemical, like mechanical, exchange is obstructed by

quenched fine-grained mafic enclave margins which likely stop the transfer of magma and crystals, and strongly inhibit chemical exchange (Barbarin & Didier, 1992).

2.6 IMPLICATIONS OF STUDY FOR UNDERSTANDING ARC DYNAMICS

Study of the Halfmoon Pluton has the potential to provide unique insights into the magmatic processes taking place in subduction-related magma chambers, and to further our understanding of the genesis and evolution of arc-related plutonic rocks. Fundamental questions persist with regard to how large volumes of rhyolitic magma are generated within arc settings. Recent publications have hypothesized that one mechanism for generating large, eruptible volumes of silicic magma is to extract melt from wet intermediate crystalline cumulate mushes that have stalled in the mid- to upper crust (Hildreth, 2004; Bachmann & Bergantz, 2004, 2008; Eichelberger *et al*., 2006; Miller & Wark, 2008). A number of authors consider it likely that the viscosities of felsic melts are too high to permit the effective sinking and accumulation of crystals (Harper *et al*., 2004) which would preclude the formation of granitic cumulates. Recent viscosity measurements however have indicated that crystal settling rates on the order of 1m/year are likely in hydrous felsic magmas at temperature of ~750-800°C (Baker, 1996; Scaillet *et al*., 1998) which is sufficient to accumulate the large volumes of cumulate material required to produce rhyolitic magmas with volumes on the order of 1000km^3. Evidence for crystal-liquid separation is rarely reported within volcanic deposits as crystal-rich intermediate rocks are very rarely erupted. Therefore, the best evidence to support the occurrence of intermediate cumulates within arc settings is to study sections of exhumed arc crust, where processes are directly observable. A growing body of field and geochemical evidence in granitic bodies supports the process of downward crystal accumulation, and indicates that it is a common process that operates within magma chambers from a variety of tectonic settings, including arc settings (i.e. Wiebe & Collins, 1998; Bachl *et al*., 2001; Harper *et al*., 2004; Kamiyama *et al*., 2007). Hornblende fractionation has also been argued to be an important process controlling geochemical trends observed within arc magmas (Davidson *et al*., 2007). Many geochemical studies have concluded that silicic magmas in arcs are generated by a combination of assimilation and crystal fractionation (Bacon & Druitt, 1988; Mahood & Halliday, 1988; Hildreth *et al*.,

1991) and highlight the importance of hornblende fractionation in controlling the trace element variations (Davidson *et al*, 2007). The exhumed Halfmoon Pluton provides direct evidence for the processes that operate at depth within currently active arc settings. Processes identified within the Halfmoon Pluton and their implications for understanding the genesis and evolution of arc-related plutonic rocks will be discussed in Chapter 7.

2.7 CONCLUSIONS

As outlined in Chapter 1, the main goal of this thesis is to identify the processes that operate within high-level composite mafic/felsic magma chambers using the Halfmoon Pluton on Stewart Island as an example. The episodic injection of mafic magma into a crystallizing intermediate-felsic magma chamber is well documented within the Halfmoon Pluton, with mingling structures and textures preserving a detailed record of magma chamber processes. Evaluation of the spatial and temporal evolution of the incrementally constructed Halfmoon Pluton magmatic system is achieved by combining whole-rock and mineral chemistry and geochronology with careful documentation of way-up structures and textures in the field. Other magmatic processes outlined in this chapter will be identified by application of whole-rock geochemistry (major, trace and REEs, and Sr/Nd Isotopes) and detailed geochemical analyses of key mineral phases within the Halfmoon Pluton rocks (i.e. plagioclase, hornblende, zircon). The Halfmoon Pluton displays spectacular field relationships typical of magma mingling of compositionally diverse but coeval magmas. Field relations document the evolving nature of these magma chambers, and will be discussed in the following chapter.

2.8 REFERENCES

Bachl, C.A., Miller, C.F., Miller, J.S. and Faulds, J.E. 2001 'Construction of a pluton: Evidence from an exposed cross section of the Searchlight pluton, Eldorado Mountains, Nevada' *GSA Bulletin* 113(9): 1213-1228

Bachmann, O. and Bergantz, G.W. 2004 'On the origin of crystal-poor rhyolites: extracted from batholithic crystal mushes' *Journal of Petrology* 45: 1565-1582

Bachmann, O. and Bergantz, G.W. 2008 'Rhyolites and their source mushes across tectonic settings' *Journal of Petrology* 49: 2277-2285

Bachmann, O., Miller, C.F. and de Silva, S.L. 2007 'The volcanic-plutonic connection as a stage for understanding crustal magmatism' *Journal of Volcanology and Geothermal Research* 167: 1-23

Bacon, C.R. and Druitt, T.H. 1988 'Compositional evolution of the zoned calcalkaline magma chamber of Mount Mazama, Crater Lake, Oregon' *Contributions to Mineralogy and Petrology* 98: 224-256

Baker, D.R. 1996 'Granitic melt viscosities: Emperical and configurational entropy models for their calculation' *American Mineralogist* 81: 126-134

Barbarin, B. and Didier, J. 1992 'Genesis and evolution of mafic microgranular enclaves through various types of interaction between coexisting felsic and mafic magmas' *Transactions of the Royal Society of Edinburgh: Earth Sciences* 83: 145-153

Blundy, J.D. and Sparks, R.S.J. 1992 'Petrogenesis of mafic inclusions in granitoids of the Adamello Massif, Italy' *Journal of Petrology* 33: 1039-1104

Bowen, N.L. 1928 *The evolution of the igneous rocks*. Princeton University Press pp 334

Coleman, D.S., Glazner, A.F., Miller, J.S., Bradford, K.J., Frost, T.P., Joye, J.L. and Bachl, C.A. 1995 'Exposure of a Late Cretaceous layered mafic-felsic magma system in the central Sierra Nevada batholith, California' *Contributions to Mineralogy and Petrology* 120: 129-136

Coleman, D.S., Gray, W. and Glazner, A.F. 2004 'Rethinking the emplacement and evolution of zoned plutons: Geochronological evidence for incremental assembly of the Tuolumne Intrusive Suite, California' *Geology* 32: 433-436

Collins, W.J., Wiebe, R.A., Healy, B. and Richards, S.W. 2006 'Replenishment, crystal accumulation and floor aggradation in the megacrystic Kameruka Suite, Australia' *Journal of Petrology* 47: 2073-2104

Davidson, J., Turner, S., Handley, H., Macpherson, C. and Dosseto, A. 2007 'Amphibole "sponge" in arc crust?' *Geology* 35: 787-790

Davies, G.R., Halliday, A.N., Mahood, G.A. and Hall, C.M. 1994 'Isotopic constraints on the production rates, crystallization histories and residence times of pre-caldera silicic magmas, Long Valley, California' *Earth and Planetary Science Letters* 125: 17-37

Eichelberger, J.C. 1980 'Vesiculation of mafic magma during replenishment of silicic magma reservoirs' *Nature* 288: 446-450

Eichelberger, J.C., Izbekov, P.E. and Browne, B.L. 2006 'Bulk chemical trends at arc volcanoes are not liquid lines of descent' *Lithos* 87: 135-154

Fernandez, A.N. and Gasquet, D.R. 1994 'Relative rheological evolution of chemically contrasted coeval magmas: example of the Tichka plutonic complex (Morocco)' *Contributions to Mineralogy and Petrology* 116: 316-326

Frost, T.P. and Mahood, G.A. 1987 'Field, chemical, and physical constraints on mafic-felsic magma interaction in the Lamarck Granodiorite, Sierra Nevada, California' *Geological Society of America Bulletin* 99: 272-291

Glazner, A.F., Bartley, J.M., Coleman, D.S., Gray, W. and Taylor, R.Z. 2004 'Are plutons assembled over millions of years by amalgamation from small magma chambers?' *GSA Today* 14(4): 4-11

Graham, I.J., Cole, J.W., Briggs, R.M., Gamble, J.A. and Smith, I.E.M. 1995 'Petrology and petrogenesis of volcanic rocks from the Taupo Volcanic Zone: a review' *Journal of Volcanology and Geothermal Research* 68: 59-87

Harper, B.E., Miller, F., Miller, G., Koteas, C., Cates, N.L., Wiebe, R.A., Lazzareschi, D.S. and Cribb, J.W. 2004 'Granites, dynamic magma chamber processes and pluton construction: the Aztec Wash pluton, Eldorado Mountains, Nevada, USA' *Transactions of the Royal Society of Edinburgh: Earth Sciences* 95: 277-295

Hawkins, D.P. and Wiebe, R.A. 2004 'Discrete stoping events in granite plutons: A signature of eruptions from silicic magma chambers?' *Geology* 32(12): 1021-1024

Hildreth, W., Halliday, A.N. and Christiansen, R.L. 1991 'Isotopic and chemical evidence concerning the genesis and contamination of basaltic and rhyolitic magma beneath the Yellowstone Plateau volcanic field' *Journal of Petrology* 32: 63-138

Hildreth, W. 2004 'Volcanological perspectives on Long Valley, Mammoth Mountain, and Mono Craters: several contiguous but discrete systems' *Journal of Volcanological and Geothermal Research* 136: 169-198

Hutton, D.H.W. 1988 'Granite emplacement mechanisms and tectonic controls: inferences from deformation studies' *Transactions of the Royal Society of Edinburgh: Earth Sciences* 79: 245-255

Iyer, H.M., Evans, J.R., Dawson, P.B., Stauber, D.A., Achauer, U., 1990 'Differences in magma storage in different volcanic environments as revealed by seismic tomography; silicic volcanic centers and subduction-related volcanoes'
In: Ryan, M.P. *Magma transport and storage* United Kingdom, John Wiley & Sons, pp 293–316

Jellinek, A.M. and DePaolo, D.J. 2003 'A model for the origin of large silicic magma chambers: precursors of caldera-forming eruptions' *Bulletin of Volcanology* 65: 363-381

Kamiyama, H., Nakajima, T. and Kamioka, H. 2007 'Magmatic stratigraphy of the tilted Tottabetsu Plutonic Complex, Hokkaido, North Japan: Magma chamber dynamics and pluton construction' *The Journal of Geology* 115: 296-314

Lipman, P.W. 2007 'Incremental assembly and prolonged consolidation of Cordilleran magma chambers: Evidence from the Southern Rocky Mountain volcanic field' *Geosphere*, **3**, 42-70

Mahood, G.A. and Halliday, A.N. 1988 'The generation of high-silica rhyolite: a Nd, Sr, and O isotopic study of the Sierra La Primavera, Mexican Neovolcanic Belt' *Contributions to Mineralogy and Petrology* 100: 183-191

Marsh, B.D. 1982 'On the mechanics of igneous diapirism, stoping, and zone melting' *American Journal of Science* 82: 808–855

Miller, C.F. and Miller, J.S. 2002 'Contrasting stratified plutons exposed in tilt blocks, Eldorado Mountains, Colorado River Rift, NV, USA' *Lithos* 61: 209-224

Miller, R.B. and Paterson, S.R. 1999 'In defense of magmatic diapirs' *Journal of Structural Geology* 21: 1161-1173

Miller, C.F. and Wark, D.A. 2008 'Supervolcanoes and their explosive supereruptions' *Elements* 4: 11-15

Paterson, S.R. and Vernon, R.H. 1995 'Bursting the bubble of ballooning plutons: a return to nested diapers emplaced by multiple processes' *Geological Society of America Bulletin* 107: 1356-1380

Petford, N., Cruden, A.R., McCaffrey, K.J.W. and Vigneresse, J.-L. 2000 'Granite magma formation, transport and emplacement in the Earth's crust' *Nature* 408: 669-673

Pitcher, W.S. 1997 *The nature and origin of granite* Chapman & Hall, London, pp 387

Pitcher, W.S. and Berger, A.R., 1972 *The geology of Donegal: a study of granite emplacement and unroofing* Regional geology series, New York, Wiley-Interscience, pp 435

Poli, G., Tommasini, S. and Halliday, A.N. 1996 'Trace element and isotopic exchange during acid-basic magma interaction processes' *Transactions of the Royal Society of Edinburgh: Earth Sciences* 87: 225-232

Rollinson, H. 1993 *Using Geochemical Data: evaluation, presentation, interpretation* Longman Scientific and Technical, pp 352

Scaillet, B., Holtz, F., Pichavant, M. 1998 'Phase equilibrium constraints on the viscosity of silicic magmas. 1. Volcanic-plutonic comparison' *Journal of Geophysical Research* 103: 27257-27266.

Snyder, D. 2000 'Thermal effects of the intrusion of basaltic magma into a more silicic magma chamber and implications for eruption triggering' *Earth and Planetary Science Letters* 175: 257-273

Snyder, D., and Tait, S. 1995 'Replenishment of magma chambers: comparison of fluid-mechanic experiments with field relations' *Contributions to Mineralogy and Petrology* 122: 230-240

Snyder, D. and Tait, S. 1998b 'The imprint of basalt on the geochemistry of silicic magmas' *Earth and Planetary Science Letters* 160: 433-445

Snyder, D. and Tait, S. 1998a 'A flow-front instability in viscous gravity currents' *Journal of Fluid Mechanics* 369: 1-21

Soo, S.H. 1967 *Fluid dynamics of multiphase systems*. Blaisdell, Waltham, Mass

Sparks, R.J., Sigurdsson, H. and Wilson, L. 1977 'Magma mixing: a mechanism for triggering acid explosive eruptions' *Nature* 267: 315-318

Sparks, R.S.J. and Marshall, L.A. 1986 'Thermal and mechanical constraints on mixing between mafic and silicic magmas' *Journal of Volcanology and Geothermal Research* 29: 99-124

Spera, F.J. and Bohrson, W.A. 2001 'Energy-constrained open-system magmatic processes I: general modeal and energy-constrained assimilation and fractional crystallization (EC-AFC) formulation' *Journal of Petrology* 42: 999-1018

Sylvester, A.G., Oertel, G., Nelson, C.A. and Christie, J.M. 1978 'Papoose Flat pluton: a granitic blister in the Inyo Mountains, eastern California' *Bulletin of the Geological Society of America* 89: 1205-1219

Tamura, Y. and Tatsumi, Y. 2002 'Remelting of an andesitic crust as a possible origin for rhyolitic magma in oceanic arcs: an example from the Izu-Bonin Arc' *Journal of Petrology* 43: 1029-1047

Vigneresse, J L., Barbey, P. and Cuney, M. 1996 'Rheological transitions during partial melting and crystallization with application to felsic magma segregation and transfer' *Journal of Petrology* 37: 1579-1600

Wada, H., Harayama, S. and Yamaguchi, Y. 2004 'Mafic enclaves densely concentrated in the upper part of a vertically zoned felsic magma chamber: The Kurobegawa granitic pluton, Hida Mountain Range, central Japan' *Geological Society of America Bulletin* 116: 788-801

Waight, T.E., Wiebe, R.A., Krogstad, E.J. and Walker, R.J. 2001 'Isotopic response to basaltic injections into silicic magma chambers; a whole-rock and microsampling study of macrorhythmic units in the Pleasant Bay layered gabbro-diorite complex, Maine, USA' *Contributions to Mineralogy and Petrology* 142: 323-335

Walker, B.A., Miller, C.F., Claiborne, L.L., Wooden, J.L. and Miller, J.S. 2007 'Geology and geochronology of the Spirit Mountain batholith, southern Nevada: implications for timescales and physical processes of batholith construction' *Journal of Volcanological and Geothermal Research* 167: 239-262

Weinburg, R.F. and Podliadchikov, Y.Y. 1994 'Diapiric ascent of magmas through power law crust and mantle' *Journal of Geophysical Research* 99: 9543-9559

Wiebe, R.A. 1993 'Basaltic injections into floored silicic magma chambers' *Eos* 74(1): 1-4

Wiebe, R.A. 1996 'Mafic-silicic layered intrusions: the role of basaltic injections on magmatic processes and the evolution of silicic magma chambers' *Transactions of the Royal Society of Edinburgh: Earth Sciences* 87: 233-242

Wiebe, R.A., Blair, K.D., Hawkins, D.P. and Sabine, C.P. 2002 'Mafic injections, in situ hybridization, and crystal accumulation in the Pyramid Peak granite, California' *GSA Bulletin* 114(7): 909-920

Wiebe, R.A. and Collins, W.J. 1998 'Depositional features and stratigraphic sections in granitic plutons: implications for the emplacement and crystallization of granitic magma' *Journal of Structural Geology* 20(9/10): 1273-1289

Winter, J.D. 2001 *An Introduction to Igneous and Metamorphic Petrology* Prentice Hall, pp 697

CHAPTER THREE

FIELD EVIDENCE FOR MAFIC-FELSIC MAGMA MINGLING IN THE HALFMOON PLUTON: OBSERVATIONS AND INTERPRETATIONS

3.1 INTRODUCTION

Field evidence from exposed plutonic rocks indicates that felsic magma chambers often trap basaltic magmas as they rise through the crust (Wiebe 1974; Fernandez & Gasquet, 1994; Wiebe & Collins, 1998; Harper *et al*., 2004; Walker *et al*., 2007). This process commonly results in the formation of spectacular mingling structures and textures where quenched mafic magmas are enclosed within a more felsic host. Mingling structures and textures have previously been ascribed to processes occurring during pluton emplacement, but detailed field observations from several authors (Wiebe, 1993; Chapman & Rhodes, 1992; Wiebe & Collins, 1998; Koyaguchi & Kaneko, 2000; Bachl *et al*., 2001; Miller & Miller, 2002) indicate that these textures represent processes operating within an active magma chamber during the process of solidification. The composite Halfmoon Pluton within the Bungaree Intrusives on the northern coast of Stewart Island preserves abundant evidence for the coeval interaction between mafic and felsic magmas, and documentation and interpretation of the mingling structures and textures preserved allows for a magma chamber stratigraphy to be reconstructed, and the processes responsible for pluton formation to be inferred.

3.2. GEOLOGICAL SETTING

The Bungaree Intrusives (Allibone & Tulloch 2004) form an approximately 2-8km wide strip of plutonic rocks exposed along the northern coast of Stewart Island (Figure 3.1 and Figure 3.2). They were emplaced ~175-140 Ma along the convergent New Zealand margin of Gondwana, and dominate the outer part of the Median Batholith (Mortimer *et al*., 1999; Tulloch & Kimbrough, 2003; Allibone *et al*., 2009), a belt of mainly subduction-related I-type plutonic rocks of Carboniferous to Early Cretaceous age that separates the Eastern and Western Provinces of New Zealand (Figure 3.1). The Bungaree Intrusives are correlatives of the Darran Suite (Muir et al., 1998; Allibone *et*

al., 2009), which comprise much of the outer belt of the Median Batholith, and are a series of I-type, hornblende-bearing calc-alkaline mafic and felsic plutonic bodies ranging in age from ~230-137Ma (Kimbrough *et al*., 1994; Muir *et al*., 1998; Tulloch & Kimbrough, 2003; Price *et al*. 2006; Allibone *et al*., 2009).

The Bungaree Intrusives were initially mapped as part of the Anglem Complex, which consisted of all plutonic rocks north of the Freshwater Fault (Figure 3.2) (Watters, 1978). Subsequently, Allibone and Tulloch (2004) further subdivided the Anglem Complex into a series of at least 16 predominantly elongate plutons with emplacement ages ranging between the Jurassic and Early Cretaceous. The Paterson Group (consisting of rhyolite, andesite and basaltic andesite) has a similar age to the Bungaree Intrusives (~146 +3/-1 Ma; Kimbrough *et al*., 1994), and is the only volcanic unit to outcrop on Stewart Island, and represents a possible correlative to the Bungaree Intrusives which lie stratigraphically below them. The Bungaree Intrusives themselves comprise several intrusions of gabbro, diorite, tonalite, granodiorite and granite. Previous work (Watters, 1978; Cook, 1988; Wiebe & Collins, 1998; Smith, 2000; Allibone & Tulloch, 2004) illustrated the heterogeneous nature of the Bungaree Intrusives, and highlighted the potential for further study of the magma mixing and mingling structures that occur.

Areas chosen for detailed structural, textural, geochemical and geochronological study within the Bungaree Intrusives were based on the degree of accessibility and the nature of coastal exposures. This was to ensure that detailed structural and textural interpretations of the mingled magmas could be made across distances of between ~5-50 m. Exposures west of Halfmoon Bay are small and discontinuous, and represent an older suite of plutonics, whereas exposures east of Halfmoon Bay are larger and more continuous, and represent a single pluton within the composite Bungaree Intrusives. This pluton, which is outlined in Figure 3.1 will be referred to as the Halfmoon Pluton (new name) throughout the rest of the thesis. The Halfmoon Pluton is distinct from the rest of the Bungaree Intrusives in that the Bungaree Intrusives north of Horseshoe Bay are older than the ~140 Ma Halfmoon Pluton (diorite at Port William dated at c. 175 Ma; A.J. Tulloch unpublished data. See Chapter 6 for geochronological results and discussion).

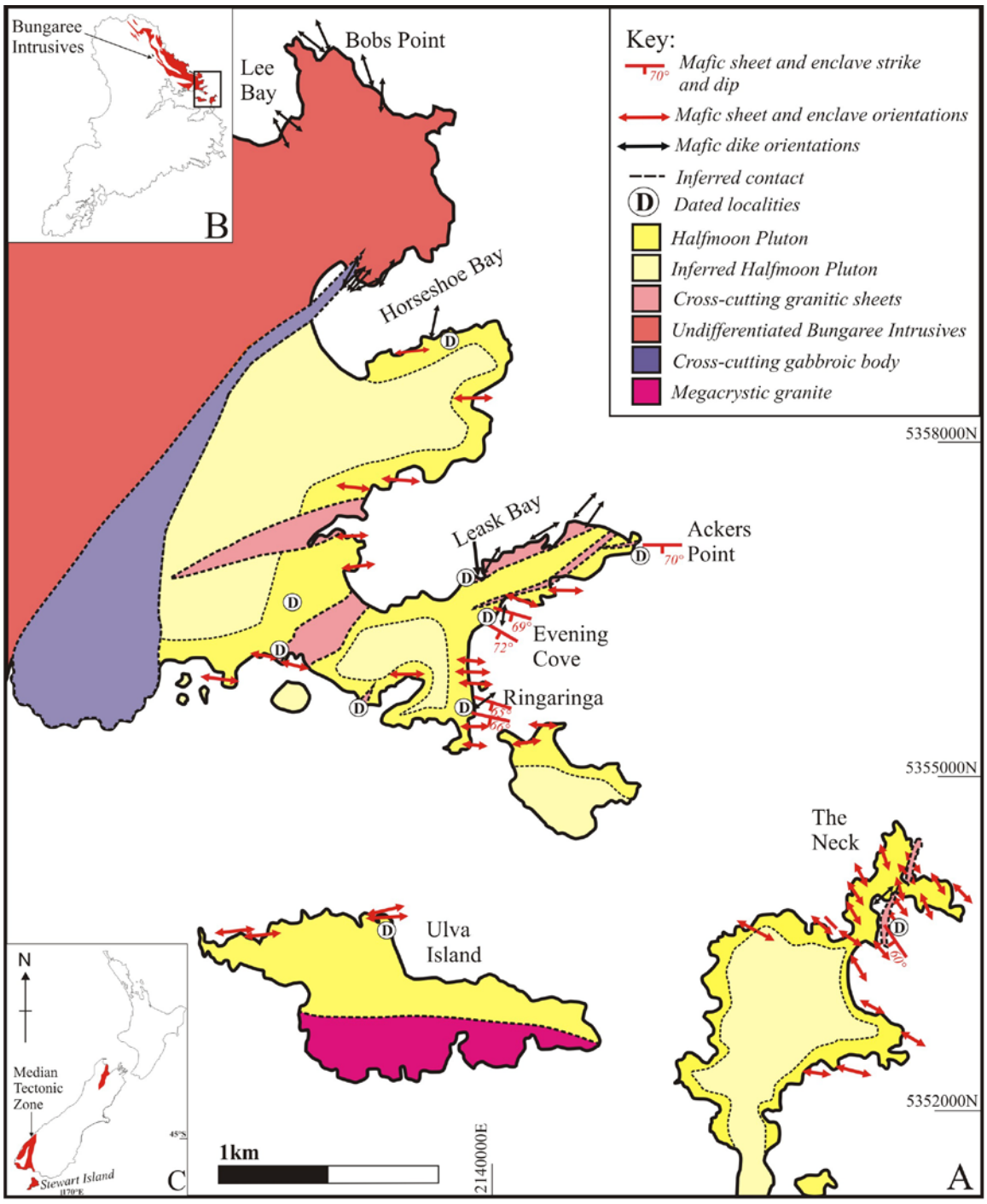

Figure 3.1. (A) Geological map of the Halfmoon Pluton and relationship with other plutonic bodies within the Bungaree Intrusives. Where no dip information was observed, strike directions of mafic sheets and enclaves are given. Mafic dikes all intrude perpendicular to the pervasive orientation of the mingled mafic sheets and enclaves. Areas without any data displayed were either not visited due to difficulties with access, or outcrop was absent. (B) Map of Stewart Island indicating the full extent of the Bungaree Intrusives, as mapped by Allibone and Yulloch (2004) (C) Map of New Zealand showing the extent of the Median Batholith (modified from Mortimer *et al.*, 1999). Supplementary field data obtained from Wilson & Barrell (2002) and Cook (1988).

Rocks north of Horseshoe Bay are also cut by numerous mafic dikes which show little to no evidence of mingling, which is the dominant magma interaction preserved within the Halfmoon Pluton. No contacts or pluton margin were identified in the field, however given changes in rock type and mafic-felsic interaction, the boundary probably lies close to the north side of Horseshoe Bay (Figure 3.1). The sections chosen for detailed study within the Halfmoon Pluton range from Ackers Point to The Neck, and occur at right angles to the strike of the magmatic layering, thus offering continuous sections through the pluton. Outcrops were generally limited in lateral extent, with outcrop widths typically 4-20m.

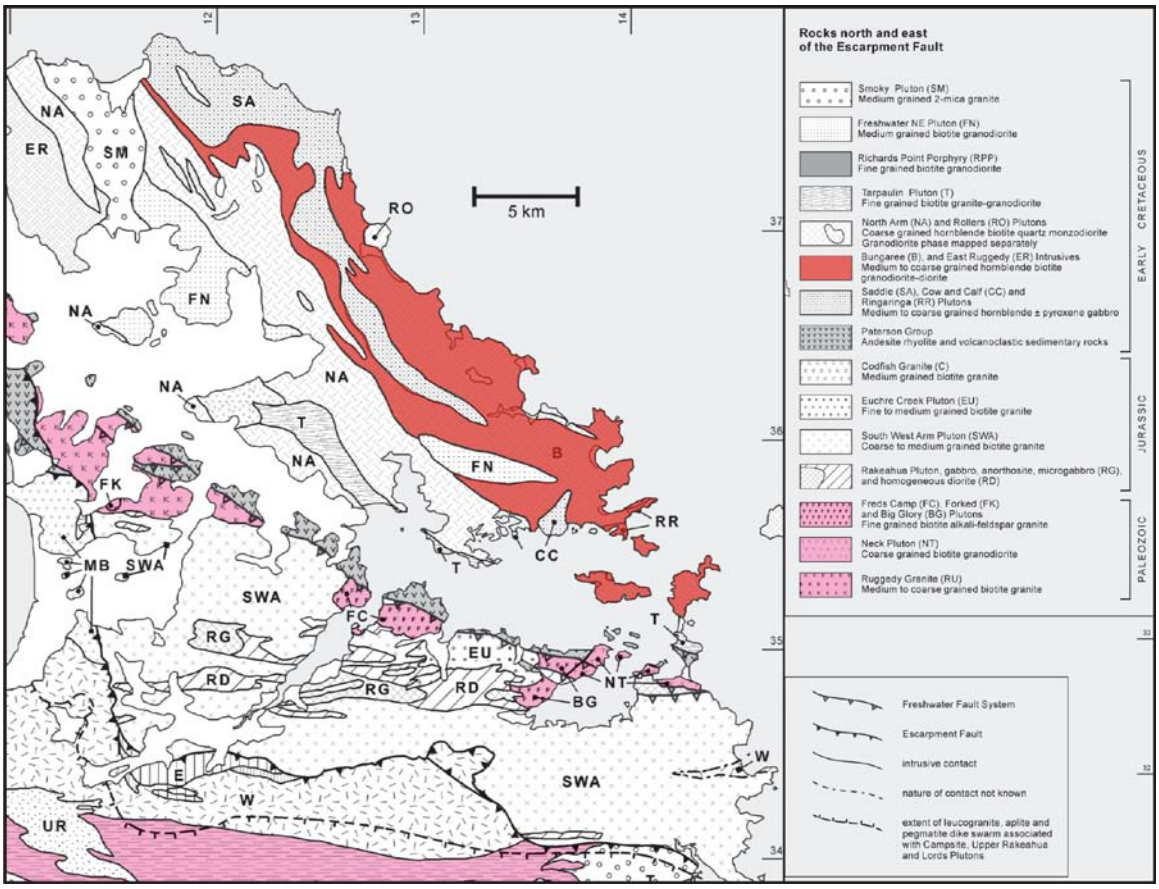

Figure 3.2. Geological map of the northeastern margin of Stewart Island illustrating the location and the nature of the boundaries between the various plutons that outcrop north of the Freshwater Fault (edited from Allibone & Tulloch, 2004)

3.3 Intrusive Bodies Within the Halfmoon Pluton, Bungaree Intrusives

The Halfmoon Pluton is characterized by a sequence of mafic sheets and enclaves of basaltic composition that have been emplaced incrementally as layers within a more felsic host. Mafic-felsic magma interaction within the Halfmoon Pluton has occurred at various stages in the crystallization history of the felsic host magma, resulting in three distinct magma interaction styles being preserved; (a) mafic sheet formation, (b) formation of mafic enclave swarms, and (c) mafic dike formation.

3.3.1 Mafic Sheets

Thick (~2 to <10m) mafic sheets are present at Ackers Point and Evening Cove, with thinner (>1.5m thick) mafic sheets present at Ringaringa and The Neck. All mafic sheets display the characteristic morphology of a mafic sheet as discussed in Chapter 2, with a fine-grained quenched basal contact, coarser-grained centre, and a gradational, enclave-rich rubbly upper contact with the overlying felsic host (Figure 3.3A).

3.3.2 Mafic Enclave Swarms

The quantity, size, shape, aspect ratio and concentration of mafic enclaves within enclave swarms vary throughout the pluton (Figure 3.3B and 3.3C). Mafic enclave swarms become more abundant at Ringaringa and The Neck. Mafic enclaves have textures, modes and mineralogy similar to those of the mafic sheets, suggesting that they are genetically related. They range from globular and nearly equant bodies with obvious magmatic textures, to highly elongate bodies in zones where magmatic foliation is well developed. The morphology of mafic enclaves within individual enclave swarms will be discussed in further detail in the following section.

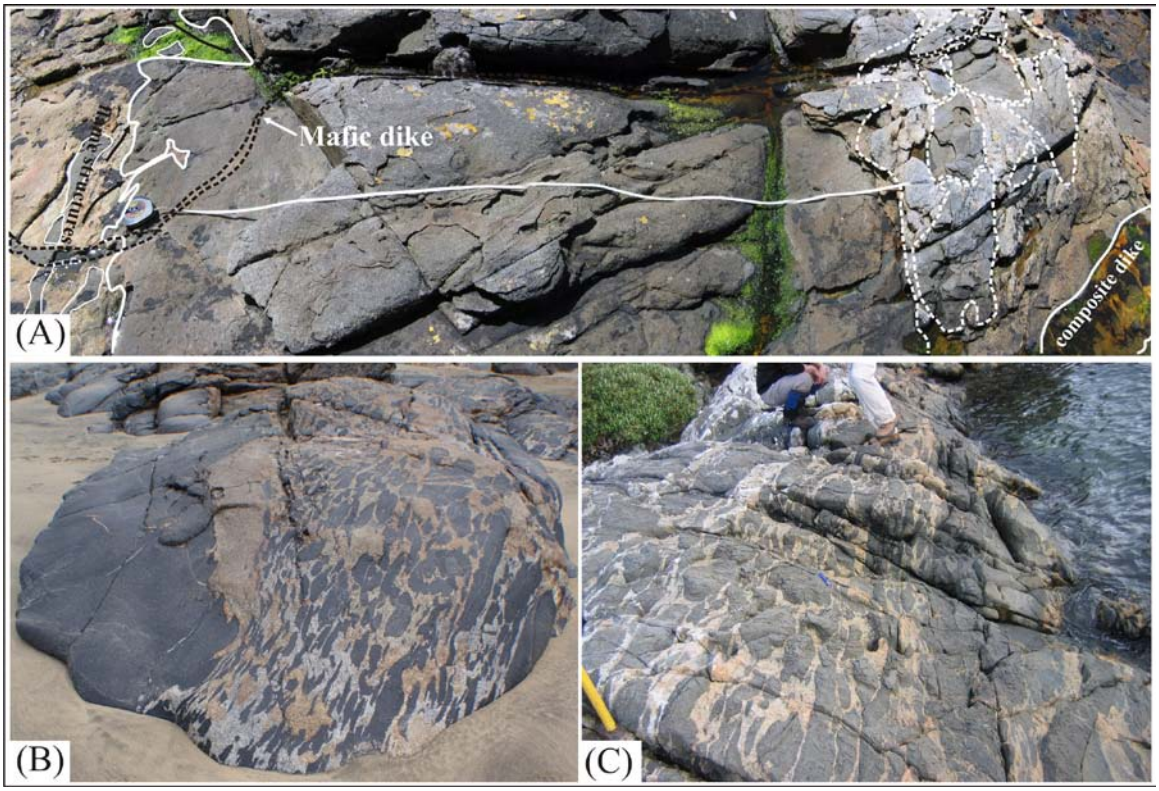

Figure 3.3. (A) Mafic sheet ~3.6m in width and at least 9m in length from Evening Cove (E48/40045650). Displays the typical morphology of a mafic sheet with a chilled base (left of photo) punctuated by flame structures, and a gradational, rubbly top with numerous enclaves (right of photo). (B) Mafic enclave swarm at Ringaringa beneath a thin mafic sheet (E48/39825566). Outcrop width is 3.2 m. Top is to the left (C) Mafic enclave swarm at The Neck (E48/43095361).

3.3.3 Mafic Dike and Composite Dike Formation

Several late mafic dikes cross-cut the pluton and differences in the form of these dikes indicate variable extents of crystallization of the host magma when the dikes were intruded. Mafic dikes with sharp, well-defined edges that cross-cut all foliations within the host magma(s) were intruded when the pluton was completely solidified (Figure 3.4C). Mafic dikes with diffuse, gradational edges, which often meander through the host rock and bend around solid objects such as mafic sheets and enclaves, or have broken apart upon entry (Figure 3.4B), were likely to have been intruded when the host magma retained enough interstitial melt to allow plastic deformation of these dikes (Wiebe, 1993). Composite dikes (Figure 3.4A), where mafic enclaves are enclosed within a felsic matrix, also occur within the pluton, though are concentrated in swarms towards the top of the chamber. Composite dikes were injected contemporaneously with pluton

crystallization, with residual/interstial felsic melt incorporated into the composite dike by the intruding mafic magma (Wiebe, 1973; Snyder *et al*., 1996; Wiebe & Ulrich, 1997). The presence of mafic dikes with varying forms and compositions, injected during different stages of pluton crystallization, is evidence for the continuous input of mafic magma into the magma chamber throughout its crystallization history.

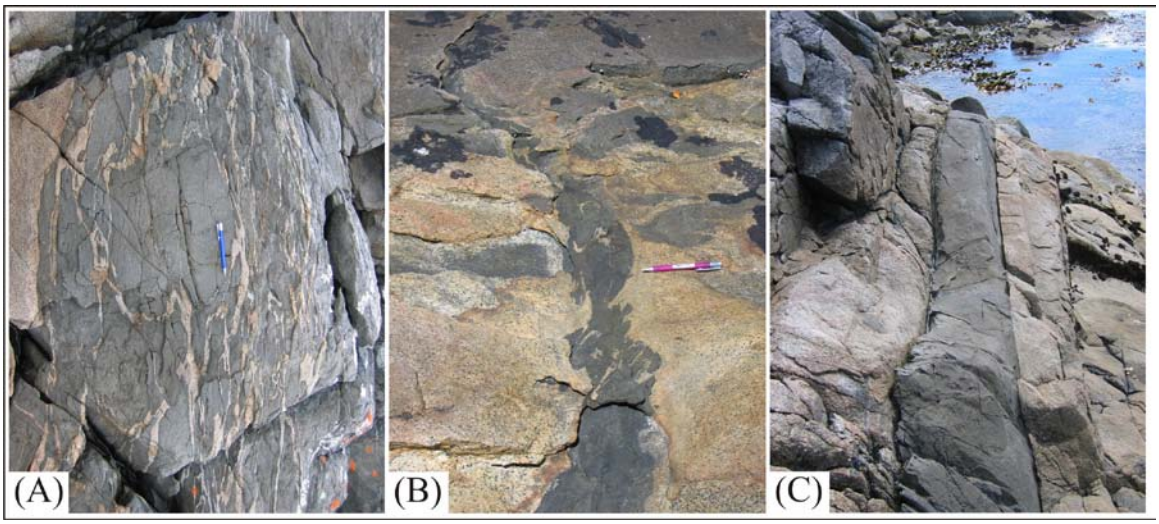

Figure 3.4. Styles of mafic dike emplacement. (A) Composite dike formed by the remobilisation and incorporation of residual felsic magma into the intruding mafic dike (The Neck; E48/43585374) (B) Mafic dike injected when the felsic host still contained some heat/melt, allowing for limited physical and chemical exchange (Evening Cove; E48/40085657) (C) mafic magma injected when the host was completely crystallized. Contacts are sharp and planar, and cross-cut foliations in the felsic host. Pencil for scale in all photos is 14 cm in length (E48/38846112).

3.4 Magma Chamber "Stratigraphy" and Way Up Indicators

Orientations of mafic sheets and enclaves are persistent throughout the sequence (Figure 3.1, and 3.5), with each mafic intrusion defining the boundary between a crystal-rich chamber floor and the overlying crystal-poor magma at any one particular time during crystallization of the felsic host magma. Consistent dip directions of mafic sheets and enclaves reveal that the magma chamber as a whole has been tilted by 60-70° from the horizontal towards the south (Figure 3.6), exposing a cross-section through the pluton and allowing for interpretations to be made with respect to height or depth within the chamber. Orientations of mafic dikes are perpendicular to orientations of mafic sheets and enclaves (Figure 3.1).

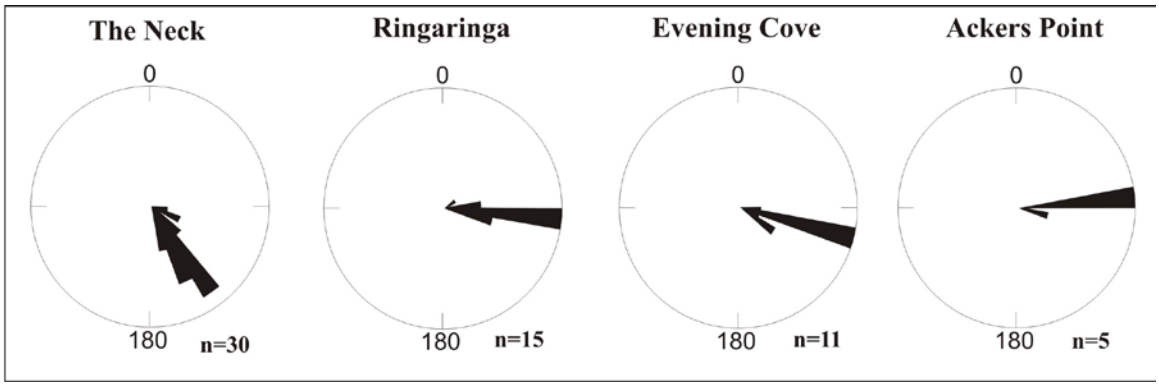

Figure 3.5. Orientations of mafic sheets and enclaves at The Neck, Ringaringa, Evening Cove and Ackers Point. n= number of orientations measured

Four key sections were chosen for detailed structural and textural analysis based on field exposures and position within the "stratigraphic" sequence; Ackers Point (AP), Evening Cove (EC), Ringaringa (RR) and The Neck (TN) (see Figure 3.1 for locations). Smaller outcrops at several other locations (Ulva Island and Horseshoe Bay) are used to link together these four key sections and to provide a more complete picture of the variation in composition and mafic-felsic magma interaction within the magma chamber from the base to the top.

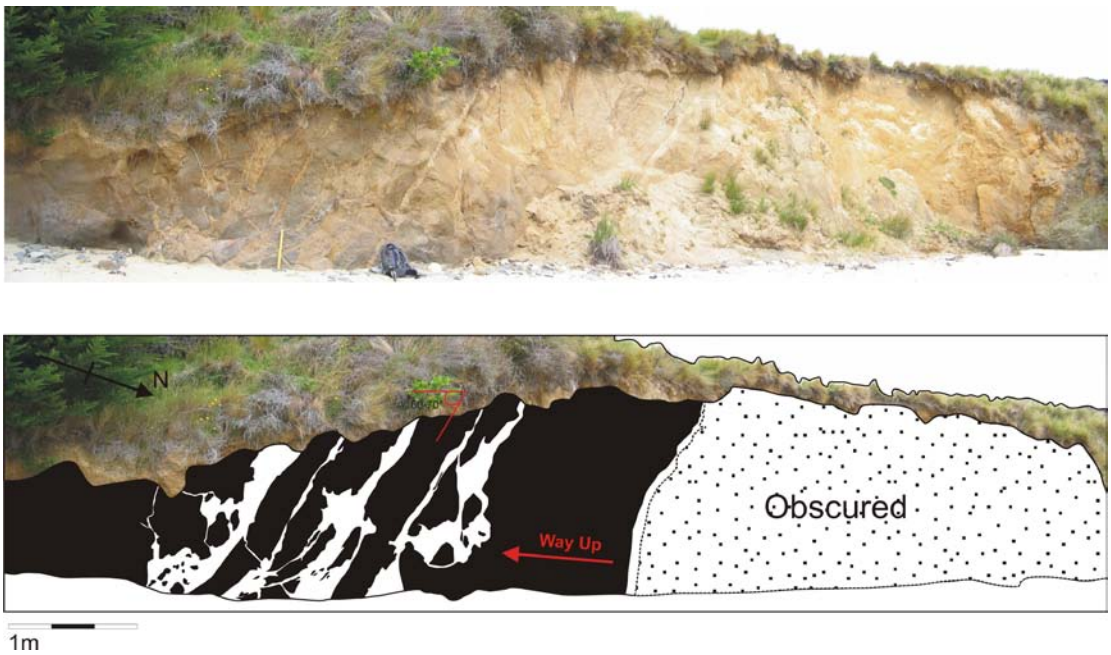

Figure 3.6. Tilted mafic sheets at Ringaringa dipping between 60-70° to the south. Way-up is inferred towards the south (E48/39775544).

A magmatic “stratigraphy” was constructed through recognition of way-up indicators and depositional structures within the mingled rocks. The inferred base of the chamber was identified at Ackers Point, and the inferred top of the chamber is at The Neck (Figure 3.1), providing an approximate magma chamber thickness of at least 4.8 km. The lateral extent of the pluton is difficult to determine due to the limited exposure, however a minimum width of ~6.5 km has been measured from Bob’s Point (E48/38476142) to Karimoni Beach at The Neck (E48/43865424). Mafic sheets and enclaves from Ackers Point to Ringaringa all preserve a pervasive preferred orientation striking between 80 and 100° and dipping between 60 an 70° towards the south, indicating the vertical extent of the magma chamber is in a N-S direction (Figure 3.1). Way-up structures in mafic sheets and enclave swarms all point towards the south. The most abundant and reliable way-up structures identified in the Halfmoon Pluton are basal contacts of mafic sheets that exhibit numerous flame structures and load casts (Figure 3.7).

Figure 3.7. Base of a mafic sheet at Evening Cove (E48/40085657) that has been punctuated by numerous flame structures. Way-up is to the top of the photo.

Amphibole accumulations at basal contacts between mafic sheets/enclaves and the felsic host are also reliable way-up indicators. Amphibole accumulations are interpreted to result from the upward escape of volatiles from magmas trapped beneath the chilled mafic contacts (Figure 3.8).

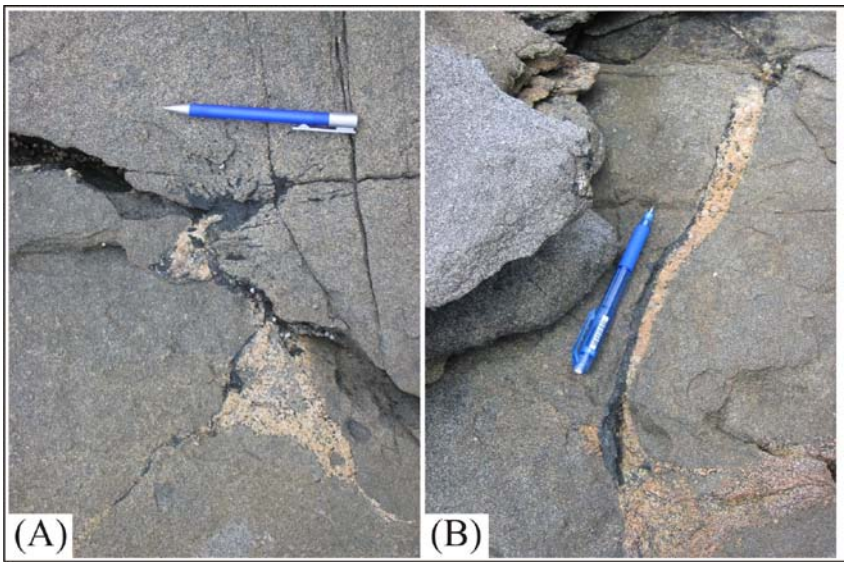

Figure 3.8. Examples of amphibole accumulation at Evening Cove (E48/40045650) (A) amphibole accumulation at the top of a flame structure, way up is to the top of the photo (B) amphibole accumulation at the base of a mafic sheet. Way-up is to the left of the photo. Pencil for scale in both photos is 14cm in length

Mafic feeder dikes are also an excellent way-up indicator. As discussed in Chapter 2, mafic feeder dikes are thought to initially intrude vertically through the crystal mush at the crystallizing base of the magma chamber, before spreading laterally at the rheological boundary between the crystal mush and the overlying crystal-poor liquid magma.

Figure 3.9 shows a mafic feeder dike at The Neck. This outcrop also shows at least three episodes of mafic magma injection of fairly similar composition.

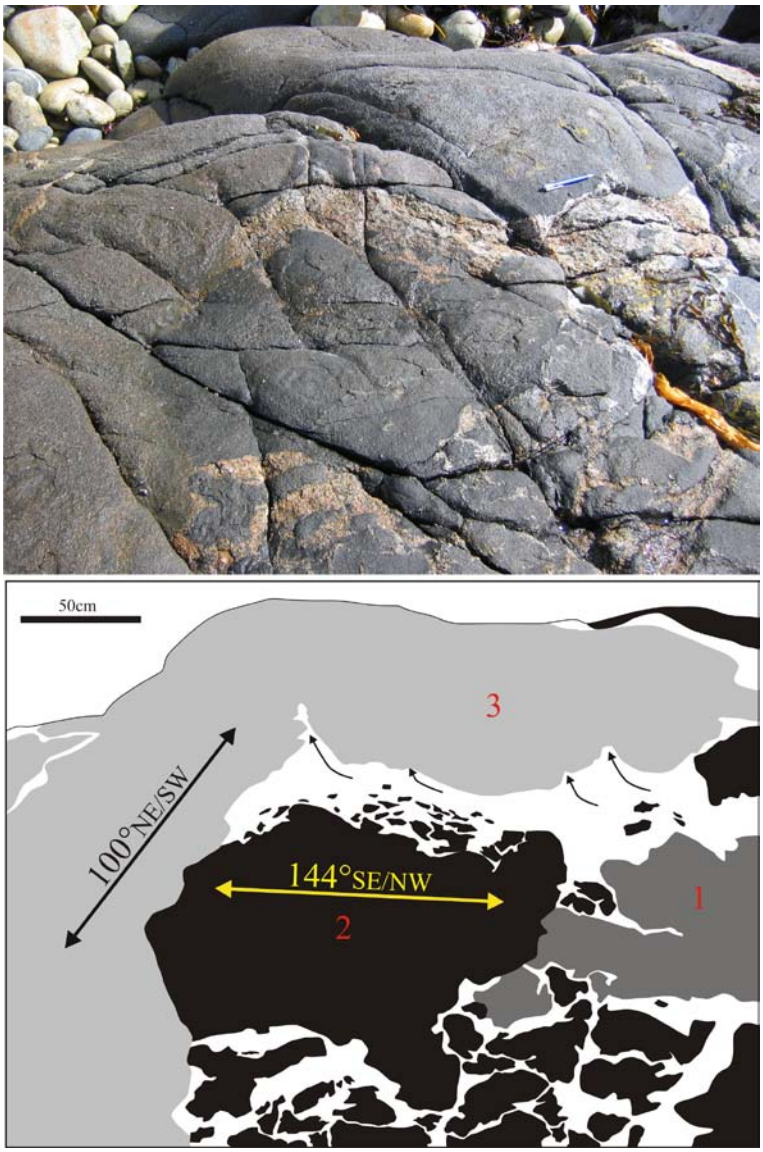

Figure 3.9. Mafic feeder dike from at The Neck (E48/43555357). Way-up is to the top of the photo.

The first mafic magma injection (1) appears to be relatively small in volume as very little of it is seen. The second episode (2) involved a mafic sheet with several smaller mafic enclaves. The final mafic magma injection was the mafic feeder dike (3) which occurred as a thick mafic sheet rising up through the earlier mafic enclaves and cross-cutting them, indicating they were relatively solid. This mafic sheet then spread laterally, and chilled against the felsic host. This mafic sheet has a medium-grained centre and a fine-grained

chilled margin at its base that is punctuated by flame structures. The width of the vertical mafic sheet is at least 6 m.

Other reliable way-up indicators include cross-cutting relationships, sinking of denser material towards the base, compaction of mafic enclaves beneath later intrusions above, and veins of filter-pressed felsic material that extend vertically into mafic sheets above (Figure 3.10). All of these way-up indicators indicate clearly the incremental construction of the pluton from the base up. Sinking of mafic enclaves and sheets suggest that the felsic host magma above was less crystalline than the felsic host magma where the mafic inclusion has come to rest. This is consistent with the model proposed by Wiebe and Collins (1998) in which magma chambers have a crystal-rich base and an overlying crystal-poor magma. Paleo-horizontal indicators are not common within the Halfmoon Pluton, however the presence of rare silicic pipes (Figure 3.10D) that dip at the same degree as the dip of mafic sheets (~70°) is clear evidence that the magma chamber as a whole has undergone significant tilting since deposition.

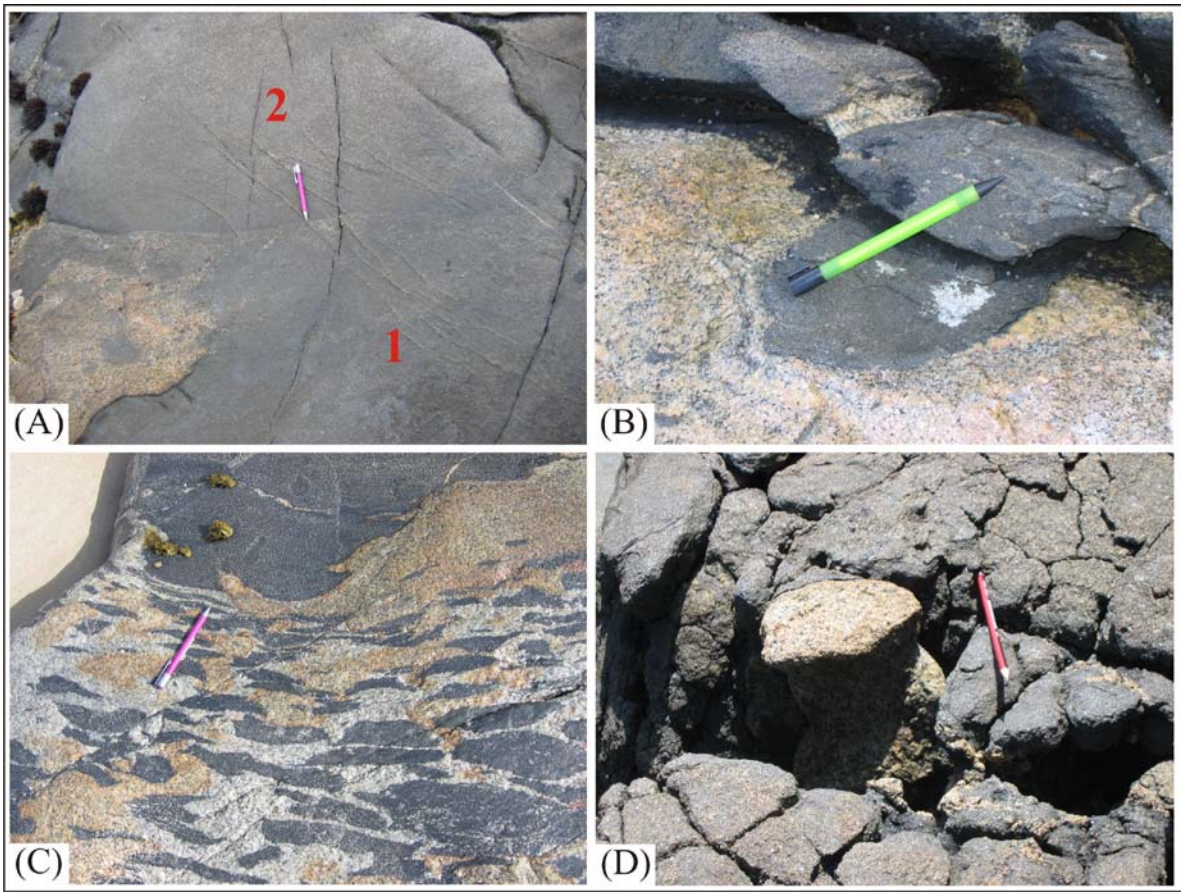

Figure 3.10. Way-up indicators, all showing way-up towards the top of the photo (A) Mafic sheet (2) at Ackers Point (E48/41265711) cross-cutting an earlier intruded mafic sheet (1). Point of pencil marks the contact between the two intrusions (B) schlieren layer being displaced by the downward movement of a mafic enclave from gravity settling (The Neck; E48/43575374) (C) Mafic enclaves being compressed beneath an overlying later intruding mafic sheet (Ringaringa; E48/39825566) (D) Felsic pipe within a mafic sheet indicating paleo-horizontal towards the top of the photo (Evening Cove; E48/40085657). Pencil for scale in all photos is 14 cm in length.

3.5. Mingling Structures and Inferred Magmatic Processes

Mafic and felsic rocks vary in petrography, composition, volume and geometry throughout the sequence, indicating that processes operating within the evolving magma chamber varied in intensity and relative importance through time. This is reflected in variations in the style of magma mingling preserved. The four key localities (Ackers Point, Evening Cove, Ringaringa, and The Neck) will be discussed in detail, and interpretations made on processes responsible for the variation in mingling style preserved.

3.5.1 ACKERS POINT

Ackers Point represents the lowermost exposed section of the pluton, and is inferred to represent the near base of the magma chamber. This section consists of at least eight thick (8-15 m) mafic sheets separated by thin (<1 m) portions of felsic host rock. Mafic sheets have an average preferred orientation of 089/70°. Mafic sheets display fine-grained chilled margins and coarser-grained centres. A sketch of a section exposed at Ackers Point is shown in Figure 3.11. This outcrop consists of two mafic sheets separated by ~1.5m of felsic host that contains numerous mafic enclaves. The upper mafic sheet has been broken apart by upwelling of felsic material immediately following mafic magma injection, as the edges of the separated mafic inclusions are all fine-grained indicating that they chilled against the felsic host. Compaction of the magma whilst it was still mobile enough to deform plastically is evident in cuspate margins that lie perpendicular to the degree of shortening (N-S).

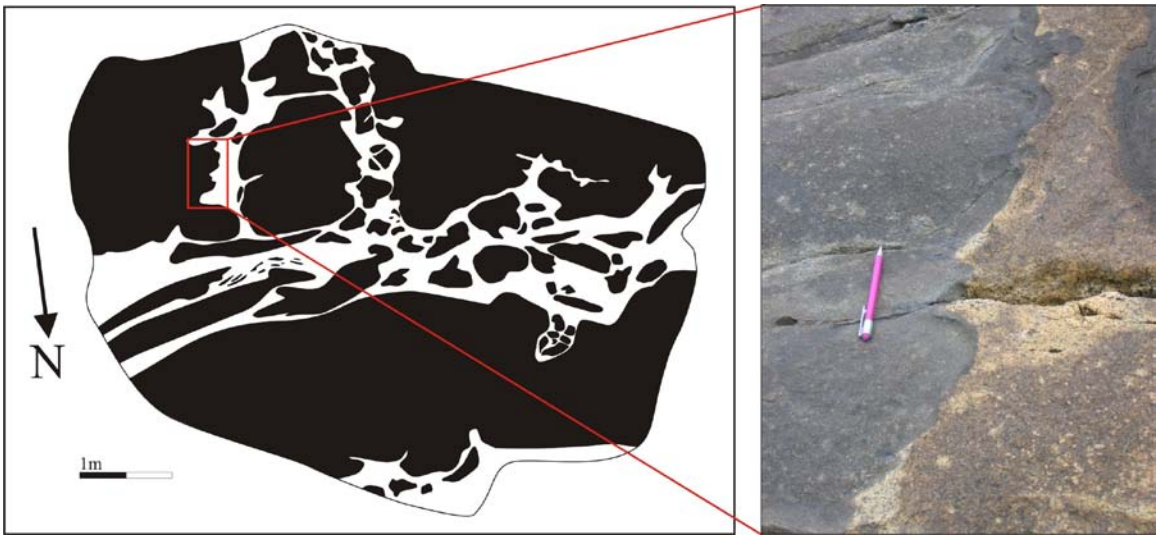

Figure 3.11. Sketch of an outcrop at Ackers Point displaying the characteristics of magma minlgling structures found at this location. Photo illustrates the cuspate margin of a mafic sheet which was caused by compaction of the magma perpendicular to this interface (E48/41265711).

3.5.2 EVENING COVE

Evening Cove sits stratigraphically above Ackers Point, and is characterized by a sequence of at least six thick (1-10 m) mafic sheets and enclave swarms that are separated by ~1-3 m portions of felsic host rock (Figure 3.12). Mafic sheets and enclaves have an average orientation of 107/70°. The mingling style remains approximately

constant throughout the Evening Cove section, indicating that magmatic processes remained similar during its construction. The section at the base of the Evening Cove sequence is different from the rest in that it is composed of multiple intrusions of thin mafic sheets and mafic enclaves (Figure 3.13). Mafic enclaves and sheets within this section typically have sharp fine-grained chilled contacts with the adjacent felsic host (Figure 3.13D), indicating that the dominant magma interaction process was mingling. Structures and textures preserved within the mingled magmas reveal that several processes were operating during crystallization of the section, including magmatic flow, magma mixing and compaction.

Magmatic flow is evidenced by discordant enclaves at an angle to the preferred orientation, and bending of mafic sheets in response to upwelling of magma from below (Figure 3.13A). Gradational contacts between mafic enclaves and adjacent felsic host indicate magma mixing (Figure 3.13B). Compaction of the unit in a N/S direction is evidenced by cuspate margins that lie perpendicular to the direction of shortening. These processes will be discussed in further detail in section 3.8. Figure 3.14 displays in greater detail a sketch of a mafic sheet that sits above the mafic enclave swarm. This mafic sheet displays the characteristic morphology of a mafic sheet as described by Wiebe and Collins (1998), with a fine-grained quenched basal contact, a coarser grained centre, and a rubbly, enclave-rich gradational upper contact with the overlying felsic host. Enclaves above the mafic sheet preserve evidence for the presence of convective currents that were operating when the mafic sheet was emplaced. These enclaves were ripped off the top of the crystallizing mafic sheet by the convective currents, and differing variations in enclave orientation indicate the direction of magmatic flow.

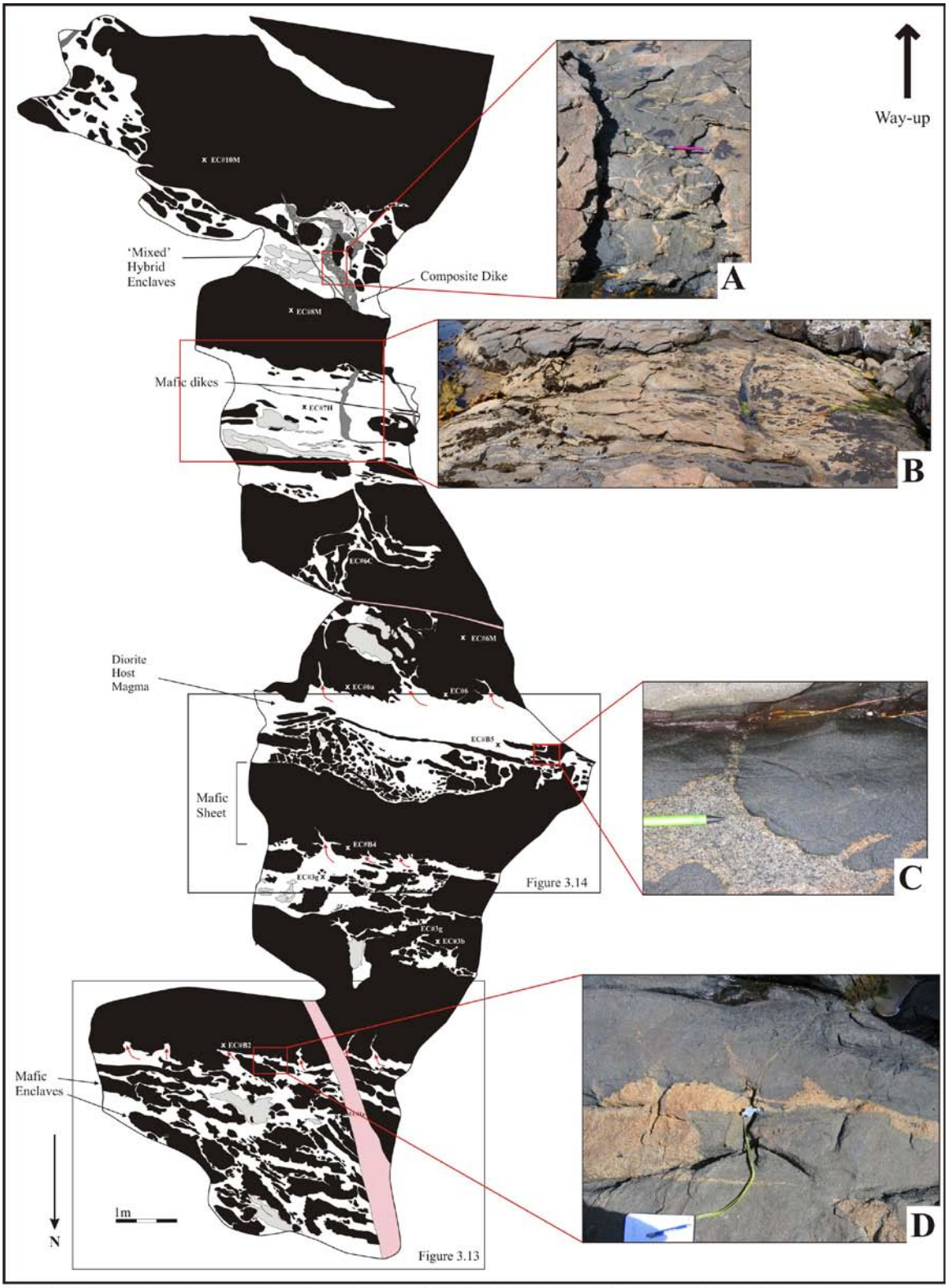

Figure 3.12. Detailed section exposed at Evening Cove (A) Composite Dike (B) Leucodiorite host between two mafic sheets (C) cuspate edges on a mafic enclave as a result of compaction (D) Flame structures in the base of a mafic sheet. Locations for samples that were analysed for geochemistry and/or geochronology are also listed, i.e. EC#B5.

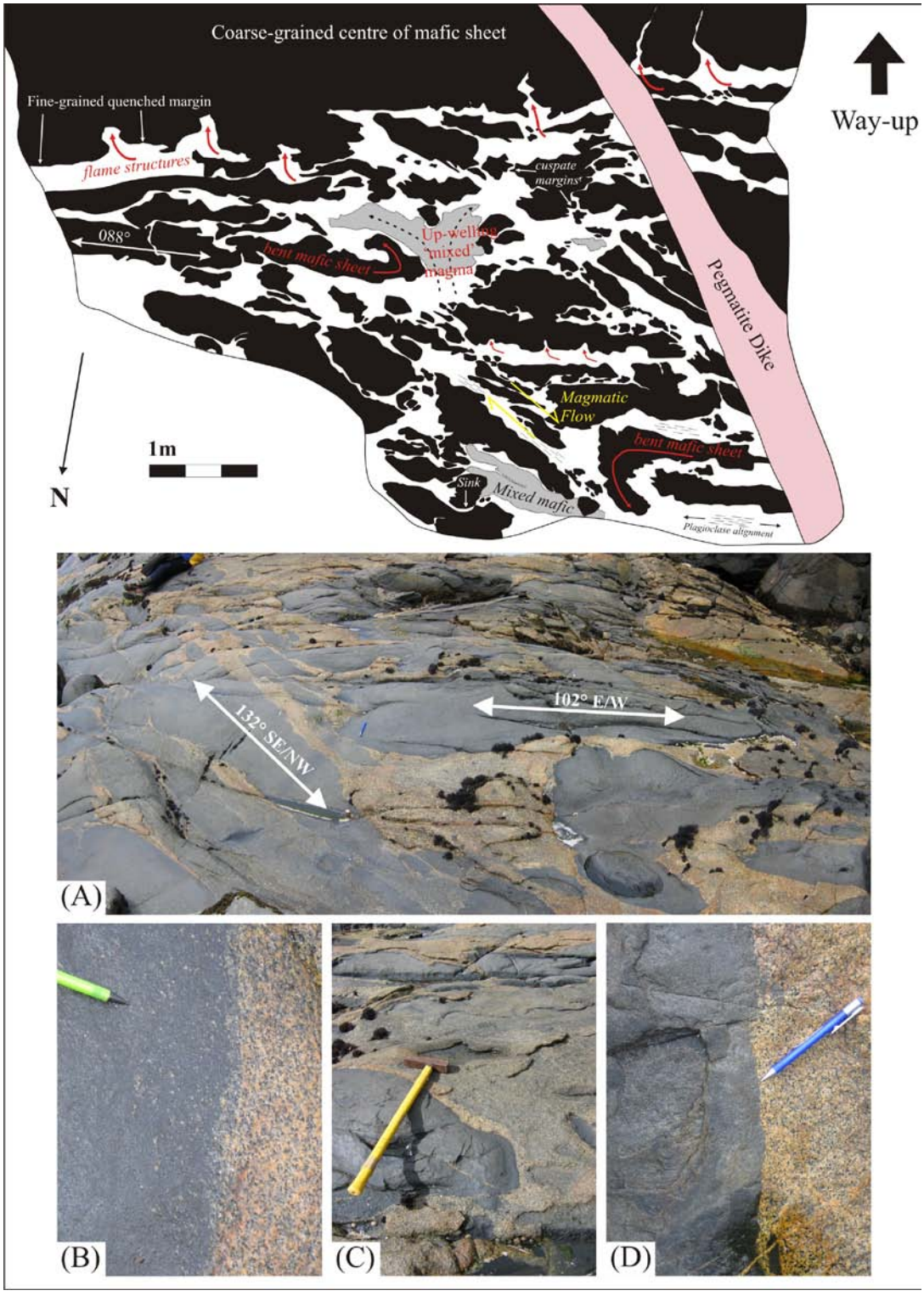

Figure 3.13. Sketch of a mafic enclave swarm at Evening Cove. (A) Enclaves orientated at132° SE/NW have been interrupted by flow, resulting in localized mixing at the edges of mafic enclaves (B) gradational contact between mafic enclave and felsic host (C) mixed mafic enclave next to a mingled mafic enclave (D) sharp, fine-grained quenched contact between mafic and felsic rocks (E48/40095658).

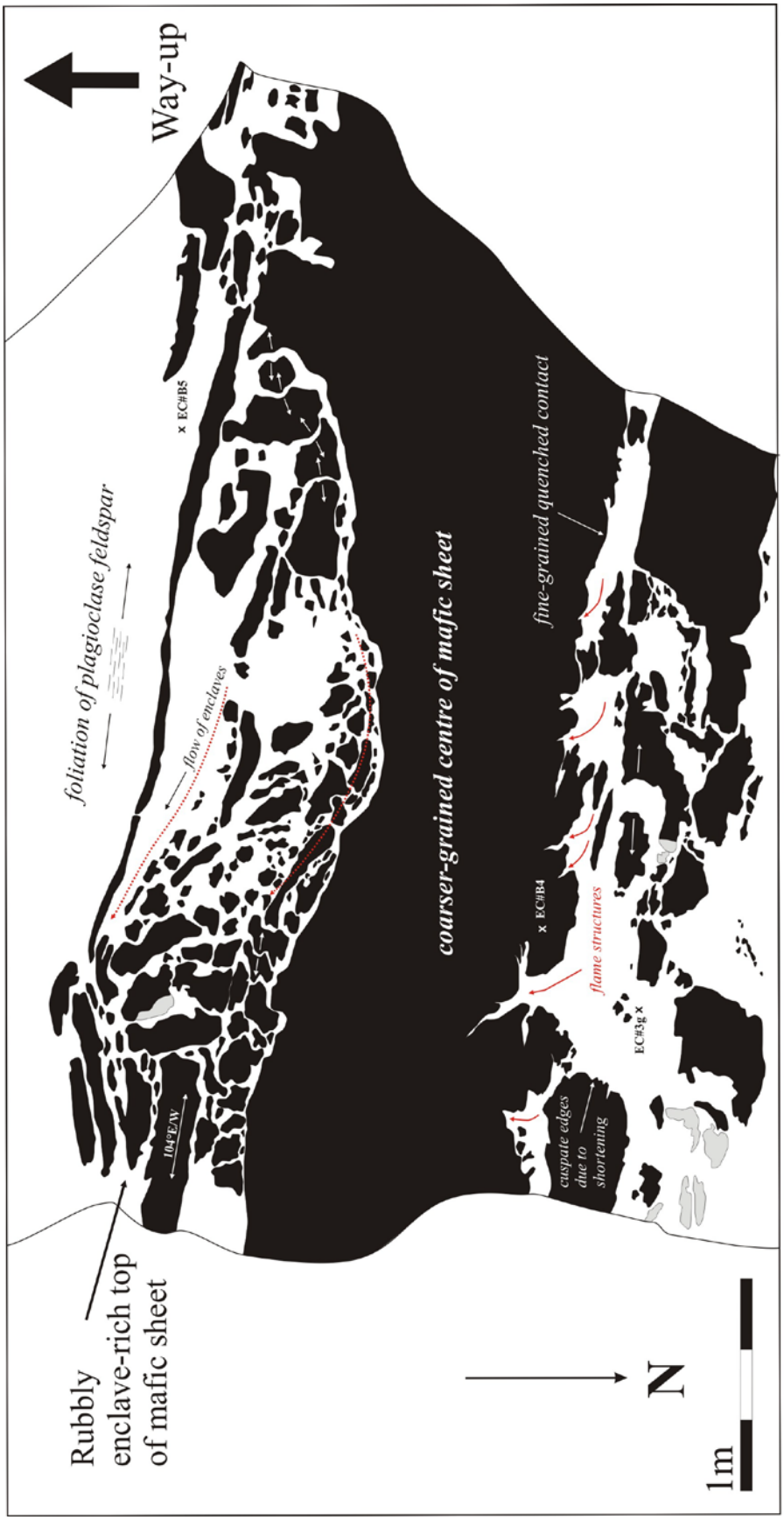

Figure 3.14 Sketch of mafic sheet at Evening Cove with interpretations made on physical processes that were operating within the crystallizing magma chamber, including compaction and magmatic flow

3.5.3 RINGARINGA

Two outcrops separated by ~60 m of beach sand occur at Ringaringa (Figure 3.15). At the first outcrop, mingling structures consist of thin (0.5-2 m) laterally discontinuous mafic sheets alternating with concentrated enclave swarms (Figure 3.16). The second outcrop is characterized by an enclave swarm at the base which has been overlain by a number of thin (1-2m thick) mafic sheets.

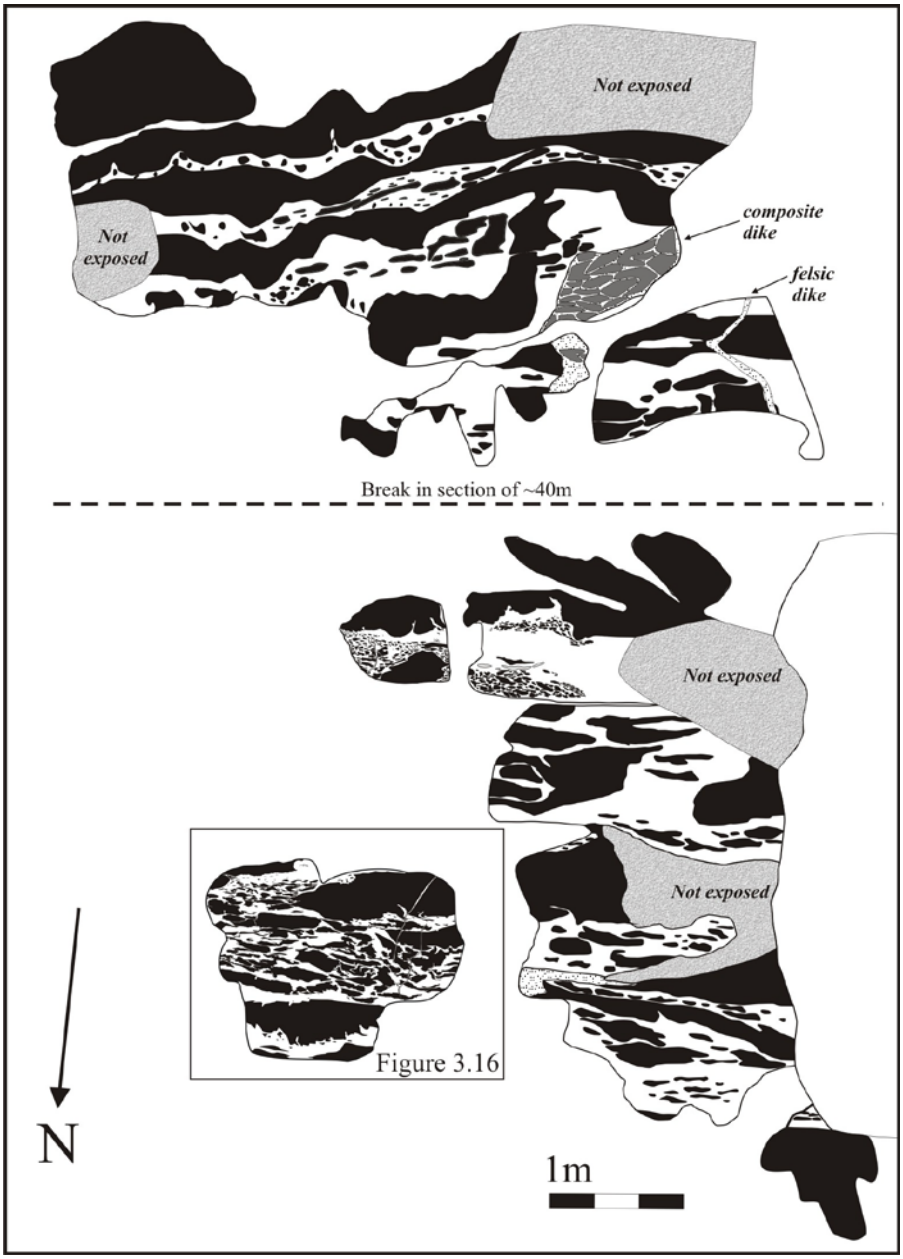

Figure 3.15. Section exposed at Ringaringa (E48/39825566).

A thick mafic sheet-like intrusion outcrops ~100m down the beach from the two main outcrops at Ringaringa, which lies stratigraphically below these two outcrops. The significance of this outcrop will be discussed in Chapter 4.

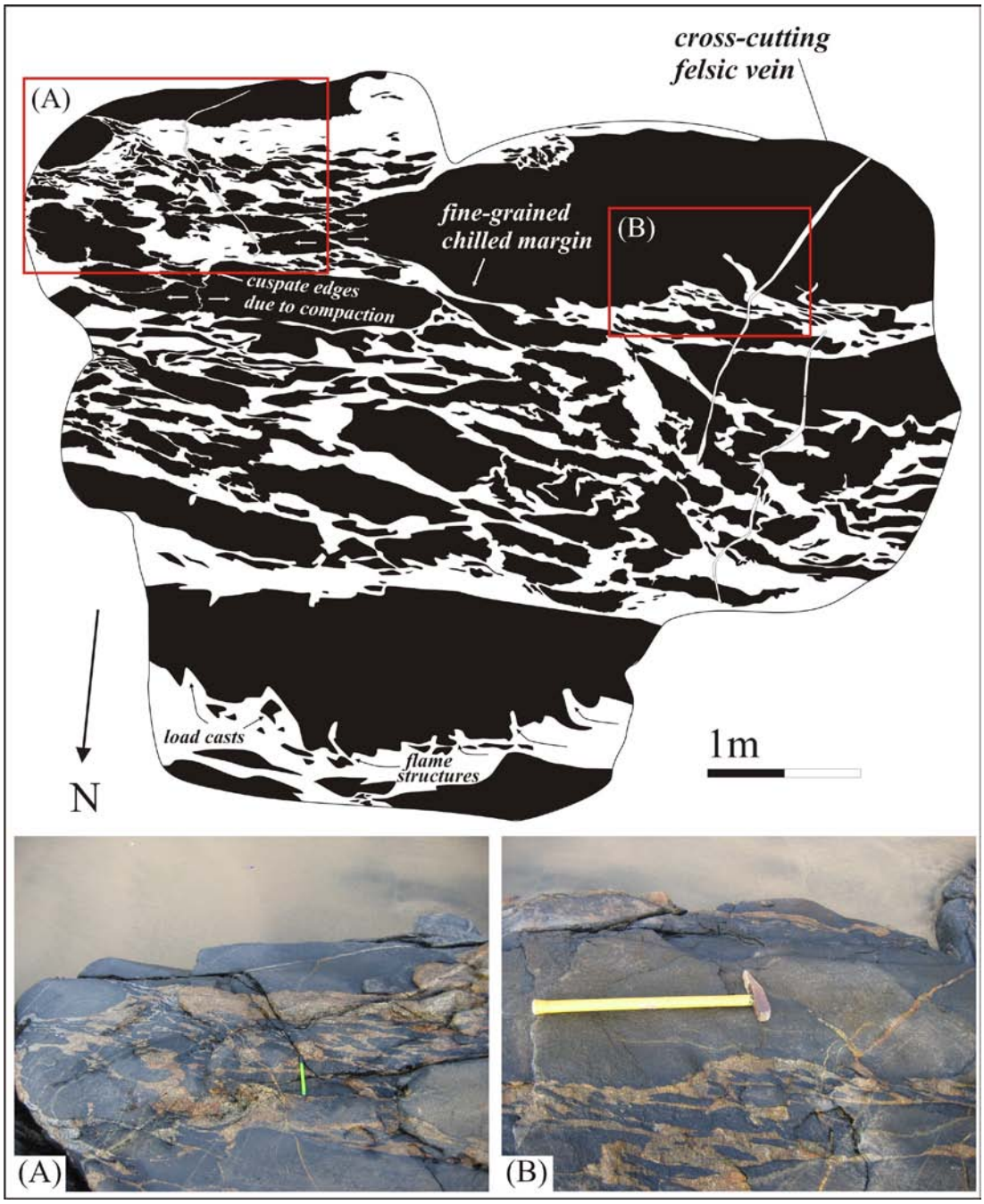

Figure 3.16. Sketch of an outcrop at Ringaringa showing the characteristic mingling style (A) Photo showing the disaggregation at the edge of a mafic sheet to form mafic enclaves. Pencil for scale is 14 cm long. (B) Photo showing the base of a mafic sheet with a cross-cutting felsic vein. Hammer for scale is 1 m long (E48/39825566).

Enclave size and shape remain relatively consistent throughout the section, and tend to form in sheet-like swarms, which probably reflect their original emplacement as mafic sheets. Mafic enclaves have a sub-rounded morphology, which indicates their magma mingling origin. This is distinct from the angular morphology of xenoliths that are derived from the break-up of solid rock. Orientations within mafic enclaves and sheets are very consistent within this section, with an average orientation of 097/65°. Magma mixing on a local scale is evident, with several small (5x10 cm) mafic enclaves containing xenocrysts of plagioclase and quartz derived from the felsic host. Mafic enclaves also occur at the thin edges of mafic sheets, and their contact shape indicates that they were once connected to the edge of the sheet, but have been ripped off (Figure 3.16A). This is likely due to flow-front instabilities forming at the ends of mafic sheets as they spread laterally (Snyder & Tait, 1998).

Flame structures at the base of sheets are commonly overturned and orientated in the same direction (Figure 3.17). In a sedimentary environment, overturned crests of flame structures that have a consistent orientation indicate the presence of some horizontal drag or movement between the two interacting materials (Boggs, 2001). Mafic enclave swarms that occur between mafic sheets typically have a sigmoidal, asymmetrical shape to them, indicating that they were deformed whilst they were still mobile as a result of shear or magmatic flow within the chamber (Figure 3.17). Magmatic flow is therefore likely to have operated immediately beneath this mafic sheet in the underlying enclave swarm. Aligned plagioclase crystals within the surrounding felsic host that do not display cumulate textures or chemistry further support the interpretation that magmatic flow operated within this section of the chamber.

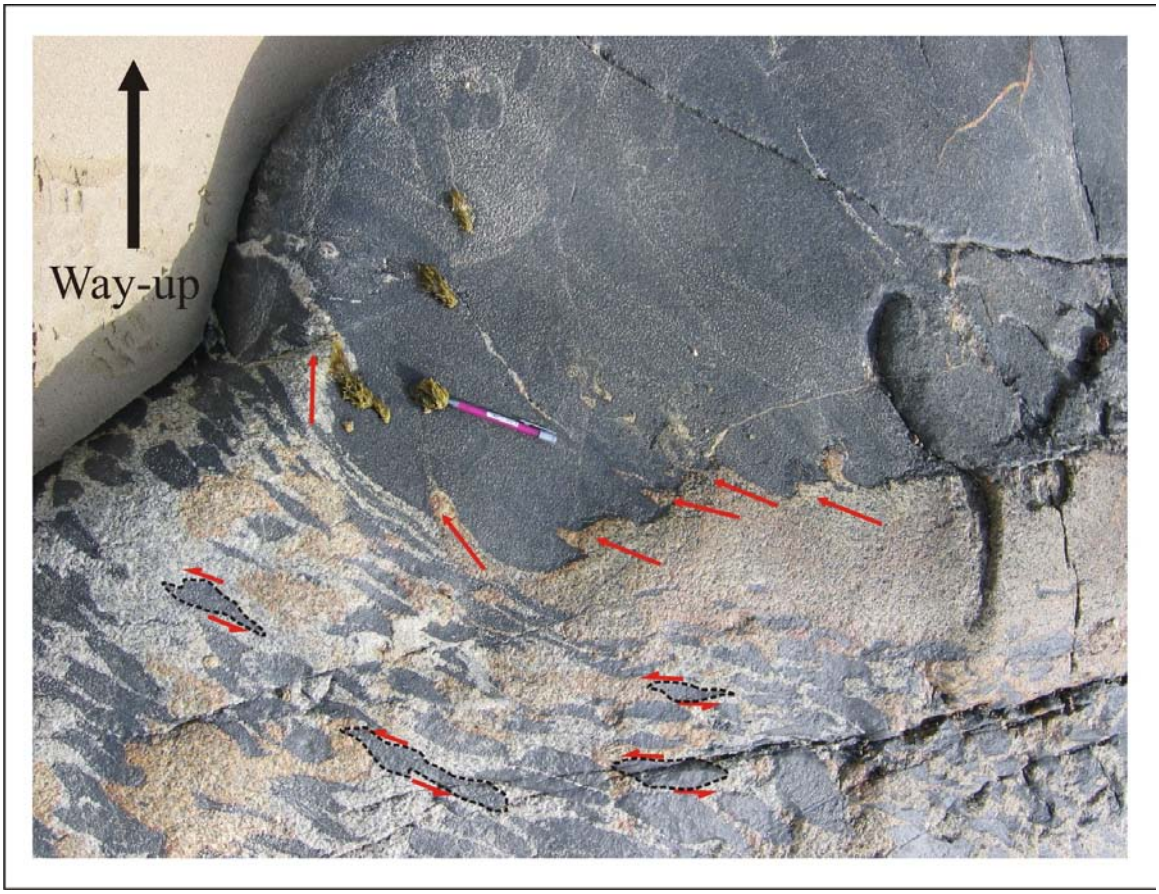

Figure 3.17. Flame structures at the base of a mafic sheet that display a common orientation towards the east (left of the photo). Underlying mafic enclaves display asymmetric sigmoidal shapes that indicate a sinistral sense of shear/flow. Pencil for scale is 14 cm long (E48/39825566).

3.5.4 The Neck

The Neck represents a large, almost continuously exposed section of ~1 km. The coeval interaction of mafic and felsic magmas at The Neck has resulted in the formation of a thick, uninterrupted succession of aligned mafic enclaves, and thin (<1m) scarce mafic sheets. The size, shape and degree of concentration of mafic enclaves vary considerably throughout the sequence. Figure 3.18 shows two examples of enclave swarms seen at The Neck; (A) represents enclaves that have undergone little compaction, which have typical aspect ratios of 1:4, and (B) represents a mafic enclave swarm that has been compacted beneath an overlying mafic sheet which has intruded above it. Aspect ratios of enclaves within this section range between 1:10 and 1:25.

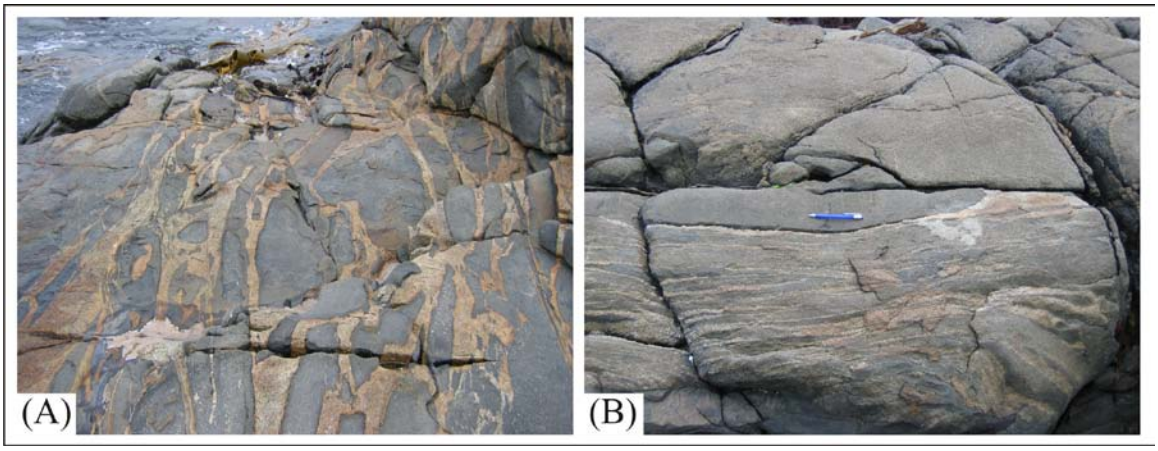

Figure 3.18. Different aspect ratios of mafic enclaves at The Neck as a result of varying degrees of compaction (A) little to no evidence for compaction (E48/43535346) (B) mafic enclaves have high aspect ratios due to emplacement of mafic sheet above (E48/43865424). Pencil for scale is 14 cm long and rests on the base of the mafic sheet.

Mafic enclave orientations within this section are at an angle to the other three sections, with average orientations of 147/60°. Towards the south (top of the chamber), these orientations become more concordant with those at the other locations, with average orientations of 110/60°. The significance of these discordant orientations will be discussed in later chapters. Sections that provide a 3D view of mafic enclaves reveal that enclaves in plan view are typically pancake shaped, having likely been flattened from a more ovoid shape as a result of compaction (Figure 3.19A).

Composite enclaves are present at several locations, and exhibit mingling textures with the surrounding host, indicating that they were still mushy when emplaced (Figure 3.19B). A few outcrops also show evidence for the presence of syn-plutonic shearing within the chamber, with mafic enclaves being smeared out along small shear planes (Figure 3.19C), indicating flow in a ductile state. Shearing within the chamber is not widespread, and its localized nature indicates that it may have been initiated as a result of compression from overlying magma intrusions which destabilized the underlying magma when it was still relatively mobile.

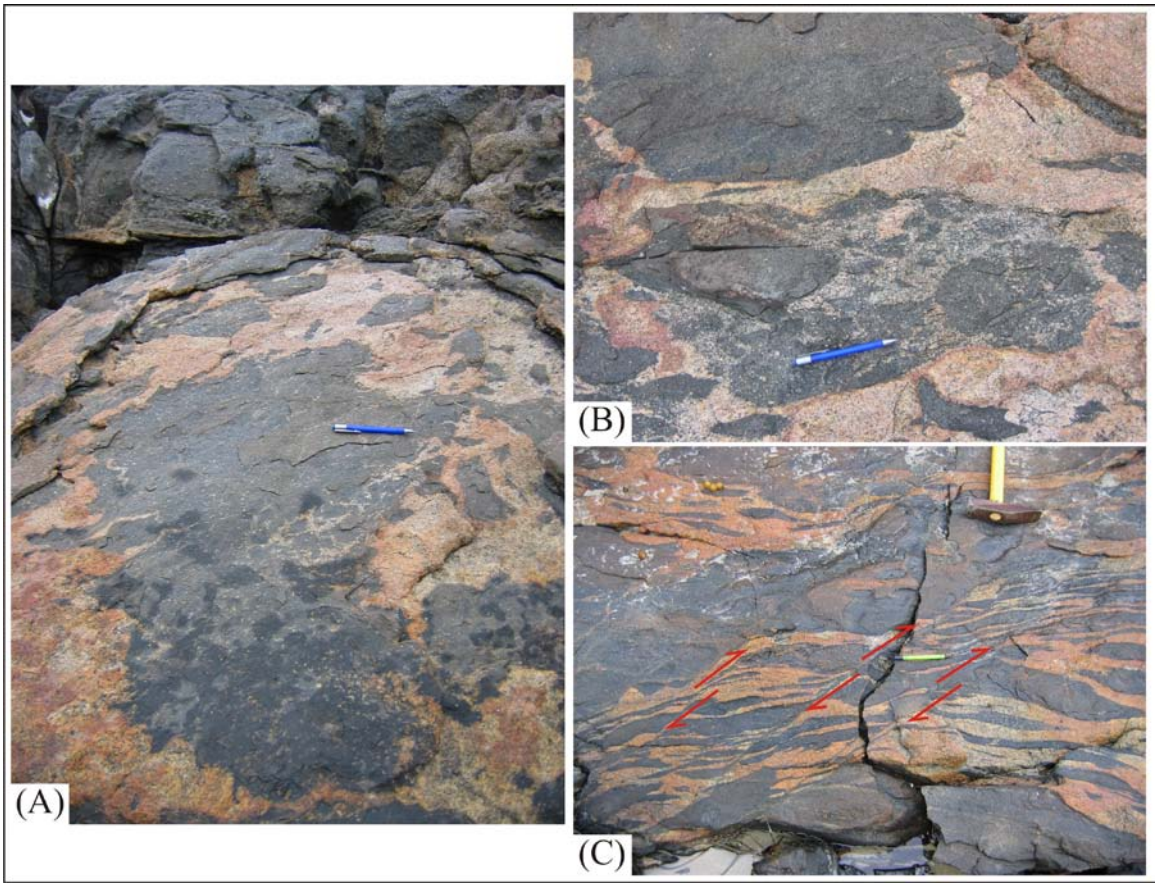

Figure 3.19. (A) Plan view of a pancake-shaped enclaves (E48/42975364) (B) composite enclave (E48/42975364) (C) Evidence for syn-plutonic shear (E48/43455406). Pencil for scale is 14 cm long; hammer head for scale is 16 cm long.

3.5.5 Other Localities

Two other localities within the pluton are described below. These localities are characterized by small, poorly accessible outcrops, where detailed structural and textural interpretations were unable to be made. They do however represent important locations within the chamber, and are used for linking the larger key localities together to provide a more complete and comprehensive understanding of the magma chamber as a whole.

3.5.5.1 Horseshoe Bay

Small outcrops occur on both sides of Horseshoe Bay. Outcrops on the north side are characterized by homogenous felsic host rocks that have been cross-cut by multiple fine-grained mafic dikes. These dikes occur at right angles to crystal foliation in the felsic rock. On the south side of Horseshoe Bay, small outcrops are characterized by felsic host

containing small mafic enclave swarms. Enclaves are typically rounded, and form as rafts, deposited as a result of magmatic flow within the chamber (Figure 3.20). Mafic enclave swarms often have concave bases indicating deposition within a channel, and enclaves are typically tightly packed. Mafic dikes at this locality are orientated at right angles to mafic enclave orientation.

The lack of exposure at Horseshoe Bay makes interpretations regarding their position within the chamber difficult. Stratigraphically they rest below the inferred base at Ackers Point, however the lack of abundant magma mingling structures that are present throughout the rest of the chamber indicate that the Horseshoe Bay section may represent a portion of the magmatic system that operated at a different time and with different processes dominating.

Figure 3.20. Photo of a mafic enclave swarm at Horseshoe Bay (E48/39285886). Backpack for scale is 50cm in length.

3.5.5.2 Ulva Island

On the north side of Ulva Island, three small (2m x 2m) outcrops were studied. Both were characterized by a felsic host rock containing small, elongated mafic enclaves. The felsic host rock is a granodiorite, and the mafic enclaves are micro-diorite. On the south side of Ulva Island, felsic host rocks are much more evolved, containing alkali feldspar megacrysts and rare small (<10cm^2) mafic enclaves (Figure 3.21). Mafic dikes cross-cut these rocks, and often become disaggregated within them suggesting intrusion when the felsic host magma still retained some residual melt. These evolved granites are quite deformed with widespread quartz ribboning, and therefore may well represent a later

cross-cutting granitic intrusion. It may also represent a cap of silicic melt that was extracted from the underlying Halfmoon Pluton.

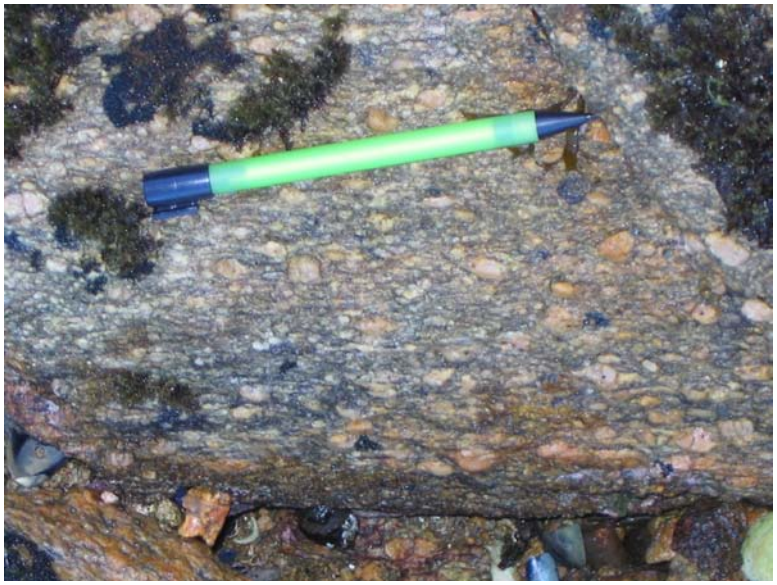

Figure 3.21. Granitic material on the south side of Ulva Island containing abundant alkali feldspar megacrysts (E48/38305266). Pencil for scale is 14 cm long.

3.6 PETROGRAPHY OF THE HALFMOON PLUTON

A full list of hand specimens and their petrographic, geochemical and geochronological treatment can be found in Appendix 1, and a full description of all thin sections and their modal abundances can be found in Appendix 2. Modal analyses were made on thin sections by counting 500 points in each thin section. Estimates of uncertainty in the modal proportions are ± 4.5% for modal proportions >50%, ± 4% for modal proportions ≥ 10 – 50%, ± 3.5% for modal estimates of 10%, ± 0.6% for modal estimates of ~1%, and ± 0.5% for modal estimates < 1% (Howarth, 1998). The intermediate-felsic host rocks are medium-grained, with compositions ranging from a hornblende leucodiorite at the inferred base of the chamber (AP and EC), to a biotite-tonalite and monzogranite (RR), and finally a biotite-tonalite towards the inferred top of the chamber (TN) (Figure 3.22). Host rocks at the inferred base of the chamber (AP and EC) are dominated by plagioclase (68%-90%), which occur as aligned, tabular crystals that define a cumulate texture. Plagioclase has an An composition between 30% and 42%. Hornblende (5%-12%) is almost always euhedral, olive-green pleochroic, commonly twinned and is aligned parallel to that of plagioclase crystal alignment. Biotite

(<1%-6%) is euhedral to subhedral, brown-straw pleochroic and appears to be a late crystallizing phase. Quartz (0%-5%) is anhedral and interstitial. Zircon crystals are abundant, euhedral and typically occur in interstices between plagioclase and hornblende. Fe-Ti oxides (<1%-3%) typically occur as euhedral cubic shaped crystals, indicating they are probably magnetite. Sphene (trace) occurs either interstitially or as anhedral rims around Fe-Ti oxides indicating it is a late crystallizing phase. Apatite is euhedral and occurs as either inclusions within plagioclase as stubby prisms or acicular crystals.

Host rocks towards the inferred top of the chamber (RR and TN) contain smaller proportions of randomly oriented sub- to euhedral plagioclase feldspar (14%-87%) and higher proportions of quartz (6%-47%), which becomes more subhedral as it increases in abundance towards the top of the chamber. Plagioclase has an An composition between 26% and 35%. Alkali feldspar (<1%-37%) is subhedral, and occurs in almost all host rocks from Ringaringa and only one host sample from The Neck (TN#7). The dominant mafic phase changes within the host rocks at Ringaringa and The Neck from hornblende to biotite. Where hornblende is present (2%-11%) it occurs as subhedral grains. Biotite (1%-12%) is brown pleochroic and sub- to euhedral and where it occurs in the same rock with hornblende it is typically intergrown, forming in clots. Accessory apatite, sphene and Fe-Ti oxides occur in abundances <1% - 2%. Zircon crystals are euhedral and are most commonly found as inclusions within biotite, displaying pleochroic haloes. Scare secondary phases of chlorite, sericite and myrmekite are present in abundances 0% -1% of all host rocks in the Halfmoon Pluton.

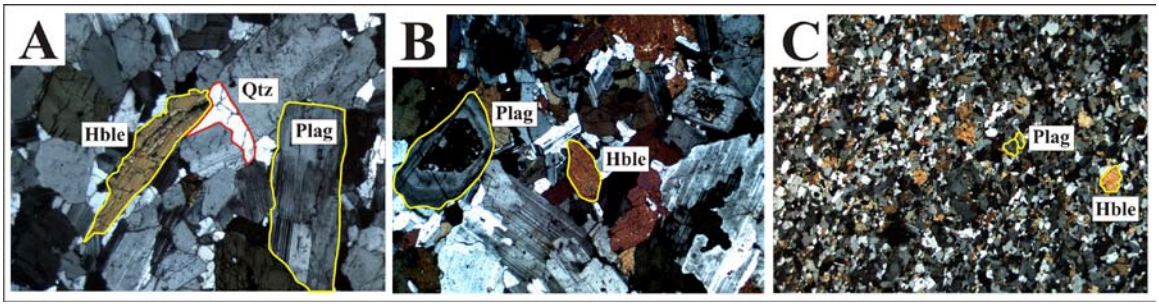

Figure 3.22. Representative CPL images showing the relative difference in grainsize between (A) Intermediate-felsic host rock (EC#6H) with sub- to euhedral medium-grained crystals (B) Mixed 'hybrid' rock (EC 3/2#CX) with juxtaposed fine and medium-grained crystals (C) Mafic sheet (EC#6) with a mosaic texture of fine-grained crystals. Width of all photos is 5mm.

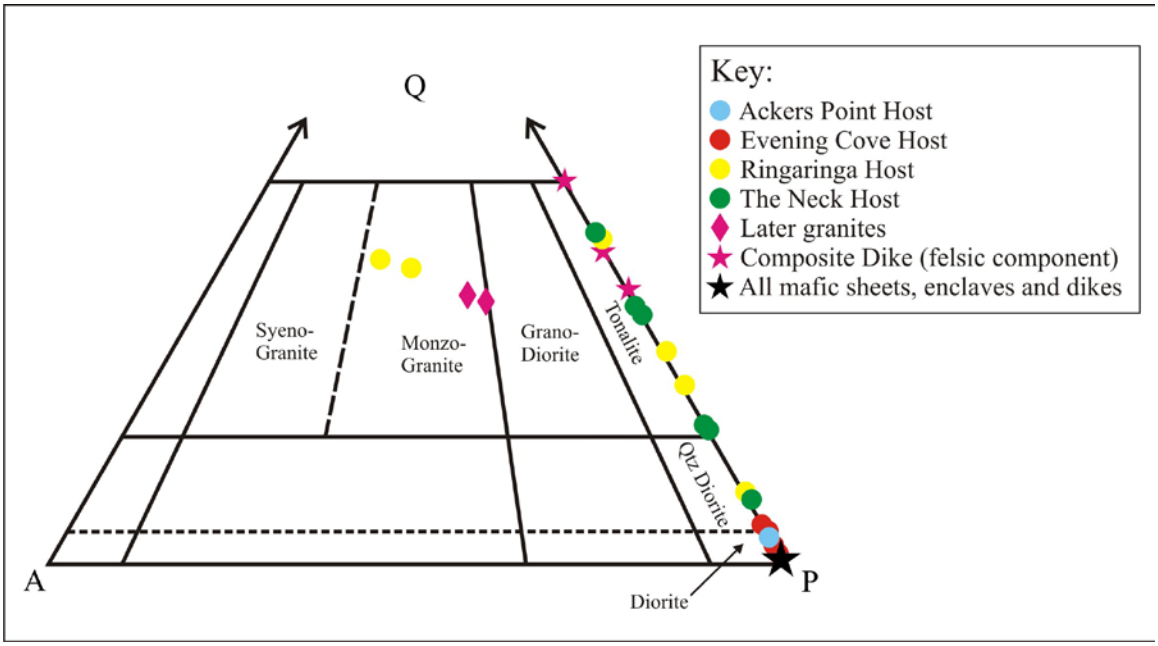

Figure 3.23. IUGS Classification of representative petrographic sections. All mafic sheets, enclaves and cross-cutting mafic dikes contain 100% plagioclase. After Streckeisen (1973). Modal amounts were determined for 22 representative samples throughout the pluton were made by point counting.

The mafic rocks (sheets, enclaves, dikes) are classified petrographically as hornblende mesodiorites (Figure 3.23. Streckeisen, 1973). The mineral assemblage remains fairly constant throughout the chamber. Mafic sheets and enclaves are characterized by ~60% mafics (hornblende and/or biotite), ~35% plagioclase, and <5% Fe-Ti oxides and sphene. Mafic enclaves often contain between 0.5 and 1% modal apatite. As in the felsic rocks, the dominant mafic phase changes from hornblende to biotite towards the top of the chamber. Hornblende-bearing mafic rocks are enclosed within hornblende-bearing intermediate-felsic rocks, whereas biotite-bearing mafic rocks are enclosed in biotite-bearing intermediate-felsic rocks. Hornblende is green pleochroic, euhedral, and typically occurs in clots. Plagioclase crystals are typically euhedral, and often define a weak preferred orientation parallel to that of sheet and enclave orientation. Plagioclase compositions range from An ~43% at the base of the chamber (AP), to An ~39% towards the top (TN). The An% within these mafic rocks is very similar to that in the surrounding host, usually only greater by 1-2%.

Mixed 'hybrid' rocks were classified as such based on their appearance in the field, petrography, and geochemistry (to be discussed in Chapter 4). In the field mixed rocks display colours intermediate to the light intermediate-felsic host rocks and the dark mafic sheets and enclaves. They also typically display mixed contacts with the surrounding rocks. Petrographically, they contain a mixture of fine and coarser-grained crystals derived from both the mafic and felsic magmas, and have the same modal mineralogy as the un-mixed rocks that enclose them. Figure 3.22 shows the differences between felsic host, mafic sheets and mixed rocks petrographically and in the field.

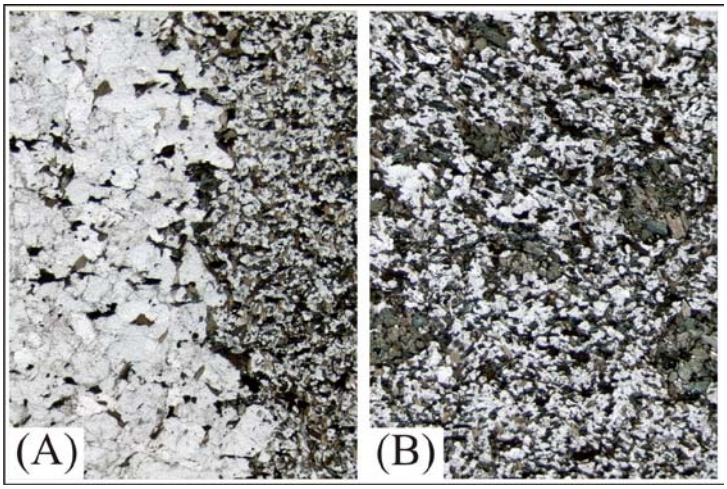

Figure 3.24. (A) Contact between mafic component of composite dike and felsic component of composite dike (B) clots of hornblende that may represent pseudomorphs of pyroxene. Photos are 5mm in length.

Mafic dikes are typically characterized by the same modal mineralogy as the mafic sheets and enclaves, though are usually more hornblende and Fe-Ti oxide-rich, and are much finer-grained (<0.2mm). Plagioclase crystals are typically lath-like, are coarser grained than the mafic minerals, and are strongly foliated parallel to the margins of the dikes. Several mafic dikes are characterized by clots of hornblende (Figure 3.24B) that may represent psuedomorphs from the replacement of pyroxene given their geometric shape (Barbarin, 2004). Composite dikes are characterized by fine-grained mafic enclaves within a fine-grained felsic host. The felsic host is typically coarser-grained than the mafic enclaves it encloses, and are dominantly composed of quartz and plagioclase crystals that have a sugary texture. The contact between the mafic and felsic rocks is

typically very sharp and planar (Figure 3.24A), though felsic material often penetrates into the mafic enclaves and seems to mix slightly with the mafic material, indicating that these dikes were liquid at the same time (Snyder *et al*., 1996).

Cummingtonite is present in four rocks at Ringaringa; occurring in the thick mafic sheet ~100 m below the main outcrops, two mafic enclaves and the adjacent felsic host at the base of the lowermost outcrop at Ringaringa. It is colourless in PPL, and displays bright (2^{nd}-3^{rd} order) interference colours in CPL (Figure 3.25). In all cases it is overgrown by hornblende. The significance of the presence of cummingtonite in only this section within the Halfmoon Pluton will be discussed in more detail in Chapter 4.

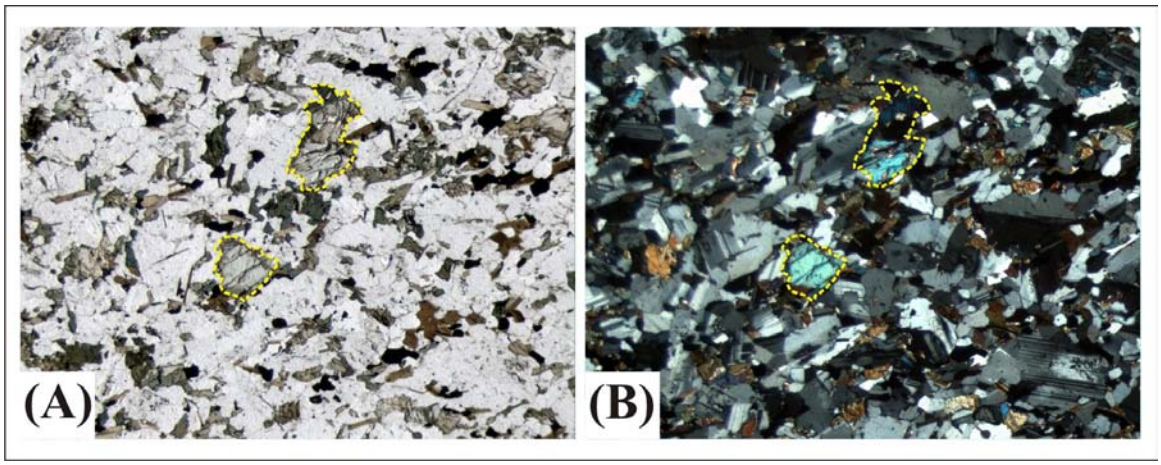

Figure 3.25. (A) PPL image of cummingtonite with hornblende overgrowths (B) CPL image of cummingtonite showing higher interference colours. Photos are 5mm in width.

3.6.1 Interpretation of Microstructures

Several microstructures are present within the rocks of the Halfmoon Pluton that support a magma mingling and mixing origin. Contact relationships between the mafic and felsic rocks vary throughout the chamber. Contacts between the two lithologies are typically sharp, with the mafic rocks generally displaying fine-grained chilled/quenched margins. Figure 3.26 shows a contact between the fine-grained quenched basal contact of a mafic sheet and the underlying coarser-grained felsic host. Plagioclase crystals in the felsic host are well aligned at the contact, with foliation becoming less pronounced further from the contact. This orientation is likely to be due to shear occurring along this interface, with

less orientation further away due to less shearing. Minerals within the mafic sheet mould around plagioclase crystals, indicating that the felsic magma must have been quite crystal-rich, though liquid enough to permit magma mingling.

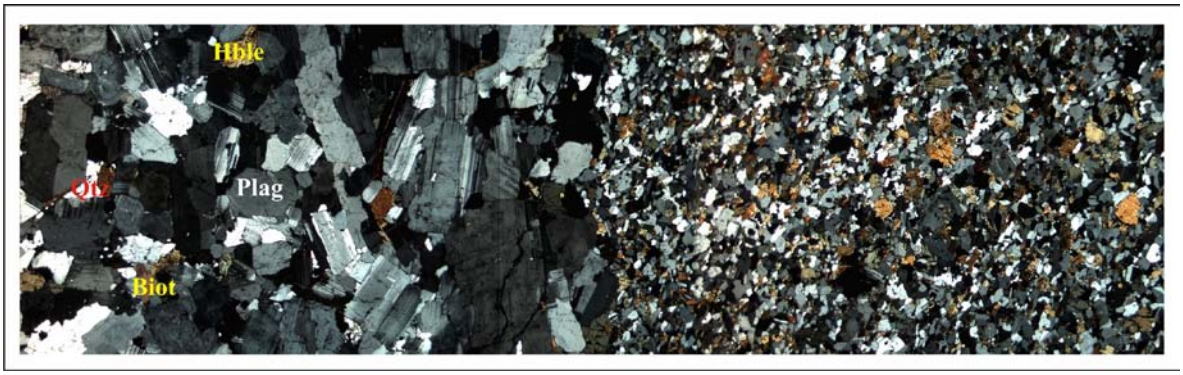

Figure 3.26. Sample EC#6 displaying fine-grained chilled mafic contact with the leucodiorite host. Minerals in the mafic margin mould around the larger plagioclase crystals in the host. Plagioclase crystals within the host are aligned. Width of the photo is 1.5cm.

Several mafic enclaves, and in some instances mafic sheets, contain petrographical evidence indicating they underwent mixing with the adjacent felsic host magma. Mafic sheets and enclaves are too basic to contain quartz, and therefore the presence of quartz xenocrysts within mafic enclaves implies that localized mixing between the mafic inclusion and the surrounding felsic host magma occurred. Figure 3.27 displays both field and petrographical examples of quartz xenocrysts within a mafic enclave at Ringaringa.

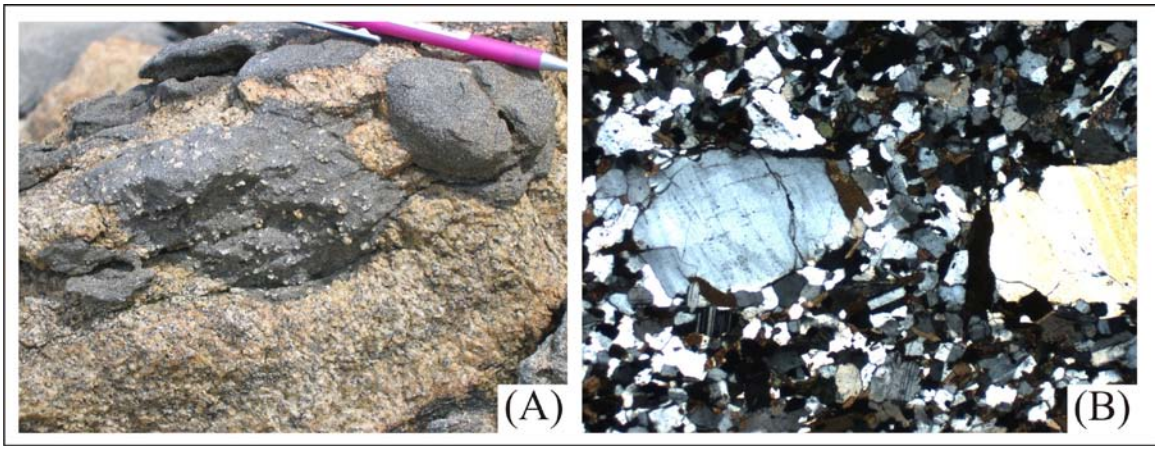

Figure 3.27. (A) Mafic enclave containing abundant plagioclase and quartz xenocryts located immediately beside a mafic enclave containing no xenocrysts (E48/39795594) (B) Cross-polar image of a mafic enclave with quartz xenocrysts. Width of the microscope photo is 5mm.

Plagioclase xenocrysts within mafic sheets and enclaves typically contained cores with a sieve-like texture, indicative of dissolution (Wada *et al.* 2004). Acicular apatite and blade biotite are often found within mafic sheets and enclaves. These mineral textures are commonly found in undercooled magmas, which have chilled rapidly against a cooler magma. An undercooling environment alters the nucleation rates of crystals, encouraging rapid growth as the crystal attempts to regain equilibrium (Hibbard, 1995). The presence of acicular apatite and blade biotite provide evidence for rapid thermal equilibration of the two interacting magmas as the mafic magmas quenched and chilled within the surrounding felsic host magma.

Amygdules are present in a handful of mafic enclaves at The Neck (Figure 3.28), and indicate H_2O coming out of solution. Amygdules form by filling of vesicles from the precipitation of aqueous solutions. The presence of amygdules towards the top of the sequence provides evidence for the vertical escape of volatiles within the magmatic system, and that The Neck represents a shallower-level of emplacement than rocks at Ackers Point, Evening Cove and Ackers Point.

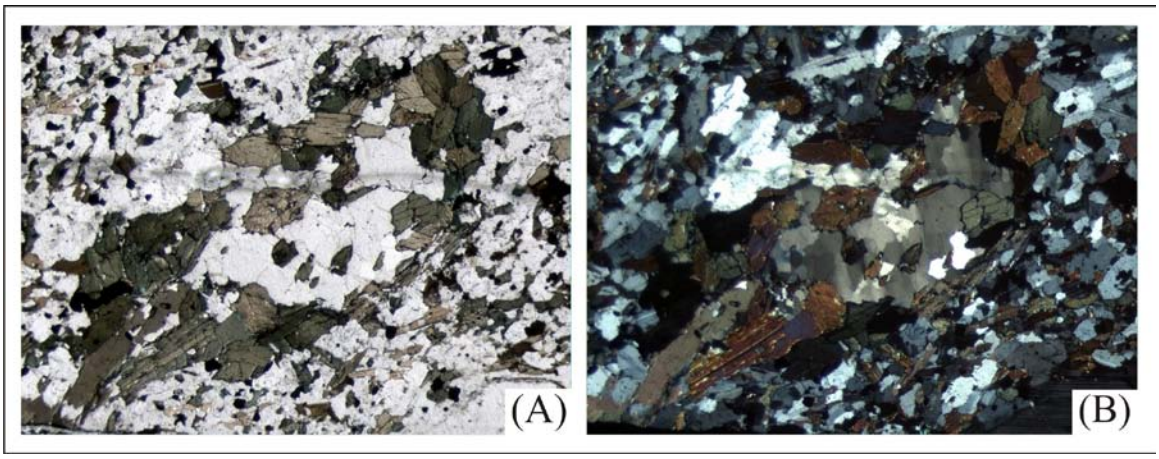

Figure 3.28. (A) PPL and (B) CPL images of amygdules. Width of the image is 5mm.

Tabular plagioclase crystals within the intermediate-felsic host rocks and mafic sheets and enclaves are commonly foliated in the same orientation as that of adjacent sheets and enclaves. This alignment is most clearly defined in the intermediate host rocks towards the base of the chamber. The alignment of crystals that define foliations within

magma chambers is often interpreted as the result of magmatic flow, or from the accumulation of crystals as a result of gravitational settling. Such textures however may also be the result of solid-state flow as a result of tectonic processes (Paterson *et al*., 1989). Outcrops that contain elongated mafic enclaves enclosed in a foliated felsic host could have deformed by solid-state deformation, and if so should be characterized by a range of microstructures indicating they were formed in the solid state, such as ribbon quartz, anastomosing foliations, shear bands, boudinage of strong minerals, undulose extinction, and recrystallization of minerals to finer aggreagates (Vernon *et al*., 1988; Paterson *et al*., 1989). None of these structures is observed in samples that have aligned plagioclase crystals, and this is strong evidence to support the conclusion that the foliations were formed by magmatic processes. The aligned plagioclase crystals are interpreted to represent a cumulate texture, formed from the gravitational settling and accumulation of crystals at the base of the chamber. Hornblende crystals that parallel the plagioclase alignment are also interpreted to have formed as a result of crystal accumulation. The presence of cumulates at the base of the chamber is further supported by the lack of cumulate textures in intermediate-felsic host rocks from the inferred top of the chamber (RR and TN). Magmatic flow is also inferred however for some areas where mineral alignment is well-defined and there is evidence that mafic enclaves enclosed within the intermediate-felsic host have also undergone flow.

A slight metamorphic overprint due to regional faulting associated with the Freshwater Fault System to the south is present. This only becomes apparent in the southernmost rocks from Ulva Island and The Neck in the form of mild quartz ribboning, and undulose extinction in biotite crystals. The rocks from these localities contain a higher proportion of quartz, which is affected more strongly by deformation. Mafic sheets and enclaves enclosed within the deformed felsic host do not contain quartz, and show no signs of solid-state deformation. This metamorphic overprint does not affect the majority of outcrops within the Halfmoon Pluton, and therefore has no significant effect on interpretation of mingling structures.

Some samples show a decrease in mafic minerals in close proximity to the contact with mafic sheets and enclaves. Such a feature is described by Blundy and Sparks (1992) as a result of the contraction of the mafic sheet as it cools, and interstitial melt from the adjacent felsic magma migrating to fill this vacated space. Mafic inclusions with this texture also typically display continuous crenulated margins which form as the mafic magma contracts. This texture has also been proposed by Wiebe (1996) as forming due to the dehydration of adjacent felsic magma as a result of the growth of hornblende and biotite at the edge of the mafic sheet or enclave. The lack of continuous crenulated margins of mafic enclaves and sheets within the Bungaree Intrusives indicates that this texture did not form from the contraction of mafic inclusions, instead it is likely to have resulted from dehydration of the adjacent felsic host.

3.8 PHYSICAL PROCESSES INFERRED

Based on interpretation of field evidence alone, several physical processes that were operational during the emplacement history of the Halfmoon Pluton have been identified, including magma mingling and mixing, magmatic flow, compaction, mechanical exchange of material between the two interacting magmas, and thermal exchange and equilibrium.

3.8.1 Magma Mingling

As established from field observations, magma mingling is the dominant physical interaction process occurring within the Halfmoon Pluton. Mingling styles vary according to position within the chamber, and are likely to have been caused by a number of factors including compositional contrasts, relative volumes of the interacting magmas, rate of mafic magma replenishment, volatile content, and contrasts in temperature and degree of crystallization (and therefore density). Acid net-veining was proposed by several early authors as the process by which mingling structures formed (Elwell *et al*., 1962). Rather than coeval mafic magma mingling within a more felsic host, many mingled rocks were attributed to felsic magma that injected into the mafic rock when it was completely crystalline, fracturing it apart to form individual chunks of mafic rock within a more felsic rock. Within the Halfmoon Pluton, acid net-veining can be ruled out

based on differences in the morphology of enclaves, clear evidence that mafic enclaves formed and were deformed whilst they were molten, and the size of crystals in the felsic host that separates the mafic enclaves and sheets. In net-veined complexes, such as that displayed in Figure 3.29 from the Longwoods Complex at Riverton, New Zealand, felsic material injects into brittle fractures within crystalline rock, separating the rock into angular inclusions with sharp contacts. This is in contrast to mafic enclaves that are sub-rounded and often display crenulate margins, a morphology that is synonymous with molten material that deforms plastically. The size of the crystals within the felsic material separating these mafic inclusions is proportional to the size of the vein, with larger crystals in wide veins, and finer-grained crystals in thin veins. In mingled magmas, the size of the crystals within the felsic host rock that separates the mafic sheets and enclaves remains uniform. All structures observed in the field are therefore interpreted to have formed as a result of magma mingling and/or mixing and not acid net-veining.

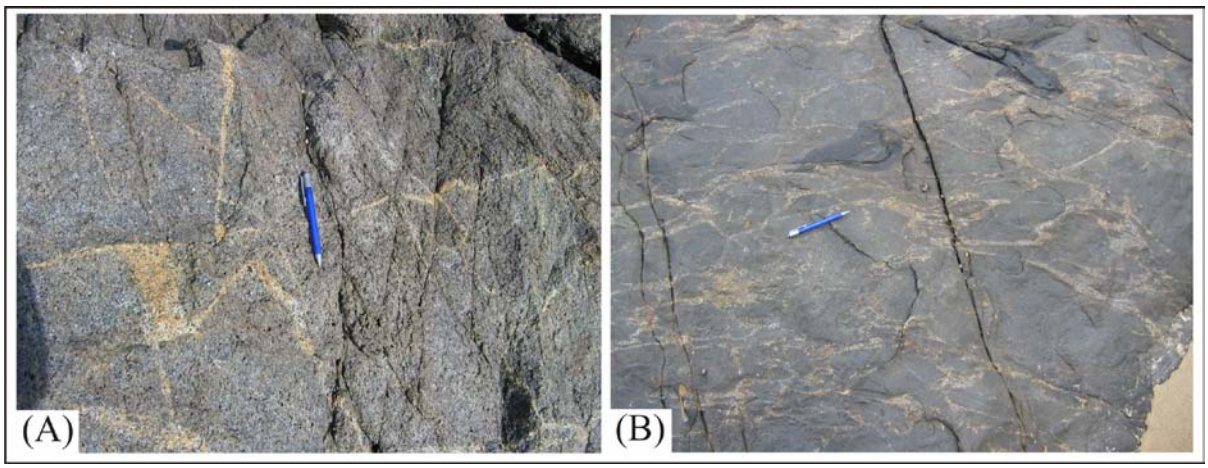

Figure 3.29. (A) Net-veined gabbro from the Longwoods complex, Riverton. Note the sharp, angular contacts with the felsic material. The thick patch of felsic material in the centre left of photo is coarser-grained than the thin veins throughout the rest of the photo (B) Tightly compacted mingled mafic enclaves within felsic host at The Neck (E48/43285331). Not the sub-rounded morphology of the enclaves and their cuspate margins. Crystal size of the felsic material separating enclaves is uniform. Pencil for scale is 14 cm in length.

Magma mingling is preserved as mafic sheets and enclave swarms within an intermediate-felsic host rock. Mingling style varies throughout the Halfmoon Pluton, and a change from mafic sheet formation at the base of the chamber to one of mafic enclave formation towards the top of the chamber coincides with a change in the modal

mineralogy and whole-rock geochemistry of the different rocks. Several petrologic processes have been proposed to account for the formation of mafic enclaves, including;

a) Restite unmixing (White & Chappell, 1977)
b) Disaggregation of chilled margins into the chamber (Huppert & Sparks, 1989)
c) Mingling of mafic magma within a more felsic magma chamber by way of;
    a. Disaggregation of mafic dikes injected into a liquid host magma (Frost & Mahood, 1987; Pitcher, 1991)
    b. Disruption of partially chilled or cumulate material from the margins of the pluton (Bonin, 1991)
    c. Disruption of mafic-intermediate magma that exists in the lower portions of compositionally stratified magma chambers (Wiebe *et al*., 1997)

Fine-grained quenched margins are observed on most mafic enclaves within the Halfmoon Pluton, indicative of an undercooled environment where hotter mafic magmas existed in a liquid state and chilled rapidly within a cooler, more felsic host magma chamber. Magma mingling is therefore preferred as the dominant process by which the mafic enclaves formed. Composite enclaves at The Neck probably represent disrupted portions of the hybrid 'mush' brought up from lower portions of the chamber. Mafic enclave formation may also have been facilitated by vesiculation of the hydrous mafic magma as it came into contact with the hotter more felsic host magma (Eichelberger, 1980; Wiebe, 1994). This process and its significance will be discussed in Chapter 7.

3.8.2 Magma Mixing

Though magma mingling is the dominant magma interaction process operating within the Halfmoon Pluton, magma mixing is also common throughout the chamber, with mixed mafic enclaves often occurring beside non-mixed mafic enclaves. Mixing between the two interacting magmas can occur at four different locations; prior to emplacement, during emplacement as a result of flow-front instabilities, interactions at the base of mafic sheets, and interactions at the top of the mafic sheet at the contact with the overlying felsic host (Wiebe *et al*., 2002). Mixing and therefore mechanical exchange of magma and/or crystals is possible only when both magmas are mobile enough for active stirring

of the two magmas to occur. The morphology and orientation of mafic enclaves compared with the flow foliation of the adjacent host provides information on the relative rheology of the coexisting and contrasting magmas during mechanical mixing (Barbarin & Didier, 1992). Most mafic enclaves within the Halfmoon Pluton appear to have undergone localized mixing with the felsic host, and are therefore likely to have had lower contrasts in temperature with the adjacent felsic host. Enclaves that occur in locations where there is evidence for vigorous flow within the chamber also often display gradational, mixed contacts with the host. Localized magma mixing involves the mechanical exchange of plagioclase and quartz crystals from the felsic host to the mafic inclusions, and gradational contacts between mafic and felsic rocks. Where mixing has occurred on a larger scale, and whole enclave swarms show evidence for mixing with the host, relative volumes and rates of mafic magma replenishment are likely to have been controlling factors promoting mixing. At The Neck, mixing either prior to or during emplacement has resulted in the formation of 'composite' enclaves, which mixed elsewhere within the chamber before being transported to the current location. These composite enclaves have mingled contacts with the adjacent felsic host rocks, indicating that they were relatively soft/mushy when they were emplaced at their current location. These enclaves may also have been sourced from disruption of lower 'hybrid' mushy portions of the stratified chamber.

3.8.3 Magmatic Flow

Foliations in plutonic bodies may develop as a result of tectonic stress and deformation, or from magmatic flow. Regional deformation following emplacement will result in foliations preserving solid-state deformation, while foliations preserving magmatic flow may be formed during ascent, or from pluton emplacement and expansion (Paterson *et a*l., 1989). Fabrics within the host and mafic rocks of the Halfmoon Pluton record evidence for magmatic flow, crystal accumulation and compaction.

Foliation within the mingled mafic rocks is defined by mafic sheet orientation and aligned enclaves showing a common elongation direction between 90-110°E/W. The consistent orientation of mafic sheets and enclaves throughout the chamber (except for

The Neck – see next section) is interpreted to represent the original orientation at which the mafic magmas injected and flowed between the lower crystal-rich mush and upper crystal-poor host magma. Magmatic foliations within the felsic host rocks are typically oriented parallel to the direction of mafic sheet and enclave orientation. Foliation within the host rocks is defined by the orientation of euhedral tabular plagioclase crystals which is strongest towards the base of the chamber. Plagioclase foliation within the felsic magmas is also typically more strongly defined when in close proximity to contacts with the mafic sheets and enclaves. Mineral foliations within mafic sheets and enclaves are always parallel to those in the surrounding host, and are parallel to the orientation of the sheets and enclaves themselves. Large melt fractions must have been present within these magmas when magmatic flow was occurring. For mingling to occur, the crystallization of the host had to be below 70% in order for the felsic host to behave like a magma (van der Molen & Paterson, 1979; Vigneresse *et al*., 1996). Melt fractions in excess of 50% are likely within felsic host magmas of the Bungaree Intrusives in order to allow for the flow of plagioclase crystals (Vernon *et al*., 1988; Vigneresse *et al*., 1996). All field and petrographic evidence shows that structural and textural features preserved in the chamber were the result of magmatic processes and not solid-state deformation. Aligned, elongated mafic enclaves show no evidence of plastic deformation or recrystallization, and therefore represent magmatic flow within the felsic host. Where quartz is present, it shows little to no sign of plastic deformation associated with solid-state deformation. A slight metamorphic overprint due to regional faulting from the Freshwater Fault System to the south only becomes apparent in the form of mild quartz ribboning in the southernmost rocks from Ulva Island and The Neck. Mafic enclaves are commonly present at the top of mafic sheets and have orientations that indicate they were affected by some magmatic flow (Figure 4). This mingling structure has been observed in several other composite plutons, and has been inferred by Wiebe and Collins (1998) to represent convective stirring in the crystal-poor felsic magma overlying the mafic sheet.

3.8.4 Crystal Accumulation

Crystal accumulation is recognized from field and petrographic evidence. Large tabular plagioclase crystals make up >85% of the host rocks at AP and EC (inferred base of the

chamber), are typically aligned, along with euhedral hornblende, apatite and zircon, and are separated by small amounts (<5%) of interstitial quartz. Whilst magmatic flow appears responsible for some of the foliation present in the host rocks, crystal accumulation is probably responsible for the strong plagioclase alignment observed in the host rocks towards the base of the chamber at AP and EC. This interpretation is supported by geochemical evidence which will be discussed in Chapter 4. Towards the inferred top of the chamber (RR & TN), alignment of plagioclase is interpreted to represent magmatic flow that parallels that in the enclosed mafic enclaves. Plagioclase foliation within these rocks is generally more strongly defined when in close proximity to contacts with the aligned mafic enclaves.

3.8.5 Compaction

Evidence for compaction of the chamber in a N-S direction is consistent throughout the pluton. Limited strain analysis carried out by Smith (2000) and in the course of this research indicate that compaction within the chamber occurred when both felsic and mafic magmas contained enough liquid to permit plastic deformation. Compaction is indicated by crenulated interfaces that lie perpendicular to the direction of shortening (N/S, Figure 3.30A), and enclaves that in cross-section view have high aspect ratios, with 3D sections revealing a more oblate, pancake shape (Figure 3.30B). The formation of symmetrical fold-forms on these interfaces indicates that a viscosity contrast must have existed between the felsic and mafic magmas, with the chilled mafic magmas becoming more viscous relative to the felsic host (Smith 2000). Smith (2000) calculated that at least 50% shortening had occurred within the chamber, however this was based on calculations taken only from Evening Cove, and are not representative of the entire sequence. Compaction is localized, with variable amounts of shortening throughout the chamber. This variation implies that shortening was not experienced at one time throughout the chamber, but instead occurred episodically, most likely in response to loading of the chamber from mafic magma input and gravitational settling from above. Areas which have experienced a high degree of shortening probably had larger inputs of mafic magma above, resulting in magma loading, than areas which display a small degree of shortening. Areas that experienced high amounts of shortening are characterized by a

high degree of mafic enclave abundance relative to felsic host, with enclaves separated by very small amounts of felsic magma, so that the two magmas have moulded around each other. The amount of shortening is probably also dependent on how soon after mafic enclave emplacement the overlying mafic sheet injected. Mafic enclaves that preserve evidence for shortening would need to have be mushy in order to accommodate the strain.

Areas that experienced high amounts of shortening are characterized by a high degree of mafic enclave abundance relative to felsic host, with enclaves separated by very small amounts of felsic magma, and subsequently have moulded around each other. This would have happened due to the squeezing out of the felsic magma following compaction. The degree of crystallization of both the host and mafic magmas would also play an important factor in the amount of shortening preserved. Experiments by van der Molen & Paterson (1979) show that there is a transition in the mechanical behaviour of magma, from solid-state to melt-dominated, at a melt fraction of ~30%. Mafic and felsic host magmas that have <30% melt remaining would therefore not accommodate shortening as readily as magma that contains >30% melt, and would more likely deform elastically. This indicates that the mafic inclusions had to have contained > 30% melt in order to plastically accommodate shortening, and therefore compaction is likely to have occurred shortly after mafic magma injection before the rapidly crystallizing mafic sheet or enclave has time to become solid. Compaction is also likely to have occurred after magmatic flow had ceased.

The degree of crystallization of both the host and mafic magmas would play an important role in allowing crystal accumulation and magmatic flow to occur, and in determining the amount of shortening preserved. Magma containing <20% crystals is able to accommodate magmatic flow and rotation of individual crystals (Vigneresse et al., 1996), and hence preserve magmatic flow textures and allow crystal settling to occur. Magmatic flow is still achievable in magmas with as much as 55% crystals, however once above 55% crystals, foliations will only develop by solid-state processes (Vigneresse *et al.*, 1996). Once crystallinities have reached ~72-75% the magma is

effectively solid, and will not accommodate shortening or magmatic flow in a magmatic fashion.

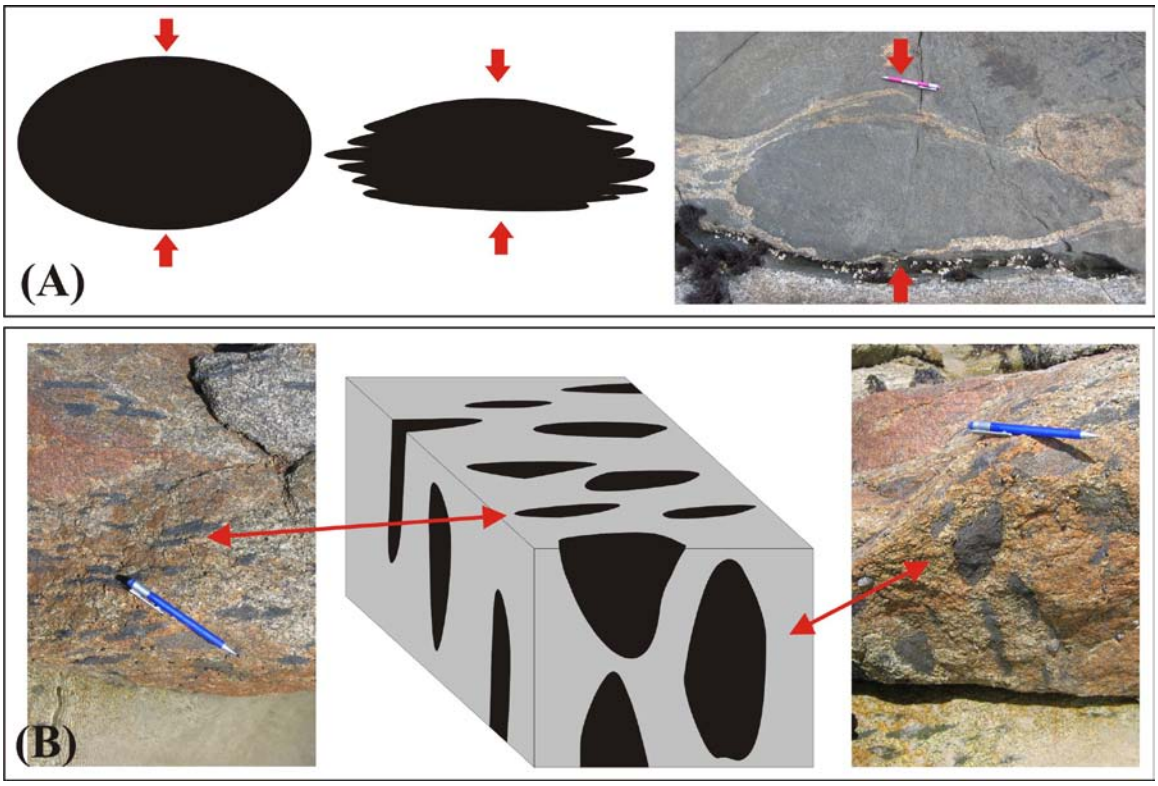

Figure 3.30. (A) Simplified model of crenulate margin formation from an oval magma blob, to a mafic blob with crenulated margins due to shortening in a N-S direction. Photo indicates crenulated E-W margins on a mafic enclave as a result from compaction beneath a thick mafic sheet. (B) 3D sketch and field examples of the morphology of compacted mafic enclaves that are ellipsoidal in cross-section, and pancake shaped in plan view.

3.8.6 Thermal Exchange

Thermal exchange between the felsic and mafic magmas probably occurred very rapidly. Textures within the mafic sheets and enclaves, such as fine-grained chilled margins, acicular apatite, blade biotite, and sieve textures in plagioclase indicate that the hot injecting mafic magmas quenched and crystallized rapidly within the cooler felsic host magma (Barbarin & Didier, 1992; Hibbard, 1995). The rate at which thermal equilibrium is attained is a function of the mass fractions of the coexisting magmas. Large volumes of mafic magma take a longer time to reach thermal equilibrium than smaller blobs of mafic magma. The rate at which thermal equilibrium is achieved is an important factor controlling the amount of chemical exchange that can occur between the two interacting

magmas. Small volumes of mafic magma reach thermal equilibrium very quickly, and become solid enough to limit and even inhibit chemical exchanges (Frost & Mahood, 1987). The importance of chemical exchange will be discussed in following chapters.

3.9 CONCLUSIONS

Detailed documentation and interpretation of mafic-felsic magma mingling structures and textures in the field reveal that the Halfmoon Pluton within the Bungaree Intrusives formed incrementally as the result of episodic replenishments of mafic magma into a more felsic magma chamber. Alternating mafic sheet and enclave swarms represent magma replenishment events onto the floor of an aggrading crystal-rich chamber, allowing for a temporal evolution of magmatic processes to be established. Magma mingling and mixing structures vary throughout the chamber, indicating that processes operating within the evolving magma chamber varied in intensity and relative importance through time. Identification of magmatic processes by interpretation of mingling structures and textures alone however is limited, as these features often only record processes that were operating towards the end of a magma chamber's life. The following two chapters therefore will combine detailed geochronological and geochemical analyses with field interpretations outlined in this chapter to provide a more complete picture of the construction and evolution of the Halfmoon Pluton.

3.10 REFERENCES

Allibone, A.H and Tulloch, A.J. 2004 'Geology of the plutonic basement rocks of Stewart Island, New Zealand' *New Zealand Journal of Geology and Geophysics* 47: 233-256

Allibone, A.H., Jongens, R., Scott, J.M., Tulloch, A.J., Turnbull, I.M., Cooper, A.F., Powell, N.G., Ladley, E.B., King, R.P. and Rattenbury, M.S. 2009 'Plutonic rocks of the Median Batholith in eastern and central Fiordland: field relations, geochemistry, correlation, and nomenclature' *New Zealand Journal of Geology and Geophysics* 52: 101-148

Bachl, C.A., Miller, C.F., Miller, J.S. and Faulds, J.E. 2001 'Construction of a pluton: Evidence from an exposed cross section of the Searchlight pluton, Eldorado Mountains, Nevada' *GSA Bulletin* 113(9): 1213-1228

Barbarin, B. 2004 'Mafic magmatic enclaves and mafic rocks associated with some granitoids of the central Sierra Nevada batholith, California: nature, origin, and relations with the hosts' *Lithos* 80: 155-177

Barbarin, B. and Didier, J. 1992 'Genesis and evolution of mafic microgranular enclaves through various types of interaction between coexisting felsic and mafic magmas' *Transactions of the Royal Society of Edinburgh: Earth Sciences* 83: 145-153

Blundy, J.D. and Sparks, R.S.J. 1992 'Petrogenesis of mafic inclusions in granitoids of the Adamello Massif, Italy' *Journal of Petrology* 33: 1039-1104

Boggs, S. 2001 *Principles of sedimentology and stratigraphy* Prentice Hall USA pp726

Bonin, B. 1991 'The enclaves of alkaline anorogenic granites: an overview' In: Didier, J. and Barbarin, B. (eds) *Enclaves and Granite Petrology. Developments in Petrology 13* Amsterdam: Elsevier pp 179-189

Chapman, M. and Rhodes, J.M. 1992 'Composite layering in the Isle au Haut Igneous Complex, Maine: evidence for periodic invasion of a mafic magma into an evolving magma reservoir' *Journal of Volcanology and Geothermal Research* 51: 41-60

Cook, N.D.J. 1988 'Diorites and associated rocks in the Anglem Complex at the Neck, northeastern Stewart Island, New Zealand: an example of magma mingling' *Lithos* 21: 247-262

Eichelberger, J.C. 1980 'Vesiculation of mafic magma during replenishment of silicic magma reservoirs' *Nature* 288: 446-450

Elwell, R.W.D., Skelhorn, R.R. and Drysdall, A.R. 1962 'Net-veining in the diorite of northeast Guernsey, Channel Islands' *Journal of Geology* 70: 215-226

Fernandez, A.N. and Gasquet, D.R. 1994 'Relative rheological evolution of chemically contrasted coeval magmas: example of the Tichka plutonic complex (Morocco)' *Contributions to Mineralogy and Petrology* 116: 316-326

Frost, T.P. and Mahood, G.A. 1987 'Field, chemical, and physical constraints on mafic-felsic magma interaction in the Lamarck Granodiorite, Sierra Nevada, California' *Geological Society of America Bulletin* 99: 272-291

Harper, B.E., Miller, F., Miller, G., Koteas, C., Cates, N.L., Wiebe, R.A., Lazzareschi, D.S. and Cribb, J.W. 2004 'Granites, dynamic magma chamber processes and pluton construction: the Aztec Wash pluton, Eldorado Mountains, Nevada, USA' *Transactions of the Royal Society of Edinburgh: Earth Sciences* 95: 277-295

Hibbard, M.J. 1995 *Petrography to Petrogenesis* Prentice Hall, USA, pp587

Howarth, R.J. 1998 'Improved estimators of uncertainty in proportions, point-counting, and pass-fail test results' *American Journal of Science* 298: 594-607

Huppert, H.E. and Sparks, R.S.J. 1989 'Chilled margins in igneous rocks' *Earth and Planetary Science Letters* 92: 397-405

Kimbrough, D.L., Tulloch, A.J., Coombs, D.S., Landis, C.A., Johnston, M.R. and Mattinson, J.M 1994 'Uranium-lead zircon ages from the Median Tectonic Zone, New Zealand' *New Zealand Journal of Geology and Geophysics* 37: 393-419

Koyaguchi, T. and Kaneko, K. 2000 'Thermal evolution of silicic magma chambers after basalt replenishments' *Transactions of the Royal Society of Edinburgh: Earth Sciences* 91: 47-60

Miller, C.F. and Miller, J.S. 2002 'Contrasting stratified plutons exposed in tilt blocks, Eldorado Mountains, Colorado River Rift, NV, USA' *Lithos* 61: 209-224

Mortimer, N., Tulloch, A.J., Spark, R.N., Walker, N.W., Ladley, E., Allibone, A. and Kimbrough, D.L. 1999 'Overview of the Median Batholith, New Zealand: a new interpretation of the geology of the Median Tectonic Zone and adjacent rocks' *Journal of African Earth Sciences* 29(1): 257-268

Muir, R.J., Ireland, T.R., Weaver, S.D., Bradshaw, J.D., Evans, J.A., Eby, G.N. and Shelley, D. 1998 'Geochronology and geochemistry of a Mesozoic magmatic arc system, Fiordland, New Zealand' *Journal of the Geological Society, London* 155: 1037-1053

Paterson, S.R., Vernon, R.H. and Tobisch, O.T. 1989 'A review of criteria for the identification of magmatic and tectonic foliations in granitoids' *Journal of Structural Geology* 11(3): 349-363

Pitcher, W.S. 1991 'Synplutonic dikes and mafic enclaves' In: Didier, J. and Barbarin, B. (eds) *Enclaves and granite petrology. Developments in Petrology 13* Amsterdam: Elsevier pp 383-391

Price, R.C., Ireland, T.R., Maas, R. and Arculus, R.J. 2006 'SHRIMP ion probe zircon geochronology and Sr and Nd isotope geochemistry for southern Longwood Range and Bluff Peninsula intrusive rocks of Southland, New Zealand' *New Zealand Journal of Geology and Geophysics* 49: 291-303

Smith, J.V. 2000 'Structures of interfaces of mingled magmas, Stewart Island, New Zealand' *Journal of Structural Geology* 22: 123-133

Snyder, D., Crambes, C., Tait, S. and Wiebe, R.A. 1996 'Magma mingling in dikes and sills' *The Journal of Geology* 105: 75-86

Snyder, D. and Tait, S. 1998 'A flow-front instability in viscous gravity currents' *Journal of Fluid Mechanics* 369: 1-21

Streckeisen, A.L. 1973 'Classification and nomenclature recommended by the IUGS subcommission on the systematics of igneous rocks' *Geotimes* 10: 26-31

Tulloch, A.J. and Kimbrough, D.L. 2003 'Paired plutonic belts in convergent margins and the development of high Sr/Y magmatism: Peninsular Ranges batholith of Baja-California and Median batholith of New Zealand' In: Johnson, S.E., Paterson, S.R., Fletcher, J.M., Girty, G.H., Kimbrough, D.L., and Martin-Barajas, A. (eds) 'Tectonic

Evolution of northwestern Mexico and the southwestern USA: Boulder, Colorado, Geological Society of America Special Paper 374, p.275-295

van der Molen, I. and Paterson, M.S. 1979 'Experimental deformation of partially melted granite' *Contributions to Mineralogy and Petrology*, **7**0, 299-318

Vernon, R.H., Etheridge, M.A. and Wall, V.J. 1988 'Shape and microstructure of microgranitoid enclaves: indicators of magma mingling and flow' *Lithos* 22: 1-11

Vigneresse, J L., Barbey, P. and Cuney, M. 1996 'Rheological transitions during partial melting and crystallization with application to felsic magma segregation and transfer' *Journal of Petrology* 37: 1579-1600

Wada, H., Harayama, S. and Yamaguchi, Y. 2004 'Mafic enclaves densely concentrated in the upper part of a vertically zoned felsic magma chamber: The Kurobegawa granitic pluton, Hida Mountain Range, central Japan' *Geological Society of America Bulletin* 116: 788-801

Walker, B.A., Miller, C.F., Claiborne, L.L., Wooden, J.L. and Miller, J.S. 2007 'Geology and geochronology of the Spirit Mountain batholith, southern Nevada: implications for timescales and physical processes of batholith construction' *Journal of Volcanological and Geothermal Research* 167: 239-262

Watters, W.A. 1978 'Diorite and associated intrusive and metamorphic rocks between Port William and Paterson Inlet, Stewart Island, and on Ruapuke Island' *New Zealand Journal of Geology and Geophysics* 21(4): 423-442

White, A.J.R. and Chappell, B.W. 1977 'Ultrametamorphism and granitoids genesis' *Tectonophysics* 43: 7-22

Wiebe, R.A. 1973 ‘Relations between coexisting basaltic and granitic magmas in a composite dike’ *American Journal of Science* 273: 130-151

Wiebe, R.A. 1974 ‘Coexisting intermediate and basic magmas, Ingonish, Cape Breton Island’ *The Journal of Geology* 82: 74-87

Wiebe, R.A. 1993 ‘Basaltic injections into floored silicic magma chambers’ *Eos* 74(1): 1-4

Wiebe, R.A. 1994 ‘Silicic magma chambers as traps for basaltic magmas: the Cadillac Mountain intrusive complex, Mount Desert Island, Maine’ *The Journal of Geology* 102: 423-437

Wiebe, R.A. 1996 ‘Mafic-silicic layered intrusions: the role of basaltic injections on magmatic processes and the evolution of silicic magma chambers’ *Transactions of the Royal Society of Edinburgh: Earth Sciences* 87: 233-242

Wiebe, R.A., Blair, K.D., Hawkins, D.P. and Sabine, C.P. 2002 ‘Mafic injections, in situ hybridization, and crystal accumulation in the Pyramid Peak granite, California’ *GSA Bulletin* 114(7): 909-920

Wiebe, R.A. and Collins, W.J. 1998 ‘Depositional features and stratigraphic sections in granitic plutons: implications for the emplacement and crystallization of granitic magma’ *Journal of Structural Geology* 20(9/10): 1273-1289

Wiebe, R.A., Smith, D., Sturm, M., King, E.M. and Seckler, M.S. 1997 ‘Enclaves in the Cadillac Mountain Granite (Coastal Maine): samples of hybrid magma from the base of the chamber’ *Journal of Petrology* 38: 393-423

Wiebe, R.A. and Ulrich, R. 1997 ‘Origin of composite dikes in the Gouldsboro granite, coastal Maine’ *Lithos* 40: 157-178

Wilson, S. and Barrell, D.J.A 2002 ‘Geological investigations for quarry rock – Oban, Stewart Island’ Client report 2002/126

CHAPTER FOUR

GEOCHEMICAL CONSTRAINTS ON MAFIC-FELSIC INTERACTION

4.1 INTRODUCTION

Whole rock geochemical data have been obtained on the mafic and felsic rocks within the Halfmoon Pluton, Bungaree Intrusives, in order to identify processes responsible for the chemical diversification of the magmas. Interpretation of geochemical trends and isotopic characteristics are used to determine the degree of chemical exchange that has occurred between the mingled mafic and felsic magmas. In addition, inferences are made on the tectonic setting in which the magmas were generated.

4.2 MAJOR AND TRACE ELEMENT GEOCHEMISTRY

Major and trace element concentrations of 100 representative samples were determined by XRF analysis. Fresh rock was crushed into a fine powder using a tungsten-tipped hydraulic ram and a tungsten-carbide ring-mill. Fusion beads for major element analysis were made using a lanthanum oxide flux, and pressed powder pellets were produced for trace element analysis. All samples were analyzed using a Philips PW2400 X-ray Fluorescence Spectrometer at the University of Canterbury. Fusion beads and pressed powder elements were irradiated with a rhodium end-window tube operating at 50kV/55mA and 60kV/46mA, respectively. Standard XRF methods were followed as reported in Weaver *et al*. (1990). A full description of XRF methodology, sample selection and locations, and all major and trace element totals can be found in electronic Appendix 3. Table 4.1 provides a key to the symbols used in all of the following figures, using the rock types as defined in Chapter 3. Representative analytical major and trace element data are displayed in Table 4.2.

Table 4.1. *Key to rock types and symbols used*

Symbol	Rock type
●	Felsic host rock
▲	Mingled mafic sheets and enclaves
▲	Cummingtonite-bearing mafic sheet (Ringaringa)
■	Mixed 'hybrid' rocks
★	Mafic dikes and mafic component of composite dikes
★	Felsic component of composite dikes
★	Felsic dike
◆	Later granite

Selected classification diagrams are displayed in Figure 4.1. Whole-rock major and trace element data are plotted on selected Harker variation diagrams in Figures 4.2A and 4.2B.

The Total Alkali-Silica (TAS) plot of Le Bas *et al*., (1986) gives different rock nomenclature from those obtained using the IUGS classification scheme (Figure 3.22, Chapter 3). As discussed in Chapter 3, all mafic sheets, enclaves and dikes are classified petrographically as micro-diorites due to their abundance of plagioclase and hornblende, and absence of pyroxene. Mafic sheets, enclaves and dikes are however classified as gabbros and monzonites using the TAS classification (Figure 4.1A). Nomenclature of felsic host rocks are also different depending on which plot is used. The lack of alkali feldspar within all but three felsic host rocks classify the felsic host rocks as hornblende leucodiorites, biotite-tonalites and biotite-monzonites using the IUGS classification. This is in contrast to several rocks being classified as monzonites using the TAS diagram. For the purposes of this thesis, the IUGS classification scheme will be used for naming of rock samples.

Table 4.2. Representative Major and Trace element compositions of plutonics from the Halfmoon Pluton

Rock Type:	Mingled Mafics						Composite Dike						
Details:	Sheet	Sheet	Sheet	Sheet	Sheet	Sheet	Enclave	Enclave	Encalve	Felsic	Mafic	Felsic	Mafic
Sample:	EC#10M	EC#B4	EC#6M	TN#37	TN#8	AP#M	RR#K1m	RR#M2	TN#6	RR#FDf	RR#FDm	TN#24f	TN#24m
SiO_2	49.87	49.22	48.32	54.53	58.70	48.07	49.86	54.05	49.88	70.05	52.01	70.78	52.87
TiO_2	1.13	1.00	1.11	1.01	0.88	1.28	1.24	1.09	1.17	0.31	0.95	0.37	1.01
Al_2O_3	17.81	17.95	17.64	18.38	18.08	18.47	19.08	18.67	19.50	15.94	16.72	15.59	17.79
Fe_2O_3	10.33	10.86	11.94	8.42	7.12	11.82	10.93	9.33	10.95	2.00	9.22	2.65	9.03
MnO	0.15	0.21	0.22	0.18	0.14	0.18	0.22	0.17	0.20	0.02	0.17	0.03	0.13
MgO	5.98	5.97	5.93	2.90	2.39	5.55	3.44	2.84	3.65	0.77	6.24	1.14	5.41
CaO	10.44	9.78	10.30	6.51	5.75	9.69	6.35	5.49	7.17	3.90	8.75	3.98	6.86
Na_2O	3.52	3.63	3.32	4.84	4.70	3.44	4.74	5.20	4.77	4.56	3.54	4.31	3.76
K_2O	0.46	0.64	0.39	1.48	1.53	0.52	1.75	1.77	1.48	0.84	1.04	0.94	1.98
P_2O_5	0.23	0.21	0.19	0.57	0.52	0.27	0.65	0.53	0.59	0.11	0.21	0.11	0.28
LOI	0.19	0.61	0.66	0.45	0.56	0.91	0.79	0.95	0.57	0.24	1.34	0.10	0.38
Total	100.10	100.08	100.01	99.26	100.37	100.21	99.09	100.10	99.92	98.74	100.19	99.99	99.50
Ba	180	155	134	451	571	187	798	1084	721	434	259	371	627
Rb	9	25	10	45	49	16	55	56	55	39	33	27	56
Sr	703	625	538	923	820	619	795	657	771	712	521	696	663
Pb	7	7	6	11	11	7	10	13	11	10	7	9	10
Zr	53	56	66	85	86	34	97	94	127	137	64	120	68
Nb	3	3	3	5	4	4	4	3	4	3	3	3	4
Y	11	22	21	26	25	19	27	23	31	4	14	3	17
V	338	283	347	53	43	385	89	75	142	34	239	51	219
Cr	103	94	35	-	-	73	-	-	-	-	276	7	52
Ni	23	17	16	-	-	20	-	-	-	5	58	12	67
Zn	93	114	114	76	67	101	108	92	122	21	95	27	96
La	-	-	-	17	9	-	16	16	11	21	8	15	12
Ce	27	24	25	40	33	20	65	35	42	42	27	25	49
Nd	18	18	-	18	15	18	25	23	18	<10	23	<10	<10
Ga	21	20	21	18	17	21	21	18	22	16	19	15	20

Data are normalized to 100% anhydrous. Major elements are given in wt% and trace elements in ppm. LOI values were calcualted by weight difference.
Dashed lines represent values below the detection limit.

Table 4.2. Continued

Rock Type:	Felsic Host								Mafic Dike		Later Granite			
Details:														
Sample:	EC#9H	EC#6C	EC#3g	RR#H1	RR#H6	TN#35	TN#31	AP#G	TN#12	EC#10D	BB#G2	UI#G1	FP#G1	LB#G1
SiO_2	56.64	57.98	61.94	65.41	75.67	73.65	70.51	52.68	50.35	49.51	69.50	76.60	77.05	70.51
TiO_2	0.89	0.40	0.50	0.57	0.24	0.33	0.48	0.76	1.34	1.18	0.37	0.17	0.14	0.26
Al_2O_3	21.11	22.41	20.57	17.68	12.75	14.18	15.29	22.57	18.16	17.45	15.43	12.82	12.38	15.80
Fe_2O_3	5.34	3.92	3.76	3.82	1.89	2.25	3.39	6.61	11.06	9.63	2.55	1.16	1.09	1.85
MnO	0.08	0.05	0.05	0.06	0.02	0.03	0.04	0.07	0.14	0.16	0.04	0.01	0.02	0.02
MgO	1.90	1.16	1.24	1.19	0.39	0.63	0.95	2.30	4.58	6.02	0.71	0.24	0.17	0.55
CaO	7.36	7.29	5.14	4.17	1.63	3.02	3.53	7.34	8.08	9.41	1.74	1.07	0.73	2.32
Na_2O	5.23	5.86	5.72	5.23	3.73	4.28	4.60	5.20	3.71	3.87	4.08	3.48	3.29	3.87
K_2O	0.78	0.58	1.35	1.22	3.05	1.32	1.08	1.29	0.85	0.85	4.52	4.33	4.86	4.14
P_2O_5	0.19	0.14	0.20	0.17	0.06	0.07	0.15	0.27	0.37	0.27	0.08	0.02	0.03	0.06
LOI	0.69	0.48	-0.19	0.57	0.42	-0.20	0.47	0.56	1.81	1.74	1.13	0.37	0.42	0.57
Total	100.21	100.27	100.29	100.10	99.84	99.55	100.48	99.65	100.44	100.09	100.15	100.28	100.17	99.95
Ba	389	273	679	614	2940	556	524	697	361	293	529	1225	522	1486
Rb	32	14	39	36	45	41	38	42	30	33	205	63	104	81
Sr	908	895	859	793	384	602	632	1001	715	679	260	225	117	427
Pb	11	12	13	14	16	12	11	8	5	11	30	24	27	26
Zr	203	193	176	209	117	146	203	239	80	91	175	82	67	112
Nb	3	2	3	2	-	3	3	3	3	4	4	-	-	3
Y	12	9	8	9	2	3	7	9	17	17	14	5	5	5
V	127	85	55	41	15	21	35	131	327	285	42	14	12	35
Cr	6	5	-	-	-	-	-	8	18	238	-	-	4	-
Ni	-	4	-	-	4	4	3	6	11	37	5	-	-	5
Zn	57	38	47	38	16	22	33	72	84	91	37	12	16	24
La	8	15	7	14	13	24	18	13	-	-	24	8	10	19
Ce	23	36	27	20	21	39	36	35	22	31	43	13	16	49
Nd	-	-	-	-	-	20	-	21	19	27	18	-	-	-
Ga	21	22	20	17	10	12	15	25	22	20	18	11	11	15

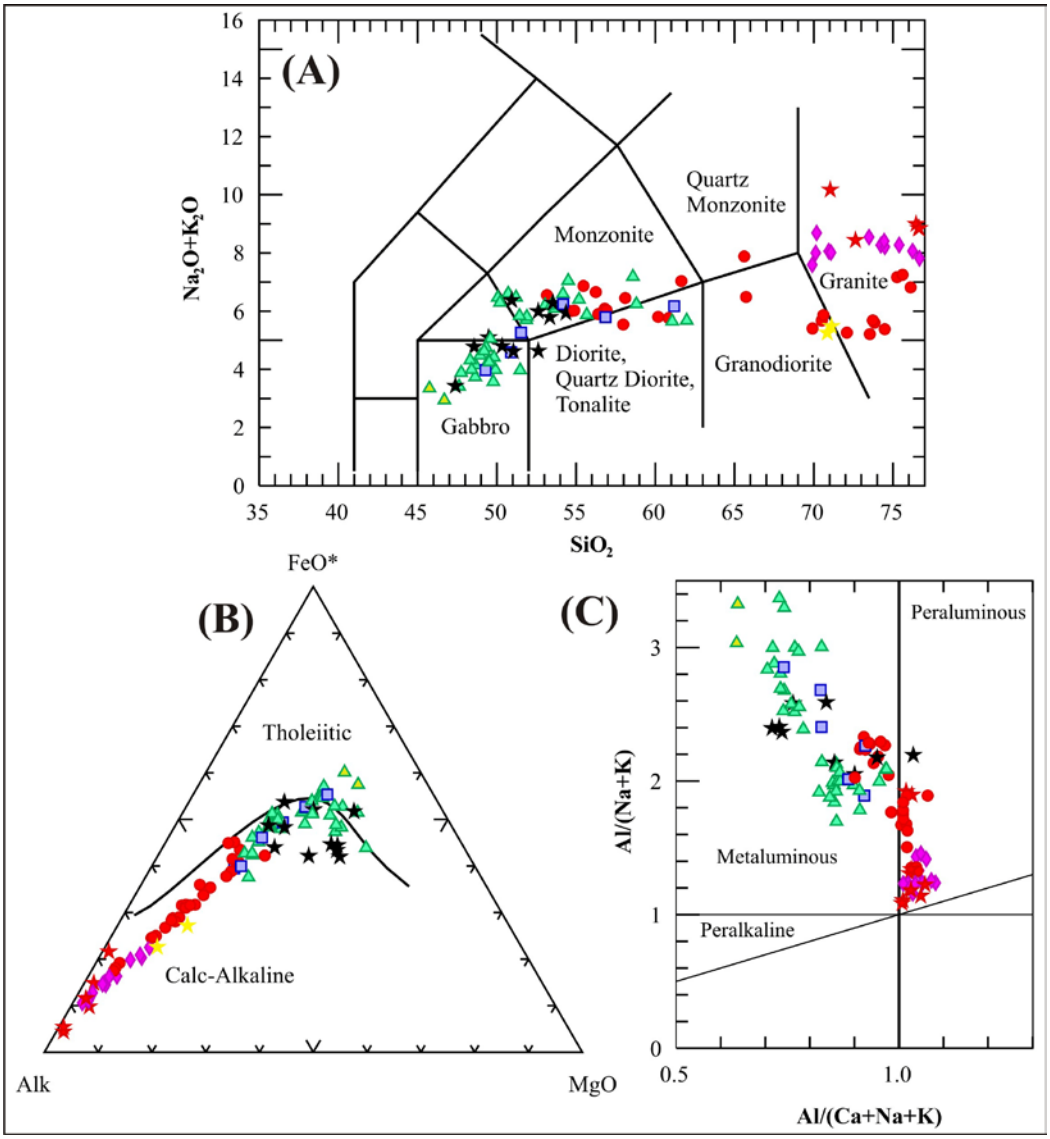

Figure 4.1. Classification diagrams applied to the Bungaree Intrusives (A) Total Alkalis vs. Silica diagram with subdivisions from Le Bas *et al*. (1986) (B) AFM diagram after Irvine & Baragar (1971) (C) Variation of Al/(Na + K) vs. Al/(Ca + Na + K) (after Maniar & Piccoli, 1989; Pearce *et al*., 1984); divisions based on Shand index.

The AFM plot of Irvine and Baragar (1971) displays a calc-alkaline trend for all rocks, consistent with their generation in an island-arc, subduction-related setting (Figure 4.1B). Classification using the Aluminium Saturation Index (ASI) indicates that the felsic host rocks towards the top of the chamber (RR and TN) are weakly peraluminous with ASI <1.1, whereas felsic host rocks towards the base of the chamber (AP and EC) are metaluminous (Figure 4.1C). All mafic sheets, enclaves and dikes are metaluminous. Mafic and felsic rocks appear to define separate linear trends. The felsic host rocks are

medium-grained, with compositions ranging from a hornblende-leucodiorite at the inferred base of the chamber (AP and EC), to a biotite-tonalite and granite (RR), and finally a biotite-tonalite towards the inferred top of the chamber (TN).

MORB-normalized trace element abundance patterns (Figure 4.2) indicate almost identical geochemical characteristics for the felsic host rocks, mingled mafic sheets and enclaves, and cross-cutting mafic and composite dikes, suggesting that they are probably cogenetic. Fluids generated at convergent margins display enrichments in large ion lithophile elements (LILE) and Pb compared with high field strength elements (HFSE) (Hawkesworth *et al*., 1993; Miller *et al*., 1994; Rollinson, 1994). An overall trend of LILE-enrichment and HFS-depletion is evident in Figures 4.2A – 4.2C, characteristic of a subduction signature. Furthermore, an island-arc subduction setting can be inferred based on depletions in Nb and Ti (Spandler *et al*., 2004; Kessel *et al*., 2005). The felsic component of composite dikes also matches the trends displayed by these mafic and felsic rocks, and not the later more evolved granite intrusions. These granite intrusions are more enriched in LILE compared with the rest of the rocks within the Halfmoon Pluton, in particular K and Rb, which may indicate either crustal contamination or that they are more fractionated melts. Significant troughs in P and Ti are also apparent, indicative of highly fractionated compositions.

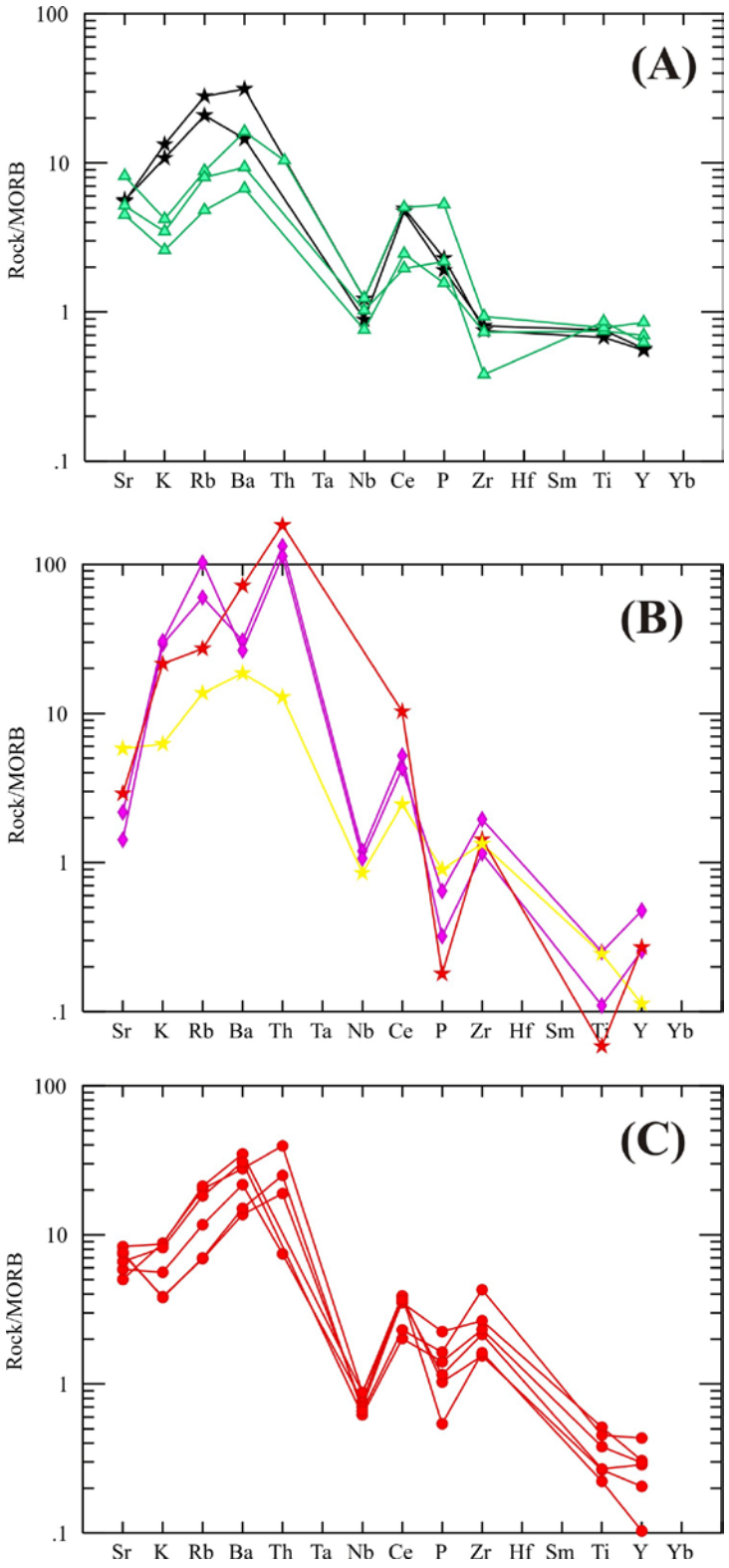

Figure 4.2. MORB-normalized trace element abundance patterns (Pearce, 1984) shown for representative rocks of (A) Mafic sheets and enclaves, mafic dikes and mafic component of composite dikes (B) Later granites, felsic component of composite dikes (C) Felsic host rocks.

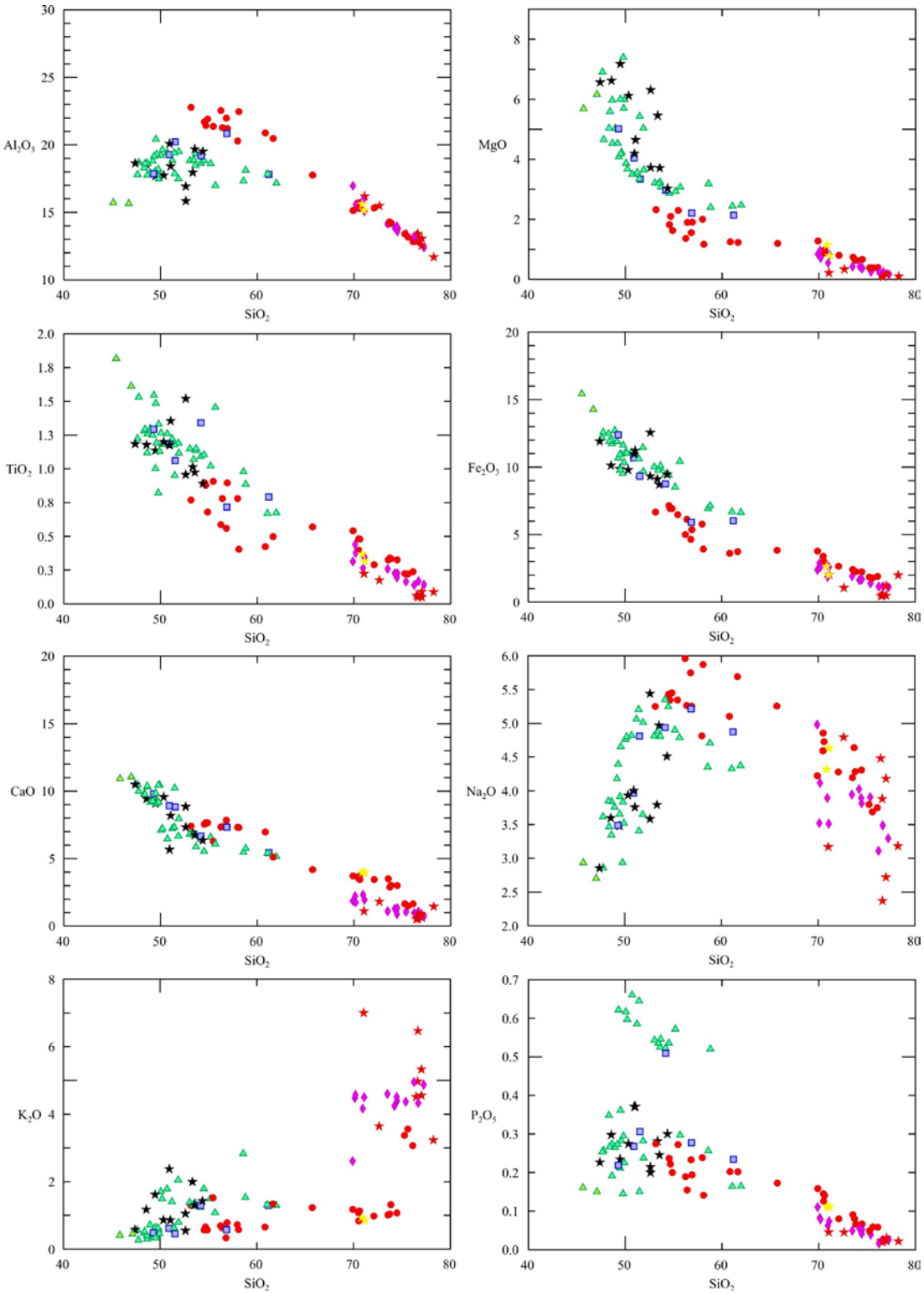

Figure 4.3(A). Harker diagrams of selected major elements for the felsic host magma, the mingled mafic sheets and enclaves, samples of mixed 'hybrid' magma, mafic dikes, felsic dikes, and composite dikes.

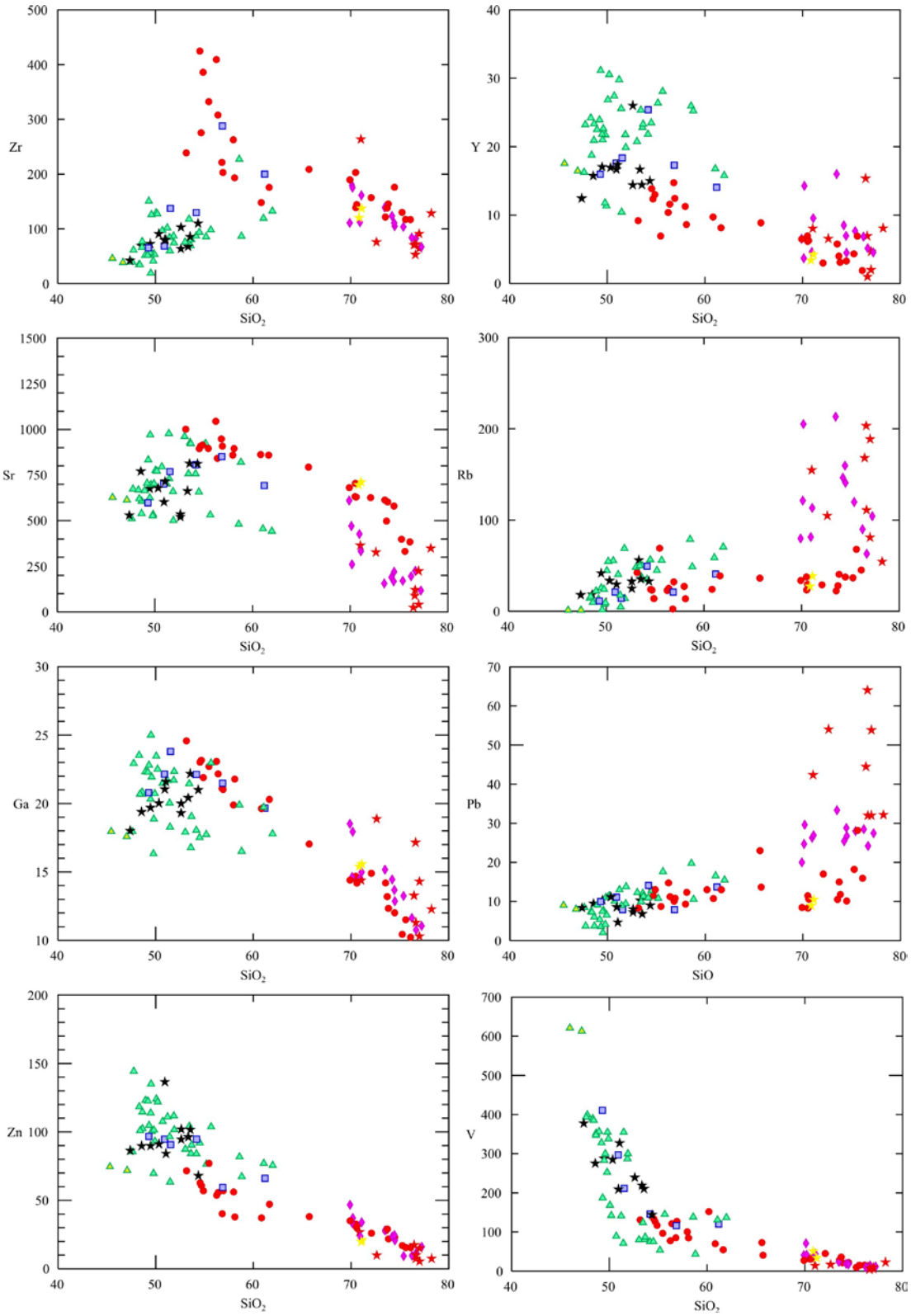

Figure 4.3(B). Harker diagram of selected trace elements for the same rocks as those plotted in Figure 3.2(B).

4.2.1 FELSIC HOST ROCKS

The felsic host rocks range in SiO_2 composition from ~53% at the inferred base of the chamber (AP) to 76% at the inferred top (TN). Major element plots typically define curvilinear arrays (Figure 4.3A). With the exception of K_2O and Na_2O, all other major elements display decreasing concentrations with increasing fractionation and height in the chamber. High values of K_2O occur in three of the felsic host samples, which are the only rocks containing alkali feldspar. Al_2O_3 abundance within the host decreases with increasing height in the chamber due largely to the early crystallization of plagioclase in the sequence, depleting the host melt in Al. CaO content within the host also decreases with increasing height in the chamber. The depletion in Ca, and the concordant rise in K coincide in the mafic phase changing from hornblende to biotite at a high level in the chamber.

Trace element plots for the host rocks also define curvilinear trends. Zr, Y, Sr, and Ga show decreases in concentration with increasing SiO_2 content. Sr decreases from the base towards the top of the chamber, which is consistent with the early crystallization and accumulation of plagioclase at AP and EC. Low Rb concentrations within rocks at AP and EC suggest that the felsic host rocks contained relatively little trapped liquid, further supporting their cumulate origin. Zr displays a large decrease in concentration with increasing SiO_2 contents probably as a result of zircon accumulation at the base of the chamber. Decreasing Zr concentrations correspond with a change in the morphology of zircon crystals, with smaller crystals forming in rocks depleted in Zr. The decrease in Zr is not linear, and the significance of this trend will be discussed in Section 4.4. Gaps within the trends of the host rocks are probably due to sampling bias as there was a paucity of locations between Ringaringa and The Neck (mid-upper part of the chamber) due to large areas without outcrops suitable for geochemical sampling.

The major and trace element variation within the felsic host does not follow a simple linear trend from the base towards the top. Small variations in major and trace element abundances in the host leucodiorites at AP and EC can be attributed to the presence of trapped liquid within these cumulate rocks, combined with the effects of minor fractional

crystallization and limited mixing with the intruding mafic sheets and enclaves, similar to variable host rock compositions within the composite Tottabetsu Igneous Complex (Kamiyama *et al*., 2007). Though SiO_2 concentration remains fairly constant between Ringaringa and The Neck, the concentrations of other major and trace elements show reverse trends, with felsic rocks at The Neck being depleted in Ca, Al, Ti and Sr relative to those at Ringaringa. These reverse trends can be explained by the effect of mafic magma replenishments on the composition of the felsic host, which may have interrupted fractionation towards more felsic compositions. This same trend is observed in the Kameruka Pluton, where mafic magma replenishments caused the composition of the host magma to vary back and forth (Collins *et al*., 2006).

4.2.2 MAFIC SHEETS AND ENCLAVES

Mafic sheets and enclaves throughout the chamber have a restricted SiO_2 composition, ranging from 48% at the base to 55% at the top. Major element trends are not as well defined as those for the felsic host, however most show linear trends of decreasing concentrations with increasing SiO_2 and increasing height in the chamber. Na_2O concentrations increase with increasing SiO_2 until ~52% SiO_2 there after Na_2O decreases. This is correlated with a change in the composition of the plagioclase crystallizing, which becomes less Ca-rich and more Na-rich with higher SiO_2 contents. Al_2O_3 concentration remains uniform throughout the sequence. Mafic enclaves from RR and TN are all enriched in Na_2O, K_2O, P_2O_5, Ce, Y, Rb and Ba relative to mafic sheets from AP, EC and TN. These enriched enclaves also have higher modal abundances of apatite (between 1-2%) and biotite. Zr, Rb, and Pb all show small increases with increasing height in the chamber. Sr concentrations increase from the inferred base of the chamber at Ackers Point to Ringaringa, but are lower at The Neck. Thick (>5m) mafic sheets and dikes all seem to show a depletion in Y relative to Y contents in mafic enclaves and thin mafic sheets.

The cummingtonite-bearing mafic sheet at Ringaringa (see Chapter 3 for description) is more primitive in composition than all the other mafic sheets, enclaves and dikes within the Halfmoon Pluton. This mafic sheet shows compositional and

mineralogical grading, becoming more fine-grained and silicic towards the top (south). It is enriched in CaO, TiO_2, Fe_2O_3, MgO and V, and depleted in Al_2O_3, Na_2O, K_2O, Zr, Sr, Zn and Y, relative to all the mafic sheets, enclaves and dikes. The unique chemistry of this mafic sheet suggests that it may represent a magma from a different source.

4.2.3 Mixed 'Hybrid' Rocks

As discussed in Chapter 3, mixed 'hybrid' rocks were classified on their appearance in the field and petrographically. As shown in Figures 4.3A, 4.3B and 4.4, these hybrid rocks have compositions intermediate between the enclosing felsic host and adjacent mafic inclusions, strongly supporting the interpretation that they are derived from mixing between the mafic and felsic rocks.

4.2.4 Mafic, Composite and Felsic Dikes

Mafic dikes and mafic components of composite dikes have chemistry indistinguishable from that of the mafic sheets and enclaves, suggesting they are derived from the same primitive source. The felsic component of the composite dikes appears to be almost identical in whole rock composition to the felsic host rocks but the isotopic compositions are different in each case (see section 4.3). This felsic material is quite different in composition from the late-stage granite dikes and larger granite intrusions, which are highly fractionated, with high SiO_2 compositions ranging between 70-80%. The later granitic intrusions are enriched in K_2O relative to the rest of the Halfmoon Pluton, with ~4.5 wt% K_2O compared with <1.5 wt% for almost all of the felsic host samples. These granitic dikes and larger intrusive bodies represent later cross-cutting magmas that intruded the Bungaree Intrusives after they were completely crystallized.

4.2.5 Comparison Between Felsic and Mafic Rocks

Figure 4.4 shows the variation in composition vs. stratigraphic height. Initially, the compositional contrast between the mafic and felsic rocks is quite small, with the host felsic rock between ~53 and 62%% SiO_2, and the mingled mafic rocks ranging between 49 and 51% SiO_2 at Ackers Point and Evening Cove. With fractionation of the felsic host, this compositional gap becomes much greater as the felsic host rocks fractionate,

and the mafic sheets and enclaves remain fairly uniform in SiO_2. A large change occurs at Ringaringa where the composition of the host changes from 65% SiO_2 to >75% SiO_2. Mafic sheets and enclaves within this section have an average SiO_2 concentration of 55%. The composition of the host rock from this point appears to remain relatively constant, with felsic host rocks at The Neck ranging between 70-75% SiO_2, and mafic rock concentrations ranging between 50-55% SiO_2.

Variations in the CaO contents within both the felsic host rocks and the mafic rocks mimic each other, with both displaying a large drop in concentration at Ringaringa. This decrease in CaO-content coincides with the disappearance of hornblende as the major mafic phase, replaced by the more abundant biotite. Al_2O_3 contents within the felsic host also decrease substantially at Ringaringa, however the Al_2O_3 content in the mafic rocks remains uniform throughout the sequence. The depletion of CaO and Al_2O_3 (both major constituents of plagioclase) in the felsic host rocks probably reflects crystallization of plagioclase to form cumulates at the base of the chamber (AP and EC). The removal of plagioclase from the melt towards the base of the chamber is further supported by a similar trend exhibited in the Sr-content of the felsic host rocks, which decreases sharply at Ringaringa. Sr-concentrations in the mafic rocks increase at Ringaringa, coinciding with a decrease in CaO and an increase in K_2O and Na_2O. This change in mafic composition is inferred to represent a change in the composition of plagioclase, becoming more sodic and less calcic with height in the chamber. The sharp increase in K_2O at Ringaringa coincides with the first appearance of alkali feldspar in the sequence, and also biotite replacing hornblende as the dominant mafic phase. The reverse pattern is shown in Na_2O, with a decrease in Na_2O concentration in the felsic rocks at Ringaringa and The Neck. Na_2O concentrations within the mafic rocks increase from the inferred base (AP and EC) to Ringaringa, before fluctuating at The Neck. This variation in Na_2O concentration can be explained by fractionation of the mafic magma from the base towards the top of the sequence. Two mafic sheets analyzed from The Neck have similar Na_2O concentrations to the mafic sheets at Evening Cove and Ackers Point, and probably represents primitive or unfractionated mafic magmas that were injected into the sequence.

The compositions of mafic dikes and mafic components of felsic dikes are uniform throughout the sequence, and have compositions very similar to those in the mafic sheets towards the base of the chamber. They are likely to represent the parent magma from which the mafic sheets and enclaves originated.

Mixed ‘hybrid’ samples display compositions that fall between those of the mafic and felsic rocks adjacent to them. The felsic component of composite dikes is identical, and seems to be slightly less evolved than the felsic host rocks in which they intrude. This suggests that the felsic material may have been derived from re-melting and remobilization of felsic rocks from the less fractionated lower portions of the chamber.

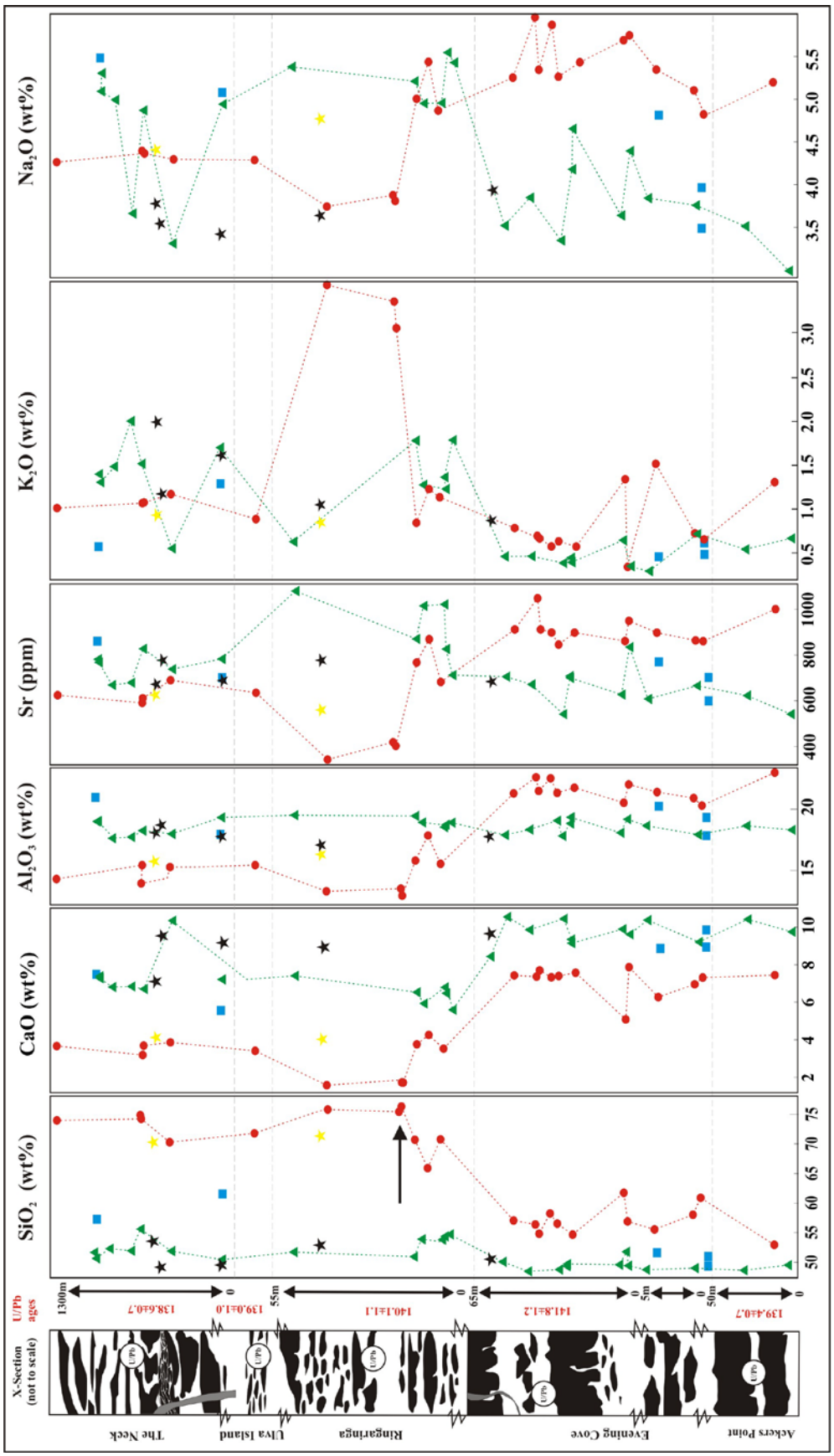

Figure 4.4 Composition vs. stratigraphic height. Arrow indicates the incoming of alkali feldspar and muscovite at ~75% SiO_2. U/Pb SHRIMP ages are given for each of the locations. Symbols are as follows; green triangles = mingled mafic sheets and enclaves; red circles = intermediate-felsic host rocks; blue squares = mixed 'hybrid' rocks; black stars = mafic dikes/mafic component of composite dikes; yellow stars = felsic component of composite dikes.

4.3 RARE EARTH ELEMENTS

Fourteen samples representing both mafic and host rocks from within the Halfmoon Pluton were analysed for rare earth elements (REE). Whole rock samples were trimmed of any weathered material, cleaned in a sonic bath of distilled water for 10 minutes to remove any surface contaminants, and then placed in an oven at 100°C for 24 hours. Dry rock samples were then milled in a Frisch Planetary agate mill. Glass disks were made using a flux of lithium tetraborate ($Li_2B_4O_7$) and ammonium nitrate (NH_4NO_3) as an oxidizer. All REE, Nb, Ta, Hf, Ba, Y, Th, U and Pb were determined by LA-ICPMS using a Cetac LSX200+ laser ablation system at Michigan State University. Trace element data reduction was done using MassLynx software. Element concentrations in the samples were calculated based on a linear regression model using well-characterized standards. Precision and accuracy of the LA-ICPMS chemical analyses are reported in Vogel *et al*., (2006).

Rare earth element (REE) data for the 14 samples analysed are displayed in Table 4.3. Chondrite-normalised REE diagrams are displayed in Figure 4.5. REE trends for the mafic sheets and enclaves (Figure 4.5A) are similar, with moderate enrichment in LREE relative to HREE and no negative Eu anomaly (Eu/Eu* ranges between 0.8 and 1.1). Absolute REE abundances between samples are variable, with mafic sheets and enclaves from Ackers Point and Evening Cove containing lower REE abundances than mafic sheets and enclaves at Ringaringa and The Neck. A mafic dike analysed from The Neck (TN#16) displays a similar, though slightly flatter LREE enriched pattern as the mafic sheets and enclaves within the Halfmoon Pluton. REE abundances within the mafic sheets and enclaves show a negative correlation with MgO, with decreasing MgO concentrations correlated with increasing REE abundances (Figure 4.6C). From the base (AP and EC) towards the top (RR and TN) of the chamber there is however no evidence within the mafic sheets and enclaves of a correlation between MgO and REE abundance; the mafic sheet from The Neck has lower abundances of MgO and REE than a mafic enclaves from Ringaringa.

Table 4.3. Rare earth element analyses for Halfmoon Pluton

Rock Type:	Mingled Mafics							Hybrid	Felsic Host						Mafic Dike
Details:	Sheet	Sheet	Enclave	Enclave	Sheet	Enclave	Sheet								
Sample:	AP#H	EC#8M	RR#K1m	TN#37	TN#16	EC#3b	EC#B2	TN#25	EC#B5	EC#9H	EC#6c	RR#K1h	RR#G1	TN#35	TN#26
Ba	190.2	176.9	830.8	432.2	159.0	202.5	138.0	370.5	259.2	346.6	291.3	440.3	1988.7	453.6	264.1
La	5.3	10.8	24.1	19.5	14.9	8.1	9.6	18.0	10.7	8.5	7.9	6.1	7.4	5.5	11.4
Ce	11.8	26.6	54.7	45.9	30.3	20.8	23.1	40.1	26.7	19.7	18.0	12.4	13.3	10.5	25.4
Pr	1.6	3.9	7.5	6.0	3.7	2.6	3.2	4.8	3.1	2.4	1.9	1.4	1.3	1.1	3.3
Nd	7.7	19.2	34.3	26.5	15.7	10.2	15.1	20.4	11.5	9.5	7.0	5.3	4.7	4.0	15.2
Sm	2.0	4.7	7.6	5.8	3.2	3.5	3.8	4.2	2.9	3.0	2.0	1.5	1.3	1.2	3.6
Eu	0.8	1.4	1.9	1.9	1.0	1.1	1.2	1.3	1.1	0.8	0.9	0.9	0.8	0.8	1.3
Gd	2.5	4.4	6.3	5.2	3.0	2.6	3.8	3.9	2.7	2.4	2.0	1.7	1.6	1.5	3.6
Tb	0.3	0.7	1.0	0.8	0.4	0.4	0.6	0.5	0.4	0.2	0.2	0.2	0.1	0.1	0.5
Y	12.7	25.0	30.6	27.3	11.0	12.0	21.8	17.3	10.6	9.2	6.3	4.4	4.1	4.2	17.4
Dy	2.2	4.3	5.8	4.8	2.1	2.1	3.6	2.9	1.8	1.5	1.1	0.8	0.7	0.7	3.1
Ho	0.5	0.9	1.2	1.0	0.4	0.4	0.8	0.6	0.4	0.2	0.3	0.2	0.2	0.2	0.7
Er	1.3	2.4	3.1	2.8	1.0	0.7	2.2	1.7	1.2	0.6	0.6	0.4	0.3	0.4	1.7
Yb	1.3	2.2	2.9	2.8	1.0	0.8	2.1	1.8	1.4	0.6	0.6	0.5	0.5	0.6	1.6
Lu	0.2	0.3	0.4	0.4	0.1	0.1	0.3	0.3	0.2	0.1	0.1	0.1	0.1	0.1	0.2
V	220.9	363.2	80.9	54.5	305.8	128.1	319.1	149.1	144.4	169.9	118.7	36.1	20.6	23.4	241.6
Cr	143.8	14.3	1.3	0.9	25.5	13.8	20.4	8.3	10.4	12.4	8.2	3.5	2.9	6.1	133.0
Nb	1.0	2.7	3.9	4.8	1.5	4.8	2.3	5.5	3.6	4.4	1.6	2.0	2.5	2.3	2.3
Hf	1.2	1.3	2.6	2.6	1.7	5.1	2.0	7.3	7.9	4.3	3.6	3.9	4.8	5.5	2.1
Ta	0.1	0.1	0.4	0.4	0.1	0.1	0.1	0.5	0.2	0.2	0.2	0.5	4.6	0.7	0.2
Pb	5.1	5.3	10.8	11.7	7.7	17.3	4.3	16.1	17.1	17.9	25.3	16.2	41.0	19.0	9.3
Th	1.7	0.5	1.7	3.5	9.9	1.7	0.4	9.7	5.6	5.3	2.6	2.9	3.6	4.9	1.8
U	0.4	0.2	0.7	0.9	1.7	1.7	0.1	3.2	2.8	2.3	1.3	1.0	1.3	1.5	0.6
Eu*	11.6	25.9	40.3	31.3	16.4	17.6	21.1	21.8	15.2	13.5	9.8	7.3	6.4	6.1	19.8
Eu/Eu*	1.1	1.0	0.8	1.0	1.0	1.1	1.0	1.0	1.2	1.1	1.5	2.1	2.3	2.2	1.1

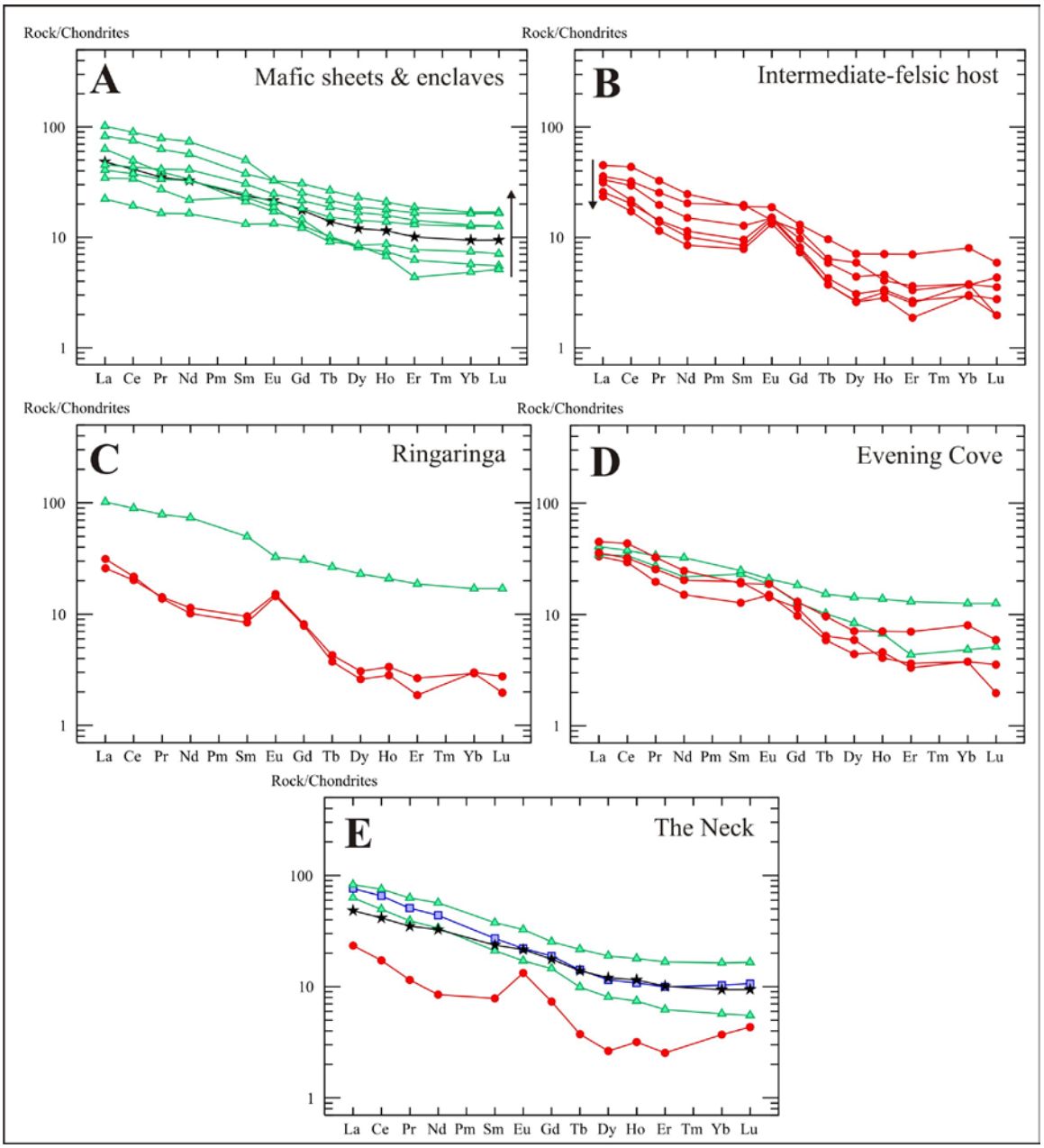

Figure 4.5. Rare earth element patterns for the Halfmoon Pluton. Red circles represent host samples, green triangles represent mingled mafic sheets/enclaves, black stars represent cross-cutting mafic dikes, and blue squares represent mixed 'hybrid' samples (A) All mafic sheet and enclave samples with arrow indicating evolutionary trend (B) All intermediate-felsic host samples with arrow indicating fractionation trend (C) Mafic enclave and granite host rock from Ringaringa (D) Mafic sheets/enclave and leucodiorite host rock from Evening Cove (E) Mafic sheet/enclave, tonalite host, mafic dike and hybrid rock from The Neck.

Dy/Yb ratios decrease with increasing SiO_2 contents, however like overall REE abundances this trend is not correlated stratigraphically.

REE trends for the intermediate-felsic host rocks also show LREE enrichment relative to HREE, however the trend is steeper with higher LREE concentrations relative to HREE (Figure 4.5B). MREE and HREE show flat trends in host rock samples. Host samples from towards the inferred top of the chamber (RR and TN) contain lower abundances of REE than host samples from Evening Cove towards the inferred base of the chamber. Host rock samples show positive Eu anomalies, with small anomalies (Eu/Eu* = 1 – 1.5) from Evening Cove samples, and more prominent anomalies (Eu/Eu* = 2 – 2.3) from Ringaringa and The Neck samples. Eu/Eu* values increase with increasing SiO_2 (Figure 4.6A) and increase with decreasing P_2O_5 (Figure 4.6D). Though Dy/Yb ratios display a slight scatter, overall they decrease with increasing SiO_2, consistent with hornblende fractionation (Davidson *et al*. 2007) (Figure 4.6B).

REE abundances of mafic sheets/enclaves and the enclosing leucodiorite host at Evening Cove are similar (Figure 4.5D), with host rock samples having slightly smaller REE abundances than the mafic sheets and enclaves. Mafic samples from Ringaringa and The Neck display much higher REE abundances than the felsic host rock that they intrude (Figures 4.5C and 4.5D). This trend is also observed within the whole-rock major and trace element abundances, with mafic and intermediate host rocks at Evening Cove having very similar SiO_2 contents, whereas there is a much larger compositional contrast between mafic and felsic host rocks at Ringaringa and The Neck.

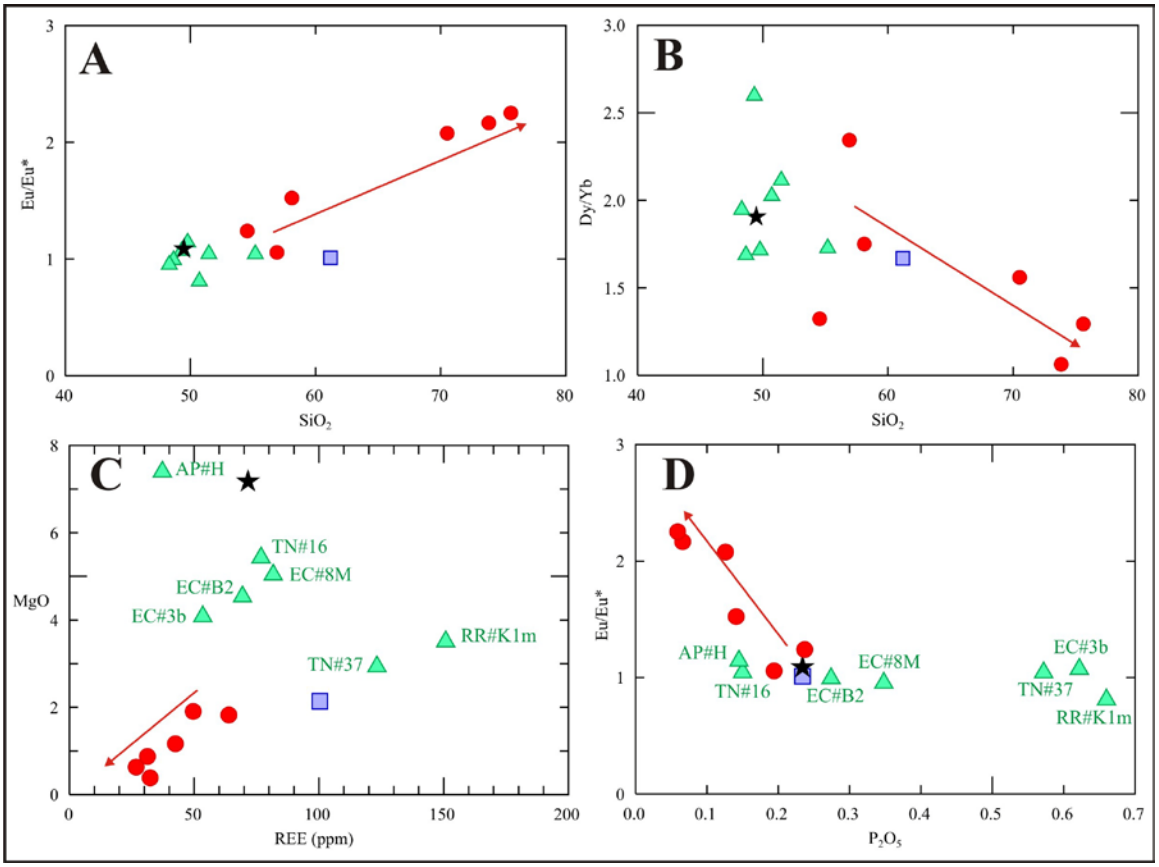

Figure 4.6. REE variation diagrams for mafic and felsic rocks within the Halfmoon Pluton (A) SiO_2 vs. Eu/Eu* (B) SiO_2 vs. Dy/Yb (C) REE vs. MgO (D) P_2O_5 vs. Eu/Eu*

4.4 Isotopic Characteristics

$^{87}Sr/^{86}Sr$ and $^{143}Nd/^{144}Nd$ isotope ratios for 14 selected samples were measured by multi-collector inductively coupled plasma mass spectrometry (MC-ICPMS) at Victoria University of Wellington. Samples for Sr isotopic analysis were digested using HF-HNO_3 techniques and Sr separated using Sr-spec Eichrom resin. Sr mass spectrometric techniques used are a modified version of those described in detail by Waight *et al.*, (2002). Samples for Nd isotopic analysis were digested using flux-fusion techniques (Ulfbeck et al., 2003) and Nd separated using conventional cation exchange and Ln-spec Eichrom resins. Rb/Sr and Sm/Nd ratios were analysed by ICP-MS on aliquots of bulk digestions of samples taken prior to chemical separation of Sr and Nd in order that age corrections could be carried out. Isotopic ratios were corrected for instrumental mass bias using the exponential law ($^{86}Sr/^{88}Sr$ = 0.1994; $^{146}Nd/^{144}Nd$ = 0.7219) and normalized to

$^{87}Sr/^{86}Sr$ = 0.710248 (SRM987) and $^{143}Nd/^{144}Nd$ = 0.5128980 (BHVO-2). External reproducibility of $^{87}Sr/^{86}Sr$ and $^{143}Nd/^{144}Nd$ ratios are better than ±0.00002.

$^{87}Sr/^{86}Sr$ and $^{143}Nd/^{144}Nd$ isotope ratios from the Halfmoon Pluton are displayed in Figure 4.7 and listed in Table 4.4 and electronic Appendix 4. Initial $^{87}Sr/^{86}Sr$ values for all felsic host, mafic sheets and enclaves, composite dikes and mafic dikes occupy a very restricted range between 0.70379-0.70427. εNd values display a slightly less restricted range, between +3.5 and +1.9. No significant crustal component can be inferred from the isotopic variation. The limited variation in initial isotopic compositions can be ascribed to small variations in mantle and crustal components such as aqueous fluids derived from the subducted slab, and minor crustal contamination. Another possible explanation for the limited strontium isotope ratios and a spread of neodymium ratios is diffusive exchange between more and less primitive materials at depth, either contrasting rocks in the source region or mafic and felsic magmas during ascent (Bachl *et al*., 2001). The isotopic values confirm that the mingled mafic and felsic magmas are genetically related, having come from the same primitive source which is depleted relative to Bulk Earth. The Halfmoon Pluton display primitive initial ratios, consistent with only a limited interval between the time of extraction from the mantle and crystallization. The field for plutonics from the Darran Suite (Muir *et al*., 1998) is also plotted on Figure 4.7, and indicates that the Halfmoon Pluton has a slightly more evolved isotopic signature. Four other samples from the Halfmoon Pluton were analyzed for Sr-isotopes only, and display almost identical $^{87}Sr/^{86}Sr$ initial ratios to those presented in Figure 4.7, ranging between 0.70387-0.70396 (see electronic Appendix 4). Included within these is a mixed 'hybrid' sample (TN#25) which has an $^{87}Sr/^{86}Sr$ initial ratio of 0.70396.

Two samples from later cross-cutting granite bodies have slightly more elevated initial $^{87}Sr/^{86}Sr$ values of 0.70404 and 0.70457, and εNd values of +5.0 and +1.5 respectively. These granites are interpreted to have been derived from a distinct source of a more fractionated composition and involving some degree of crustal contamination. They are not petrogenetically related in any simple way to the Halfmoon Pluton magmas.

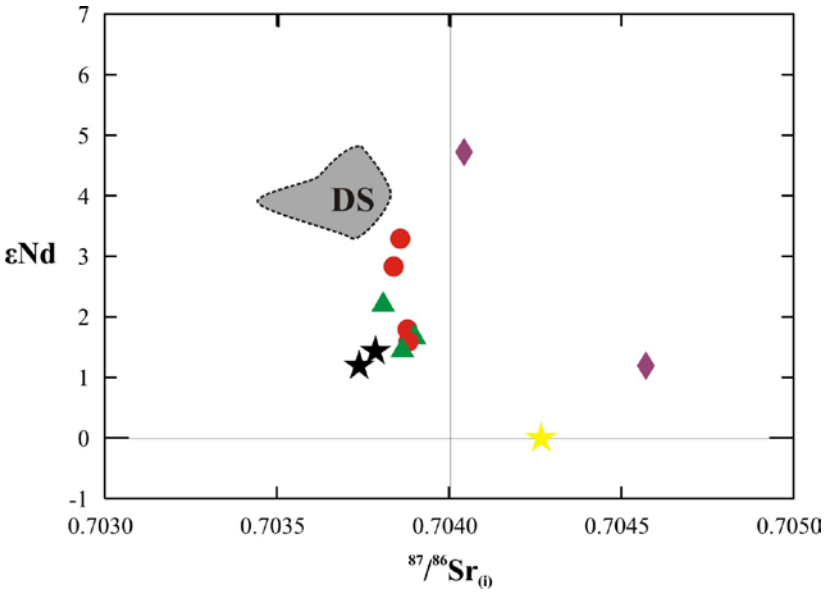

Figure 4.7. εNd (140Ma) vs. initial $^{87}Sr/^{86}Sr$ for the Halfmoon Pluton. Darran Suite field (DS) from Muir *et al*. (1998).

As discussed previously, the felsic component of the composite dikes that cross-cut the chamber have similar whole-rock compositions to the felsic host rocks that enclose them, however their Sr-Nd isotopic signature is more comparable with the later cross-cutting granites. This felsic material is inferred to represent granitic dikes from a more evolved source, which was subsequently incorporated into a composite dike along with intruding mafic dikes.

Figure 4.8 represents a simplified map of the north eastern section of the Halfmoon Pluton, the Bungaree Intrusives and other adjacent plutonic bodies. Plutonic rocks that share similar isotopic characteristics to the Halfmoon Pluton include the younger North Arm Pluton which rests immediately above the inferred top of the Halfmoon Pluton, and a slightly older (~145 Ma) basalt-andesite dike that cross-cuts the older (~175 Ma) composite diorite at Lee Bay that is included within the Bungaree Intrusives, but is separate in time and space from the ~140 Ma Halfmoon Pluton that is the focus of this study. This basalt-andesite dike is identical in isotopic composition to the Darran Suite. Allibone and Tulloch (2004) suggested that the Saddle Pluton (see Figure 3.2, Chapter 3) may be related to the Bungaree Intrusives as gabbroic rocks similar to those seen within the Saddle Pluton are found within the Bungaree Intrusives at

Table 4.4 Sr and Nd isotopic data from selected samples of the Halfmoon Pluton

Sample	Type	Sr (ppm)	Rb (ppm)	$^{87}Rb/^{86}Sr$	$^{87}Sr/^{86}Sr_{(m)}$	$^{87}Sr/^{86}Sr_{(i)}$	$^{147}Sm/^{144}Nd$	$^{143}Nd/^{144}Nd$	εNd (T)
AP#G	Diorite Host	1001	42	0.045	0.704140	0.703879	0.207	0.512739	1.97
AP#M	Mafic Sheet	619	16	0.015	0.703964	0.703879	0.238	0.512753	2.25
EC#6C	Diorite Host	895	14	0.019	0.703966	0.703859	0.210	0.512819	3.53
EC#6M	Mafic Sheet	538	10	0.005	0.703835	0.703809	0.258	0.512807	3.30
RR#H6	Host Granite	384	45	0.097	0.704443	0.703882	0.106	0.512720	1.59
TN#35	Tonalite Host	602	41	0.056	0.704162	0.703839	0.144	0.512734	1.88
TN#37	Mafic Enclave	923	45	0.053	0.704189	0.703884	0.223	0.512746	2.12
TN#24m	Mafic Comp Dike	663	56	0.089	0.704254	0.703739	0.133	0.512699	1.20
TN#24f	Felsic Comp Dike	696	27	0.040	0.704495	0.704268	0.095	0.512638	0.00
LB#G1	Granite (later?)	427	81	0.178	0.705053	0.704044	0.215	0.512896	5.04
BB#G2	Granite (later)	260	205	0.770	0.708941	0.704572	0.213	0.512714	1.47
TN#26	Mafic Dike	675	42	0.067	0.704171	0.703787	0.241	0.512752	2.23

For εNd calculations, $^{143}Nd/^{144}Nd$ CHUR = 0.512638; $^{147}Sm/^{144}Nd$ CHUR = 0.1967

Cow and Calf Point and Ringaringa Beach. The Saddle Pluton is more mafic than the Bungaree Intrusives, composed largely of gabbro, norite, troctolite and dunite, and smaller bodies of quartz monzonite, granodiorite and granite. Gradational contacts between some of these units, and the presence of enclave-rich zones, indicates that like the Bungaree Intrusives, magma mingling and/or mixing occurs within the Saddle Pluton.

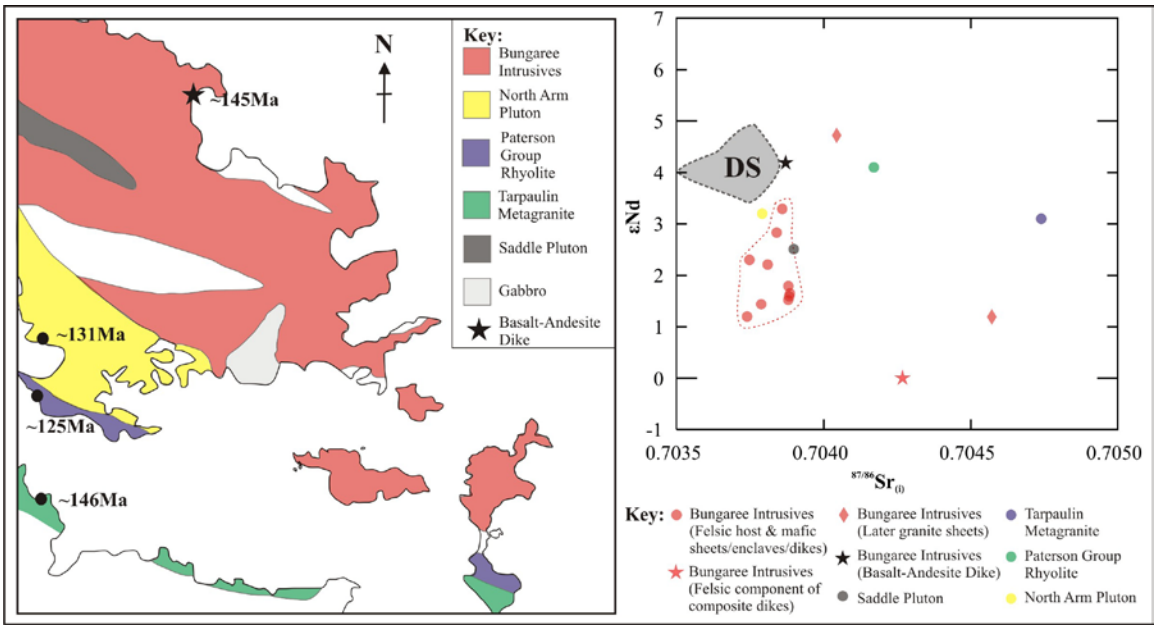

Figure 4.8. Simplified geological map of north eastern Stewart Island outlining the location of the various plutons that intrude or are intruded by the Bungaree Intrusives. $^{87/86}Sr_{(i)}$ vs. ε Nd of these plutonic bodies and their ages are also given. DS represents the Darran Suite field (Allibone & Tulloch, 2004). Isotopic values for Tarpaulin Metagranite, Saddle Pluton, North Arm Pluton and the Paterson Group are unpublished data from A. Tulloch.

As Figure 4.8 reveals, the Sr-Nd isotopic composition of the Saddle Pluton is identical to that of the Halfmoon Pluton. The more mafic compositions within the Saddle Pluton, plus their identical isotopic compositions may indicate that the Saddle Pluton represents the deeper mafic root from which the Halfmoon Pluton was extracted.

The Paterson Group, which sits stratigraphically above the Halfmoon Pluton, has been postulated by Wiebe and Collins (1998) as a possible volcanic equivalent of the Halfmoon Pluton. It however gives an older (~146 Ma) age, and has a more evolved isotopic signature, enriched in $^{87/86}Sr_{(i)}$.

4.5 SUMMARY OF GEOCHEMISTRY AND PROCESSES INFERRED

A distinct compositional change occurs in both the felsic host and mafic rocks at the Evening Cove – Ringaringa horizon. Here the mafic rocks become more enriched in incompatible elements (Ba, Rb, Sr, Na, K). This sudden enrichment between rocks at EC and those at RR may represent a separate batch of mafic melt, or change in the degree of partial melting in the source. An increase in these elements may also indicate an increase in melting of feldspar in the source. Melting of feldspar in the source may indicate melting at higher pressure or drier conditions, which are required in order to destabilize feldspar. A gap in continuity exists between the outcrops at Evening Cove and Ringaringa. SiO_2 concentrations within the mafic rocks however remains uniform, suggesting that all the mafic rocks represent repeated tapping of a mafic magma reservoir at depth that was recharging with magma of uniform composition.

4.4.1 FRACTIONAL CRYSTALLIZATION

Fractional crystallization occurred within both the mafic and felsic magmas of the Halfmoon Pluton and was probably the dominant petrogenetic process driving compositional differentiation. The magma composition of the felsic host rocks became progressively more silicic, changing from an intermediate diorite (SiO_2 55%) towards the base of the chamber at AP and EC, becoming a more felsic tonalite-granodiorite (SiO_2 75%) towards the top of the chamber at RR and TN. Figure 4.4 shows the change in SiO_2, CaO, Al_2O_3 and Sr with stratigraphic height in the chamber. A difference in the compositional contrast between the mingled rocks coincides with observed changes in the style of magma mingling preserved. Mafic and felsic rocks at Ackers Point and Evening Cove have small compositional contrasts (<10 wt% SiO_2) and the dominant magma mingling style is one of mafic sheet formation. Mafic enclave formation is favoured at Ringaringa and The Neck, which coincides with larger (>15 wt% SiO_2) compositional contrasts between the interacting rocks. This suggests that composition may influence the style of magma interaction that occurs. This will be discussed in Chapter 7.

The observed REE trends for the intermediate-felsic host rocks are consistent with crystallization and accumulation of a plagioclase – hornblende – apatite – zircon

assemblage. Competition between this crystallizing assemblage complicates the observed REE trends. A commonly used indicator of crystal accumulation in arc magmas is the Eu anomaly, which becomes progressively more negative with fractionation. Despite textural evidence for plagioclase accumulation towards the base of the chamber (AP and EC), there is no corresponding Eu-depletion, instead Eu/Eu* increases in value (Figure 4.6 and 4.9). No depletion in Eu is observed because the crystallization of apatite and hornblende are masking the plagioclase effect. The partition coefficient (Pc) for Eu and the adjacent REE (which are used to calculate the Eu anomaly) in amphibole and apatite are such that these phases will enrich the melt in Eu. The amphibole and apatite Pc are up to an order of magnitude larger than, and opposite to, plagioclase (Table 4.5) and thus creates a competition between these phases for determining the magnitude and direction of the Eu anomaly.

Table 4.5. *Mineral/melt partition coefficients for dacitic and andesitic liquids*

Element	Plagioclase	Hornblende	Apatite
La	0.302		14.5
Ce	0.221	0.899	21.1
Nd	0.149	2.890	32.8
Sm	**0.102**	**3.990**	**46**
Eu	**1.214**	**3.440**	**25.5**
Gd	**0.067**	**5.480**	**43.9**
Dy	0.050	6.200	34.8
Er	0.045	5.940	22.7
Yb	0.041	4.890	15.4
Lu	0.015	4.530	13.8

Pc for plagioclase are from Fukimaki et al., (1984); Pc for hornblende are from Arth (1972); Pc for apatite are sourced from Fujimaki (1986) and Watson and Green (1981).

As discussed in Chapter Three, amphibole and apatite (as well as plagioclase) are early crystallizing phases within the intermediate cumulate host rocks at the inferred base of the chamber, and therefore will exert a strong influence on the observed REE trends. However, in the Halfmoon Pluton, the plagioclase/amphibole + apatite + oxides ratio observed in the cumulate rocks at Ackers Point and Evening Cove (Plag/amph+ap+ox: 5.3) is sufficient to generate a steep negative Eu anomaly with increasing SiO_2, exactly

opposite to that observed in the rocks (Figure 4.6 and 4.9). This discrepancy can only be resolved by considering the models of magma evolution and melt extraction from an intermediate mush, which have shown that the most efficient crystallinity interval for melt extraction is between 50-70 vol. % (Bachmann & Bergantz, 2004). In the Halfmoon Pluton, the total amphibole and apatite contents in the cumulate host are ~12% and 0.5% respectively, providing a maximum estimate of these three phases during early crystallization, settling and compaction. If the remaining crystal contents are plagioclase and oxides, 50-70% crystallization is reached with an additional 30-50% plagioclase. At 25% plagioclase and 45% crystallinity, the ratio of plagioclase to amphibole/apatite/oxides (1.4) is such that it increases the Eu anomaly the appropriate magnitude from intermediate (~55% SiO_2) to felsic (~75% SiO2) host (see Figure 4.9). The early crystallization of hornblende and apatite in the cumulate host rocks at the base of the chamber are therefore masking the plagioclase effect. The effect of hornblende crystallization is evident in the flattening of the MREE and HREE, however if the REE trend were attributed solely to hornblende crystallization, a smooth convex curve would be generated. The effect of hornblende and apatite crystallization on the observed REE trends is further supported by trends of increasing Eu anomalies with decreasing P_2O_5 and Dy/Yb ratios with stratigraphic height in the chamber. Sphene is another accessory mineral that has high Pc for REE, however as discussed in Chapter Three it crystallized late in the host rocks and therefore did not have any influence on the trace element concentrations.

A similar REE trend to the Halfmoon Pluton occurs in cumulate leucodiorites within the Tottabetsu Plutonic Complex. The authors attributed the steep LREE, positive Eu-anomalies and flat MREE-HREE patterns to plagioclase and zircon accumulation (Kamiyama *et al*., 2007). The observed REE trends indicate that the presence or absence of a Eu anomaly cannot be used as an indicator of a plagioclase cumulate alone, and that the effect of crystallization of other mineral phases needs to be taken into consideration.

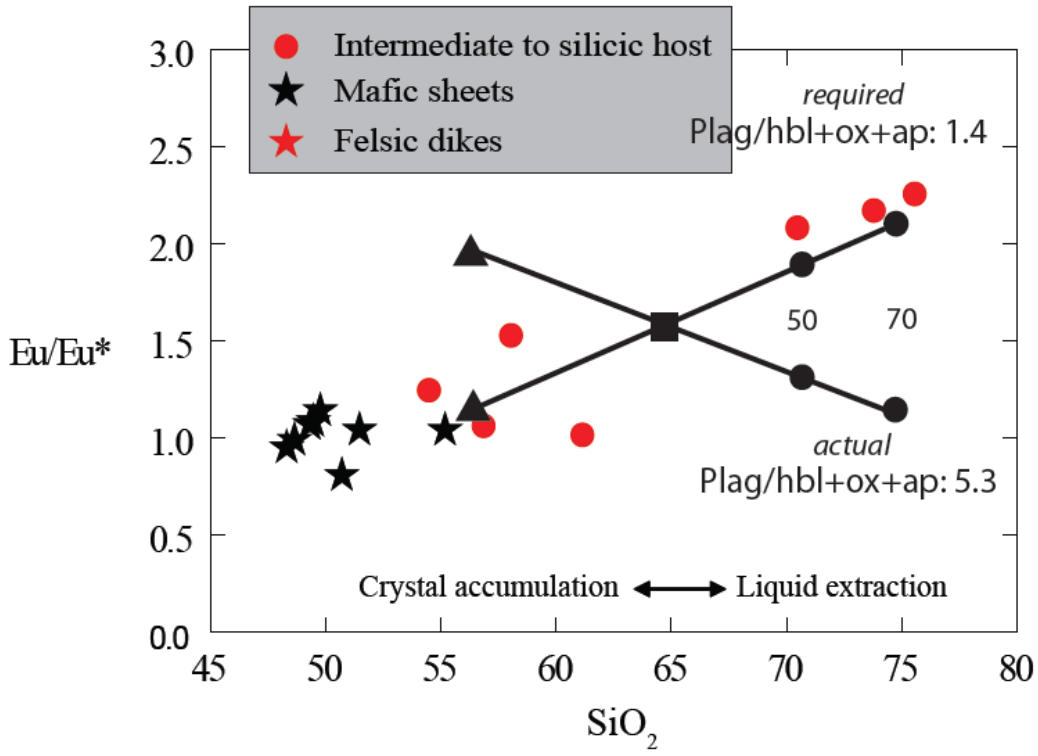

Figure 4.9. Fractional crystallization trends based on the actual modal concentrations in the host cumulates and required modal concentrations. Filled circles represent 50 and 70% crystallization intervals of dacite with differing plag/hbl+ox+ap ratios. Filled triangles represent cumulate compositions, and filled boxes are the estimated dacitic recharge compositions.

A lack of Eu anomaly within the mafic rocks indicates that there was no apatite fractionation within these rocks. Intermediate-felsic host rocks display steeper LREE trends and flatter MREE and HREE trends than the mafic rocks. These trends can be explained by fractionation of hornblende (MREE) and zircon (HREE). Hornblende fractionation is also indicated by decreasing Dy/Yb ratios with increasing SiO_2 contents and stratigraphic height. Amphibole fractionation is consistent with intermediate crustal depths and with the high water contents that characterize primitive magmas at subduction zones (Davidson *et al*., 2007). Amphibole may also influence the distinctive major element characteristics of arc lavas. Amphibole contains significantly less SiO_2 and more TiO_2 than basalt, such that fractionation will efficiently drive liquid compositions to higher SiO_2 and lower TiO_2 (Davidson *et al*., 2007), which is the trend observed within Halfmoon Pluton rocks.

Fractionation within the mafic rocks is indicated by trends of decreasing MgO with increasing REE abundance. All REE are incompatible in mafic systems (Rollinson, 1993), which supports this interpretation. Unlike the intermediate-felsic host rocks, no discernable stratigraphic correlation exists within the mafic rocks, with a mafic sheet from The Neck (TN#16) having more primitive compositions than a mafic enclave sample from Ringaringa which is interpreted to lie stratigraphically beneath it. Mafic rocks display identical isotopic signatures indicating they came from the same mantle source. Different mafic components coming into the intermediate-felsic host magma chamber is therefore consistent with varying amounts of partial melting from the same mantle source and/or ponding of these mantle melts at different levels in the crust and differences in the amount of fractionation of these mafic melts. Differences in chemistry within the mafic rocks are probably caused by diffusion, which is discussed in Section 4.4.3 below.

4.4.2 Crystal Accumulation

The occurrence of granite cumulates is considered by many to be unlikely due to the high viscosities of felsic melts which would inhibit the sinking and accumulation of crystals (Harper *et al*., 2004). However, recent viscosity measurements have shown that crystals within a hydrous felsic magma at temperatures of 750-800°C may settle at rates of >1m/year, which would be sufficient for crystal accumulation to occur (Baker, 1996; Scaillet *et al*., 1998).

Crystal accumulation may also result from the disruption and removal of crystals at the margins of a chamber. Crystals are envisaged to nucleate along the margins and roof of a magma chamber during peripheral cooling, and crystallize from the margins inwards, forming a solidification front that grades from a solid exterior to a liquid interior (Marsh, 1988). External events (earthquakes, replenishments, eruptions) and internal events (convection) may dislodge these semi-coherent accumulations of crystals, which would then sink with gravity and accumulate as a crystal-rich mush at the base of the chamber (Collins *et al*., 2006). These crystal packages would sink more rapidly than

single crystals. Crystals may therefore come from different parts of the chamber, juxtaposing crystals with different P-T histories.

A number of both composite and homogenous plutons exhibit compelling field and geochemical evidences supporting downward crystal accumulation (Wiebe & Collins, 1998; Bachl *et al*., 2001; Collins *et al*., 2006; Kamiyama *et al*., 2007). As discussed in section 4.4.1, extraction of cumulates rich in plagioclase, hornblende, apatite and zircon explains most of the compositional variability in the felsic host rocks of the Halfmoon Pluton. Increasing concentrations of initially incompatible elements (K, Rb, Ba) suggest that the rocks at Ringaringa are melt-rich extracts from the initial cumulate magma. The dominant control over the Eu anomaly is crystallization and accumulation of a plagioclase – hornblende – apatite – zircon mineral assemblage. Zr accumulation is indicated by unusually high Zr contents within intermediate host rocks at Ackers Point and Evening Cove (Figure 4.10). Rocks with SiO_2 concentrations as low as those at EC and AP (<60%) would not normally exhibit such high Zr concentrations, indicating accumulation of zircon within the plagioclase – hornblende - apatite cumulates at the base of the chamber. Despite the lack of a negative Eu-anomaly within the cumulate host rocks at Evening Cove, the decrease in Sr with stratigraphic height in the chamber, combined with textural evidence and the higher modal abundance of plagioclase (>90%) indicates that host rocks at Ackers Point and Evening Cove were accumulating plagioclase. Cumulate textures are weaker and often absent in rocks further up the stratigraphic sequence at Ringaringa and The Neck. These rocks also contain much lower abundances of plagioclase (generally <60%) and contain less Sr.

4.4.3 Chemical Exchange/Magma Mixing/Isotopic Equilibration

Multiple mafic magma replenishments within a more felsic magma body can cause significant chemical and isotopic diffusion between the two magmas. Both mafic enclaves and sheets are susceptible to chemical and isotopic diffusion with the surrounding felsic magma. The large volume of mafic enclave swarms at Ringaringa created a large surface area where the two magmas were in contact, and provided an opportunity for significant chemical and isotopic exchange by diffusion. Many of these

enclave swarms also display evidence for strong magmatic flow. Continuous flow of fresh felsic magma between the enclaves will enhance diffusion by maintaining the chemical contrast between the two magmas (Barbarin & Didier, 1992). Mafic sheets may be susceptible to chemical exchange due to the prolonged period over which it takes to attain thermal equilibrium with the felsic host. Rapid crystallization of the mafic magmas would result in a rapidly established thermal equilibrium between the two interacting magmas, therefore limiting any significant chemical or isotopic diffusion of the mafic sheets and enclaves to occur (Sparks & Marshall, 1986).

Chemical exchange does seem to have occurred within the felsic host cumulate rocks towards the base of the chamber. As Figure 4.10 displays, the Zr trend within the felsic host rocks doesn't follow a simple linear trend that is typically found in a fractionating felsic magma chamber. This trend can best be explained by chemical exchange with the mafic sheets that intruded them. The felsic cumulates are enriched in Zr relative to both the mafic sheets and enclaves, and to the fractionated felsic rocks towards the top of the chamber. A distinct bend in the Zr trend is indicative of mixing of these cumulates with the mafic sheets that intruded them, as mafic sheets take longer to reach thermal equilibrium, allowing for a longer period over which chemical exchange can occur.

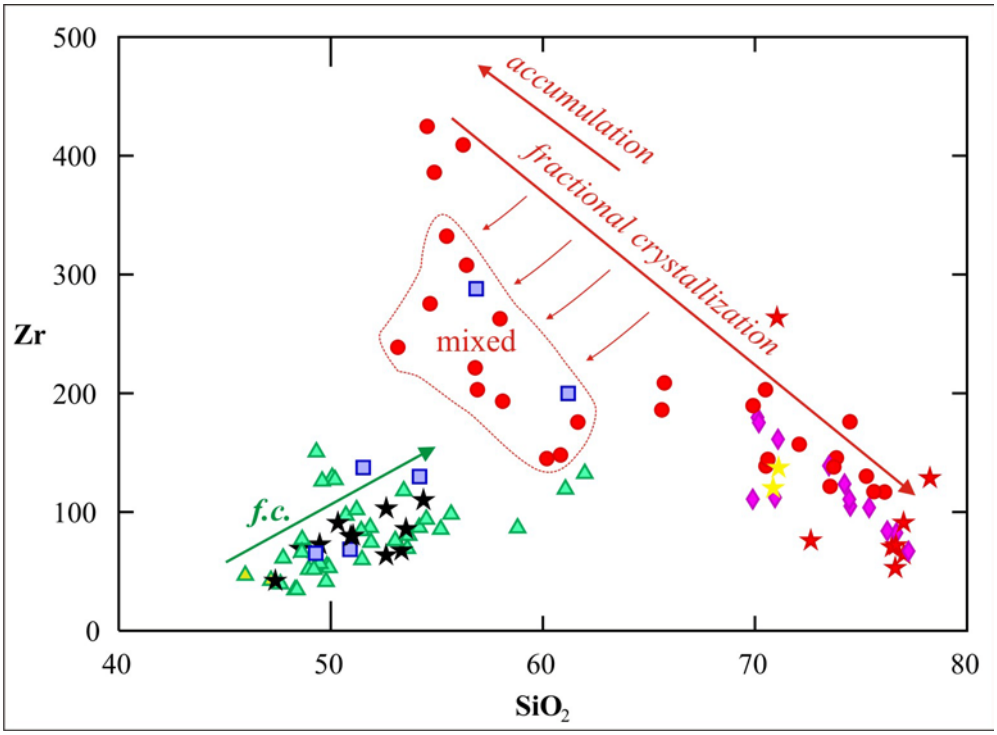

Figure 4.10. SiO_2 vs. Zr showing fractional crystallization of both the mafic sheets and enclaves, and the felsic host rocks. Felsic cumulate host which has mixed with the mafic sheets are outlined.

The more fractionated felsic rocks towards the top of the chamber are unaffected by mixing and/or chemical exchange with the mafic magmas as a smaller volume of mafic magma was injected, favouring the formation of mafic enclaves, which chilled quickly and inhibited any significant chemical exchange.

As discussed in the preceding section, there is very little evidence to suggest that complete chemical and isotopic equilibration occurred between the interacting mafic and felsic magmas. Mafic enclaves are however enriched in more mobile elements (Na_2O, K_2O, P_2O_5, Rb, Ba, Y) relative to the thicker mafic sheets and later cross-cutting mafic dikes that are inferred to represent the parent composition from which they originated. This probably reflects diffusion of these more mobile elements from the host magma into the mafic enclaves. Mafic enclaves within the Adamello Massif were shown by Blundy and Sparks (1992) to be enriched in trace and mobile elements relative to the enclosing host rock, which they attributed to diffusion of these elements from the melt phase of the enclosing host, into the mafic enclave. No enrichment in these elements is observed

within mafic sheets and dikes, which indicates that these larger volume bodies were not affected by diffusion. Mafic enclaves also display a slight enrichment in MnO and Zn, which was attributed by Blundy and Sparks (1992) to represent equilibrium between the Fe-Ti oxides in the mafic enclaves and the host. Diffusion of elements between mafic and felsic magmas is most likely to occur while both the enclave and host have high proportions of liquid, and therefore probably occurs immediately after mafic enclaves have quenched. Snyder and Tait (1998) have shown that multiple mafic magma injections can cause chemical diffusion into the felsic host magma, affecting the trace element and isotopic character of the felsic host magma. Chemical and isotopic equilibration of the host appears unlikely as the composition of the enclosed mafic magma does not mimic that in the felsic host (Figure 3.4), and felsic host rocks often display more primitive $^{87}Sr/^{86}Sr$ and εNd than the mafic sheets and enclaves.

Some authors suggest that complete isotopic equilibrium between coeval mafic and felsic magmas can occur, with mafic enclaves equilibrating with the surrounding felsic host (Barbarin & Didier, 1992; Poli *et al*., 1996; Waight *et al*., 2001). Chemical and isotopic equilibrium has generally been proposed within plutons that contain small quantities of mafic enclaves, whereby there is a larger effect of the felsic host on the enclosed mafic enclaves. Chemical exchange and isotopic equilibration of the mafic magmas is likely to have been obstructed by the quickly-formed fine-grained quenched margins of the mafic sheets and enclaves. These chilled margins stop the mechanical transfer of mass and crystals between the two magmas, and probably inhibit chemical exchange and therefore isotopic equilibration (Barbarin & Didier, 1992). The isotopic similarity between the mafic and felsic rocks within the Halfmoon Pluton is therefore interpreted to indicate that the magmas originated from the same primitive mantle source and that there was only minor isotopic modification through interaction with other mantle or crustal components.

4.4.4 PLUMBING OF A DEEPER SOURCE?

The cummingtonite-bearing mafic sheet at Ringaringa is interpreted to represent plumbing of a primitive mafic magma from a deeper source, perhaps the source from

which the rest of the mafic and felsic magmas within the Halfmoon Pluton fractionated from. Cummingtonite is most commonly found in low pressure-temperature metamorphic rocks, however it has been found in some igneous rocks. Experiments by Nichols et al. (1992) on cummingtonite-bearing rhyolites from the Taupo Volcanic Zone (TVZ) showed that the stability field of cummingtonite was restricted to pressures less than 0.35 GPa, and a temperature of ~750°C. Magmatic cummingtonite has been recognized in volcanic deposits from the 1991 Pinatubo eruption (Luhr & Melson, 1996) and some rhyolites from the Taupo Volcanic Zone (Nicholls *et al*., 1992; Deering, 2009), where it is interpreted to represent crystallization in response to a rapid decrease in temperature. Cummingtonite within mafic enclaves and felsic host rocks immediately above the mafic sheet are probably the result of mixing with the mafic sheet below.

4.5 CONCLUSIONS

The mingled mafic and intermediate-felsic host rocks within the Halfmoon Pluton exhibit many geochemical features consistent with being products of calc-alkaline island-arc magmatism. Compositional changes within the intermediate-felsic host rocks were driven by crystallization and accumulation of a plagioclase – hornblende – apatite – zircon mineral assemblage. Both field and petrographic evidence demonstrate that crystallization of the host magma was interrupted episodically by variable volumes of mafic magma replenishment in several discrete episodes throughout the history of the pluton. Chemical variation within the Halfmoon Pluton indicates that the intermediate-felsic host rocks crystallized from a relatively homogenous magma that underwent fractional crystallization that was periodically interrupted and often reversed by frequent mafic magma injections. The felsic host and mafic magma identified in the Halfmoon Pluton are themselves most probably the fractionated products of a primitive basaltic parent. The conclusions presented above reflect a qualitative assessment of geochemical results. A quantitative assessment of amounts of fractional crystallization has not been undertaken owing to the difficulty in obtaining appropriate and reliable partition coefficients.

4.6 REFERENCES

Allibone, A.H and Tulloch, A.J. 2004 'Geology of the plutonic basement rocks of Stewart Island, New Zealand' *New Zealand Journal of Geology and Geophysics* 47: 233-256

Arth, J.G. 1976 'Behaviour of trace elements during magmatic processes – a summary of theoretical models and their applications' *Journal of Research of the U.S. Geological Survey* 4: 41-47

Bachl, C.A., Miller, C.F., Miller, J.S. and Faulds, J.E. 2001 'Construction of a pluton: Evidence from an exposed cross section of the Searchlight pluton, Eldorado Mountains, Nevada' *GSA Bulletin* 113(9): 1213-1228

Bachmann, O. and Bergantz, G.W. 2004 'On the origin of crystal-poor rhyolites: extracted from batholithic crystal mushes' *Journal of Petrology* 45: 1565-1582

Baker, D.R. 1996 'Granitic melt viscosities: Emperical and configurational entropy models for their calculation' *American Mineralogist* 81: 126-134

Barbarin, B. and Didier, J. 1992 'Genesis and evolution of mafic microgranular enclaves through various types of interaction between coexisting felsic and mafic magmas' *Transactions of the Royal Society of Edinburgh: Earth Sciences* 83: 145-153

Blundy, J.D. and Sparks, R.S.J. 1992 'Petrogenesis of mafic inclusions in granitoids of the Adamello Massif, Italy' *Journal of Petrology* 33: 1039-1104

Collins, W.J., Wiebe, R.A., Healy, B. and Richards, S.W. 2006 'Replenishment, crystal accumulation and floor aggradation in the megacrystic Kameruka Suite, Australia' *Journal of Petrology* 47: 2073-2104

Davidson, J., Turner, S., Handley, H., Macpherson, C. and Dosseto, A. 2007 'Amphibole "sponge" in arc crust?' *Geology* 35: 787-790

Deering, C.D. 2009 'Cannibalization of an amphibole-rich andesite progenitor induced by caldera-collapse during the Matahina eruption: evidence from amphibole compositions' *American Mineralogist* 94: 1162-1174

Harper, B.E., Miller, F., Miller, G., Koteas, C., Cates, N.L., Wiebe, R.A., Lazzareschi, D.S. and Cribb, J.W. 2004 'Granites, dynamic magma chamber processes and pluton construction: the Aztec Wash pluton, Eldorado Mountains, Nevada, USA' *Transactions of the Royal Society of Edinburgh: Earth Sciences* 95: 277-295

Hawkesworth, C.J., Gallagher, K., Hergt, J.M. and McDermot, F. 1993 'Mantle and slab contributions in arc magmas' *Annual Reviews in Earth and Planetary Sciences* 21: 175-204

Irvine, T.N. and Baragar, W.R.A. 1971 'A guide to the geochemical classification of the common volcanic rocks' *Canadian Journal of Earth Sciences* 8: 523-548

Kamiyama, H., Nakajima, T. and Kamioka, H. 2007 'Magmatic stratigraphy of the tilted Tottabetsu Plutonic Complex, Hokkaido, North Japan: Magma chamber dynamics and pluton construction' *The Journal of Geology* 115: 296-314

Kessel, R., Schmidt, M.W., Ulmer, P. And Pettke, T. ,Trace element signature of subduction-zone fluids, melts and supercritical liquids at 120-180 km depth' *Nature* 437: 724-727

Le Bas, M.J., LeMaitre, R.W., Streckeisen, A.L. and Zanettin, B. 1986 'A chemical classification of volcanic rocks based on the total alkali-silica diagram' *Journal of Petrology* 27: 745-750

Luhr, J.F. and Melson, W.G. 1996 'Mineral and glass compositions in June 15, 1991 pumices: Evidence for dynamic disequilibrium in the Pinatubo dacite' In: Punongbayan, R.S. and Newhall, C.G. *Fire and mud eruptions and lahars of Mount Pinatubo, Phillipines*, University of Washington Press pp 733-750

Maniar, P.D. and Piccoli, P.M. 1989 'Tectonic discrimination of granitoids' *GSA Bulletin* 101: 635-643

Marsh, B.D. 1988 'Crystal capture, storage and retention in convecting magma' *Geological Society of America Bulletin* 100: 1720-1737

Miller, D.M., Goldstein, S.L. and Langmuir, C.H. 1994 'Cerium/lead and lead isotope ratios in arc magmas and the enrichment of lead in the continents' *Nature* 368: 514-520

Muir, R.J., Ireland, T.R., Weaver, S.D., Bradshaw, J.D., Evans, J.A., Eby, G.N. and Shelley, D. 1998 'Geochronology and geochemistry of a Mesozoic magmatic arc system, Fiordland, New Zealand' *Journal of the Geological Society, London* 155: 1037-1053

Nicholls, I.A., Oba, T. and Conrad, W.K. 1992 'The nature of primary rhyolitic magmas involved in crustal evolution: evidence from an experimental study of cummingtonite-bearing rhyolites, Taupo Volcanic Zone' *Geochimica et Cosmochimica Acta* 56: 955-962

Pearce, J.A., Harris, B.W. and Tindle, A.G. 1984 'Trace element discrimination diagrams for the tectonic interpretation of granitic rocks' *Journal of Petrology* 25: 956-983

Poli, G., Tommasini, S. and Halliday, A.N. 1996 'Trace element and isotopic exchange during acid-basic magma interaction processes' *Transactions of the Royal Society of Edinburgh: Earth Sciences* 87: 225-232

Rollinson, H. 1993 *Using Geochemical Data: evaluation, presentation, interpretation* Longman Scientific and Technical, pp 352

Scaillet, B., Holtz, F., Pichavant, M. 1998 'Phase equilibrium constraints on the viscosity of silicic magmas. 1. Volcanic-plutonic comparison' *Journal of Geophysical Research* 103: 27257-27266.

Snyder, D. and Tait, S. 1998 'The imprint of basalt on the geochemistry of silicic magmas' *Earth and Planetary Science Letters* 160: 433-445

Spandler, C., Hermann, J., Arculus, R. and Mavrogenes, J. 2004 'Geochemical heterogeneity and element mobility in deeply subducted oceanic crust; insights from high-pressure mafic rocks from New Caledonia' *Chemical Geology* 206: 21-42

Sparks, R.S.J. and Marshall, L.A. 1986 'Thermal and mechanical constraints on mixing between mafic and silicic magmas' *Journal of Volcanology and Geothermal Research* 29: 99-124

Ulfbeck, D., Baker, J., Waight, T. and Krogstad, E. 2003 'Rapid sample digestion and chemical separation of Hf for isotopic analysis by MC-ICPMS' *Talanta*, 59, 365-373

Vogel, T.A., Flood, T.P., Patino, L.C., Wilmot, M.S., Maximo, R.P.R., Apra, C.B., Arcilla, C.A., Stimac, J.A. 2006 'Geochemistry of silicic magmas in the Macolod Corridor, SW Luzon, Philippines: evidence of dinstinct, mantle-derived, crustal sources for silicic magmas' *Contributions to Mineralogy and Petrology* 151: 267-281

Waight, T.E., Baker, J.A. and Peate, D.W. 2002 'Sr isotope ratio measurements by double-focusing MC-ICPMS: techniques, observations and pitfalls' *International Journal of Mass Spectrometry* 221, 229-244

Waight, T.E., Wiebe, R.A., Krogstad, E.J. and Walker, R.J. 2001 'Isotopic response to basaltic injections into silicic magma chambers; a whole-rock and microsampling study

of macrorhythmic units in the Pleasant Bay layered gabbro-diorite complex, Maine, USA' *Contributions to Mineralogy and Petrology* 142: 323-335

Weaver, S.D., Gibson, I.L., Houghton, B.F. and Wilson, C.J.N. 1990 'Mobility of rare earth and other elements during crystallization of peralkaline silicic lavas' *Journal of Volcanology and Geothermal Research* 43, 57-70

Wiebe, R.A. and Collins, W.J. 1998 'Depositional features and stratigraphic sections in granitic plutons: implications for the emplacement and crystallization of granitic magma' *Journal of Structural Geology* 20(9/10): 1273-1289

CHAPTER FIVE

MINERAL COMPOSITIONS AND INTENSIVE PARAMETERS: A RECORD OF FLUCTUATING MAGMATIC CONDITIONS

5.1 INTRODUCTION

In this chapter mineral chemical data are used to evaluate the magmatic processes that were involved in the evolution of intermediate-felsic host rocks of the Halfmoon Pluton. These are argued to include a complex interplay between crystal accumulation, fractional crystallization, convection and mafic magma replenishment.

Compositional variations within minerals provide insights into magmatic processes and changing conditions within magma chambers that cannot be determined through fieldwork and whole-rock geochemistry alone. The record of dynamic processes preserved in plutonic bodies in the field and whole-rock geochemistry are likely to be biassed towards the later stages of a chamber's history. Mineral compositions provide a record of magma composition at the time they crystallized, are sensitive to changes in magma composition, and may be influenced by changes of intensive parameters such as pressure, temperature and oxygen fugacity. Fluctuations in crystal chemistry can therefore provide important clues to the chemical history and evolution of a magma chamber, and reveal processes such as mafic magma replenishment that are otherwise obscured within the whole-rock chemistry. Hornblende crystals in particular are excellent indicators of the intensive variables that governed the formation of the melt in which they grew, as their composition is affected by pressure, temperature, PH_2O and fO_2. Detailed geochemical transects across hornblende crystals are discussed in this chapter as well as a smaller data set of mineral analyses on plagioclase and biotite. Transects across hornblende crystals reveal that the conditions within the chamber fluctuated as a result of the interplay between mafic magma replenishments and the influence of H_2O pressure.

5.2 ANALYTICAL METHODS

Major element compositions (SiO_2, TiO_2, Al_2O_3, FeO, MnO, MgO, CaO, Na_2O and K_2O) of hornblende, plagioclase and biotite crystals were determined using a JEOL Superprobe equipped with three wavelength dispersive spectrometers at Victoria University of Wellington (VUW), and a Cameca SX 100 EPMA equipped with five wavelength spectrometers at the University of Michigan. Major element concentrations obtained at VUW were determined using the ZAF correction method. Analyses were performed using an accelerating voltage of 15kV under a focused electron beam with a >2 µm spot size, counting time of ~5 min/spot, and operating at 8nA. The instrument was calibrated daily using natural and synthetic standards; Al, Ti, Fe, Mn and Mg – synthetic element oxides; Si and Ca – wollastonite; Na – jadeite; K – orthoclase. The homogeneous reference minerals Hornblende P.S.U. Px-1 and Albite Amelia Ab-1 were frequently analysed throughout the analysis period. Major element concentrations obtained at the University of Michigan were corrected using natural and synthetic standards. Standards used were natural fluor-topaz (FTOP); natural jadeite (JD-1); natural Grossular, Quebec (GROS); natural adularia, St. Gothard, Switzerland (GKFS); synthetic apatite (BACL); and synthetic $FeSiO_3$ (FESI). Analyses were performed using an accelerating voltage of 15 kV, a focused beam with a >1 µm spot size, counting time of ~3 min/spot, and a 10 nA beam current. Tables of all EPMA analyses are presented in electronic Appendix 5.

5.2 BIOTITE COMPOSITIONS

As discussed in Chapter 3, biotite is not uniformly distributed throughout the Halfmoon Pluton sequence, displaying a trend of increasing biotite abundance with inferred height in the chamber. EPMA analyses of biotite crystals were obtained from nine rocks within the Halfmoon Pluton. Each rock analysed represents a different position within the chamber (from the base to the top) so that changes in mineral chemistry and therefore magma chamber chemistry could be traced throughout the stratigraphic sequence. Samples chosen also reflect the different host rock types that were identified in Chapter 3 (i.e. leucodiorite, granodiorite, tonalite, granite) as well as a single sample representing a mafic enclave from The Neck (TN#30), and the mafic component of a composite dike (TN#17). Representative biotite analyses from

the nine samples analysed are shown in Table 5.1. All biotite crystals analyzed were euhedral to subhedral, and brown pleochroic.

Table 5.1. Representative major element analyses of Biotite from the Halfmoon Pluton

Sample:	TN#17	AP#G	EC 1/5	EC#6	RR#M4	TN#7	TN#30	TN#4	HB#M2
Type:	Comp. Dike	Felsic Host	Felsic Host	Felsic Host	Felsic Host	Felsic Host	Mafic Enclave	Mixed Host	Mixed Enclave
SiO_2	37.06	37.12	36.63	36.85	36.43	36.26	36.66	36.50	36.42
TiO_2	3.85	4.00	2.48	3.45	2.25	3.39	3.93	3.38	4.10
Al_2O_3	15.42	15.62	16.13	15.48	15.99	15.73	15.22	16.13	14.89
FeO	18.31	19.01	20.35	20.24	20.79	20.50	21.15	21.00	21.08
MnO	0.26	0.00	0.00	0.00	0.00	0.48	0.31	0.39	0.00
MgO	12.09	11.90	11.23	11.42	11.14	10.78	10.19	9.80	9.86
CaO	0.00	0.00	0.00	0.00	0.00	0.00	0.00	0.00	0.00
Na_2O	0.00	0.00	0.00	0.00	0.00	0.00	0.00	0.18	0.00
K_2O	8.88	8.91	8.98	8.93	8.58	9.11	9.01	8.91	8.64
Total	95.87	96.56	95.80	96.37	95.18	96.25	96.47	96.29	94.99
Number of ions on the basis of 22 oxygens									
Si	5.57	5.55	5.56	5.56	5.57	5.51	5.56	5.54	5.60
Al^{iv}	2.43	2.45	2.44	2.44	2.43	2.49	2.44	2.46	2.40
Σ(Z)	8.00	8.00	8.00	8.00	8.00	8.00	8.00	8.00	8.00
Al^{vi}	0.30	0.30	0.44	0.31	0.45	0.32	0.28	0.42	0.29
Ti	0.44	0.45	0.28	0.39	0.26	0.39	0.45	0.39	0.47
Fe	2.30	2.38	2.58	2.55	2.66	2.60	2.68	2.67	2.71
Mn	0.03	0.00	0.00	0.00	0.00	0.06	0.04	0.05	0.00
Mg	2.71	2.65	2.54	2.57	2.54	2.44	2.30	2.22	2.26
Σ(Y)	5.78	5.78	5.85	5.82	5.90	5.82	5.76	5.74	5.73
Na	0.00	0.00	0.00	0.00	0.00	0.00	0.00	0.05	0.00
K	1.70	1.70	1.74	1.72	1.67	1.76	1.74	1.72	1.69
Σ(X)	1.70	1.70	1.74	1.72	1.67	1.76	1.74	1.78	1.69
Σ(cat)	15.48	15.48	15.59	15.54	15.57	15.58	15.50	15.52	15.43
Fe/(Mg+Fe)	0.46	0.47	0.50	0.50	0.51	0.52	0.54	0.55	0.55

Structural formulae of biotites were calculated on the basis of 24 (O, OH, Cl, F) and 8 cations. Biotites typically contain ~4wt% H_2O + F + Cl, and therefore anhydrous oxide totals (SiO_2, Al_2O_3, FeO_{tot}, MgO, CaO, Na_2O, K_2O, TiO_2 and MnO) of 96 ± 1 wt% were retained. According to the nomenclature of Speer (1984), the biotite crystals within the Halfmoon Pluton are all classified as biotite (Annite – Siderophyllite) (Figure 5.1A). Biotites show a trend of decreasing Mg and increasing Fe, and increasing Fe/(Fe+Mg) with stratigraphic height in the chamber, with biotites at the inferred base of the chamber (Ackers Point) having FeO values of ~19 wt% and MgO values of ~12 wt%, whereas those towards the top of the chamber (The Neck) have FeO and MgO values of ~21 wt% and ~10 wt% respectively (Figure 5.1B and Figure 5.1C). Biotite crystals from the mafic component of composite dikes have the lowest FeO values (~18 wt%) and the highest MgO values (~13 wt%) (sample TN#17, Table 5.1). The mafic component of the composite dikes is inferred to represent the parental magma from which the magmas represented by the rocks of the Halfmoon Pluton evolved.

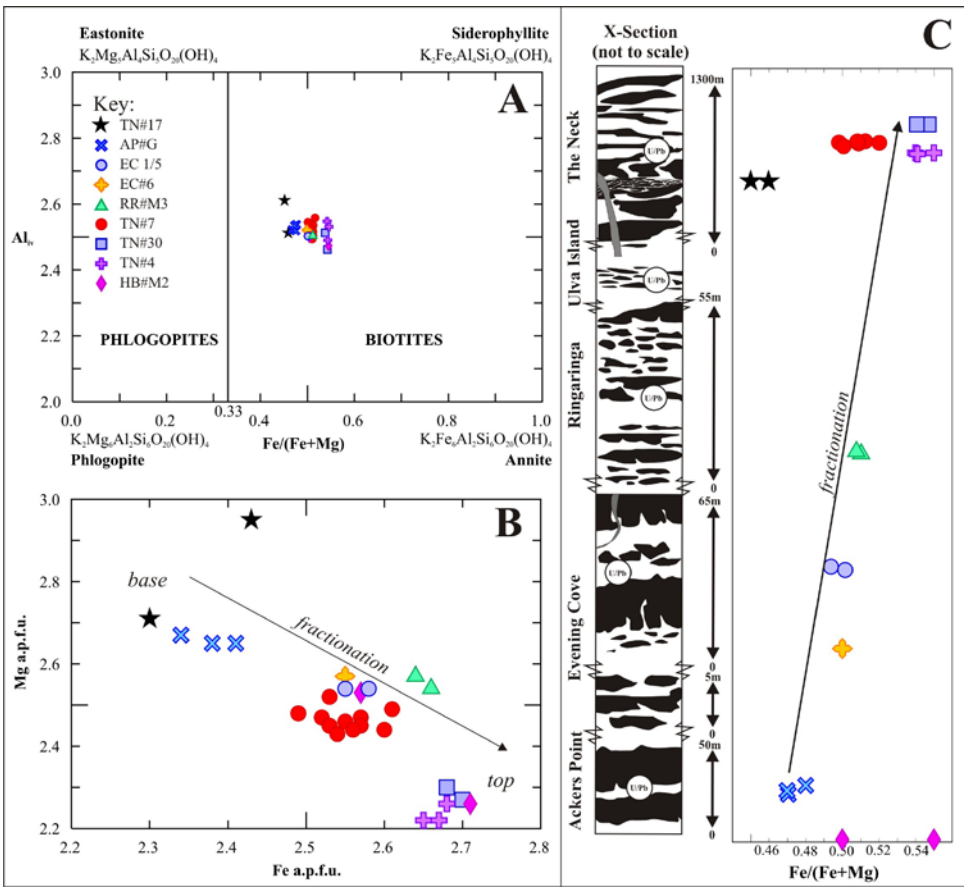

Figure 5.1. (A) Classification of biotite according to the nomenclature of Speer (1984) (B) Mg and Fe compositions of biotite from both mafic and felsic rocks within the Halfmoon Pluton (HP) (C) Fe/(Fe+Mg) vs. stratigraphic height within the magmatic sequence of HP.

Biotite crystals analyzed within a mixed mafic enclave at Horseshoe Bay (HB#M2) do not plot together, exhibiting different compositions. This sample is inferred to represent a 'mixed' mafic enclave, and therefore the variety in biotite compositions may reflect juxtaposed biotites from different melts. The significance of this sample will be discussed in further detail in Section 5.5 of this chapter.

5.3 PLAGIOCLASE COMPOSITIONS

Core and rim spots were obtained to determine the compositions of plagioclase crystals within both the mafic and felsic host rocks. Representative plagioclase analyses are presented in Table 5.2, with all results presented in Electronic Appendix 5. Plagioclases with oxide totals >99 and <101% were retained. Plagioclases within mafic sheets and enclaves display more scatter in An-content, with the majority ranging between Andesine and Labradorite compositions (Figure 5.2A). Plagioclases within host rocks have a more defined compositional range, with almost all plagioclases analysed being Andesine (Figure 5.2B). There is an overall decrease in An% with increasing height in the chamber. Mafic sheets at Ackers Point and Evening Cove have plagioclases with An% values between 41 and 46% (Figure 5.2A), with their enclosing leucodiorite host having slightly lower An% values between 34 and 41% (Figure 5.2B). Plagioclases from a granodiorite host rock at Ringaringa (RR#M4) have an average An% of 31, whereas those from a thick mafic sheet have much higher An% of 52. Plagioclases within mafic enclaves from The Neck have An% ranging between 30 and 32%, with tonalite host plagioclases having slightly lower average An-values of 30%. Plagioclase crystals within the mafic component of a cross-cutting composite dike (TN#17) have higher average An% of ~38.

Three core-rim transects were undertaken on euhedral plagioclase crystals from three different samples in the chamber, two from leucodiorite host rocks at Evening Cove, and one from a leucodiorite host rock at Ackers Point (Figure 5.2). Short transects from mid-section to rim were also done on plagioclases from samples EC 3/2#CX and EC#9H to compare with the more detailed core-rim transects done. A transect across a plagioclase phenocryst within a mixed mafic enclave from Horseshoe Bay was also undertaken, however the results from this will be discussed in Section 5.5. Crystals chosen as suitable for transects were euhedral, with sizes

ranging between 1.5mm and 2.5mm. Plagioclase crystals all displayed faint oscillatory compositional zoning. All three plagioclase crystals come from the inferred base of the magma chamber, and occur within rocks that have well defined plagioclase cumulate textures and geochemical signatures (see Chapter 4 for further discussion on cumulate textures and geochemistry).

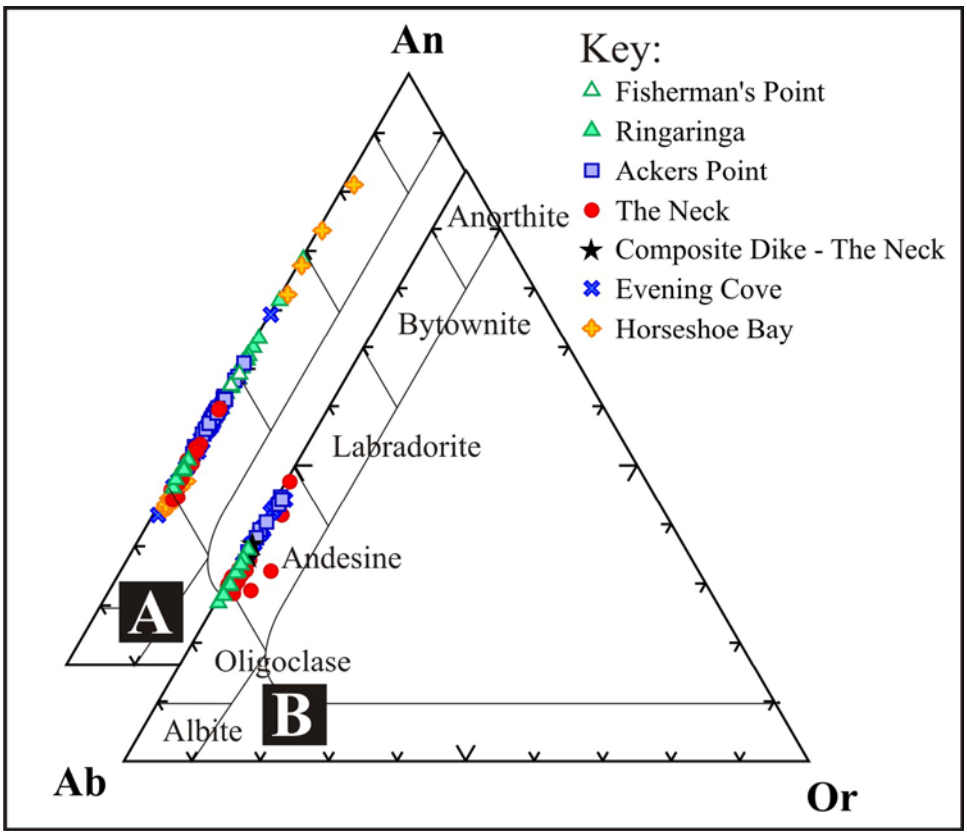

Figure 5.2. Ternary feldspar diagrams based on single spot EMPA analysis of (A) plagioclase within mafic enclaves and sheets and (B) plagioclase within intermediate-felsic host rocks

As Figure 5.3 shows, all transects on cumulate plagioclase crystals show variations in their An-composition from core to rim, which reflect changing concentrations of Ca and Na. Plag#1 from sample EC 3/2#CX (Figure 5.3A) displays a decrease in An from the core, until it reaches zone C where An-content increases from An_{39} to An_{46} at zone A. An-content decreases sharply from zone A towards the rim, before a small increase again at the rim with an An-content of 40. The shorter transect on plag#2 shows the same decreasing trend from mid-rim, and subsequent small increase in An% immediately at the rim. Plag#1 from sample EC#9H (Figure 5.3B) shows a remarkably similar trend to plag#1 in EC 3/2#CX, with increasing An-contents from its core to mid-section, and then a sharp decrease in An% towards the rim.

Table 5.2. Representative major element analyses of Plagioclase from the Halfmoon Pluton

Sample:	HB#M2	HB#M2	AP#H	AP#G	EC 3/2#CX	EC#6	EC#6	EC1/5	EC#8M	EC#9H	RR#M8
Type:	Mafic Enclave	Mafic Enclave	Mafic Sheet	Host	Host	Mafic Sheet	Host	Host	Mafic Sheet	Host	Mafic Sheet
Domain:	Core	Rim	Rim	Rim	Rim	Rim	Rim	Rim	Rim	Rim	Rim
SiO_2	46.43	60.20	56.45	57.76	58.13	57.52	58.43	59.30	57.88	59.97	55.20
Al_2O_3	34.74	25.43	27.65	26.79	27.30	27.23	26.68	26.40	27.04	25.77	29.08
FeO	0.26	0.14	0.25	0.19	0.09	0.07	0.15	0.16	0.17	0.23	0.16
CaO	17.01	5.71	9.31	8.36	8.13	8.98	8.23	7.64	8.49	6.90	10.88
Na_2O	1.91	8.19	6.16	6.74	6.56	6.50	6.82	7.26	6.67	7.21	5.45
K_2O	0.06	0.08	0.06	0.13	0.18	0.14	0.12	0.08	0.11	0.03	0.09
Total	100.5	100.1	99.9	100.0	100.5	100.44	100.4	100.8	100.4	100.4	100.9
An	82.7	27.4	45.4	40.4	40.2	42.9	39.7	36.6	41.0	34.2	52.2
Ab	16.8	71.4	54.3	58.9	58.7	56.3	59.6	62.9	58.3	64.7	47.3
Or	0.5	1.3	0.3	0.7	1.0	0.8	0.7	0.5	0.6	1.1	0.5

Table 5.2. Continued

RR#M4	FP#C2	TN#7	Sample:	TN#4	TN#7	TN#17	TN#30
Host	Mafic Enclave	Mafic Enclave	Type:	Mixed Host	Host	Composite Dike	Mafic Enclave
Rim	Rim	Rim	Domain:	Rim	Rim	Rim	Rim
59.56	55.89	59.90	SiO_2	60.25	60.15	58.79	60.65
25.05	28.49	25.42	Al_2O_3	25.19	25.00	26.23	25.08
bdl	0.25	0.11	FeO	0.22	0.11	0.19	0.12
6.53	10.04	6.98	CaO	6.38	6.38	7.71	6.32
7.61	5.74	7.64	Na_2O	7.69	7.89	7.07	8.16
0.13	0.11	0.22	K_2O	0.21	0.20	0.16	0.07
98.9	100.5	100.3	Total	99.9	99.7	100.2	100.4
31.9	48.8	33.1	An	31.1	30.5	37.3	29.9
67.3	50.5	65.6	Ab	67.7	68.3	61.8	69.8
0.8	0.6	1.2	Or	1.2	1.1	0.9	0.4

bdl = below detection limit

This trend is also observed in the shorter mid-rim transect of plag#2. A more complex trend is observed within a plagioclase crystal from Ackers Point (AP#G), with the An-content showing two increases; one from the core the zone D, and the other from zone A towards the rim. Small fluctuations in plagioclase chemistry occur between zones D and A, which correlate with observed changes in zoning. The reversed zoning trends observed in core to mid-sections are not simply diffusion controlled oscillatory zoning. They are indicative of a dynamic system in which temperature and melt composition fluctuated in response to multiple mafic magma replenishments.

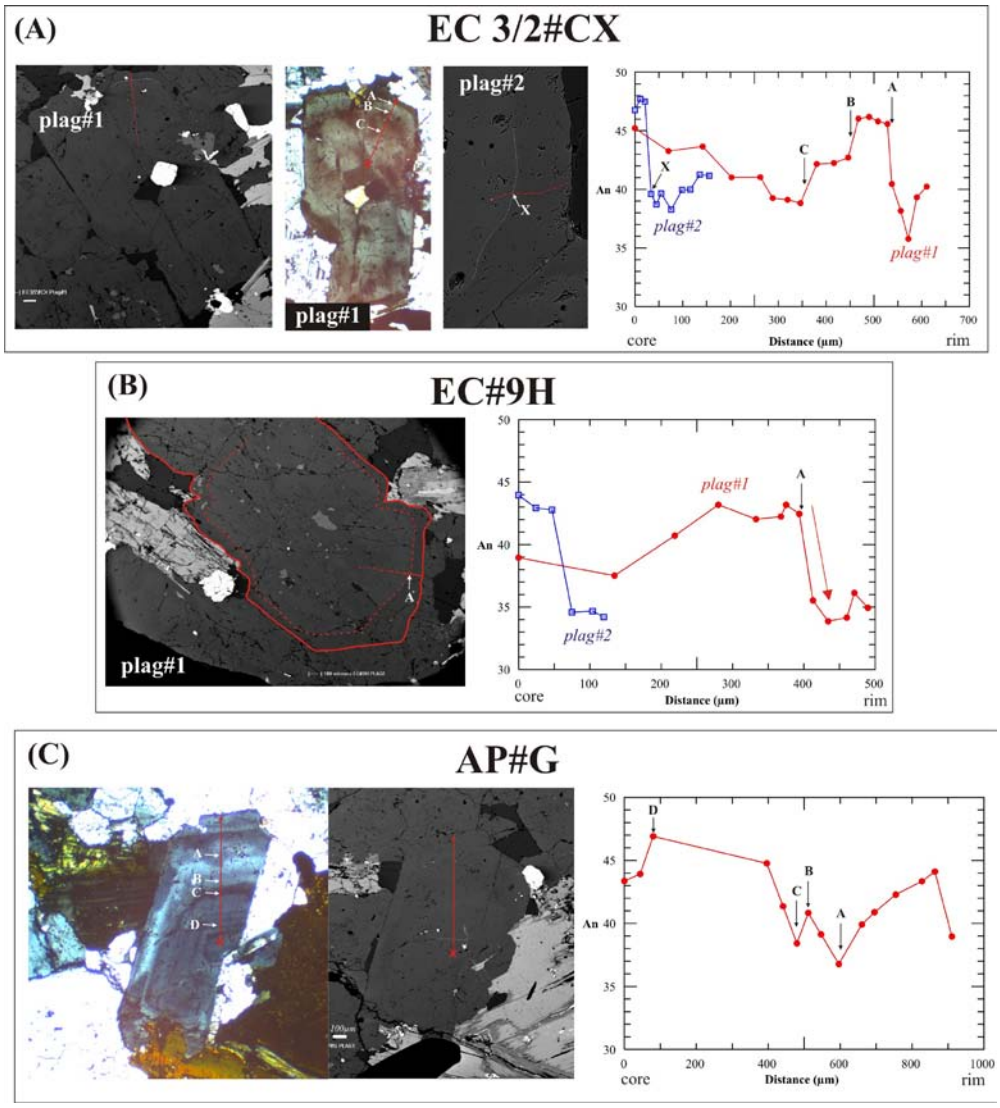

Figure 5.3. Core-rim transects across plagioclase crystals within cumulate felsic host samples towards the inferred base of the chamber (A) EC 3/2#CX towards the base of the section. Locations A, B and C along transect of plag#1 can be identified on the CPL image as distinct changes in colouration. (B) EC#9H towards the top of the section. Location A along transect of plag#1 occurs at a boundary showing a subtle change in colour on the BSE image. (C) AP#G from the inferred base of the chamber.

5.4 AMPHIBOLE COMPOSITIONS AND GEOTHERMOBAROMETRY

Results from detailed traverses across hornblende crystals from six samples within the Halfmoon Pluton are presented in this section. Almost all rocks within the Halfmoon Pluton contain amphibole and the appropriate buffering assemblage to utilize the plagioclase-hornblende geothermometer (Holland & Blundy, 1994) and the Al-in-hornblende geobarometer (Schmidt, 1992; Anderson & Smith, 1995), which makes amphibole the most useful mineral for evaluating the magmatic and tectonic evolution of the Halfmoon Pluton. Fourteen core-rim traverses across large (1-2mm) euhedral hornblende crystals were obtained from four felsic host rock samples and one mixed 'hybrid' sample within the Halfmoon Pluton. Averaged results from all 14 analysed amphiboles are presented here, as well as five representative transects. The remaining transects are presented in Electronic Appendix 5.

Table 5.3 displays average hornblende compositions and structural formulae from the analysed samples. Traverses range from 200 to 600μm in length, with analytical steps typically less than 25μm, however some larger crystals had steps of <50μm. Variation in analytical step distances occurs in all traverses in order to avoid cleavage planes, cracks and mineral inclusions. Samples were chosen to reflect different positions within the inferred stratigraphic sequence (see Chapter 3), however no samples were obtained from rocks at Ackers Point as all leucodiorite rocks lacked a sufficient amount of primary euhedral hornblende. Core and rim analyses were also obtained for fine-grained hornblendes within a resorbed plagioclase crystal, and the significance of these crystals will be discussed in Section 5.5.

Table 5.3. Average major element analyses and structural formulae of different amphiboles within the Halfmoon Pluton

Sample	HB#M2†	EC3/2#CX†	EC#9H†	RR#J3†	EC1/5*	TN#25*	TN#25†
Rock Type	Mafic Enclave	Host	Host	Host	Host	Hybrid	Hybrid
n =	11	63	36	47	125	104	29
SiO2	45.48	45.99	46.79	47.34	46.28	46.57	46.30
TiO2	1.05	1.26	1.31	1.17	1.15	1.18	1.50
Al2O3	8.33	8.60	7.77	7.30	7.54	6.71	7.76
FeO*	17.46	16.05	16.02	14.83	15.23	16.26	16.56
MgO	11.77	12.63	12.90	13.82	12.49	11.93	12.05
MnO	0.42	0.47	0.49	0.42	0.48	0.59	0.65
CaO	11.70	11.16	11.48	11.60	11.57	11.71	11.41
Na2O	1.01	1.09	0.99	0.88	1.11	1.00	1.06
K2O	0.80	0.31	0.51	0.42	0.51	0.60	0.61
F	nm	0.31	nm	0.05	0.14	0.17	nm
Cl	0.09	0.25	0.05	0.26	0.04	0.06	0.12
Total	98.10	98.14	98.31	98.11	96.55	96.77	98.02
Structural formulae							
Si	6.70	6.72	6.80	6.87	6.86	7.11	6.80
Al_{tot}	1.45	1.48	1.33	1.25	1.32	0.96	1.34
Al_{iv}	1.30	1.28	1.20	1.13	1.14	0.89	1.20
Al_{vi}	0.14	0.20	0.13	0.12	0.18	0.07	0.14
Ti	0.12	0.14	0.14	0.13	0.13	0.12	0.17
Fe2+	1.39	1.11	1.20	1.05	1.31	1.33	1.37
Fe3+	0.72	0.75	0.67	0.67	0.56	0.50	0.60
Mg	2.58	2.75	2.79	2.99	2.76	2.90	2.64
Mn	0.05	0.06	0.06	0.05	0.06	0.07	0.08
Ca(M4)	1.84	1.75	1.79	1.80	1.84	1.91	1.79
Na(M4)	0.11	0.15	0.13	0.12	0.14	0.09	0.14
Na+K(A)	0.33	0.25	0.24	0.21	0.28	0.18	0.27
Sum cations	15.33	15.25	15.24	15.21	15.28	15.28	15.27

Structural formulae of amphiboles calculated using the method of 13 cations excluding Ca, Na and K (13eCNK) described in Leake *et al*., (1997).
nm = not measured. † measured at VUW; * measured at the University of Michigan

All amphiboles analyzed were euhedral, pleochroic olive green, and commonly contained inclusions of plagioclase and Fe-Ti oxides. Amphiboles typically contain ~2wt% H_2O + F + Cl, and therefore anhydrous oxide totals (SiO_2, Al_2O_3, FeO_{tot}, MgO, CaO, Na_2O, K_2O, TiO_2 and MnO) of 98 ± 1 wt% were retained. Amphiboles analyzed at the University of Michigan (UM) had lower oxide totals of ~96.5 wt% relative to amphiboles analysed at Victoria University of Wellington (VUW) (see Table 5.3). Sample TN#25 was analysed on the EPMA at both VUW and the UM, and comparison between major element concentrations indicates that those obtained from UM yielded lower abundances for almost all major elements. These lower abundances are thought to be a consequence of a slightly too thick carbon coat. Despite totals being low, the relative trends observed within the amphibole transects are interpreted to be sound as they parallel trends observed in amphiboles with higher oxide totals. For each sample, with the exception of HB#M2, detailed core to rim transects were completed on between one and four euhedral amphibole crystals. For HB#M2, core, mid and rim analyses were undertaken on three amphibole crystals.

Significant variations within and between samples are evident in major element trends of Halfmoon Pluton amphiboles (Figure 5.4). SiO_2 displays negative correlations with Al_2O_3, Na_2O, K_2O and FeO*, whereas MgO displays a positive correlation, and TiO_2, CaO and MnO remain relatively constant. Amphiboles from HB#M2 display scattered compositions, which may be a reflection of the small number of analyses performed, or that this sample has plumbed a deeper source and therefore has amphiboles with different compositions from the rest. This will be discussed in greater detail in Section 5.5.

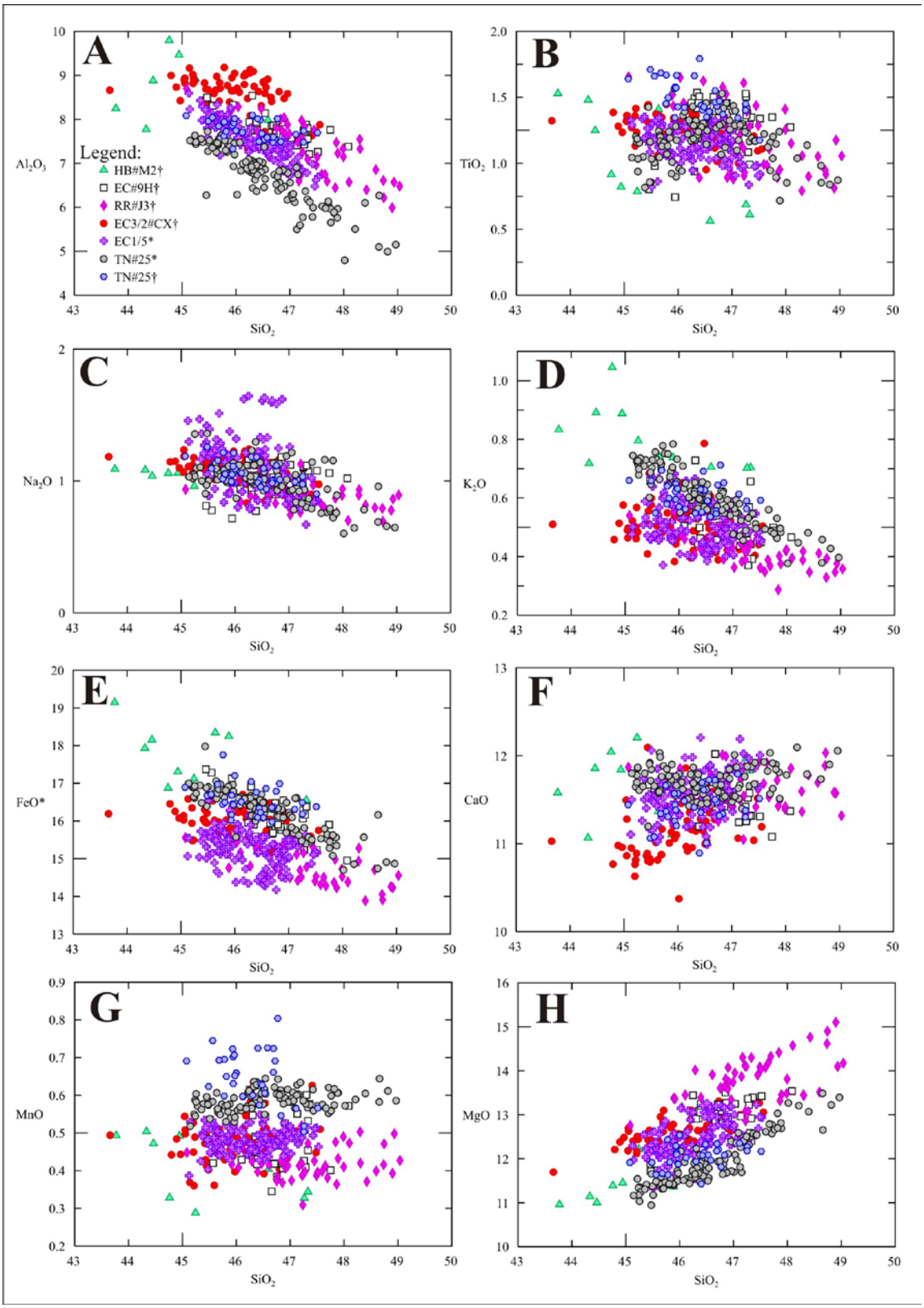

Figure 5.4. Major-element variation diagrams for amphiboles within the Halfmoon Pluton. Note that all amphiboles display compositional overlap and exhibit the same trends despite being from different rocks throughout the stratigraphic sequence. * = analyses performed at the University of Michigan; † = analyses performed at Victoria University of Wellington.

Cation distributions for structural formulae were recalculated following the method of Leake *et al*. (1997), which assumes a formula cation sum of 13, excluding Ca, Na and K (13eCNK), and all Fe as FeO. The strong positive correlation between Fe^{2+} and Mg (Figure 5.4f) indicates that Fe^{2+} changes were entirely counterbalanced by Mg (Bachmann & Dungan, 2002). Mg also displays a strong negative correlation with Al_{tot}. Amphiboles are all classified as magnesio-hornblendes (Leake *et al*., 1997; see Figure 5.4G-H), with MgO contents ranging between 12 and 14 wt% and low TiO_2 contents of 1-1.5 wt%.

Amphibole compositions are affected by a combination of intensive parameters including pressure, temperature and oxygen fugacity. Initial field observations regarding emplacement depths of plutons (Hammarstrom & Zen, 1986) and subsequent experimental studies have shown that the total Al-content of amphibole is a function of both temperature and pressure (Johnson & Rutherford, 1989; Thomas & Ernst, 1990; Schmidt, 1992; Blundy & Holland, 1990; Anderson & Smith, 1995). These studies have show that the Al-Tschermak substitution ($^{T}Si + {}^{M1\text{-}M3}Mn = 2Al_{tot} + {}^{M1\text{-}M3}Ti$) is sensitive to changes in pressure, whereas the Ti-Tschermak ($^{2T}Si + {}^{M1\text{-}M3}Mn = 2Al_{tot} + {}^{M1\text{-}M3}Ti$) and edenite ($^{T}Si + {}^{A}X = Al_{tot} + {}^{A}(Na+K)$) exchanges in response to changes in temperature and pressure. As shown in Figure 5.5, most of the variation in Al_{tot} within Halfmoon Pluton amphiboles can be accounted for by the pressure dependent Al-Tschermak exchange. The temperature dependent edenite exchange displays a weak positive correlation (Figure 5.5C), whereas the temperature dependent Ti-Tschermak exchange displays a poor correlation (Figure 5.5B). This indicates that pressure played a more important role in controlling amphibole composition than temperature.

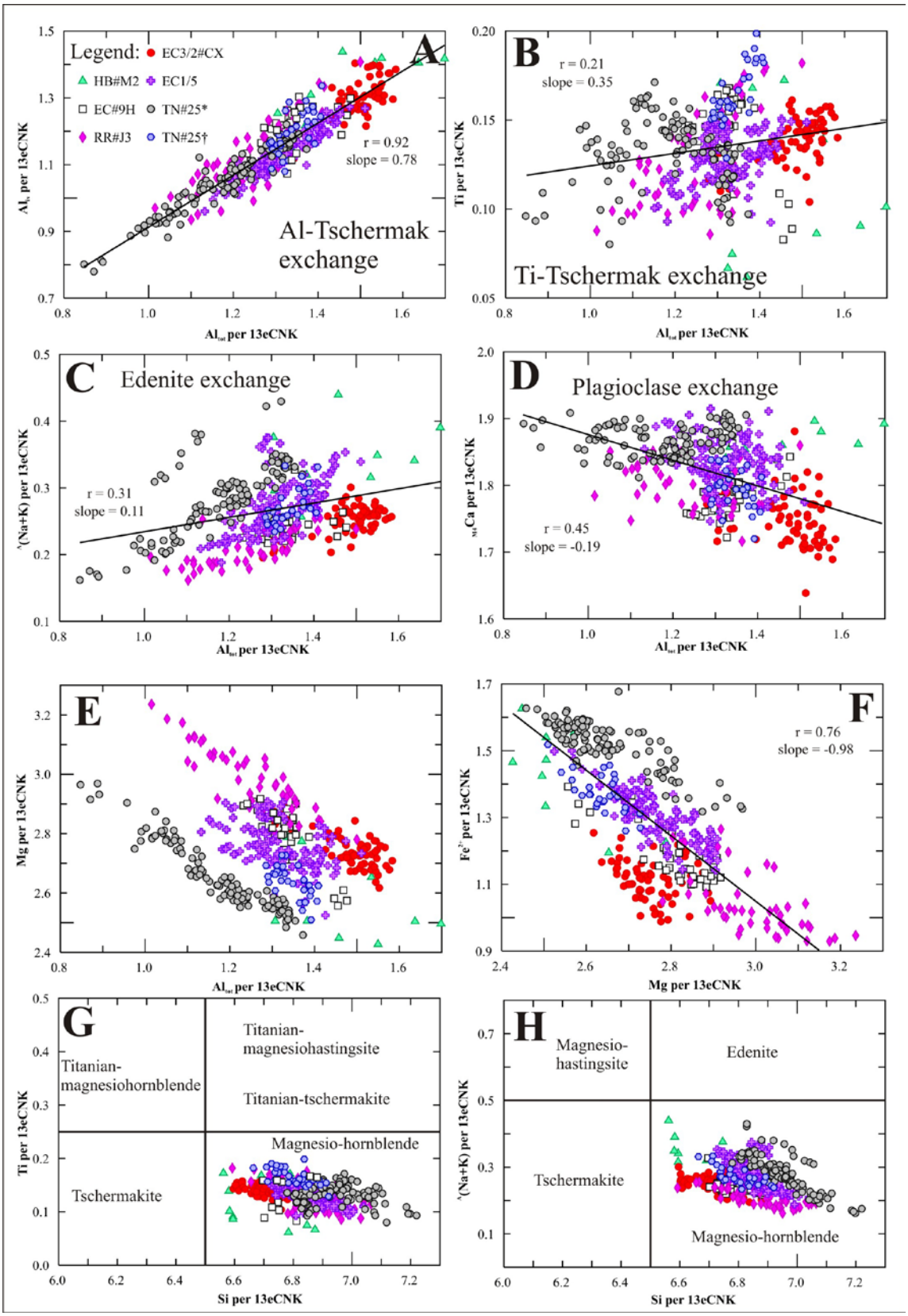

Figure 5.5. Plots of Al_{tot} vs. (A) Al_{iv}, (B) Ti, (C) Na+K(A), (D) Ca(M4), (E) Mg, (F) Mg vs. Fe^{2+} illustrating substitutions mechanisms in Halfmoon Pluton hornblendes (G)-(H) Amphibole classification diagrams using structural formulae as recommended by Leake *et al.*, (1997).

Table 5.4. Calculated pressures and temperatures for rims and cores from representative amphiboles within the Halfmoon Pluton

Holland & Blundy (1994) thermometer			Femenias *et al* ., (2006) thermometer		
	Core	**Rim**		**Core**	**Rim**
HB#M2†	723	724	HB#M2†	732	709
EC3/2#CX†	766	750	EC3/2#CX†	729	716
EC1/5*	710	673	EC1/5*	722	638
EC#9H†	782	702	EC#9H†	734	621
RR#J3†	767	749	RR#J3†	741	665
TN#25*	701	676	TN#25*	715	646
TN#25†	701	681	TN#25†	735	694

Schmidt (1992) barometer				
	P (core)	**P (rim)**	**Depth (core)**	**Depth (rim)**
HB#M2†	3.2	4.4	12	16
EC3/2#CX†	4.3	4.3	16	16
EC1/5*	3.7	3.8	14	14
EC#9H†	3.4	3.9	13	14
RR#J3†	3.0	3.4	11	13
TN#25*	2.9	3.5	11	13
TN#25†	3.3	3.3	12	12

Anderson & Smith (1995) barometer				
	P (core)	**P (rim)**	**Depth (core)**	**Depth (rim)**
HB#M2†	2.7	3.7	10	14
EC3/2#CX†	2.9	3.2	11	12
EC1/5*	3.3	3.8	12	14
EC#9H†	1.8	3.6	7	13
RR#J3†	1.8	2.4	7	9
TN#25*	2.7	3.5	10	13
TN#25†	3.1	3.2	11	12

† = VUW analysed samples; * = UM analysed samples. Samples are listed in inferred "stratigraphic" order with TN#25 representing the inferred top of the chamber

Early geobarometers only took into account the Al-content of amphibole as an indicator of crystallization pressures (Hammarstrom & Zen, 1986; Hollister *et al*., 1987). Anderson and Smith (1995) showed that temperature also had an affect on Al_{tot}, and they therefore modified the Al-in-hornblende geobarometer to also take temperature into account. Pressure estimates for Halfmoon Pluton amphiboles were therefore calculated using the temperature-corrected Anderson and Smith (1995)

geobarometer outlined below, and pressures listed in Table 5.4 and shown in Figures 5.6 and 5.7.

P(±0.6 kbar) = 4.76Al – 3.01 - [(T°C - 675/85) x (0.530Al + 0.005294) (T°C – 675)]

Application of this technique relies on the presence of the appropriate buffering assemblage of hornblende, plagioclase, orthoclase, biotite, quartz, Fe-Ti oxide (magnetite or ilmenite), apatite, titanite plus melt and a fluid phase. Almost all samples within the Halfmoon Pluton were too mafic to contain orthoclase, however Hollister *et al.*, (1987) have suggested that the absence of orthoclase would result in pressure overestimates, perhaps as high as 1 kbar. Therefore, results presented in Table 5.4 and Figures 5.6 and 5.7 represent maximum pressures and depths of emplacement for the Halfmoon Pluton. The Al-in-hornblende geobarometer is not sensitive enough to be able to quantitatively differentiate pressure differences between rims and cores of individual hornblende crystals as there is considerable uncertainty as to the mineral assemblage that was actually crystallizing at the time hornblende cores were crystallizing. Therefore, while actual pressures cannot be quantified, relative numbers and observed trends will be discussed with respect to what processes may be responsible.

Oxygen fugacity may also affect the calculated pressures. Changes in fO_2 affect the valence state of iron, which in turn affects the cation ratios and site vacancies within amphiboles. Crystallization under low fO_2 conditions (i.e. reduced) decreases the Mg/Fe and Fe^{3+}/Fe^{2+} ratios, thereby increasing Al-substitution. Crystallization under high fO_2 conditions (i.e. oxidised) increases Al values in amphiboles, and can therefore over estimate crystallization pressures (Anderson & Smith, 1995). Anderson and Smith (1995) therefore recommend that the Al-in-hornblende geobarometer be used only for hornblendes that have Fe/(Fe + Mg) < 0.65. Amphiboles from Halfmoon Pluton samples have Fe/(Fe + Mg) ratios ranging between 0.32 and 0.48 and therefore are appropriate for application of the Al-in-hornblende geobarometer.

It is difficult to establish the original fO_2 of plutonic rocks using the Fe-Ti oxide geothermometer/oxygen barometer algorithm of Ghiorso and Sack (1991) as

magnetite usually becomes Ti-free due to exsolution during slow cooling of the pluton, and ilmenite undergoes oxidation and exsolution (Haggerty, 1976). Inferences on the oxidation state of the primary magma and therefore fO_2 can however be made based on mineral assemblages and chemistry. The Mg-rich nature of the hornblendes and the occurrence of euhedral magnetite and titanite as early-crystallizing phases within all the host rocks suggests that the magma remained relatively oxidized (Leake & Said, 1994).

Pressure estimates vary within amphibole crystals and between samples, however no clear trend is recognized. Pressures estimates from core analyses from hornblendes within the section from Evening Cove to The Neck range from 3.3 kbar to 1.8 kbar (based on the Anderson & Smith 1995 calibration), and display an overall trend of decreasing pressure from the Evening Cove (inferred base) to The Neck (inferred top) (Figure 5.7). Associated errors on pressure calculations are ±0.6 kbar, therefore calculated pressures from all samples overlap within error. These results suggest that all the cores analysed from amphiboles from Evening Cove, Ringaringa and The Neck crystallized at pressures between ~1.8 and 3.3 kbar (7 and 12 km) and therefore mid- to upper-crustal levels. Because crystallization of the magma must be well advanced to produce the entire mineral assemblage required for the Al-in-hornblende barometer, such plutons are likely to be largely solidified and the calculated pressures probably represent the conditions during final emplacement (Leake & Said, 1994). As previously discussed, there is considerable uncertainty regarding the mineral assemblage that was crystallizing at the time hornblende cores formed. Pressure estimates on rims are much higher than those obtained for cores (Figure 5.7), possible reasons for which will be discussed in further detail in Section 5.5. Therefore, interpretations regarding actual emplacement depths using the Al-in-hornblende geobarometer are problematic. Quantification of actual emplacement depths is challenging, however some inferences regarding likely depths can be made based on petrographic evidence. The presence of amygdules within mafic enclaves at The Neck (inferred top of the chamber) indicates much shallower depths of crystallization than those obtained using the Al-in-hornblende geobarometer, perhaps shallower than 5 km. Actual pressure estimates for the Halfmoon Pluton cannot therefore be made. Instead, magmatic processes operating within the chamber will be discussed based on observed trends in hornblende chemistry from core to rim.

Temperature estimates for Halfmoon Pluton amphiboles were made using the plagioclase-hornblende geothermometer of Holland and Blundy (1994) and the Ti-in-amphibole geothermometer (using calculations from Femenias *et al*., 2006), which is a thermometer that is independent of magma composition. The Ti-hornblende geothermometer has been shown to be an acceptable geothermometer within the P-T envelope; P = 0.1 – 0.6 GPa and T = 700 - 950°C (Otten, 1984; Ernst & Liu, 1998; Femenias *et al*., 2006; Deering, 2009). The Halfmoon Pluton falls within this envelope, and the inclusion of titanite within all rock types indicates that these magmas are Ti-saturated, and therefore appropriate for applying the Ti-hornblende geothermometer.

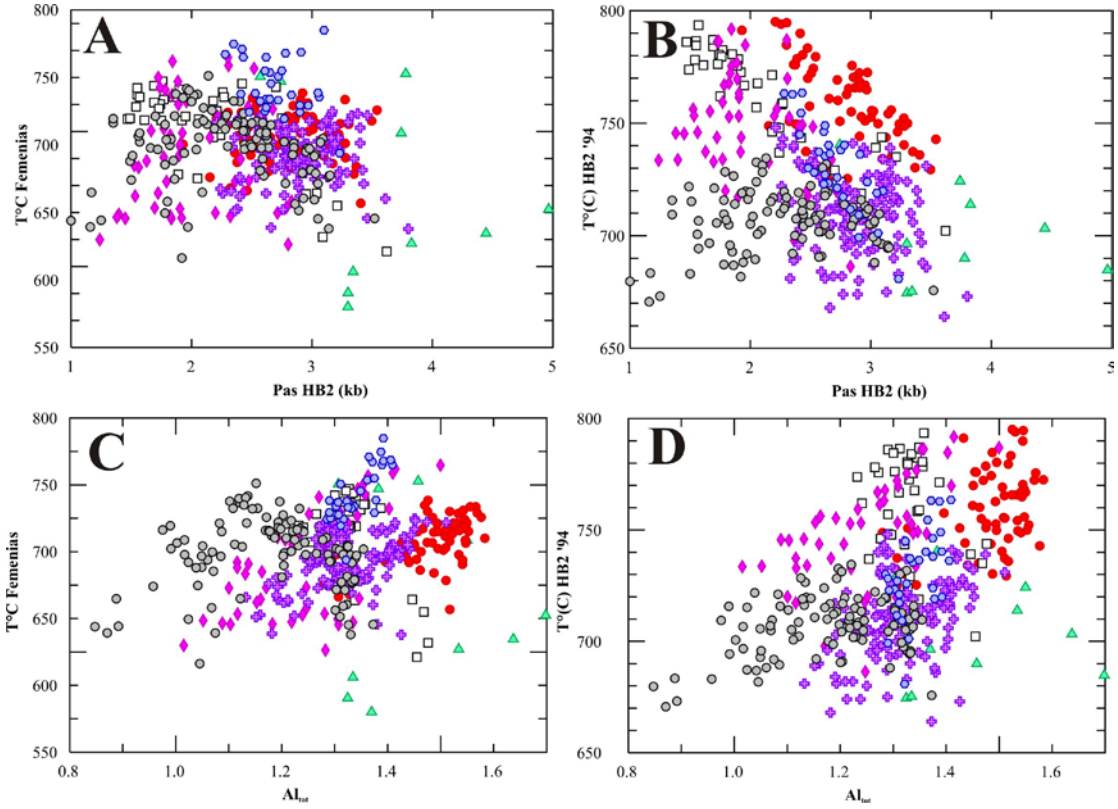

Figure 5.6. Pressure and temperature estimates for amphiboles within the Halfmoon Pluton. Pressures estimates based on Anderson & Smith (1995) and temperature estimates based on the geothermometers of (A) Femenias *et al*., (2006) and (B) Holland & Blundy (1994). (C) & (D) Temperature vs. Al_{tot}. Symbols are the same as those used in Figure 5.5.

Temperatures calculated using the plagioclase-hornblende geothermometer of Holland and Blundy (1994) display a trend of decreasing temperature with increasing pressure (Figure 5.6B) which seems counter intuitive. These temperatures however display a positive correlation with Al_{tot} (Figure 5.6D). Temperature estimates for

cores of hornblende crystals using the plagioclase-hornblende geothermometer show an overall trend of decreasing temperature from the inferred base of the chamber (EC 3/2#CX and EC#9H; T = 766 - 782°C) to the inferred top (TN#25; T = 701°C), however with geothermometer uncertainties of ± 75°C, calculated temperature differences are not significant.

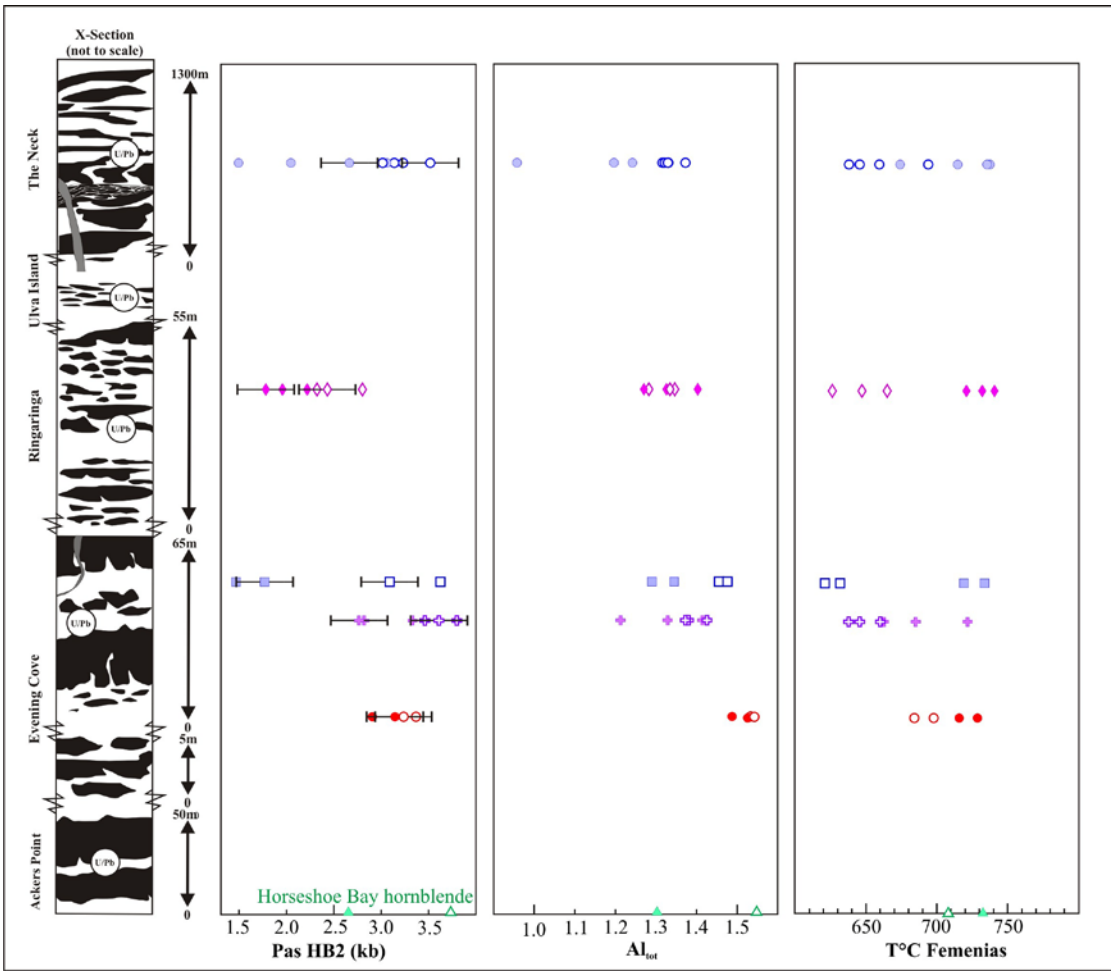

Figure 5.7. Pressure estimates (based on the Holland & Blundy 1994 calibration), Al_{tot} and temperature estimates (Ti-in-hornblende; Femenias *et al*., 2006) for core and rim analyses vs. stratigraphic height within the layered sequence of Halfmoon Pluton. Hollow symbols represent rim analyses and full-coloured symbols represent core analyses. Error bars (0.6 kbar) associated with pressure estimates are disaplayed for core and rim analyses from individual hornblende samples. In almost all examples differences within calculated pressure are larger than errors. Symbols are as follows; blue circles = TN#25; pink diamonds = RR#J3; blue squares = EC#9H; purple crosses = EC1/5; red circles = EC3/3#CX; green triangles represent HB#M2 which does not plot on the stratigraphic column but is inferred to represent a sample from deeper in the plutonic system.

Ti-hornblende temperatures (Femenias *et al*., 2006) remain relatively constant against changing pressure (Figure 5.6A). No trend with temperature and stratigraphic height is observed with temperature estimates based on the Femenias *et al*., (2006)

calibration, with core temperatures ranging from 715°C (TN#25) to 741°C (RR#J3). Rim temperatures calculated using both thermometers reveal temperatures much cooler than their cores (Table 5.4). The Ti-in-hornblende geothermometer results in much larger temperature differences between core and rim spots, with an average temperature difference of 60°C (Figure 5.7). The Ti-hornblende geothermometer gives temperature estimates that are consistently lower than those obtained from the plagioclase-hornblende geothermometer by 10-50°C.

In order to identify the processes controlling the observed compositional variations in amphiboles within the Halfmoon Pluton, detailed core-rim transects were made across 14 hornblende crystals, and five of these transects are shown in Figures 5.8 to 5.11. Chemical variation along these transects provides clues as to the changing magma compositions and fluctuating intensive parameters throughout the crystallization history of the intermediate-felsic host rocks. Al_{tot} concentrations of hornblende fluctuate from core-rim and also between samples. An overall trend of initially decreasing Al_{tot} from the core to mid-sections, and increasing Al_{tot} towards the rim is observed. Increasing Al_{tot} generally correlates with decreasing Mg and Ti. Al_{tot}-variations from core to rim within the hornblendes show a strong correlation with Al_{iv} (Al-Tschermak exchange), whereas Al_{vi} generally has a more scattered correlation with Al_{tot} concentrations (i.e. Figure 5.11). These increases in Al equate to trends of increasing pressure from core to rim (i.e Figure 5.11E). Temperature estimates based on both the plagioclase-hornblende and Ti-hornblende geothermometers show decreasing temperatures towards the rim, which correlates with increasing pressure.

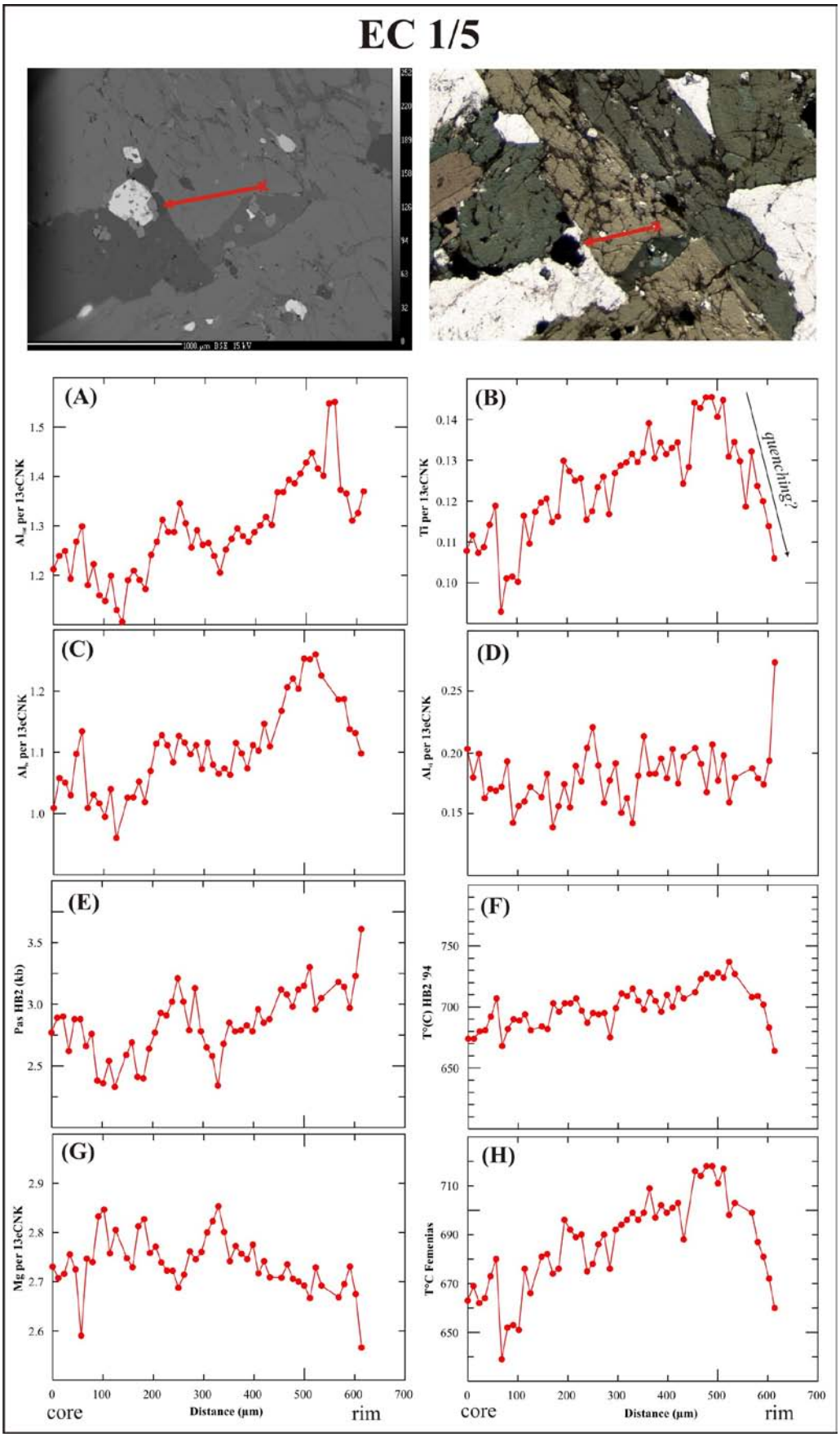

Figure 5.8. Core-rim traverse of a hornblende crystal from a leucodiorite rock at Evening Cove (EC1/5). This sample represents an intermediate cumulate host rock.

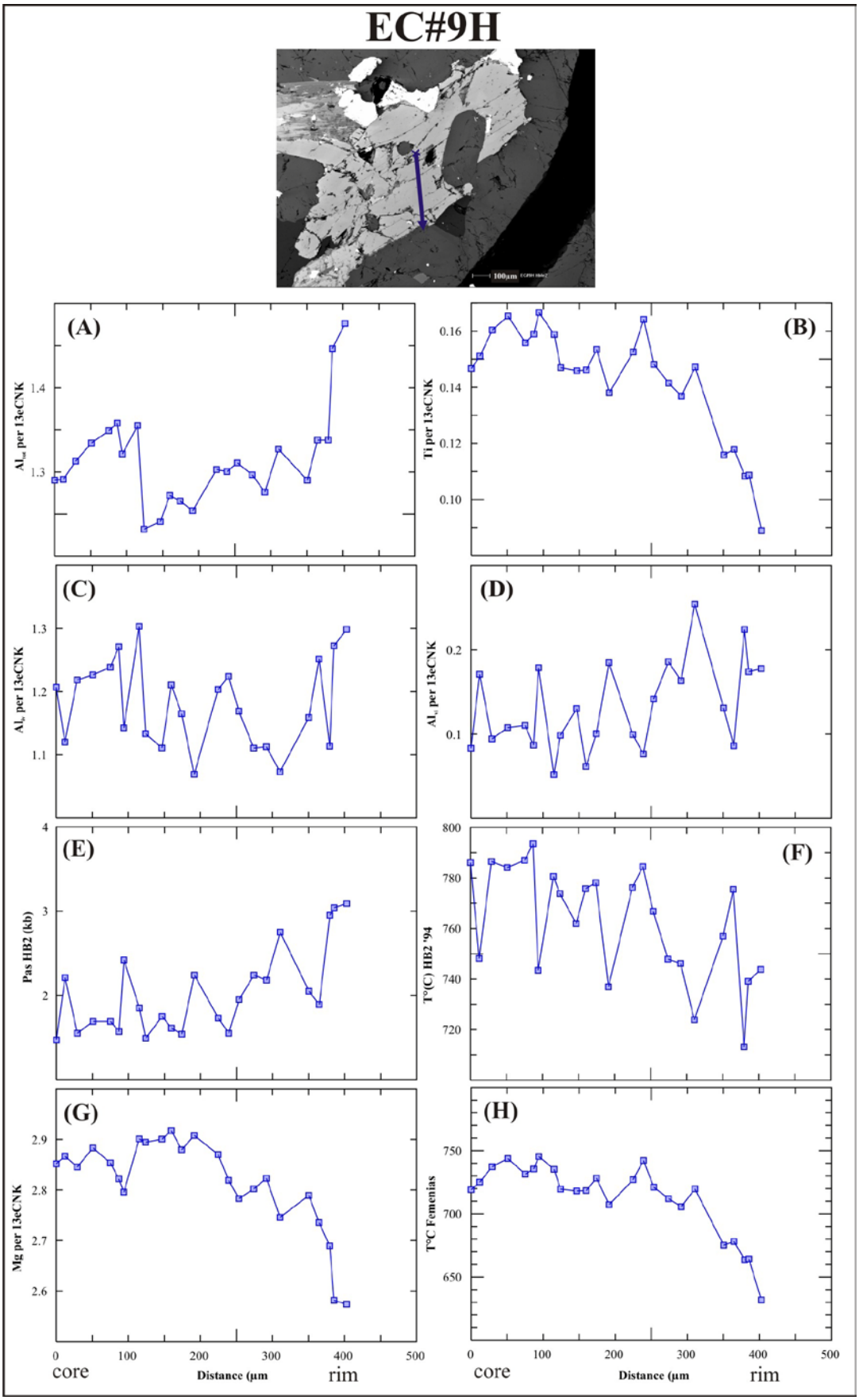

Figure 5.9. Detailed traverse across a hornblende crystal from leucodiorite host rock at Evening Cove (EC#9H).

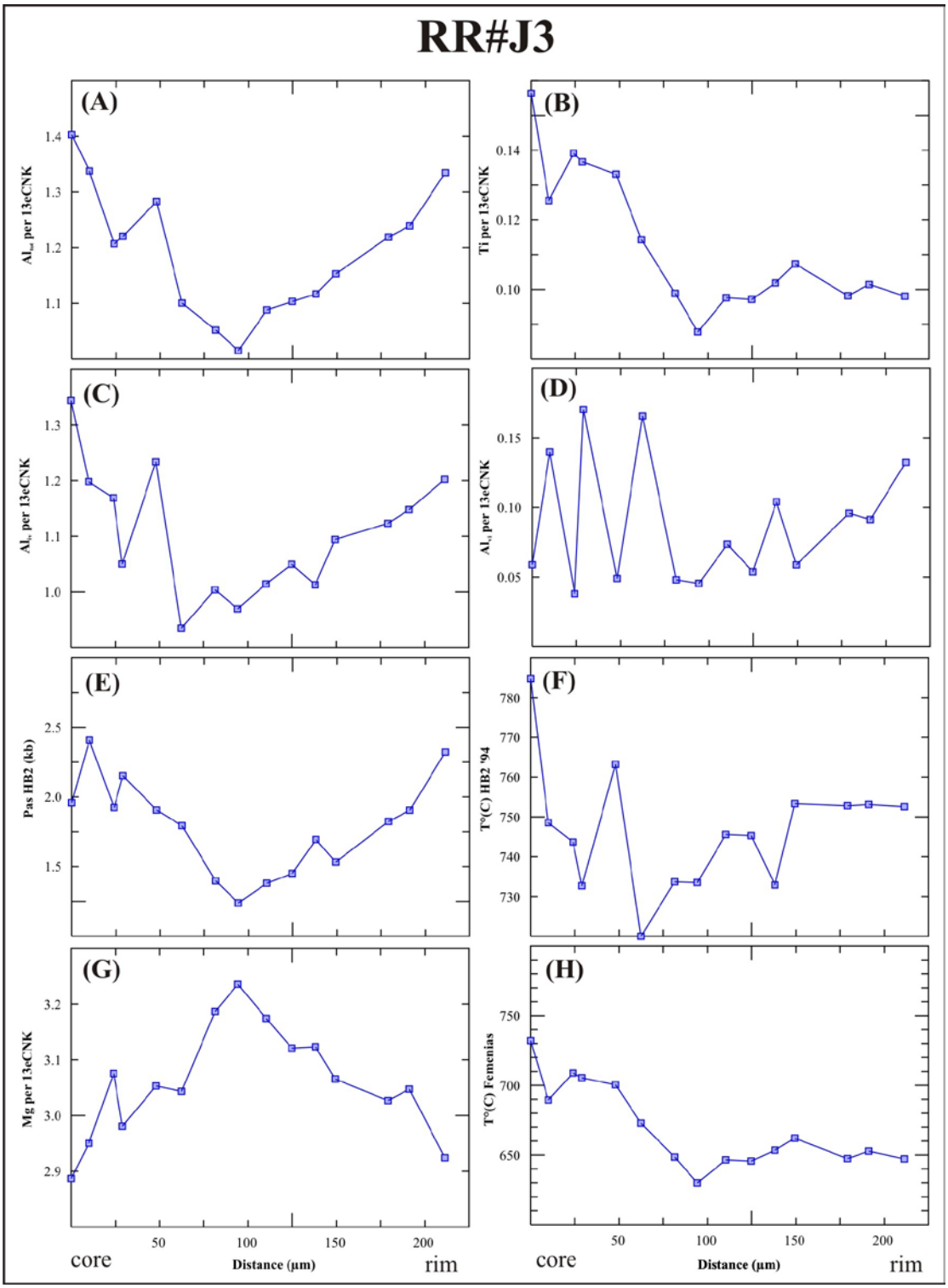

Figure 5.10. Transect from core-rim across a hornblende crystal from a granodiorite host rock at Ringaringa (RR#J3)

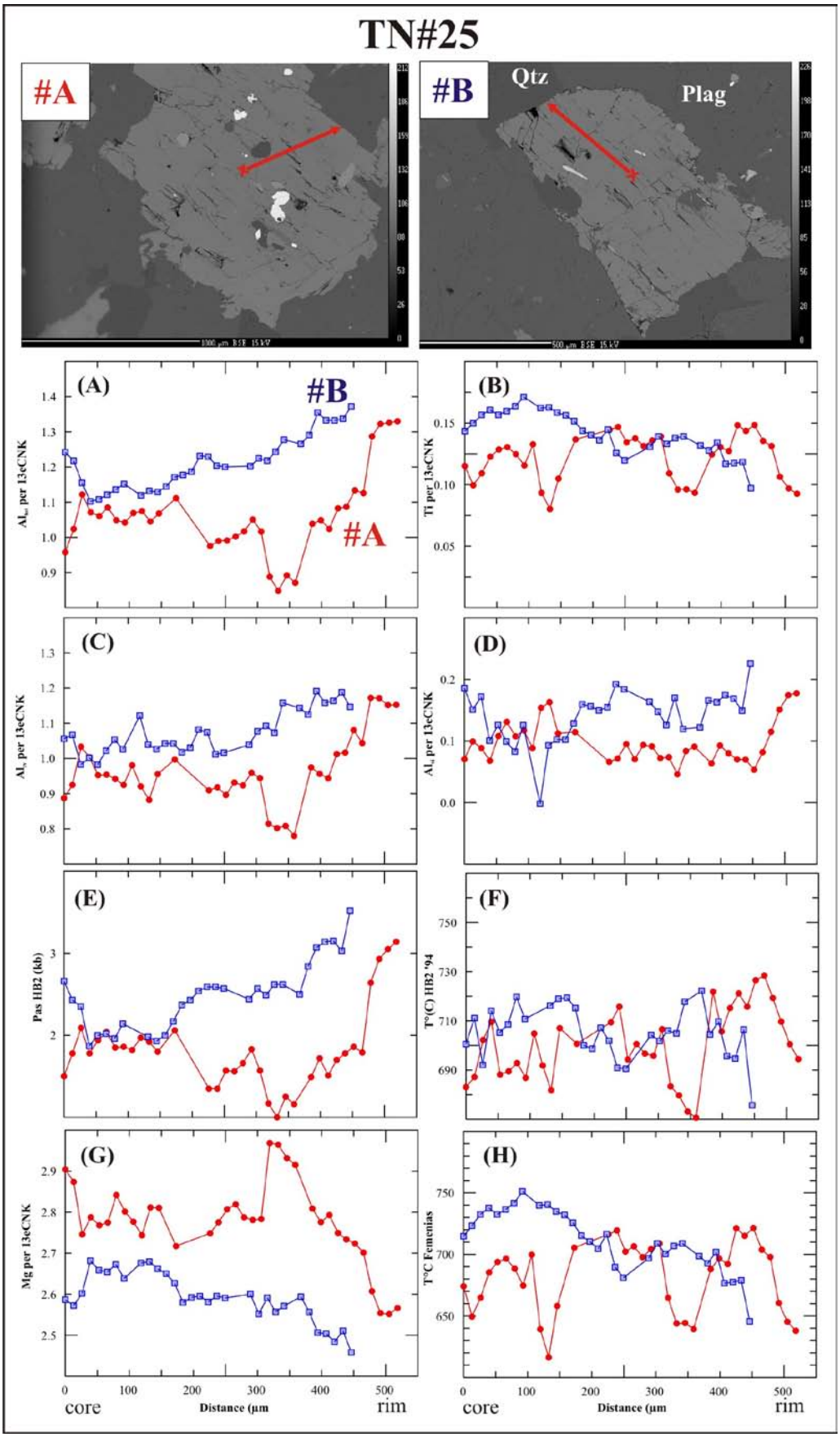

Figure 5.11. Two transects from core to rim of hornblendes from a hybrid 'mixed' rock at The Neck (TN#25).

5.5 INTERPRETATION OF MAGMATIC PROCESSES

Mineral compositions record the physical and chemical conditions of the magma from which they crystallized. Variations in the average composition of biotite show trends of decreasing MgO coupled with increasing FeO from the inferred base of the chamber towards the inferred top, consistent with fractional crystallization. Average compositions of plagioclase show a trend of decreasing An% with stratigraphic height in the chamber, which is also consistent with fractional crystallization of the host magma. These compositional changes in biotite and plagioclase are further evidence to support the conclusion reached in Chapter 4 that the main process driving chemical diversification within the Halfmoon Pluton is fractional crystallization of a mafic parental magma. Variations in plagioclase composition from core to rim however indicate that fractional crystallization was periodically interrupted. Increases in An% reflect increases in the Ca-content of the melt, which was probably caused by replenishment of the magma chamber by hotter, Ca-rich mafic magmas.

Transects across hornblende crystals also reveal variations in composition from core to rim. Maximum Al_{tot} concentrations occur at the rims of almost all hornblendes analysed. If it is to be believed that the observed increases in Al_{tot} within the hornblendes from the Halfmoon Pluton are caused by an increase in pressure, this would indicate that some of the hornblendes have experienced increases in pressure from core to rim of 0.8 and 1.6 kbar, which equates to increases in depth of crystallization of 3 – 6km. There are four possible processes that may cause the total Al_{tot} content to increase in response to increasing pressure;

1) Crystal settling of hornblendes from the top of the chamber gives lower core pressures; accumulation of these crystals at the base of the chamber gives higher pressures
2) Convection
3) Tectonic event that caused the magma chamber to be thrust to deeper pressure whereby the rims crystallized with higher Al_{tot}
4) Metamorphic re-equilibration
5) Exchange with adjacent aluminous phases in the melt

Each of these hypothesized processes has been rejected for the following reasons;

1) Large-scale crystal settling does not seem possible given that the Halfmoon Pluton appears to have been incrementally emplaced. Only small portions of the chamber were active at any one time, and crystallization and crystal settling were constantly being interrupted by the episodic injection of hotter, more mafic magmas. Therefore, crystal-rich portions of the chamber and the mingled mafic sheets and enclave swarms would inhibit crystal settling over the distances indicated by the pressure estimates

2) The morphology of the Halfmoon Pluton layered "stratigraphic" sequence would not permit the large-scale convection required to generate the large increases in pressure observed. Multiple replenishments of mafic magma into the host magma chamber resulted in the formation of a sequence of mafic sheets and enclave swarms, whose injection would have effectively sealed off large portions of the intermediate-felsic crystal mush at the base of the chamber, choking off this part of the reservoir and limiting large-scale convection

3) If a tectonic event resulting in burial of the crystallizing Halfmoon Pluton occured, then structural and/or textural evidence of such an event would be expected. Temperatures of the Halfmoon Pluton hornblendes decrease with increasing pressure, which seems to indicate that burial did not occur as you would expect temperature to increase simultaneously with pressure. However, if the still crystallizing Halfmoon Pluton were buried, it would be hotter than ambient crust, and therefore cooling would occur. Nevertheless, no obvious tectonic features are observed within the Halfmoon Pluton, and therefore the hypothesis that increasing Al-contents of hornblende are the result of burial is not favoured.

4) Metamorphic equilibration also seems an unlikely process as it seems improbable that this process would only affect the rims of the hornblendes. All hornblendes analysed also plot within the igneous field of Fleet and Barnett (1978), indicating that these hornblendes are primary magmatic hornblendes (Figure 5.12)

5) Tulloch and Challis (2000) suggested that taking analyses on hornblende rims adjacent to aluminous phases may increase the Al-content of amphibole rims for at least the outermost 30µm, by as much as 1.2 wt% Al_2O_3. This effect does not appear to be responsible for the rim-ward increase in Al observed within the Halfmoon Pluton, as increases in Al_{tot} at the rims is independent of what mineral the rim is in contact with. Furthermore, most samples show increasing Al_{tot} contents over distances greater than 200µm.

These results indicate the caution that is required when using the Al-in-hornblende geobarometer to estimate emplacement pressures as the site chosen for analysis (i.e. rim vs. core) may give pressures that do not reflect actual emplacement/crystallization depths.

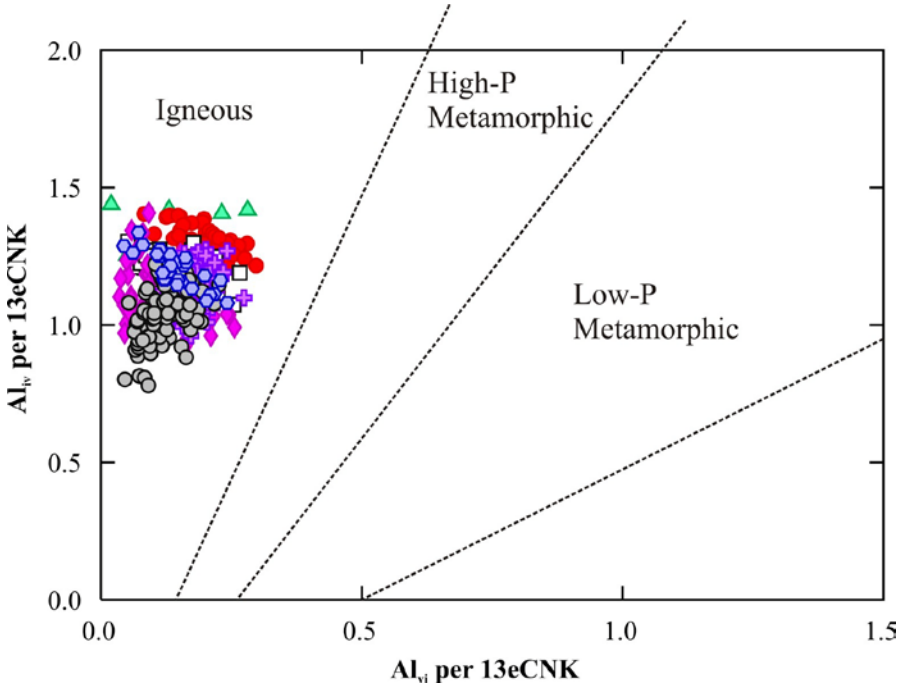

Figure 5.12. Calcic amphibole discrimination diagram from Fleet & Barnett (1978) indicating that all amphiboles within the Halfmoon Pluton are igneous.

Al_{tot}-contents within the hornblendes are therefore not controlled by increasing crystallization pressure/depth, but some other intensive variable. As discussed previously other intensive variables that may control Al_{tot}-contents are temperature, fO_2 and PH_2O. Almost all hornblendes show decreasing temperature with increasing Al_{tot}, regardless of which geothermometer is used and minimal evidence for the temperature-sensitive edenite and Ti-Tschermak substitutions. This suggests that temperature did not play a significant role in controlling the observed Al_{tot} trends. Experiments by Scaillet and Evans (1999) on the Mount Pinatubo Dacite indicated that increasing fO_2 causes Al_{tot} to increase, however these changes were small (1.64 to 1.81 Al_{tot}; 5.7 to 7.0 wt% H_2O, respectively) in relation to the Al_{tot} range for the Halfmoon Pluton amphiboles (0.85 to 1.63), and therefore fO_2 cannot account solely for the observed variation in Al_{tot}.

The sustained increase of Al_{tot} towards the rims of hornblendes may occur in response to a change in the PH_2O of the melt. As crystallization of a water-bearing melt progresses, PH_2O may increase as hydrous minerals (hornblende and biotite) can only incorporate a certain amount of the H_2O from the melt into their crystal structures. Another process that may increase PH_2O may be replenishment of the magma chamber by hydrous mafic magmas. The influence of PH_2O is hard to quantify, however increases in PH_2O might be revealed by increases in Cl- and F-contents. A lack of precision on the EMPA utilized within this study unfortunately meant that obtaining accurate concentrations for these elements was not possible.

Evidence for limited edenite-exchange (Figure 5.5C) suggests that the Al-content of hornblende is not entirely controlled by pressure, but that temperature may also have contributed to increasing Al_{tot} contents. The effect of temperature on the Al-content of Halfmoon Pluton hornblendes is difficult to resolve. Temperature estimates based on the plagioclase-hornblende geothermometer do not seem to be accurate, displaying trends of decreasing temperature with increasing pressure (Figure 5.6B). This indicates that temperature is probably acting independently of the An% of plagioclase and/or the Al-content of amphibole, and that the Ti-hornblende geothermometer may be a more reliable indicator of fluctuating hornblende crystallization temperatures.

If the magma chamber was a closed-system (i.e. there are no inputs of hot mafic or felsic magma) than the elemental concentrations within the hornblende and plagioclase crystals should decrease or increase as crystallization occurs. Fluctuations in composition profiles across both plagioclase and hornblende imply that the Halfmoon Pluton is characterized by open-system processes, and that individual crystals experienced different growth histories (i.e. composition of the melt, temperature, water content). Crystals within the same rock also commonly display different compositional histories, which indicates that crystals have been juxtaposed by processes such as magma mixing, convection and/or crystal settling.

5.6 PLUMBING OF DEEPER SOURCE?

A transect across a plagioclase crystal within a mixed 'hybrid' mafic enclave inferred to have come from lower portions of the Halfmoon Pluton (from Horseshoe Bay) was undertaken, and single spot analyses on the fine-grained mafic minerals present in its core, and growing around it. As shown in Figure 5.13, this mafic enclave contains large phenocrysts of plagioclase that display textures suggestive of disequilibrium.

A transect across this plagioclase phenocryst reveals that the corroded core of the crystal (lighter colour in BSE image) is calcic-rich, with An% ~83. This core has been resorbed, and a Na-rich rim crystallized around it, with An% of ~28. Lower An% within the core at points B and C in Figure 5.13C probably represent equilibration of the core as a result of diffusion between the adjacent mafic minerals. Anhedral clinopyroxene crystals are located in the core of this plagioclase phenocryst (Figure 5.13B). This sample represents the only rock within the entire Halfmoon Pluton to contain clinopyroxene. Core-mid-rim spots on amphibole crystals within the core of this plagioclase phenocryst were also analyzed, and display very deep crystallization pressures (4.4 - 5.0 kbar), which equates to crystallization depths between 16.4 and 18.4 km respectively. The assumption is made that these amphiboles crystallized in equilibrium with the full buffering assemblage, however because this cannot be determined, caution is required when making interpretations based on the calculated pressure estimates. These amphibole crystals display steadily decreasing Al concentrations towards the rim, with rim crystallization depths of ~12.3 km. One core

to rim analytical transect was carried out on an amphibole crystal that was in contact with the outside of the plagioclase phenocryst but still within the mafic enclave. Both the core and rim of this amphibole have compositions indicative of shallower crystallization pressures/depths with each giving estimates of 3.7 kbars/13.8 km and 2.6 kbars/9.8 km respectively. These differences in crystallization depth are interpreted as real.

This plagioclase phenocryst is interpreted to represent a Ca-rich plagioclase sourced from a deeper basaltic magma, which probably injected into the host magma chamber as a dike before breaking apart and mixing with the more silica- and sodium-rich magma. The Ca-rich core of this plagioclase was resorbed, and nucleation of Na-rich plagioclase was initiated around the rim of the resorbed core, due to crystallization within a more silicic melt. The greater crystallization depths of the amphiboles in the core of this plagioclase and the high An-contents of the plagioclase core indicates that it comes from a deeper more mafic source than the rest of the mingled mafic sheets and enclaves within the Halfmoon Pluton, and may represent the primitive parental magma from which all the mingled mafic and felsic rocks evolved.

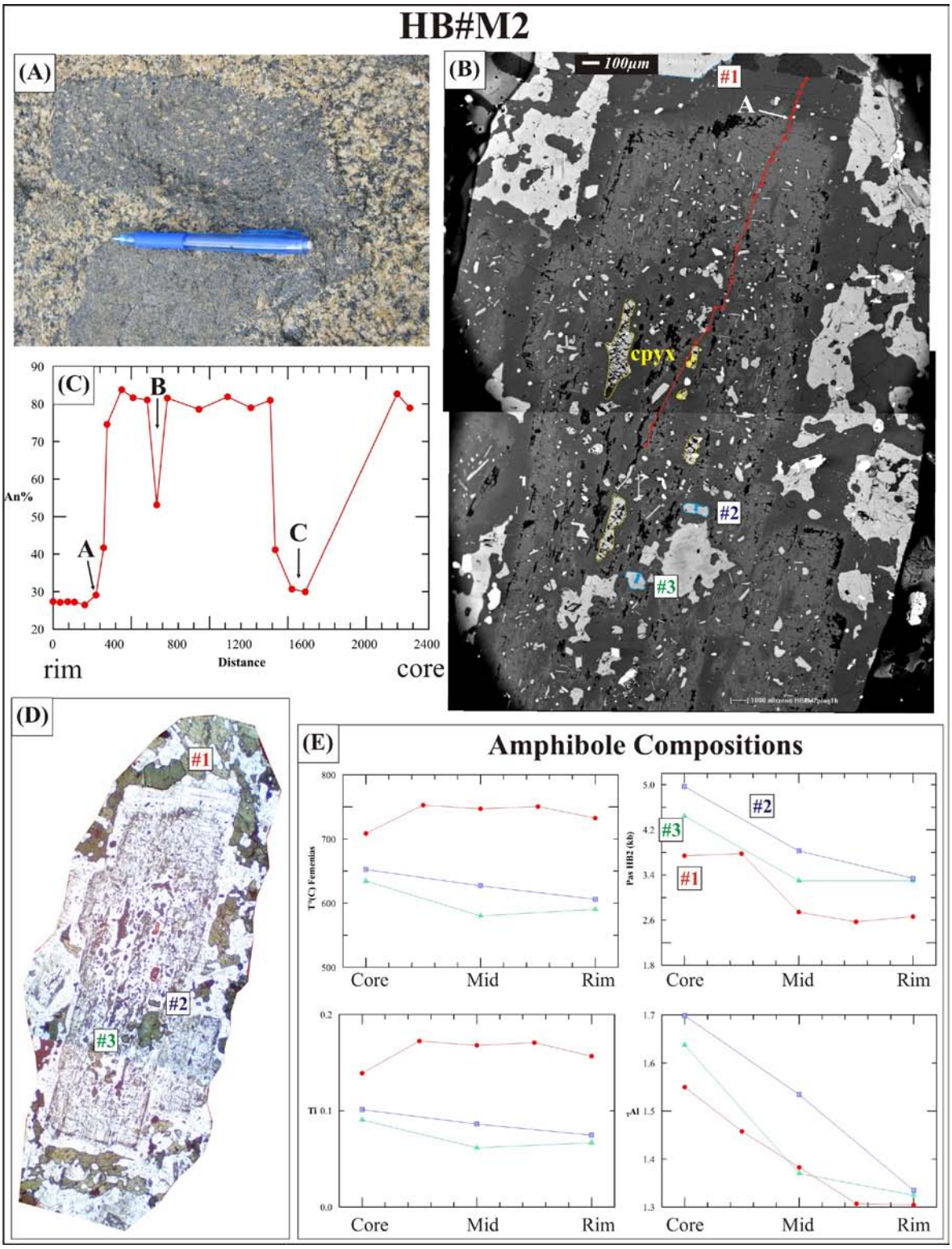

Figure 5.13. (A) Photograph showing mixed mafic enclave (top) next to a mingled mafic enclave (B) BSE image of analyzed plagioclase. Amphiboles analyzed (#1, #2 and #3) are identified and correlate with compositional results in (E). Clinopyroxene crystals are outlined in yellow (C) An% values from core-rim (D) PPL image of analyzed plagioclase. Analyzed amphiboles are again identified (E) Compositional information for amphiboles from core, mid and rim spots.

5.7 CONCLUSIONS

Minerals are sensitive to a range of important intensive parameters, including temperature, pressure, oxygen fugacity, and melt composition, and therefore the record of growth, compositional changes (zoning) and dissolution of minerals is a sensitive indicator of the history of the enclosing magma.

Variations in mineral zoning and composition indicate that the Halfmoon Pluton crystallized within an open-system at depths ≤5 km and <12km where melt composition fluctuated in response to repeated mafic magma replenishments that increased the Ca-content, temperature and PH_2O of the resident intermediate-felsic host magma. Magma chambers with mushy cumulates at their base may contain a mixture of crystals with different thermal and geochemical histories; some crystals experienced many heat pulses, whereas others crystallized from melt associated with the last heat pulse. Different zoning profiles across plagioclase and hornblende crystals within and between samples indicate that the crystals do not have the same crystallization histories, and therefore probably came together during formation of a cumulate.

These results indicate that hornblende is an effective tool for assessing the chemical evolution of magma chambers, however, the inherent complexity of the crystal structure of amphiboles and the different exchanges that occur in response to intensive parameters, makes quantification of the processes responsible for compositional changes in hornblende difficult. Actual pressure estimates should therefore be used with caution due to the uncertainty of the mineral assemblage that was actually crystallizing at the time the hornblende crystals were growing.

5.8 REFERENCES

Anderson, J.L. and Smith, D.R. 1995 'The effects of temperature and f_{O2} on the Al-in-hornblende barometer' *American Mineralogist* 80: 549-559

Bachmann, O. and Dungan, M.A. 2002 'Temperature-induced Al-zoning in hornblendes of the Fish Canyon magma, Colorado' *American Mineralogist* 87: 1062-1076

Blundy, J.D. and Holland, T.J.B. 1990 'Calcic amphibole equilibria and a new amphibole-plagioclase geothermometer' *Contributions to Mineralogy and Petrology* 104: 208-224

Deering, C.D. 2009 'Cannibalization of an amphibole-rich andesite progenitor induced by caldera-collapse during the Matahina eruption: evidence from amphibole compositions' *American Mineralogist* 94: 1162-1174

Ernst, W.G. and Liu, J. 1998 'Experimental phase-equilibrium study of Al- and Ti-contents of calcic amphibole in MORB – A semiquantitative thermobarometer' *American Mineralogist* 83: 952-969

Femenias, O., Mercier, J-C, C., Nkono, C., Diot, H., Berza, T., Tatu, M. and Demaiffe, D. 2006 'Calcic amphibole growth and compositions in calc-alkaline magmas: Evidence from the Motru Dike Swarm (Southern Carpathians, Romania)' *American Mineralogist* 91: 73-81

Fleet, M.E. and Barnett, R.L. 1978 'Al_{iv}/Al_{vi} partitioning in calciferous amphiboles from the Frood Mine, Sudbury, Ontario' *The Canadian Mineralogist* 16: 527-532.

Ghiorso, M.S. and Sack, R.O. 1991 'Fe-Ti oxide geothermometry: thermodynamic formulation and the estimation of intensive variables in silicic magmas' *Contributions to Mineralogy and Petrology* 108: 485-510

Haggerty, S.E. 1976 'Opaque mineral oxides in terrestrial igneous rocks' *Reviews of Mineralogy* 3: 101-300

Hammarstrom, J.M. and Zen, E-An. 1986 'Aluminium in hornblende: An empirical igneous geobarometer' *American Mineralogist* 71: 1297-1313

Hollister, L.S., Grissom, G.C., Peters, E.K., Stowell, H.H. and Sisson, V.B. 1987 'Confirmation of the empirical correlation of Al hornblende with pressure of solidification of calc-alkaline plutons' *American Mineralogist* 72: 231-239

Holland, T. and Blundy, J. 1994 'Non-ideal interactions in calcic amphiboles and their bearing on amphibole-plagioclase thermometry' *Contributions to Mineralogy and Petrology* 116: 433-447

Johnson, M.C. and Rutherford, M.J. 1989 'Experimentally determined conditions in the Fish Canyon Tuff, Colorado, magma chamber' *Journal of Petrology* 30: 711-737

Leake, B.E. and Said, Y.A. 1994 'Hornblende barometry of the Galway Batholith, Ireland: an emperical test' *Mineralogy and Petrology* 51: 1438-1168

Leake, B.E., Wooley, A.R., Arps, C.E.S., Birch, W.D., Gilbert, M.C., Grice, J.D., Hawthorne, F.C., Kato, A., Kisch, H.J., Krivovichev, V.G., Linthout, K., Laird, J., Mandarino, J.A., Maresch, W.V., Nickel, E.H., Rock, N.M.S., Schumacher, J.C., Smith, D.C., Stephenson, N.C.N., Ungaretti, L., Whittaker, E.J.W. and Youzhi, G. 1997 'Nomenclature of amphiboles: Report of the subcommittee on amphiboles of the international mineralogical association, commission on new minerals and mineral names' *The Canadian Mineralogist* 35: 219-246

Otten, M.T. 1984 'The origin of brown hornblende in the Artfjallet gabbro and dolerites' *Contributions to Mineralogy and Petrology* 86: 189-199

Scaillet, B. and Evans, B. 1999 'The 15 June 1991 eruption of Mount Pinatubo. I. Phase equilibria and pre-eruption *P*-T-fO_2-fH_2O conditions of the dacite magma' *Journal of Petrology* 40: 381-411

Schmidt, M.W. 1992 'Amphibole composition in tonalite as a function of pressure: an experimental calibration of the Al-in-hornblende barometer' *Contributions to Mineralogy and Petrology* 110: 304-310

Speer, J.A. 1994 'Micas in igneous rocks' In: Bailey, S.W. (ed) *Micas.* Reviews in Mineralogy Vol. 13: 299-356

Thomas, W.M. and Ernst, W.G. 1990 'The aluminium content of hornblende in calc-alkaline granitic rocks: a mineralogic barometer calibrated experimentally to 12 kbars' In: Spencer, R.J. and Chou, I-M (eds) 'Fluid-mineral interactions: a tribute to H.P. Eugster' *Geochemical Society Special Publication* 2: 59-63

Tulloch, A.J. and Challis, G.A. 2000 'Emplacement depths of Paleozoic-Mesozoic plutons from western New Zealand estimated by hornblende-Al geobarometry' *New Zealand Journal of Geology and Geophysics* 43: 555-567

CHAPTER SIX

ZIRCONS: GEOCHRONOLOGY AND ELEMENTAL ZONING

6.1 INTRODUCTION

The history of a magma chamber may be very complex, involving such processes as replenishment, mixing and mingling between contrasting magmas, convection, crystal settling, assimilation of country rock, and fractional crystallization. Recent work (Davies *et al*., 1994; Bachl *et al*., 2001; Jellinek & DePaolo, 2003; Coleman *et al*., 2004; Glazner *et al*., 2004; Harper *et al*., 2004; Hawkins & Wiebe, 2004; Walker *et al*., 2007) has indicated that magma chambers are commonly active over long periods of time ($>10^6$ years), and remain so through the episodic replenishment of both mafic and felsic magmas which result in changing physico-chemical conditions within the chamber. Whole-rock geochemistry is often a poor indicator of these processes, as the composition of the bulk rock typically reflects the final state of the magma, rather than revealing the full spectrum of processes involved throughout a chamber's history.

As outlined in Chapter Five, microanalytical analysis of mineral phases has the potential to provide a more detailed record of fluctuating compositions and intensive parameters within magma chambers. Of all minerals, zircon is proving to be the most promising as a tool for unraveling the history of magmatic processes. Several recent publications (Griffin *et al*., 2002; Belousova *et al*., 2006; Lowry Claiborne *et al*., 2006; Bolhar *et al*., 2008) have utilized a combination of relatively new techniques in zircon microanalytical geochemistry in combination with U-Pb geochronology to provide a more robust history of magmatic evolution within plutonic and volcanic systems. The purpose of this chapter is to accurately determine crystallization temperatures, fluctuations in magma chemistry, and the timing and temporal evolution of the Halfmoon Pluton using a combination of U-Pb SHRIMP dating and LA-ICPMS analyses of zircon crystals.

6.2 ZIRCON

Zircons are reliable as an indicator of magmatic processes as they are extremely resilient both physically and chemically. Zircons commonly comprise different zones that may preserve different periods of zircon formation, and indicate periods of consumption and fluctuating magmatic conditions (Corfu *et al*., 2003). Zircons are particularly useful as they are a common accessory mineral in many if not most igneous rocks, and though modal abundance is typically low, they strongly affect the behaviour of many trace elements during the crystallization of magma (Belousova *et al*., 2006). Trace elements that are incorporated into zircon that are of particular interest in geochemical and geochronological studies include U, Pb, Th, Hf, P, Y and the REE (Finch & Hanchar, 2003).

Classification of zircon morphology, zoning and indications of inheritance, metamorphism and alteration is typically achieved through images obtained using Cathodoluminescence (CL) or Back Scattered Electron (BSE) Imaging. The shape of a crystal can provide important clues as to the geological history of the zircon, and therefore the petrogenesis of the rocks in which it occurs. Assimilation from melting of source rock and as magma rises up through the crust can be inferred if zircons contain inherited cores, whereas zircon growth within a magma chamber that has experienced little disturbance is reflected in angular/euhedral grains (Hoskin & Schaltegger, 2003). Application of CL or BSE imaging typically reveals a zoning pattern, with oscillating zones reflecting different growth stages, and differences in light intensity reflecting different chemistries. Zoning patterns typically develop in response to variable concentrations of Zr, Hf, P, Y, U, Th, Ti and REE's, with dark zones in CL typically reflecting U- and Th-rich zones, and light zones in CL representing U-poor and REE-rich sections (Corfu *et al*., 2003).

6.3 ANALYTICAL TECHNIQUES

Five samples of host rock and one sample of a late granitic body were selected for geochronological analysis. The six samples chosen represent different inferred positions within the magma chamber; AP#G and EC#6C represent a leucodiorite host rock from the inferred base of the chamber, RR#H7 a granitic host rock from the middle of the chamber, and P62077 (Ulva Island) and TN#29 which represent granitic

host and tonalitic host respectively from the inferred top of the chamber. LB 3/3#7 represents a late stage granitic body which cross-cuts the Halfmoon Pluton. The five host samples represent key locations (as discussed in Chapter Three) within the stratigraphic section from the inferred base (AP#G) to the inferred top (TN#29).

Zircons from the six samples were separated from ~1kg samples of fresh rock using standard crushing and heavy-liquid techniques. Approximately 50 zircons were hand picked under a binocular microscope, mounted in epoxy, and polished to reveal mid-sections. All zircons were imaged with reflected and transmitted light to identify cracks and inclusions, and thus to guide analysis locations. Prior to SEM imaging and U-Pb SHRIMP analysis, zircons mounts were cleaned in an ultrasonic bath with petroleum spirits, ethanol, diluted lab detergent, 1M HCL solution, and deionized H2O before being dried in an oven at 60°C. Au-coated zircons were then imaged by CL in a Hitachi SEM to reveal zoning patterns and to aid in identification of any inherited cores. Zircons were also imaged under transmitted and reflected light to identify cracks and any mineral and melt inclusions (Figure 6.1).

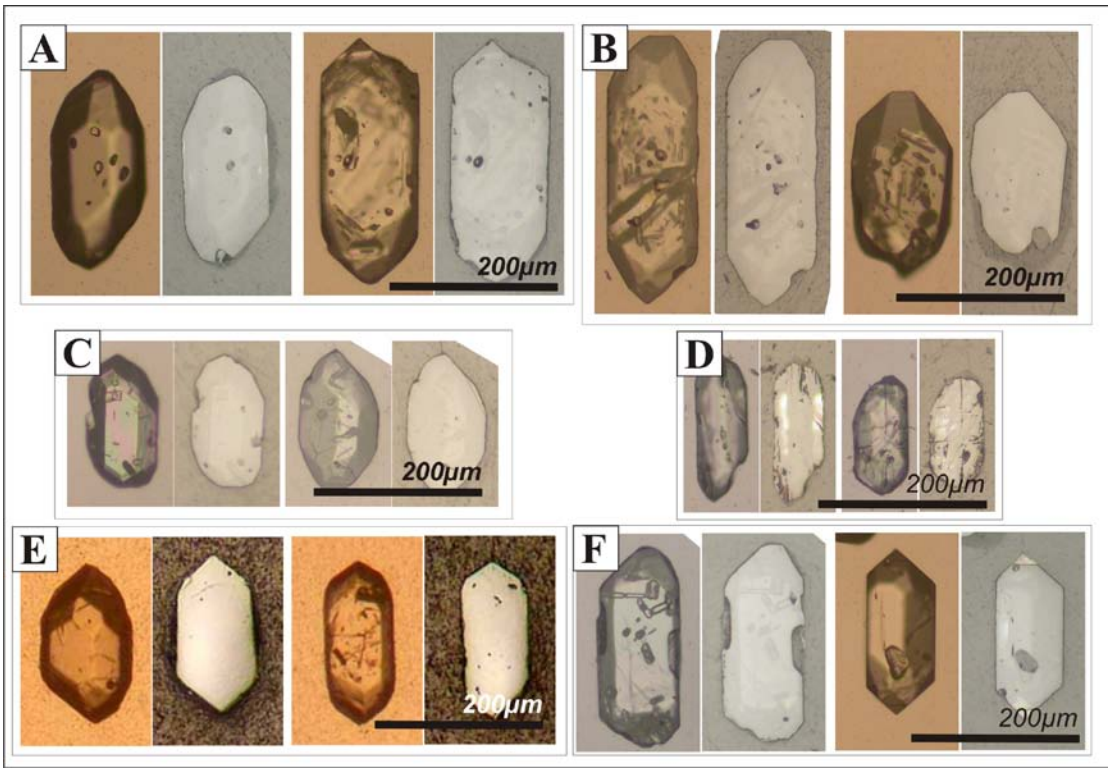

Figure 6.1. Transmitted and reflected light images of zircons from Halfmoon Pluton (A) Ackers Point - AP#G (B) Evening Cove - EC#6C (C) Ringaringa - RR#H7 (D) The Neck - TN#29 (E) Ulva Island - P62077 (F) Leask Bay - LB 3/3#7.

6.3.1 U-Pb Dating (SHRIMP-RG)

Based on CL images, between 20 and 30 grains were selected for analysis on the Sensitive High Resolution Ion Microprobe Reverse Geometry (SHRIMP-RG) at the Research School of Earth Sciences, Australian National University, Canberra. Five samples (AP#G, EC#6C, RR#H7, TN#29 and LB 3/3#7) were analysed by the author, whereas sample P62077 from Ulva Island was analszed at a later date by Trevor Ireland. Sample locations are displayed in Figure 6.2. U-Th-Pb isotopes were analyzed in-situ on small areas within single zircon crystals. Data were referenced to the zircon standard TEMORA (Black *et al*., 2003), which was analysed repeatedly during the analysis period. Operating procedures used are described in Muir *et al*. (1997), and a more detailed description can be found in electronic Appendix 6. Representative U-Th-Pb isotope and U-Th elemental data are reported in Table 6.1, and full results are found in electronic Appendix 6. Previously published and unpublished geochronological data for the Halfmoon Pluton and other plutonic bodies within the Bungaree Intrusives are displayed in Table 6.2, and locations given in Figure 6.2.

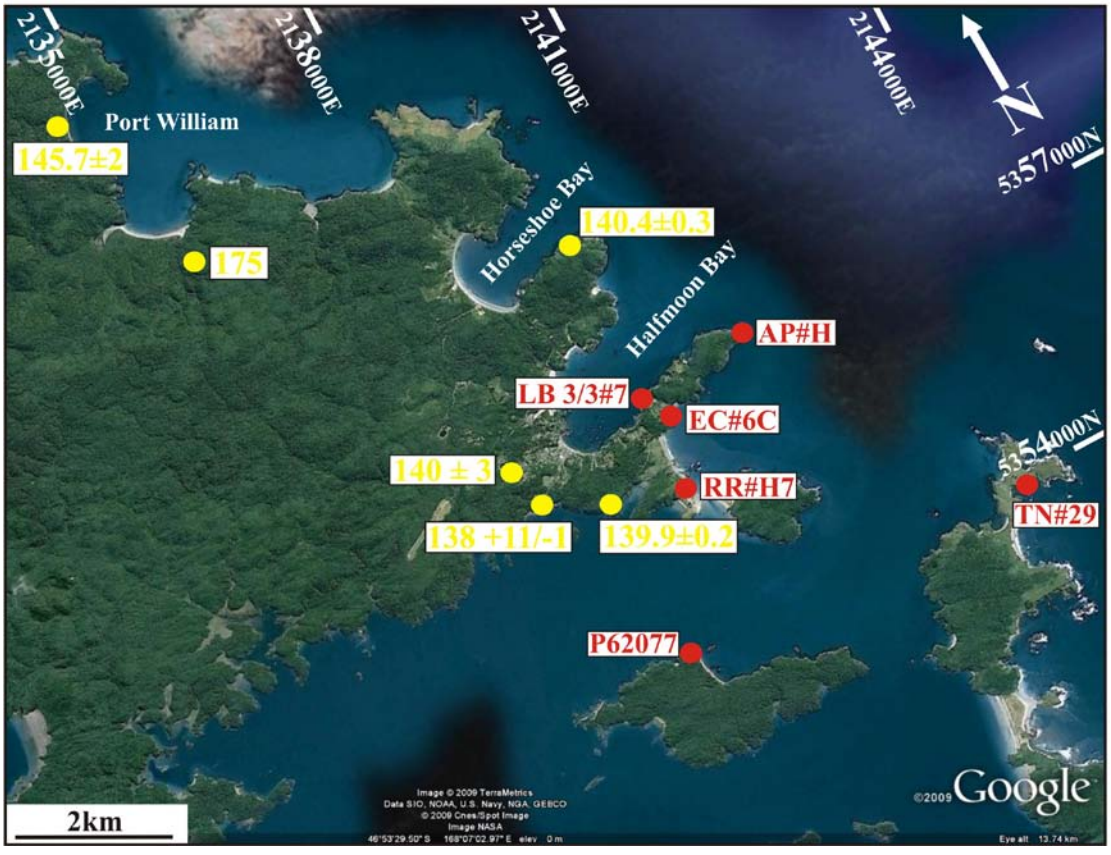

Figure 6.2. Dated samples within the Bungaree Intrusives. Figures in yellow represent geochronological data from Kimbrough *et al*., (1994) and unpublished data from A.J. Tulloch. Samples dated during this research are outlined in red. Image sourced from Google Earth.

Table 6.1: *Representative U-Th-Pb isotope data for zircons from host rock samples within the Halfmoon Pluton*

Analysis	Domain	U (ppm)	Th (ppm)	Atomic Th/U	$^{238}U/^{206}Pb$	± (1σ)	$^{207}Pb/^{206}Pb$	± (1σ)	Age (Ma)	± (1σ)
AP#G										
1.1	rim	551	291	0.55	45.22	0.7	0.05	2.1	139.6	1.0
5.1	rim	427	195	0.47	45.97	1.1	0.05	2.3	138.8	1.5
5.2	core	396	218	0.57	45.48	0.8	0.05	2.4	139.1	1.2
6.1	rim	413	193	0.48	45.71	0.7	0.05	2.3	139.5	1.0
EC#6C										
1.1	rim	141	60	0.44	44.92	1.6	0.05	3.6	138.6	2.7
1.2	core	578	261	0.47	44.77	1.4	0.05	1.9	141.7	2.0
18.1	rim	507	262	0.53	45.09	1.8	0.05	2.1	140.2	2.5
19.1	rim	574	348	0.63	45.09	1.3	0.05	1.9	141.2	1.8
RR#H7										
4.1	rim	842	432	0.53	44.78	1.2	0.06	2.6	139.9	1.8
5.1	rim	456	208	0.47	44.80	1.3	0.05	2.2	141.2	1.9
18.1	rim	632	427	0.70	44.73	1.3	0.05	1.9	142.3	1.8
19.1	rim	1486	1005	0.70	45.12	1.2	0.05	1.2	141.0	1.7
TN#29										
5.1	rim	1322	805	0.63	46.25	1.3	0.05	1.2	137.8	1.8
6.1	rim	613	347	0.58	46.14	1.5	0.05	1.8	138.3	2.1
18.1	rim	741	405	0.57	45.79	1.5	0.05	1.6	138.9	2.0
19.1	rim	1580	1269	0.83	45.99	1.3	0.05	1.1	138.5	1.8
P62077										
5.1	rim	1426	1071	0.78	45.84	1.0	0.05	1.6	139.1	1.4
6.1	rim	1879	1002	0.55	45.25	0.9	0.05	1.3	140.9	1.3
7.1	rim	3437	2041	0.61	46.51	0.9	0.05	1.2	137.2	1.2
8.1	rim	447	218	0.50	45.15	1.1	0.05	2.7	140.7	1.6
LB 3/3#7										
27.1	rim	219	99	0.47	45.18	1.0	0.05	3.1	138.9	1.6
27.2	core	243	119	0.51	46.53	1.0	0.05	3.0	136.5	1.3
30.1	rim	274	130	0.49	45.69	1.4	0.05	2.9	138.6	2.1
30.2	core	299	191	0.66	45.19	0.9	0.09	2.4	134.3	1.9

Errors associated with the measured isotope ratios and the age are 1σ

Table 6.2 *: Geochronological data for plutonic bodies within the Bungaree Intrusives*

Unit &/or sample number	Rock Type	Grid Reference	Age (Ma)	Reference
Deep Bay - P62093	Granite dike	E48/388556	139.9 ± 0.2	A.J. Tulloch unpublished
Traill - OU49148	Qtz Diorite	E48/383563	141 +2/-1	Kimbrough *et al* ., 1994
Golden Bay - OU49146	Granite sheet	E48/381560	138 +11/-1	Kimbrough *et al* ., 1994
Horseshoe Bay - P60200	Monzonite	E48/396590	141 +7/-1	Kimbrough *et al* ., 1994
Port William - P62078	Diorite	E49/545608	c. 175	A.J. Tulloch unpublished
Lee Bay - P65510	Basalt-Andesite dike	E49/460626	145.7 ± 2	A.J. Tulloch unpublished

6.3.2 Trace and Rare Earth Elements (LA-ICPMS)

Trace (P, Sc, Ti, Sr, Y, Nb, Hf, Th and U) and REE abundances were obtained by laser-ablation inductively coupled plasma mass spectrometry (LA-ICPMS) at Victoria University of Wellington. Representative trace and REE data are reported in Table 6.3, and full results are found in electronic Appendix 7.

Background data were acquired for ~30 seconds followed by ~120 seconds of laser ablation, yielding ~315 mass scans and a penetration depth of ~20 µm. All spot sizes were 20 µm. Raw data were converted to concentrations (in parts per million) by normalizing count rates for each element to those for Si, assuming SiO_2 to be stochiometric in zircon with a concentration of ~32.8 wt%, and multiplying by a correction factor based on measurement of standard glass NIST 610 with concentration values recommended by Pearce *et al*., (1997). The low abundance ^{49}Ti isotope was chosen to avoid interference with ^{96}Zr and/or ^{48}Ca (from apatite inclusions) on the major ^{48}Ti peak. Laser ablation spots on zircon were chosen to avoid inclusions and cracks, however several zircons contained a large number of apatite inclusions which affected several analyses (Figure 6.1). Apatite is enriched in phosphorous and LREE, and therefore any zircon analyses which displayed unusually high P and LREE count rates were excluded from concentration calculations. To ensure precise elemental concentrations, analysis of standard glass NIST 610 was undertaken prior to, and following analyses of Halfmoon Pluton samples. Analytical errors (based on 2% standard deviations from NIST-610 analyses and Halfmoon Pluton analyses) are <1% for Sr, Y and Nb at the ppm concentration level, between 1-5% for the REEs, and between 5 and 7% for U, Th, Ta and W.

Table 6.3. Representative trace and rare earth element concentrations (in ppm) for zircons from the Halfmoon Pluton

Domain	Sample	P	Y	La	Ce	Sm	Eu	Dy	Lu	Ti	Hf	Th/U	Eu/Eu*
Evening Cove (EC#6C)													
core	EC#6C B3	373.1	1220.7	3.2	23.3	4.8	0.7	98.1	95.2	5.9	11900.6	0.63	0.066
mid	EC#6C B2	231.8	1023.7	0.0	22.5	2.4	0.3	81.3	79.7	3.2	12040.6	0.71	0.046
rim	EC#6C B1	105.0	200.8	0.1	4.4	0.4	0.2	13.7	26.0	4.4	12079.0	0.30	0.277
core	EC#6C A3	189.5	564.4	0.1	6.8	1.7	0.3	46.5	39.1	12.4	10401.8	0.54	0.068
mid	EC#6C A2	207.4	833.0	0.1	16.4	2.2	0.3	64.8	68.0	2.3	12167.2	0.66	0.060
rim	EC#6C A1	59.3	174.2	0.0	3.1	0.2	0.2	11.2	25.5	11.7	12554.7	0.27	0.251
Ackers Point (AP#G)													
rim	AP#G 7.1	231.5	633.8	0.6	12.0	1.7	0.3	48.2	52.2	2.0	12022.7	0.53	0.069
core	AP#G 7.2	263.9	1010.8	0.3	11.4	3.6	0.4	91.1	60.3	19.4	10827.5	0.69	0.040
mid	AP#G 7.3	162.9	437.5	0.0	7.3	1.0	0.1	33.9	33.9	4.5	13057.8	0.40	0.040
rim	AP#G 8.1	258.2	577.4	0.4	9.4	1.6	0.2	48.2	39.1	5.8	11342.4	0.56	0.058
core	AP#G 8.2	283.6	2180.4	0.3	17.0	11.5	0.9	208.3	111.4	9.5	11591.1	0.82	0.036
The Neck (TN#29)													
rim	TN#29 7.1	273.0	1343.9	0.1	17.3	3.4	1.1	100.0	108.2	5.2	9543.0	0.59	0.132
core	TN#29 7.2	634.8	2273.8	13.6	71.4	11.2	2.7	176.3	147.5	7.6	11039.8	0.84	0.127
rim	TN#29 9.1	197.0	1113.4	0.0	8.3	5.1	1.6	97.4	80.0	3.4	10252.1	0.64	0.146
core	TN#29 9.2	418.4	3083.8	0.2	21.5	13.9	2.4	274.3	183.1	8.8	9441.2	0.87	0.078
rim	TN#29 16.1	615.0	1836.0	1.2	31.8	6.6	0.8	140.4	134.0	2.7	12327.6	0.52	0.053
core	TN#29 16.2	366.0	1703.7	0.2	29.4	4.0	0.5	125.9	135.8	4.1	11560.2	0.55	0.046
Ringaringa (RR#H7)													
rim	RR#H7 5.1	203.4	835.9	0.1	15.9	1.6	0.3	64.3	71.8	3.6	11680.2	0.52	0.066
core	RR#H7 5.2	260.5	1964.0	1.8	27.3	9.5	2.0	159.7	130.4	13.6	11674.4	0.63	0.106
rim	RR#H7 7.1	281.9	2074.6	0.0	22.2	7.4	0.6	172.9	141.5	3.8	11503.4	0.72	0.036
core	RR#H7 7.2	351.8	926.7	0.4	12.6	2.6	0.6	69.7	83.5	7.7	12190.4	0.43	0.111
rim	RR#H7 9.1	327.6	1306.8	0.2	25.4	3.6	0.6	101.4	104.3	20.7	11004.3	0.61	0.072
core	RR#H7 9.2	341.1	1513.2	0.0	26.4	3.5	0.5	115.3	125.8	3.6	10352.7	0.67	0.060
Leask Bay (LB 3/3#7)													
rim	LB3/3#7 13.1	253.7	963.0	0.1	12.4	2.7	0.3	82.0	61.9	8.2	12329.9	0.71	0.039
core	LB3/3#7 13.2	215.8	1281.2	bdl	11.1	6.3	0.5	113.7	69.4	11.0	11910.4	0.84	0.036
rim	LB3/3#7 12.1	285.0	907.1	0.5	15.6	2.4	0.2	75.1	59.3	4.7	12428.6	0.72	0.036
mid	LB3/3#7 12.2	291.9	1022.3	0.2	13.2	3.5	0.3	85.0	66.6	7.2	11725.7	0.68	0.040
core	LB3/3#7 12.3	776.3	2841.4	3.0	30.9	14.2	1.3	268.6	145.8	11.7	9899.0	0.89	0.040

bdl = below detection limit

6.4 ZIRCON MORPHOLOGY AND U-PB GEOCHRONOLOGY

Field interpretations made in Chapter 3 indicate that the Halfmoon Pluton crystallized upwards and was subsequently tilted to expose a cross-section through the magma chamber. To test interpretations made in the field based on the identification of way-up structures, and to determine the precise age and crystallization history of the pluton, U/Pb dating of six samples of the felsic host rocks was undertaken. Zircon CL images are shown in Figure 6.3, and data obtained from SHRIMP-RG analysis are discussed below and presented in the form of Tera-Wasserburg concordia diagrams in Figure 6.4. Representative U-Th-Pb isotopic data are given in Table 6.1. Rims were analyzed in order to determine the age of crystallization of the zircon within the magma. Several cores were analysed to ascertain if there was inheritance within any of the rock samples.

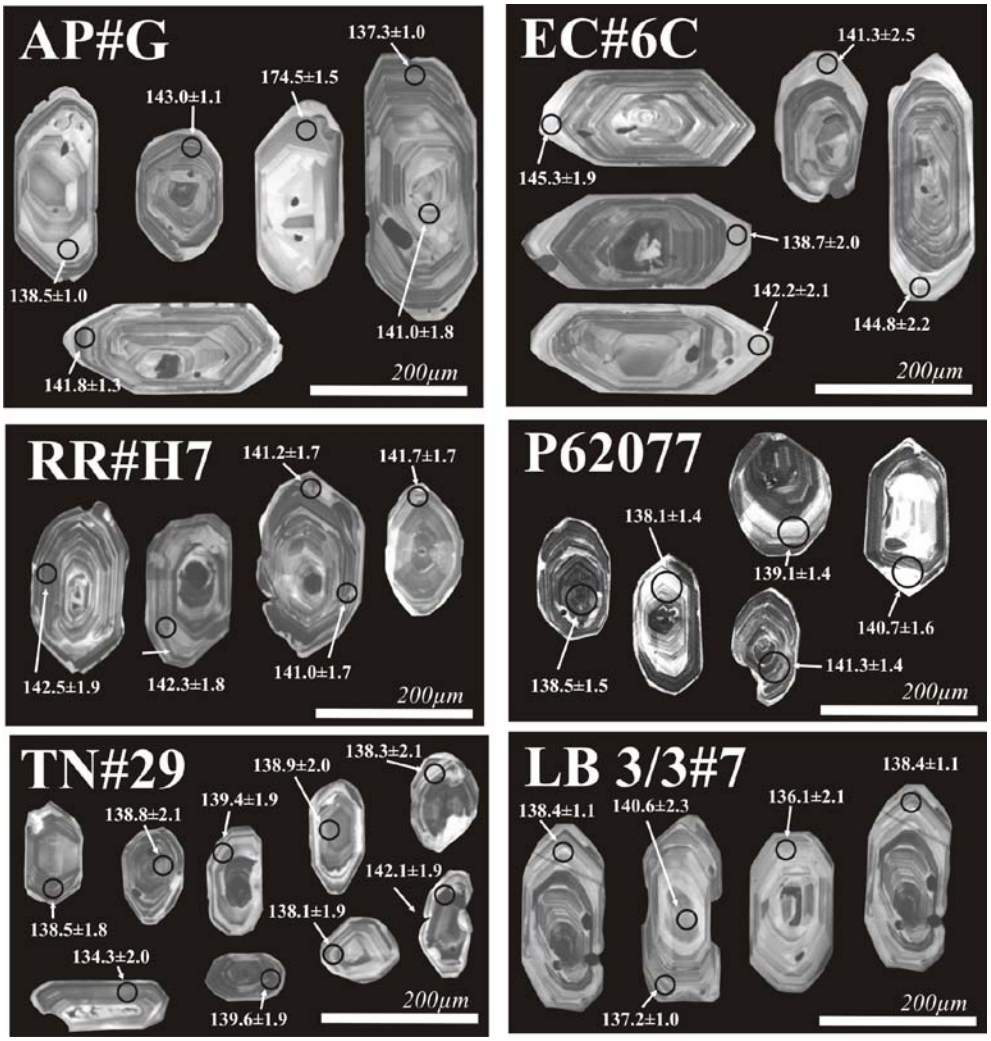

Figure 6.3. Cathodoluminescence images of selected zircons analysed from six samples within the Halfmoon Pluton. $^{238}U/^{206}Pb$ ages are given in Ma with one sigma errors. Black circles show approximate spot size and location.

6.4.1 AP#G – Leucodiorite host rock from Ackers Point (E48/41265711)

Zircons are euhedral and range in length from ~160 – 320 µm (aspect ratios range from 1:1.4 to 1:3). Transmitted light images reveal that the zircons commonly contain inclusions (see Figure 6.1A) which are probably apatite and melt inclusions. Internal structures are variable, however most zircons display relatively homogeneous cores surrounded by narrowly spaced uninterrupted oscillatory zoning (Figure 6.3A). These cores are typically darker than the enclosing zones and have boundaries parallel to oscillatory zoning and therefore are not likely to be inherited cores. This is supported by a lack of inherited ages, with only one zircon displaying an older age of 175.6 ± 2 Ma, which is interpreted to represent an inherited zircon from the older heterogeneous diorites within the Bungaree Intrusives, such as those at Port William (Figure 6.2 and Table 6.2). Zircons also commonly exhibit a bright rim that is enriched in LREE and depleted in U relative to the darker interior of the zircons. These rims have Th/U ratios between 0.4 and 1.7 indicating that they are clearly magmatic (Table 6.3). Twenty-two zircons were analysed from Ackers Point. Three outliers which show spurious backgrounds (i.e. high Th/U ratios), are discordant or were interpreted to represent an older inherited age were excluded from age calculations. The remaining 19 analyses have a weighted mean age of 139.4 ± 0.7 Ma (95% confidence) and an MSWD of 1.1 (Figure 6.4A).

6.4.2 EC#6C – Leucodiorite host rock from Evening Cove (E48/40045650)

Zircons are large (~150 - 310 µm in length, aspect ratios range from 1:1.7 to 1:3.4), and are all euhedral. Transmitted light images reveal that the zircons contain a large number of inclusions (apatite + melt) which were often difficult to avoid analyzing (see Figure 6.1B). CL images show that from core to rim the zircons are characterized by numerous repeating zones and a distinctive thick brighter outside rim (Figure 6.3B), which analysis shows has Th/U ratios between 0.2 and 0.7 (Table 6.3). No sign of inherited cores is evident in CL images, which is supported by the absence of distinctly older U-Pb ages and four core spot analyses. Twenty-seven zircons were analysed from Evening Cove. One outlier was excluded, with the remaining 26 analyses giving a weighted mean age of 141.8 ± 1.2 Ma (95% confidence) and an MSWD of 1.16 (Figure 6.4B).

6.4.3 RR#H7 – Granite host rock from Ringaringa (E48/39835562)

Zircons from RR#H7 are smaller than those from AP#G and EC#6C, ranging in length from ~100 to 240 µm, with aspect ratios between 1:1 and 1:2.5. All zircons analyzed are euhedral and stubby, and they commonly contain inclusions (Figure 6.1C). Under CL, all zircons are homogeneous, contain no obvious inherited cores, and display closely spaced oscillatory zoning (Figure 6.3C). Like samples AP#G and EC#6C, zircons commonly contain a brighter rim, but it is much less pronounced in these zircons. Rims have Th/U ratios between 0.4 and 1.1 (Table 6.3). Twenty zircons were analyzed from Ringaringa, 19 of which yield a weighted mean age of 140.1 ± 1.1 Ma (95% confidence) and an MSWD of 1.05 (Figure 6.4C). One anomalously old age was excluded from these age calculations.

6.4.4 P62077 – Leucogranite host rock from Ulva Island (E48/39055365)

Zircons are euhedral to subhedral, with several displaying irregular, embayed edges, which may have been due to sample processing, or may represent corrosion. Zircons are quite stubby in appearance, ranging in length from ~90 to 200 µm, with aspect ratios between 1:1.2 and 1:2.2. Most zircons under transmitted light contain few if any inclusions (Figure 6.1E). Closely spaced oscillatory zoning is evident in CL imaging, with almost all zircons displaying dark cores and progressively lighter mid sections and rims (Figure 6.3D). Poor picture quality limits further interpretations on the internal character of these zircons. Fourteen zircons were analyzed, with 13 of these having a weighted mean age of 139.0 ± 1.0 Ma (95% confidence) and an MSWD of 1.4 (Figure 6.4E).

6.4.5 TN#29 – Tonalite host rock from The Neck (E48/43095361)

Zircons are euhedral to subhedral, with most appearing slightly rounded in shape and containing several embayments at their edges. This appearance may have been caused by sample processing or represent corrosion of the crystal within the magma. Zircons within this sample are much smaller than in all other samples, with lengths ranging from ~80 to 170 µm, and aspect ratios ranging between 1:1.1 and 1:3.7. Transmitted light images reveal that zircons contain small concentrations of inclusions (Figure 6.1D). CL images show that the zircons from TN#29 don't exhibit the same degree or complexity of zoning as the other four samples discussed above, with faint oscillatory zoning and a lack of any significant bright rim (Figure 6.3E). All 26 zircon analyses

from The Neck provide a single age population with an age of 138.6 ± 0.7 Ma (95% confidence) and an MSWD of 1.4 (Figure 6.4D).

6.4.6 LB 3/3#7 – Cross-cutting Granite body from Leask Bay (E48/39795681)

Zircon crystals are almost generally all euhedral and range in length from ~170 to 370 µm, with aspect ratios between 1:1.4 and 1:3.2. Transmitted light images reveal that all zircons contain an abundance of inclusions (Figure 6.1F) (likely to be both apatite and melt inclusions). Zircons show oscillatory zoning from core to rim, and lack the bright CL rims that characterize the rest of the zircons discussed above (Figure 6.3F). As Figure 6.4(F) shows, zircons analysed from LB 3/3#7 display significant scatter in U-Pb ages. Seven of the 28 zircons analysed contained much younger ages than the remaining 21 analyses. These analyses yield age differences of between ~6 and 12 Ma with one sigma errors, and are still considerably younger with two sigma errors. These anomalously young dates are attributed to Pb-loss and are therefore excluded from age calculations. The remaining 21 zircon analyses provide a single age population of 139.1 ± 0.7 Ma (95% confidence) and an MSWD of 1.13.

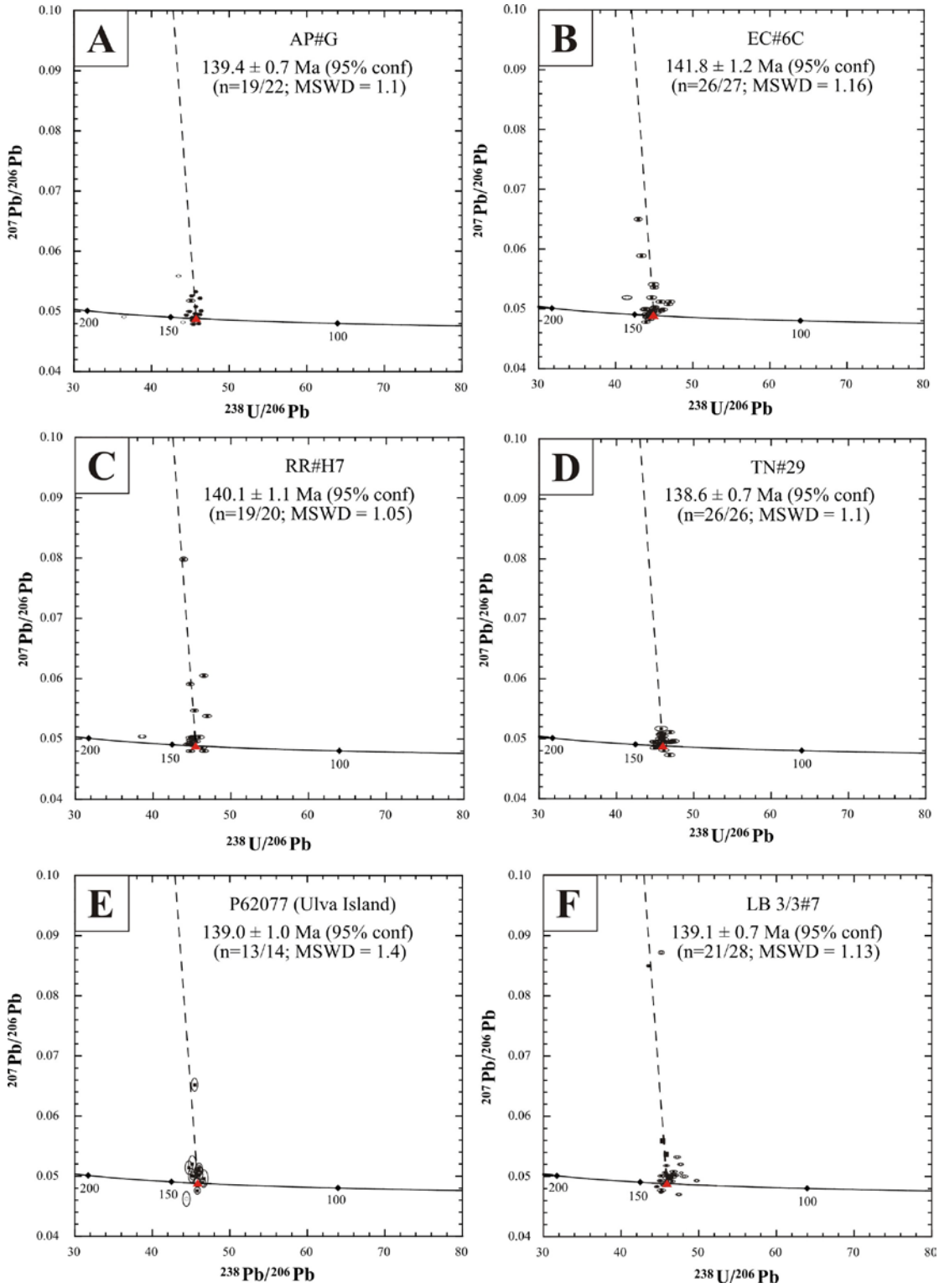

Figure 6.4. Tera-Wasserburg (Tera & Wasserburg, 1972) U/Pb concordia diagrams for samples within the Halfmoon Pluton. The amount of common Pb in each analysis is inferred from the offset of the point from concordia along the trajectory of common Pb mixing. Outliers may be caused by inheritance (left of mixing line) or Pb loss (right). Computed weighted mean $^{238}U/^{206}Pb$ ages are given with two sigma errors.

6.5 TRACE AND RARE-EARTH ELEMENTAL CHARACTERISTICS

Correlation of changes in trace element patterns with zircon zoning patterns can be indicative of changes in magma chemistry during zircon crystallization. Representative analyses of trace and REE concentrations within zircons from the Halfmoon Pluton are displayed in Table 6.3, with full results in electronic Appendix 7. Table 6.4 gives a brief summary of the rock types, whole-rock geochemistry and location within the Halfmoon Pluton "stratigraphic" sequence of the five samples analysed for LA-ICP-MS, and Figure 6.5 displays the localities of the five samples analysed for trace and REE in zircon. Figure 6.6 displays representative chondrite-normalised (Sun & McDonough, 1989) REE trends for zircons from within these five samples. All graphs display a characteristic trend of LREE depletion relative to HREE enrichment. This REE pattern is typical for unaltered igneous zircons, and reflects the preferential incorporation of HREE's over LREE's within crystallizing zircons (Hoskin & Schaltegger, 2003). Ce- and Eu-anomalies are variable within and between samples, however most show large positive Ce-anomalies and small negative Eu-anomalies. REE concentrations from core to rim and between samples are also displayed in Figure 6.5. Almost all samples show very little variation between core and rim, with rims either being slightly more enriched or depleted in REE compared with their core or mid-section analyses. Rim analyses for zircons from EC#6C however show depletions in total REE abundance, a smaller Ce-anomaly, and no Eu-anomaly relative to core and mid-section analyses (Figure 6.5).

A small number of spot analyses are enriched in LREE and P (i.e. EC#6CB3 see Table 6.3), which probably reflects analyses of apatite inclusions. Almost every zircon analyzed from sample RR#H7 displayed data intervals with high LREE and P concentrations, which were interpreted to represent the laser passing through from the zircon into apatite inclusions. These data intervals were deleted during data processing, however this meant that in many samples there were very low count rates remaining, which may have affected the reliability/accuracy of trace and REE concentrations. Interpretation of results from RR#H7 therefore requires caution.

Table 6.4. Petrographic and geochemical data for the samples analysed for trace and REEs

Sample	Locality	Grid reference	Rock Type description	SiO_2	Zr	$^{87}Sr/^{86}Sr_{(i)}$	εNd	Age
AP#G	Ackers Point	E48/41265715	Leucodiorite host	53	239	0.7039	1.97	139.4 ± 0.7
EC#6C	Evening Cove	E48/40045650	Leucodiorite host	58	193	0.7039	3.53	141.8 ± 1.2
RR#H7	Ringaringa	E48/39835563	Monzogranite host	76	117	0.7039	1.59	140.1 ± 1.1
TN#29	The Neck	E48/43095361	Tonalite host	57	208	n/a	n/a	138.6 ± 0.7
LB 3/3#7	Leask Bay	E48/39705678	Granitic sheet	71	112	0.704	5.04	139.1 ± 0.7

Note all samples are listed in "stratigraphic" order with AP#G representing the inferred base of the chamber and TN#29 representing the inferred top. LB 3/3#7 represents a later cross-cutting granitic sheet. n/a = not analysed.

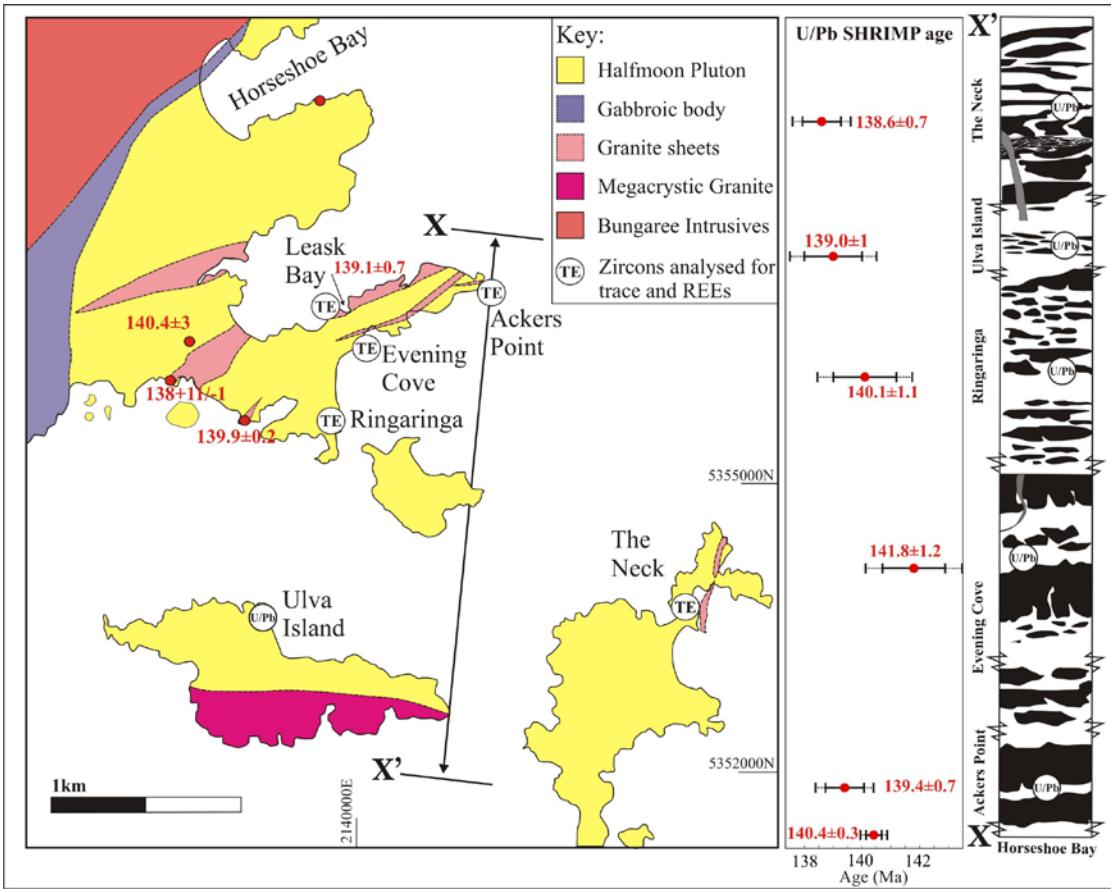

Figure 6.5 Simplified geological map of the Halfmoon Pluton showing samples dated throughout the pluton and localities of samples analysed for trace and REE in zircon. The "stratigraphic" column displayed outlines the main magmatic sequence studied between X and X' with associated U/Pb SHRIMP ages and errors. Note that errors displayed are 2σ (full line) and 3σ (dashed line). Dated localities are a combination of geochronological analyses undertaken within this research (TE and U/Pb symbols), published (Kimbrough *et al*., 1994) and unpublished (A.J. Tulloch) data (both identified by red circles).

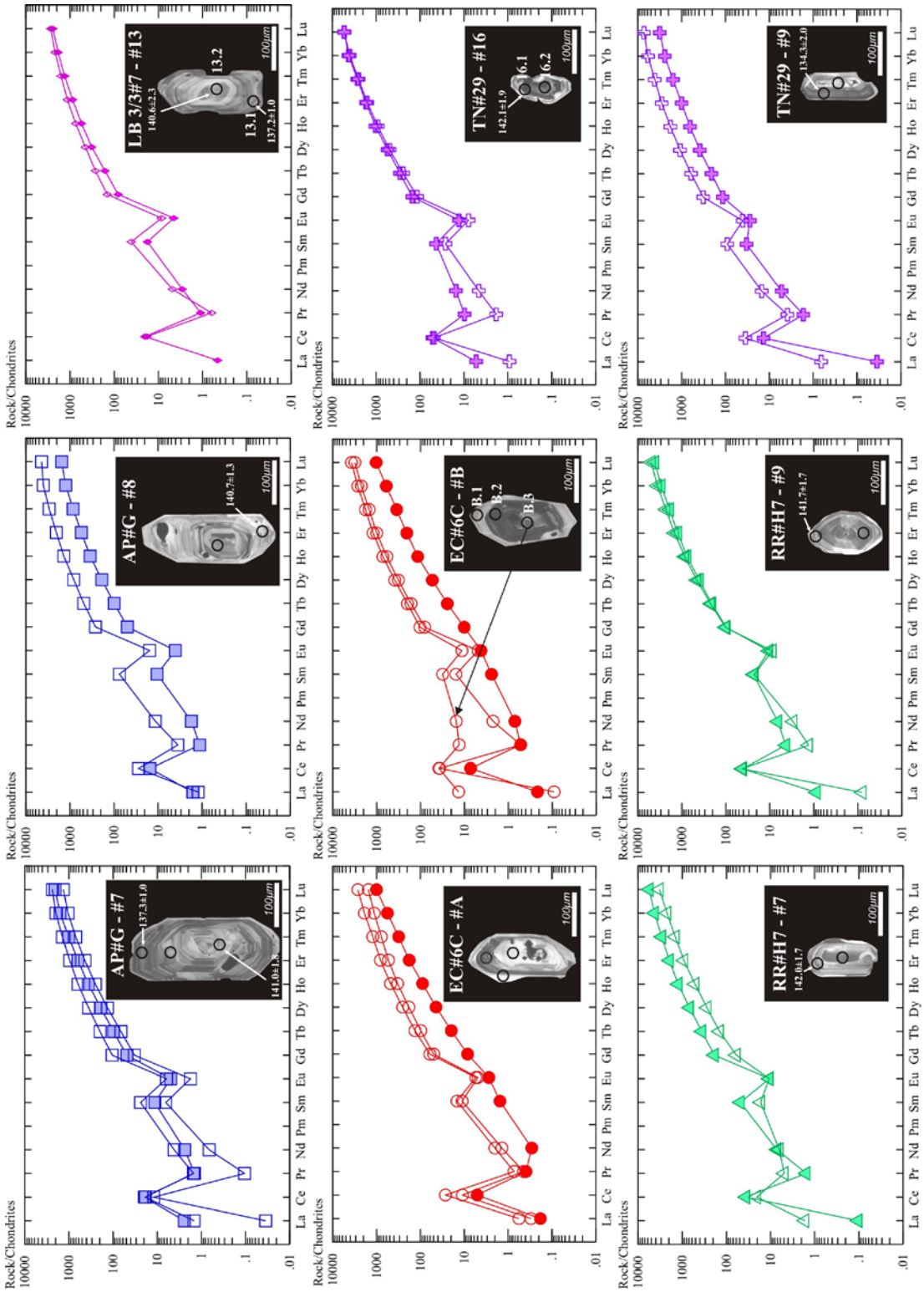

Figure 6.6 Chondrite-normalised REE diagrams for selected zircons from samples within the Halfmoon Pluton. All hollow symbols represent core or mid-section analyses, and full-coloured symbols represent rim analyses.

Hafnium (Hf) is an element that is readily incorporated during zircon growth, and therefore is a useful tracer of compositional changes in magmas and can also be used as an index of fractionation (Lowery Claiborne *et al*., 2006; Bolhar *et al*., 2008). During zircon crystallization, the residual melt typically becomes progressively more depleted in Hf and therefore decreasing Hf contents can be used to infer fractionation. Dy and Y were plotted against Hf in order to determine if amphibole fractionation had any observable effect on the chemistry of the zircon crystals.

Hf concentrations vary within and between samples. Zircons from Ackers Point display increases in Hf concentration from core to rim (Figure 6.7A), whereas zircons from Evening Cove generally show decreases in Hf concentration from core to rim (Figure 6.7C). Zircons from both these samples also show decreases in Y content from core to rim. Hf and Y concentrations are variable in zircons from Ringaringa, The Neck and Leask Bay, however zircons from Ringaringa have higher Hf concentrations than those from The Neck and Leask Bay (Figure 6.7E). There is no correlation with Y or Dy content (Figure 6.7H). Dy contents within zircons from Ackers Point and Evening Cove display trends of decreasing Dy abundance from core to rim (Figure 6.7G). Core analyses from Evening Cove zircons remain constant at ~50ppm (with one outlier) whereas those at Ackers Point vary dramatically, ranging from ~210µm to ~35µm. Dy contents within these core analyses also display a correlation of decreasing Dy with decreasing Hf. No pattern of Dy abundance is observed within zircons from Ringaringa and The Neck (Figure 6.7H).

Eu and Ce are both redox sensitive, and therefore can provide evidence on the oxidation state of the magma at the time the zircon was crystallizing (Ballard *et al*., 2002). Assuming equilibrium partitioning, the magnitude of the Ce-anomaly observed within REE patterns is governed by the abundance of Ce^{4+} in the melt, which is related to the Ce^{4+}/Ce^{3+} ratio, which is a function of oxygen fugacity (Ireland & Williams, 2003). Ce-anomalies within almost all zircons decrease from core-rim, consistent with preferential incorporation of Ce^{4+}. The Eu-anomaly in zircon may also indicate oxidation conditions within the melt. The Eu-anomaly is calculated as Eu/Eu*, where Eu is the chondrite-normalised Eu value and Eu* is the average of the chondrite-normalised Sm and Gd concentrations (Lowery Claiborne *et al*., 2006). Eu/Eu* values within zircons from Ringaringa (RR#H7) and The Neck (TN#29) show

no correlation from core to rim, with average Eu/Eu* anomalies of 0.101 and 0.110 respectively (Figure 6.7F). Samples from Ackers Point (AP#G) and Evening Cove (EC#6C) however show moderate to marked increases in Eu/Eu* from core to rim respectively (Figure 6.6B and Figure 6.7D). Eu/Eu* within samples EC#6C and AP#G also correlate with Y contents, with increasing Eu/Eu* values corresponding with decreasing Y contents. Eu/Eu* values are constant for both core and rim spots in zircons from the later cross-cutting granite at Leask Bay (LB 3/3#7) (Figure 6.7F). Eu/Eu* averages for all zircon from core analyses only show an overall trend of increasing Eu/Eu* with stratigraphic height in the chamber, consistent with higher magmatic oxidation states (fO_2) within more evolved/fractionated compositions (Ballard *et al*., 2002; Hoskin & Schaltegger, 2003).

Trace and REE abundance has been used by Belousova *et al*., (2002) as an indication of the source/origin of magmas. Low REE abundances were correlated with more primitive mafic magmas, whereas higher REE abundances were correlated with more evolved magmas. Zircon analyses from Halfmoon Pluton samples seem to fit these diagrams, with almost all zircons plotting in the fields for granodiorites and tonalites, or mafic rocks (Figure 6.8). The exceptions are the rim compositions in sample EC#6C. These are characterized by lower REE and other trace element abundances, which means that they plot either in the field for lamproites on the Y versus U diagram (Figure 6.8A) and in no particular field on the Y versus Yb/Sm diagram (Figure 6.8B).

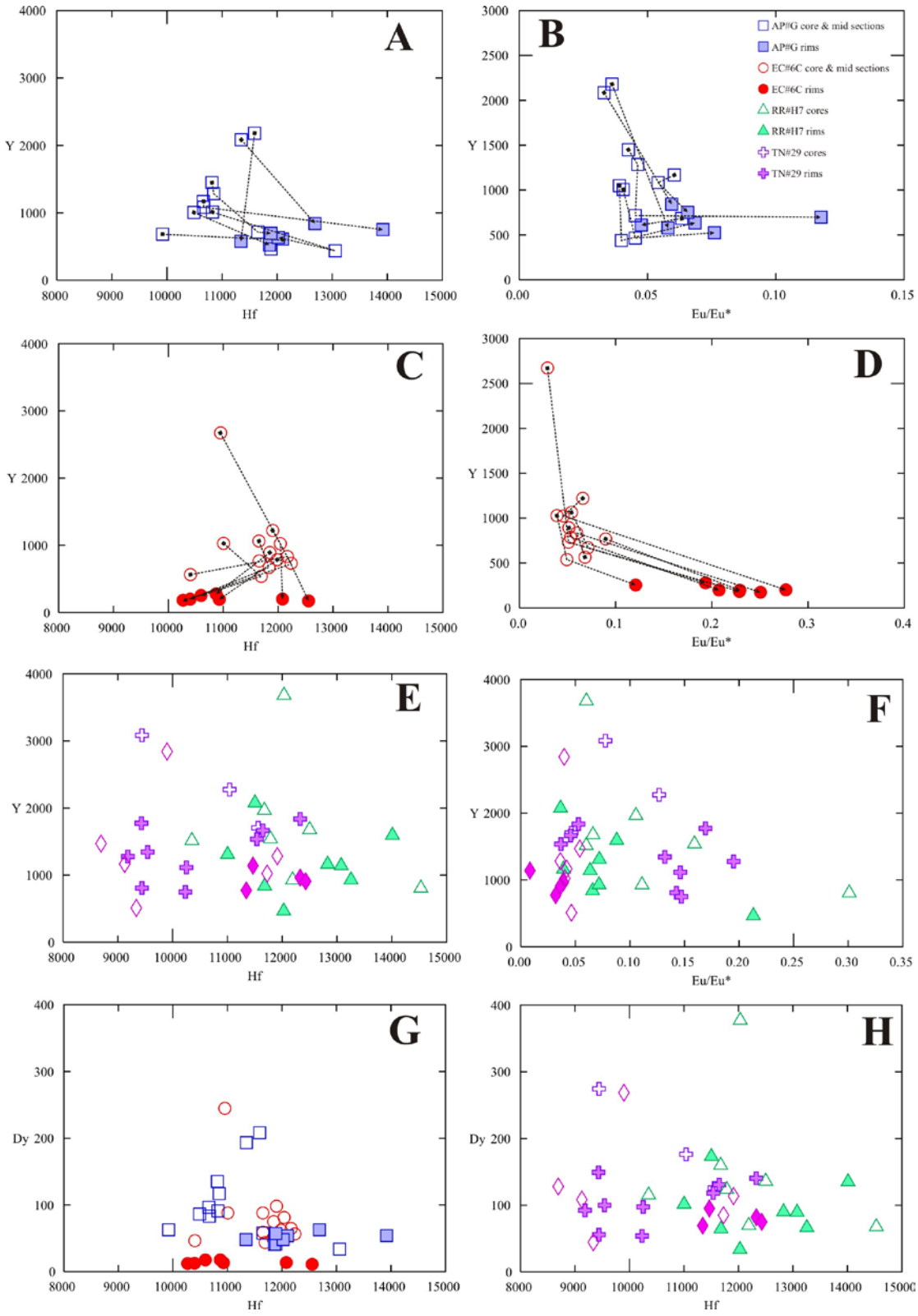

Figure 6.7. Trace element variation diagrams for zircons from the Halfmoon Pluton. Dy, Y and Hf are all measured in ppm.

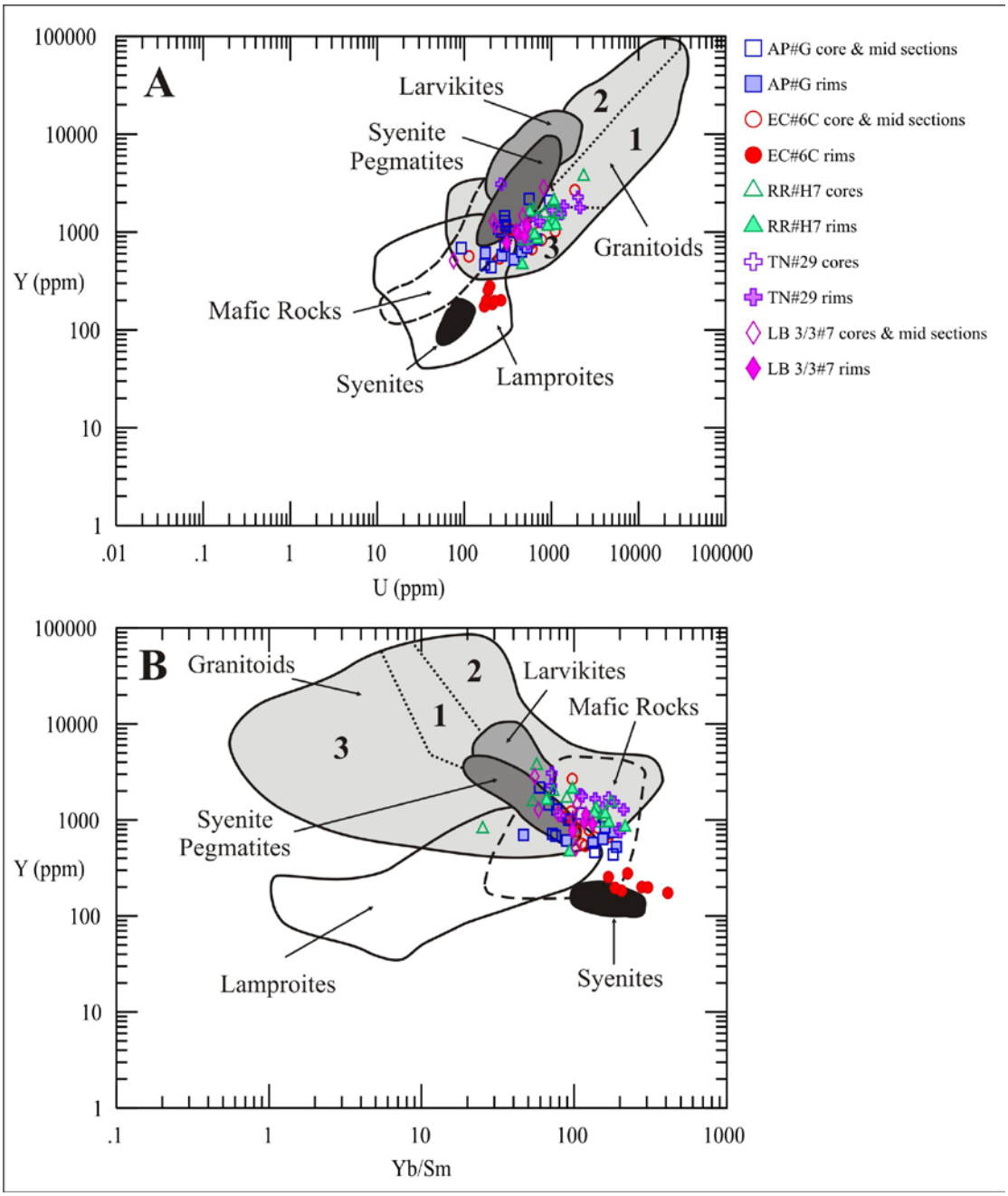

Figure 6.8. Rock-type discrimination diagrams using zircon compositions. Granitoids field includes: (1) aplites and leucogranites (2) granites and (3) granodiorites and tonalites. Fields obtained from Belousova *et al*., (2002)

6.6 Ti-in-Zircon Thermometry

The Ti-in-zircon geothermometer, which was developed by Watson *et al*., (2006) has already shown to be an excellent tracer of the thermal history of igneous rocks (Lowery Claiborne *et al*., 2006; Bolhar *et al*., 2008; Fu *et al*., 2008; Heiss *et al*., 2008). This geothermometer is based on the temperature dependant incorporation of Ti^{4+} into crystallizing zircon under TiO_2-saturated conditions (i.e. rutile is present).

Application of this technique allows assessment of the temperatures of the magmas from which the zircons crystallized, and can be compared with the temperatures obtained in Chapter 5 using the plagioclase-amphibole geothermometer. The Ti-in-zircon geothermometer was calibrated under rutile-saturated conditions ($\alpha TiO_2 = 1$). Rutile was not present within any of the rocks analyzed from the Halfmoon Pluton, and therefore the ideal equation of Watson and Harrison (2005) was adjusted to reflect ($\alpha TiO_2 \approx 0.7$) which Lowery Claiborne *et al*., (2006) suggested was appropriate for rocks with titanite and titanomagnetite saturation. The adjusted formula used to calculate temperatures based on the Ti-content of zircons is as follows;

$$T°(C) = \frac{5080}{6.01 - \log((10/7) \times Ti(ppm))} - 273$$

Uncertainty in the true activity of TiO_2 can introduce tens of °C uncertainty in absolute temperature, however because αTiO_2 remains close to constant as long as the melt remains saturated in a Ti phase (i.e. titanite, titanomagnetite), relative temperature differences indicated by the Ti-in-zircon geothermometer within individual samples will be real (Lowery Claiborne *et al*., 2006).

Ti-in-zircon temperatures (°C) from the five samples analysed from the Halfmoon Pluton are given in Figure 6.9, and plotted against Hf-content in Figure 6.10. Zircons from Ackers Point (AP#G) and Ringaringa (RR#H7) display scattered core and rim temperatures, however both display cooler average rim temperatures and hotter average core temperatures (AP#G 676°C rims, 762°C cores; RR#H7 696°C rims, 740°C cores). Rims on zircons in EC#6C give an average temperature estimated at 681°C and an average core temperature of 728°C. Zircons within sample TN#29 display quite clustered temperatures, which are on average cooler than all other zircons analysed from the other samples. Core analyses are hotter (704°C) than rim analyses (666°C). Zircons from the later cross-cutting granite at Leask Bay (LB 3/3#7) have hotter core and rim averages than all the other samples (714°C rims, 770°C cores). Rim temperatures obtained using Ti-in-zircon thermometer are low relative to the estimated solidus temperatures of the host rocks (Johannes & Holtz, 1996). Possible reasons for these low temperatures will be discussed in section 6.7.3.

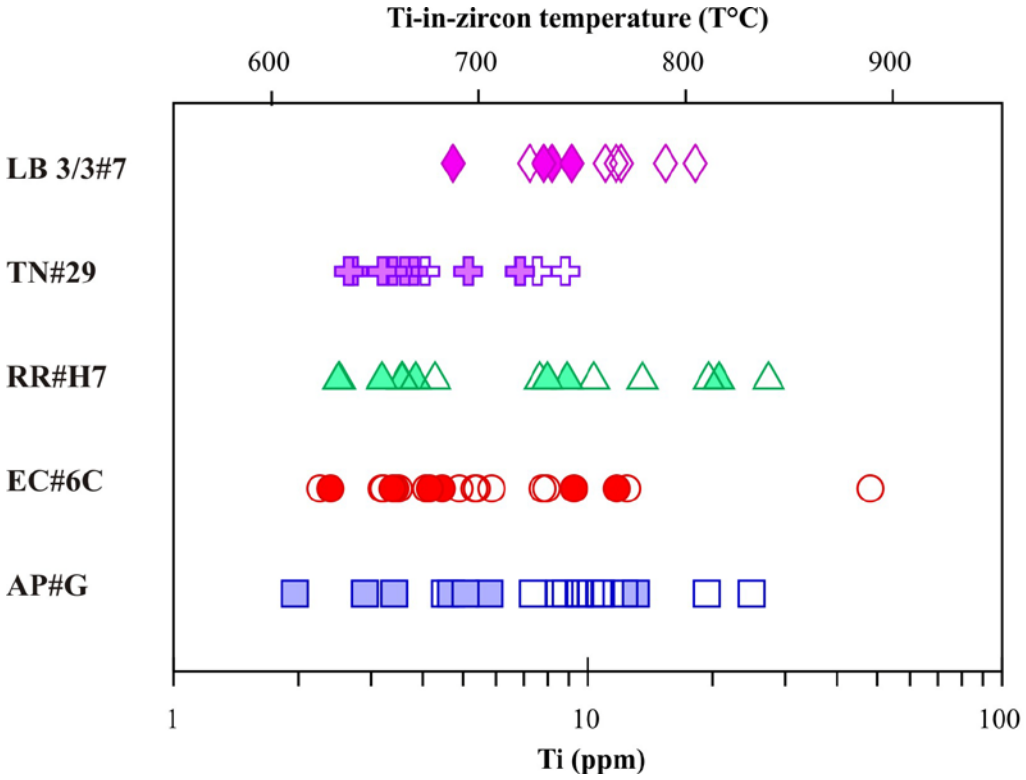

Figure 6.9. Ti concentrations and Ti-in-zircon temperatures (°C) for five samples within the Halfmoon Pluton. Filled symbols represent rim analyses whereas hollow symbols represent either mid-sections or core spot analyses.

Zircons from granitic plutons that experienced mafic magma replenishment were analysed by Lowery Claiborne *et al.*, (2006), with zircons displaying inverse relationships between Hf-content and $T°C_{TiZ}$. This trend is observed in core analyses from AP#G and EC#6C and core-rim analyses from TN#29 and LB 3/3#7 which display strong linear correlations between increasing Hf-content and decreasing $T°C_{TiZ}$ (Figure 6.10). Core and rim analyses from RR#H7 show poor correlations between Hf-content and $T°C_{TiZ}$ (Figure 6.7C). Rim analyses from EC#6C show the opposite trend to that observed in core analyses, with a strong correlation between increasing Hf-content and increasing $T°C_{TiZ}$ (Figure 6.7B and Figure 6.11).

All zircons from samples AP#G, RR#H7, TN#29 and LB 3/3#7 show trends of progressive cooling from core to rim, with zircons at AP having the largest difference in temperature between core and rim (average of 86°C), and the rest having smaller variations in temperature from core-rim (average between 38 and 56°C). These trends are consistent with progressive fractional crystallization during cooling of zircon-saturated magmas (Bolhar *et al.*, 2008). Zircons anaylsed from sample EC#6C also typically display decreasing temperatures from core to rim (average of

47°C), however two of the seven zircons analysed showed temperature reversals from core-rim, and one zircon showed an increase in temperature from core to mid-section (Figure 6.11). These zircons show temperature reversals of 24°C, 130°C (core-rim) and 31°C (core-mid), which are interpreted to represent real increases in temperature given the <10°C (2σ) uncertainty in the Ti-in-zircon thermometer (Watson *et al.*, 2006).

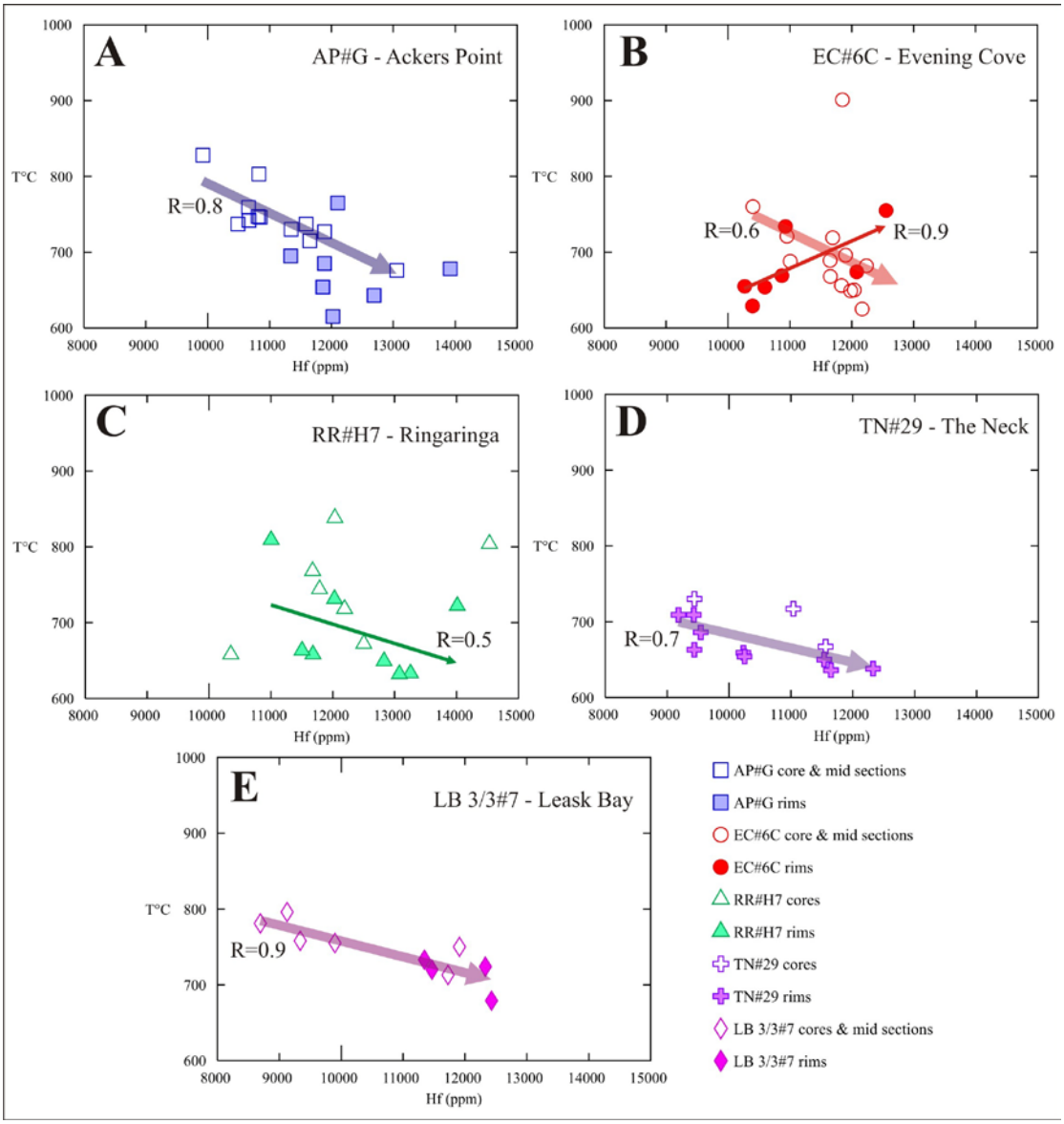

Figure 6.10. Diagrams of Hf-content versus crystallization temperature for zircon (using Ti-in-zircon thermometer of Watson *et al.*, (2006)). Well-defined linear correlations for core and mid-section analyses for AP#G and EC#6C are indicated by thick transparent arrows, rim analyses for EC#6C and RR#H7 by thin solid arrows, and correlations for all core and rim analyses from TN#29 and LB 3/3#7 by thick transparent arrows.

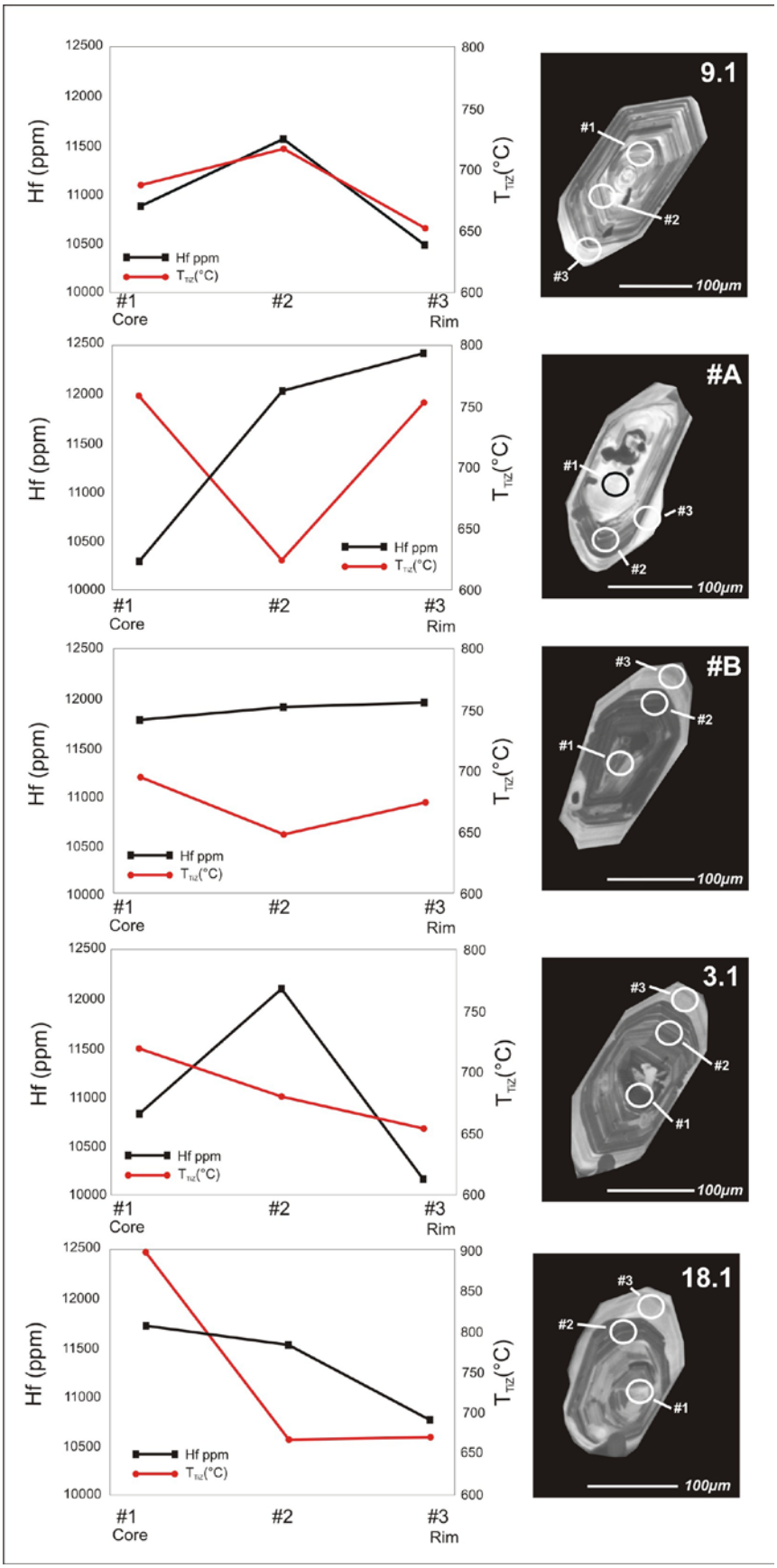

Figure 6.11. CL images of zircons from Evening Cove (EC#6C) showing locations of LA-ICP-MS analysis spots. Core-mid-rim spots correlate with the graphs showing Hf-contents and calculated $T°C_{TiZ}$.

6.7 INTERPRETATION OF MAGMATIC PROCESSES

6.7.1 Zircon morphology and internal structure

The shape of a zircon crystal is indicative of the conditions within which it has grown (Hoskin & Schaltegger, 2003). The internal make-up of zircons is also a reflection of magmatic processes, with growth zoning resulting from the interplay between a number of different factors including the stage of crystal growth, the nature of the crystal-liquid interface, the degree of zircon saturation in the melt, rates of diffusion, and the oxidation state of the melt (Mattinson *et al*., 1996). Most zircons within samples from the Halfmoon Pluton are euhedral, and are characterized by narrowly spaced uninterrupted oscillatory zoning. These features are consistent with primary growth within a melt with a high degree of zircon saturation that has not experienced much disturbance (Hoskin & Schaltegger, 2003). Zircons within host rocks from Ackers Point (AP#G) and Evening Cove (EC#6C) are much larger than those at Ringaringa (RR#H7) and The Neck (TN#29), and also display thick bright white rims. This change in zircon size may reflect a decrease in the degree of zircon saturation in the melt due to crystallization and accumulation of zircons in the plagioclase-hornblende cumulate at the base of the chamber which depleted the melt in Zr.

6.7.2 Geochronology

U-Pb dating of the five host rock samples discussed above support the field interpretations made in Chapter 3 that the sequence studied was part of a large active pluton that was active between ~139 and 141 Ma. A sample of later granite dated from Leask Bay gave an age of 139 ± 0.7 Ma, which overlaps in age. Other later cross-cutting granites have been dated by other authors, and provide similar ages to that obtained for Leask Bay (Golden Bay granite, 138 +11/-1; Deep Bay granite dike, 139.9 ± 0.2), indicating that more evolved granitic magmas intruded the Halfmoon Pluton shortly after it had crystallized. The age calculated at Ackers Point (139.4 ± 0.7 Ma) gives an age slightly younger than the section stratigraphically above it at Evening Cove (141.8 ± 1.2 Ma). The supposedly 0.5 Ma age difference (using 2σ errors) is unlikely to reflect an actual age difference between these two sections as field interpretations are robust. These sections are separated by < 500m of continuous coastal outcrop that record no discontinuities or intrusive contacts between the two

sections, with way-up structures consistently indicating way-up towards the south. Mingling style also remains very similar, as thick mafic sheets separated by thin amounts of intermediate host. The ages of these two samples do overlap at the 99% (3σ) confidence level so the apparent inconsistency is not significant.

Towards the top of the chamber at Ulva Island, sample P62077 records a slightly younger age than that at Evening Cove (with 2σ error), however with associated errors, all of the ages obtained from the bottom four sections overlap at the 2σ confidence level (see Figure 6.5). An age from a monzonite host sample at Horseshoe Bay of 141 +7/-1 (Kimbrough *et al*., 1994) indicates that these rocks are probably also part of the younger Halfmoon Pluton within the composite Bungaree Intrusives, however a lack of unaltered, in situ outcrop at this location makes it difficult to assess mingling structures and textures and therefore where this section fits into the stratigraphic sequence of the Halfmoon Pluton. Differences in the style of magma mingling (small volumes of mafic rocks preserved only as mafic enclave swarms) and more evolved host rock compositions than those at Ackers Point and Evening Cove (SiO_2 ~65% for Horseshoe Bay monzonite vs. SiO_2 ~52-62% for Ackers Point and Evening Cove) indicate that rocks at Horseshoe Bay probably represent a different magma chamber within the same active magmatic system. The youngest age obtained comes from The Neck (138.6 ± 0.7 Ma) and this indicates that this section of the Halfmoon Pluton is indeed the youngest, which supports interpretation of mingling structures that suggest that The Neck represents the upper part of the chamber. A minimum age difference of 1.3 Ma between Evening Cove and The Neck exists with 2σ errors, and 0.4 Ma with 3σ errors (see Figure 6.5). The Neck is therefore interpreted to represent a younger adjacent magmatic 'pod', though it is still considered part of the same continuously active Halfmoon Pluton magmatic system. Only one anomalously old age was obtained from an Ackers Point zircon (174.6 ± 2.1 Ma), and this is interpreted to have been inherited from the older granitoids within the Bungaree Intrusives through which the magmas of the Halfmoon Pluton intruded (i.e. the ~175 Ma diorite from Port William). Zircon morphology and apparent lack of inheritance therefore indicate that these zircons represent primary growth solely from the enclosing magmatic system, and the magmatic evolution of their host magmas did not therefore involve contamination with continental crust.

6.7.3 Compositional and thermal evolution

As indicated in Chapter 5, detailed transects across hornblende and plagioclase crystals indicate that pressure, temperature and PH_2O conditions within the Halfmoon Pluton magma chamber fluctuated in response to episodic injections of hot, wet mafic magma. LA-ICP-MS analyses of core-mid-rim spots within zoned zircons also reveal changes in the chemistry and thermal condition of the Halfmoon plutonic system during crystallization. Oscillatory zoning within almost all zircons reflects variations in the concentrations of trace (Th, U, Pb, P, Y, Ti, Hf) and REE's as a result of zircon crystallization from a fractionating magma chamber that was interrupted by repeated mafic magma injections. REE compositions for cores and rims for individual samples are very similar, with similar abundances and sizes in the Ce- and Eu-anomalies. The similarity in the overall REE patterns indicates that changes in the evolving melt composition did not effect the REE systematics in crystallizing zircon, which is a common feature within granitic systems (Hoskin *et al*., 2000; Sawka, 1988; Bolhar *et al*., 2008). Eu/Eu* values increase with stratigraphic height in the chamber, and are interpreted to denote higher magmatic oxidation states within the more evolved rocks towards the top of the chamber.

Zircons from Ringaringa (RR#H7) and The Neck (TN#29) also lack compositional variations from core to rim, indicating that the melt from which the zircons crystallized experienced no discernable changes in composition. Rim analyses on zircons from AP#G and EC#6C do however show variations in elemental concentrations, indicating that changes in melt chemistry occurred. Rims on zircons from Ackers Point and Evening Cove display increases in Eu/Eu*, and decreases in Y and Dy abundances. Decreases in Y and Dy probably reflect crystallization of hornblende in the cumulate host rocks from EC and AP which depleted the melt in these elements. Observed increases in Eu/Eu* ratios are more difficult to explain as although Eu is redox sensitive, the concentration of Eu within zircons is further complicated by the effects of plagioclase crystallization. Crystallization of plagioclase has the effect of depleting the melt in Eu(II), thereby decreasing Eu/Eu* in the melt. Eu(II) is strongly partitioned into feldspar relative to Eu (III), however the oxidation state of the melt also has an effect on how much Eu(II) can be removed from the melt in response to plagioclase crystallization, with increasing oxidation reducing the amount of Eu(II) that can be taken up by plagioclase. As outlined in Chapters 4 and 5,

plagioclase crystallization and accumulation within intermediate host rocks at Ackers Point and Evening Cove exerts a significant control on the observed whole-rock, hornblende and plagioclase chemistry, and therefore increases in Eu/Eu* ratios in zircon rims from these cumulate host rocks may reflect plagioclase crystallization and accumulation. Increases in Eu/Eu* may also be attributed to increasing oxidation states of the melt as the result of either fractionation or replenishment by hot wet mafic magmas.

Although the Halfmoon Pluton preserves abundant field evidence for episodic injection of mafic magma into a more felsic magma chamber in the form of mingled mafic sheets and enclaves, no zircons (excluding those from Evening Cove) record evidence of thermal perturbations to the system (when applying the Ti-in-zircon geothermometer). Ti behaves incompatibly in zircon, with typical concentration levels in most terrestrial zircons being between 0.3 and 50ppm (corresponds to temperatures between ~500 and 900°C) (Watson *et al*., 2006). Competition between other minerals that incorporate Ti into their crystal structures (i.e. quartz, titanite, ilmenite, amphibole) may effect the Ti concentrations within zircon. There are also other factors that influence the substitution of Ti into zircon and complicate the accuracy of the Ti-in-zircon thermometer, including; variation in TiO_2 and/or SiO_2 activity, pressure, subsolidus alteration or diffusion, or accuracy of the thermometer calibration itself (Fu *et al*., 2008). The influence of these factors may account for the low Ti concentrations and therefore the low estimated temperatures for the majority of zircons. Calculated zircon temperatures are lower than zircon saturation temperatures for intermediate-silicic plutonic rocks, and the temperature estimates made for the same rocks in Chapter Five using the Ti-in-hornblende and plagioclase-hornblende geothermometers. Zircons analysed by Fu *et al*., (2008) from a variety of different rocks and tectonic settings have shown that the Ti-in-zircon geothermometer commonly produces temperatures lower than zircon saturation temperatures, and therefore the accuracy of the Ti-in-zircon geothermometer is somewhat problematic. Absolute temperatures therefore have been used with caution in identifying magmatic processes, and instead relative temperature differences have been used to identify actual trends and processes.

The only zircons that display increases in Ti-content and therefore temperature from core to rim are those from Evening Cove. Temperature increases are only observed in three zircons, and correlate with increases in Hf content and REE content. Increases in temperature are probably in response to mafic magma replenishment.

The host rocks at Ackers Point and Evening Cove have very low SiO_2 (between 52 and 62 wt%) contents relative to their high whole-rock Zr-contents (~150-420 ppm). Melts with SiO_2 contents as low as 52% are normally zircon undersaturated, and therefore the high Zr-contents and presence of large, euhedral zircons within these rocks suggests that they represent cumulates. This is supported by whole-rock major, trace and REE compositions as discussed in Chapter Four. Fluctuating compositions from core-rim within zircons from Ackers Point and Evening Cove can therefore be explained by zircon accumulation, with these zircons having crystallized in different parts of the magma chamber with differing trace and REE contents. Other possible reasons for these fluctuating zircon compositions include a convecting magma chamber, or magma mixing. Increases in rim temperatures from zircons at Evening Cove coupled with large increases in Eu/Eu* are probably a reflection of replenishment of the magma chamber by hotter, wetter more mafic melts. Convective movement of thermally zoned magma or crystal mush may also have caused increases in temperature and Eu/Eu* by exposing zircons to hotter, wetter, and more compositionally less evolved melt (Bolhar *et al*., 2008).

6.8 CONCLUSIONS

Whole-rock analyses likely reveal compositional, mineralogical and textural traits that may represent late-stage processes that operate within magma chambers, rather than a more extended and detailed record of the fluctuating magmatic conditions that likely operated throughout a chamber's history. Detailed studies of zircons combining morphological, zoning, trace and REE profiles from core to rim are an important tool for tracking processes involved in the generation and evolution of magmatic systems. Zircons from Ackers Point and Evening Cove provide a record of evolving melt compositions in the intermediate cumulate host rocks from the inferred base of the chamber. Observed trends are best explained by the effect of fractional crystallization of a plagioclase – hornblende cumulate assemblage which variably

depleted the melt in Dy, Y and H_2O, resulting in corresponding depletions in Eu/Eu*, Dy and Y at the rims of zircons from Ackers Point and Evening Cove. Fluctuations in the chemical and thermal state of the host magma are also consistent with perturbation of the system by the episodic replenishment of hot, wet basaltic magmas, which is further supported by changing composition and intensive parameters within hornblende and plagioclase crystals from core to rim as discussed in Chapter 5. U/Pb SHRIMP ages obtained from intermediate-felsic host rocks throughout the magmatic sequence indicate that ages from the bottom four sections within the magmatic sequence all overlap within error, whereas The Neck represents a slightly younger adjacent magmatic "pod" that is interpreted to represent the upper part of the same continuously active Halfmoon Pluton magmatic system. These dates indicate that the Halfmoon Pluton was active over a period of at least 400 000 years.

6.9 REFERENCES

Bachl, C.A., Miller, C.F., Miller, J.S. and Faulds, J.E. 2001 'Construction of a pluton: Evidence from an exposed cross section of the Searchlight pluton, Eldorado Mountains, Nevada' *GSA Bulletin* 113(9): 1213-1228

Ballard, J.R., Palin, J.M. and Campbell, I.H. 2002 'Relative oxidation state of magmas inferred from Ce(IV)/Ce(III) in zircon: application to porphyry copper deposits of northern Chile' *Contributions to Mineralogy and Petrology* 144: 347-364

Belousova, E.A., Griffin, W.L., O'Reilly, S.Y. and Fisher, N.I. 2002 'Igneous Zircon: trace element composition as an indicator of source rock type' *Contributions to Mineralogy and Petrology* 143: 602-622

Belousova, E.A., Griffin, W.L. and O'Reilly, S.Y. 2006 'Zircon crystal morphology, trace element signatures and Hf isotope composition as a tool for petrogenetic modeling: examples from Eastern Australian granitoids' *Journal of Petrology* 47: 329-353

Black, L.P., Kamo, S.L., Allen, C.M., Aleinikoff, J.N., Davis, D.W., Korsch, R.J. and Foudoulis, C. 2003 'TEMORA 1: a new zircon standard for phanerozoic U-Pb geochronology' *Chemical Geology* 200: 155-170

Bolhar, R., Weaver, S.D., Palin, M.J., Cole, J.W. and Paterson, L. 2008 'Systematics of zircon crystallization in the Cretaceous Separation Point Suite, New Zealand, using U/Pb isotopes, REE and Ti geothermometry' *Contributions to Mineralogy and Petrology* 156:133-160

Coleman, D.S., Gray, W. and Glazner, A.F. 2004 'Rethinking the emplacement and evolution of zoned plutons: Geochronological evidence for incremental assembly of the Tuolumne Intrusive Suite, California' *Geology* 32: 433-436

Corfu, F., Hanchar, J.M., Hoskin, P.W.O. and Kinny, P.D. 2003 'Atlas of zircon textures' In: Hanchar, J.M. and Hoskin, P.W.O. *Zircon* Reviews in mineralogy and geochemistry 53: pp 469-500

Davies, G.R., Halliday, A.N., Mahood, G.A. and Hall, C.M. 1994 'Isotopic constraints on the production rates, crystallization histories and residence times of pre-caldera silicic magmas, Long Valley, California' *Earth and Planetary Science Letters* 125: 17-37

Finch, R.J. and Hanchar, J.M. 2003 'Structures and chemistry of zircon and zircon-group minerals' In: Hanchar, J.M. and Hoskin, P.W.O. *Zircon* Reviews in mineralogy and geochemistry 53: pp 1-21

Fu, B., Page, F.Z., Cavosie, A.J., Clechenko, C.C., Fournelle, J., Kita, N.T., Lackey, J.S., Wilde, S.A. and Valley, J.W. 2008 'Ti-in-zircon thermometry: applications and limitation' *Contributions to mineralogy and petrology* 156: 197-215

Glazner, A.F., Bartley, J.M., Coleman, D.S., Gray, W. and Taylor, R.Z. 2004 'Are plutons assembled over millions of years by amalgamation from small magma chambers?' *GSA Today* 14(4): 4-11

Griffin, W.L., Wang, X., Jackson, N.J., Pearson, N.J., O'Reilly. S.Y., Xu, X. and Zhou, X. 2002 'Zircon chemistry and magma mixing, SE China: In-situ analysis of Hf isotopes, Tonglu and Pingtan igneous complexes' *Lithos* 61: 237-269

Harper, B.E., Miller, F., Miller, G., Koteas, C., Cates, N.L., Wiebe, R.A., Lazzareschi, D.S. and Cribb, J.W. 2004 'Granites, dynamic magma chamber processes and pluton construction: the Aztec Wash pluton, Eldorado Mountains, Nevada, USA' *Transactions of the Royal Society of Edinburgh: Earth Sciences* 95: 277-295

Hawkins, D.P. and Wiebe, R.A. 2004 'Discrete stoping events in granite plutons: A signature of eruptions from silicic magma chambers?' *Geology* 32(12): 1021-1024

Heiss, J., Nutman, A.P., Bennett, V.C. and Holden, P. 2008 'Ti-in-zircon thermometry applied to contrasting Archean metamorphic and igneous system' *Chemical Geology* 247: 323-338

Hoskin, P.W.O. 2000 'Patterns of chaos: Fractual statistics and the oscillatory chemistry of zircon' *Geochemica at Cosmochimica Acta* 64: 1905-1923

Hoskin, P.W.O. and Schaltegger, U. 2003 'The composition of zircon and igneous and metamorphic petrogenesis' In: Hanchar, J.M. and Hoskin, P.W.O. (eds) *Zircon* Reviews in mineralogy and geochemistry, 53*:* pp 27-62

Jellinek, A.M. and DePaolo, D.J. 2003 'A model for the origin of large silicic magma chambers: precursors of caldera-forming eruptions' *Bulletin of Volcanology* 65: 363-381

Johannes, W. and Holtz, F. 1996 *Petrogenesis and experimental petrology of granitic rocks* Springer Verlag, Heidlelburg, pp 165

Kimbrough, D.L., Tulloch, A.J., Coombs, D.S., Landis, C.A., Johnston, M.R. and Mattinson, J.M 1994 'Uranium-lead zircon ages from the Median Tectonic Zone, New Zealand' *New Zealand Journal of Geology and Geophysics* 37: 393-419

Lowery Claiborne, L., Miller, C.F., Walker, B.A., Wooden, J.L., Mazdab, F.K. and Bea, F. 2006 'Tracking magmatic processes through Zr/Hf ratios in rocks and Hf and Ti zoning in zircons: An example from the Spirit Mountain batholith, Nevada' *Mineralogical Magazine* 70: 517-543

Mattinson, J.M., Graubard, C.M., Parkinson, D.L. and McClelland, WC. 1996 'U-Pb reverse discordance in zircons: the role of fine scale oscillatory zoning and sub-micron transport of Pb' In: Basu, A. and Hart, S. (eds) *Reading the isotopic code*. Geophysical Monograph 95. American Geophysical Union, 355-370

Muir, R.J., Ireland, T.R., Weaver, S.D., Bradshaw, J.D., Waight, T.E., Jongens, R. and Eby, G.N. 1997 'SHRIMP U-Pb geochronology of Cretaceous magmatism in

northwest Nelson-Westland, South Island, New Zealand' *New Zealand Journal of Geology and Geophysics* 40: 453-463

Pearce, N.J.G., Perkins, W.T., Westgate, J.A., Gorton, M.P., Jackson, S.E., Neal, C.R., Chenery, S.P. 1997 'A compilation of new and published major and trace element data for NIST SRM 610 and NIST SRM 612 glass reference materials' *Geostandards Newsletter* 21: 115-144

Sawka, W.N. 1988 'REE and trace element variations in accessory minerals and hornblende from the strongly zoned McMurry Meadows Pluton, California' *Transactions of the Royal Society of Edinburgh* 79: 157-168

Sun, S.-S. and McDonough, W.F. 1989 'Chemical and isotopic systematics of oceanic basalts: Implications for mantle composition and processes' *In:* Saunders, A.D. and Norry, M.J. (eds) *Magmatism in the Ocean Basins,* Geological Society, London, Special Publications, 42: 313-345

Tera, F. and Wasserburg, G.J. 1972 'U-Th-Pb systematics in three Apollo 14 Basalts and the problem of initial Pb in lunar rocks' *Earth and Planetary Science Letters* 14: 281-304

Walker, B.A., Miller, C.F., Claiborne, L.L., Wooden, J.L. and Miller, J.S. 2007 'Geology and geochronology of the Spirit Mountain batholith, southern Nevada: implications for timescales and physical processes of batholith construction' *Journal of Volcanological and Geothermal Research* 167: 239-262

Watson, E.B. and Harrison, T.M. 2005 'Zircon thermometer reveals minimum melting conditions on earliest earth' *Science* 308: 841-844

Watson, E.B., Wark, D.A. and Thomas, J.B. 2006 'Crystallization thermometers for zircon and rutile' *Contributions to Mineralogy and Petrology* 151: 413-433

CHAPTER SEVEN

MODEL OF MAGMA CHAMBER CONSTRUCTION AND EVOLUTION

7.1 INTRODUCTION

The Halfmoon Pluton of Stewart Island, New Zealand is characterized by a sequence of mingled mafic sheets and enclaves preserved within an intermediate-felsic host which provides insight into the role of coeval mafic magma in the initiation and evolution of calc-alkaline granitic magma, and the nature of mafic and felsic magma interactions. Magmatic processes that operated within the chamber are interpreted from structures and textures preserved in the mingled rocks, field and petrographic evidence, and geochemical and geochronological analyses. A model of pluton construction and evolution is presented in this chapter which shows that the Halfmoon Pluton consisted of at least two adjacent magma pods that formed incrementally by episodic replenishments of mafic magma into a fractionating chamber of intermediate-felsic composition.

Physical and chemical processes identified within the exhumed Halfmoon Pluton hold important clues to the petrogenetic processes that operate within active arc settings/systems globally. Processes identified within the Halfmoon Pluton and their implications for understanding the generation and evolution of arc-related magma chambers will also be addressed in this chapter.

7.2 PROCESSES IDENTIFIED WITHIN THE HALFMOON PLUTON

Interpretation of magma mingling and mixing structures and textures in the field, in combination with detailed geochemical and geochronological analyses, have enabled the identification of several physical and chemical processes operating within the chamber.

7.2.1 Magma mingling and mixing

Evidence for mafic magma replenishment within the Halfmoon Pluton is preserved as a sequence of mingled mafic sheets and enclaves within a more intermediate-felsic host rock. As established from field observations, magma mingling is the dominant physical interaction process occurring within the Halfmoon Pluton. Mingling styles and textures vary according to position within the magmatic sequence, with mafic sheets forming towards the inferred base of the chamber (Ackers Point and Evening Cove), and mafic enclaves, the dominant magma mingling style, towards the inferred top of the chamber (Ringaringa and The Neck). The change from mafic sheets to the predominance of mafic enclaves indicates that processes controlling the magma mingling style changed from the base towards the top of the chamber. As discussed in Chapter 2, changes in the thermal, chemical and physical parameters of two interacting magmas can have a significant effect on the style of magma interaction preserved. Mingling styles and textures are likely to have been governed by factors including, but not limited to:

- temperature contrast
- degree of crystallization
- relative magma volumes
- compositional contrasts
- rate of mafic magma replenishment
- volatile contents

Frost and Mahood (1987) concluded from fluid dynamic studies that homogenous mixing is only possible between magmas with a SiO_2 difference of less than 10%, or if the mass fraction of the mafic magma is >50%. In the Halfmoon Pluton, the volume of mafic magma injected into the felsic host varies throughout the chamber. Towards the base of the chamber (AP and EC), large volumes (50 - 60% of the total sequence) of mafic magma injection resulted in the formation of thick mafic sheets. Towards the top of the chamber, volumes of mafic rocks vary, with mafic enclaves consisting of ~40% of the sequence exposed at Ringaringa, and volumes of mafic rocks at The Neck ranging between 40 and 60%. This suggests that the formation of mafic sheets and enclaves within the Halfmoon Pluton was not controlled by the relative volumes of the two

interacting magmas as mafic sheets and enclaves occur in similar volumes throughout parts of the chamber. However, it must be noted that the amount of felsic host magma that once resided above the injected mafic sheet/enclave swarms may not be faithfully preserved in the rock record owing to eruption, making quantification of the relative volumes of the interacting magmas difficult.

The mingled rocks within the Halfmoon Pluton are very similar in composition towards the base of the chamber (Ackers Point and Evening Cove), especially with respect to SiO_2, TiO_2, K_2O, P_2O_5, with microdiorite mafic rocks between 48 and 51 wt% SiO_2, and leucodiorite host rocks between 53 and 60 wt% SiO_2. The compositional contrast between the mafic and felsic rocks becomes much greater towards the inferred top of the chamber (Ringaringa and The Neck), with mafic rocks between 52 and 53 wt% SiO_2, and granodiorite-tonalite-monzogranite host rocks between 66 and 75 wt% SiO_2. This change in compositional contrast coincides with a change in mingling style from mafic sheet formation at the base, to mafic enclave formation towards the top. Comparison with well-studied plutons that exhibit either large or small compositional contrasts between the mafic-felsic mingled rocks (Wiebe, 1993, Wiebe *et al*., 2001; Miller & Miller, 2002; Harper *et al*., 2004; Collins *et al*., 2006; Chapter 8 of this thesis) shows that mingling structures and textures are very similar regardless of the observed differences in composition. Contrast in composition is therefore not envisaged to have played a major role in the mingling style preserved.

The widespread occurrence of fine-grained quenched margins of mafic sheets and enclaves indicates that the key parameter controlling the style of magma interaction observed in the Halfmoon Pluton is temperature. Without a sufficient temperature contrast, rapid chilling of injected mafic magmas against the host magma will not occur, and therefore mixing and hybridization will be favoured. The degree of crystallization of the host magma will be a function of temperature, with liquid-poor melts being too crystalline to permit mixing or mingling, and instead results in the formation of dikes. Mafic sheets and enclaves within the Halfmoon Pluton display fine-grained chilled margins, and coarser-grained centres, indicating that the mafic magma chilled against

cooler resident intermediate-felsic host magma. Thermal equilibration between the host and the injecting mafic magmas would have occurred relatively quickly as a result of rapid quenching of the mafic magmas (Blundy & Sparks, 1992). Rapid crystallization of the mafic magma is also indicated by the presence of blade biotite and acicular apatite within mafic sheets and enclaves. Temperature contrasts therefore played the most important role in inhibiting mixing between the two interacting magmas.

Variations in temperature and crystallinity alone however cannot account for the observed change in mingling style from mafic sheet formation to mafic enclave formation. Three mechanisms have been proposed to account for mafic enclave formation;

1. Injection of mafic magma as dikes into a liquid host magma which subsequently break up into enclaves (Frost & Mahood, 1987; Pitcher, 1991; Wiebe *et al*., 1997)
2. Disrupted portions of partly chilled or cumulate material from the margins of the chamber (Bonin, 1991)
3. Disrupted portions of mafic-intermediate magmas that exist in the lower portions of compositionally stratified magma chambers (Wiebe *et al*., 1997)

The majority of enclaves within the Halfmoon Pluton probably formed as a result of the dike-like injection of mafic magma. Composite enclaves seen at The Neck however are likely to have represented disrupted portions of mixed mafic-intermediate magma from lower down in the chamber. However, the question still remains – why did the injected mafic magma break-up to form mafic enclaves?

The water contents of the two interacting magmas may have played a role in promoting the formation of enclaves. Magma water content is an important parameter as it influences melt composition, crystallization conditions and the viscosity of granitic magmas (Johannes & Holtz, 1996). It is difficult to quantify the H_2O-contents of granitic magmas, however Scaillet *et al*, (1998) indicated that most silicic volcanic rocks and their plutonic equivalents have dissolved H_2O-contetns of 4-6 wt% between the temperature range of 700-900°C. The high modal abundance of hydrous minerals

(hornblende and biotite) within both the mafic and host rocks of the Halfmoon Pluton indicates that these magmas were relatively H_2O-rich, consistent with their calc-alkaline chemistry and proposed generation in a hydrous arc-setting. The dominant mafic phase within mafic rocks changes from hornblende (at the base) to biotite (at the top) in conjunction with the change in mingling style from mafic sheets to mafic enclaves. Biotites contain higher amounts of H_2O than hornblende, indicating that mafic rocks with higher abundances of modal biotite to modal hornblende probably represent more H_2O-rich magmas. The mafic Halfmoon Pluton magmas therefore probably became more H_2O-rich through time as a result of fractionation.

Wiebe (1994) suggested that the presence of small pieces of variably chilled mafic material indicates that the process responsible for mafic enclave formation may have been promoted by the release of H_2O vapour. Mafic enclave formation may therefore be facilitated by vesiculation of the hydrous mafic magma as it comes into contact with the cooler more felsic host magma, causing it to break apart. Subsequent magmatic flow results in deposition of flow-aligned mafic enclave swarms that retain an orientation parallel to magmatic stratigraphy. The prevalence of orientated mafic enclave swarms within hydrous arc-related magma chambers as opposed to widely dispersed enclaves within less hydrous magma systems seems to point to the importance of water in the formation of mafic enclaves. The distribution of widely dispersed enclaves within granitic bodies is attributed to the effect of convective currents (Pitcher, 1991). Higher H_2O-content within the mafic magmas would also have the effect of lowering the temperature of the injected mafic magmas, meaning that these magmas may also have not been able to quench as rapidly within the cooler host magma, which would make them easier to break apart.

There are two possible processes by which mafic magmas can become relatively more H_2O-rich. Firstly by an increase in H_2O-flux from the subdecting slab, or by concentration of relatively incompatible H_2O by fractionation within the underplated basaltic magmas. Determining which process is responsible for increasing the H_2O-content within the mafic magma is difficult. Whole-rock and zircon Eu/Eu* values

increase with stratigraphic height in the chamber, and are interpreted to denote higher magmatic oxidation states within the more evolved rocks towards the top of the chamber. Fractionation of the under-plated basaltic magma is consistent with their higher SiO_2 contents relative to the earlier-injected hornblende-bearing mafic sheets towards the base of the chamber. Fractionation of mafic sheets and enclaves is further supported by their REE trends, with mafic rocks towards the top of the chamber containing progressively higher abundances of REE (Figure 4.5, Chapter 4).

Faster rates of mafic magma replenishment may also have promoted the formation of mafic enclaves towards the top of the chamber, however this parameter is difficult to quantify.

Temperature contrast and degree of crystallinity of the two interacting magmas are still considered the key factors controlling whether interacting magmas will mingle or mix.

7.2.2 Fractional crystallization and crystal accumulation

As demonstrated in Chapter 4, fractional crystallization was probably the dominant petrogenetic process driving compositional differentiation of the Halfmoon Pluton. Compositional changes within the intermediate-felsic host rocks were governed by crystallization and extraction of cumulates rich in plagioclase, hornblende, apatite and zircon. Harker diagrams displaying whole-rock major and trace element concentrations display trends consistent with fractional crystallization that correlate well with the reconstructed magmatic sequence. REE trends are the result of integrated effect of the crystallizing assemblage in which different minerals have different partition coefficients for the REEs. Hornblende, plagioclase and apatite all have high partition coefficients for certain REEs, and appear to have exerted the strongest influence on REE concentrations. Compositional changes in biotite (decreasing MgO and increasing FeO) and plagioclase (decreasing An% with increasing SiO_2) support the conclusion that fractional crystallization from a more mafic parent magma is the main process driving compositional diversification with the Halfmoon Pluton rocks.

Crystallization and accumulation of a plagioclase – hornblende – apatite – zircon mineral assemblage is recognized from petrographic and geochemical evidence. Large tabular plagioclase crystals comprise >85% of the leucodiorite host rocks at Ackers Point and Evening Cove, and show a strong preferred alignment, along with euhedral hornblende and biotite. Whereas magmatic flow probably contributes to some of the observed foliation present in the host rocks, crystal accumulation of euhedral tabular plagioclase and hornblende is probably the dominant process causing mineral alignment towards the base of the chamber. Accumulation of a plagioclase – hornblende – apatite – zircon mineral assemblage towards the base of the chamber is supported by whole-rock geochemistry. Host rocks at Ackers Point and Evening Cove have higher concentrations of the elements that comprise the aforementioned minerals (i.e. CaO, Sr, P_2O_5, Zr, MREE) than the host rocks towards the inferred top of the chamber (Ringaringa and The Neck) which do not display cumulate textures. Further support for crystal accumulation is the juxtaposition of plagioclase and hornblende crystals with contrasting *P*-T histories within host rocks from Ackers Point and Evening Cove. Fluctuating compositions from core-rim within zircon crystals from Ackers Point and Evening Cove are also consistent with accumulation of zircon. Zircons from AP and EC are depleted in Y (MREE proxy) and Dy (MREE) relative to their cores, which indicates that the rims and cores crystallized in different parts of the chamber with differing trace and REE contents. Y and Dy are two elements that are strongly partitioned into hornblende, and therefore decreases in Y and Dy probably reflect crystallization of hornblende in the cumulate host rocks from EC and AP which depleted the melt from which these zircons crystallized in these elements. Distinctive bright white rims coupled with increases in Eu/Eu* on zircons from AP and EC are interpreted to reflect higher oxidation states of the melt caused be replenishment of the crystal mush by hotter, wetter, more mafic melts.

7.2.3 Compaction and magmatic flow

Crystal alignment within host and mafic rocks cannot be accounted for by crystal accumulation alone. The consistent orientation of mafic sheets and enclaves is interpreted to represent the original orientation at which the mafic magmas injected and flowed

between the lower crystal-rich mush and upper crystal-poor host magma. Subsequent compaction of the still mushy magmas in response to loading from further input of dense mafic magma higher in the sequence resulted in compaction of the underlying magma.

7.3 IMPLICATIONS FOR UNDERSTANDING ARC-MAGMATISM

The Halfmoon Pluton is a correlative of the Darran Suite, which represents a belt of mafic and felsic plutonic rocks at least 15 km wide and 300 km long that extends from the Bungaree Intrusives in Stewart Island to the Darran Mountains in Eastern Fiordland (Allibone *et al*., 2009). Based on whole-rock geochemistry, primitive isotopic signatures and an absence of inherited zircons, the Darran Suite rocks have been interpreted to represent intra-oceanic arc magmas rather than continental margin magmas (Muir *et al*., 1998; Wandres *et al*., 1998). Major, trace and REE concentrations and Sr/Nd isotopic signatures obtained for the Halfmoon Pluton rocks during the course of this research support this conclusion. As such, the Halfmoon Pluton provides an opportunity to directly observe the processes that operate within active island-arc systems. The origin and evolution of silicic magmas in arc settings has recently been the topic of much debate (Arculus, 1994; Tamura & Tatsumi, 2002; Smith *et al*., 2003, 2006; Shukuno *et al*., 2006; Wright *et al*., 2006; Tamura *et al*., 2009). Magmas produced in arc settings rarely represent primary mantle-derived melts, more typically displaying differentiated compositions reflecting such processes as magma mixing, fractional crystallization and assimilation. Exposed sections of arc crust provide direct field evidence for the processes that operate within arc settings, and therefore conclusions outlined above for the exhumed arc-related Halfmoon Pluton provide an opportunity for further discussion of the processes that operate within arc settings that lead to the bulk composition of arc crust.

7.3.1 The role of amphibole in the differentiation of arc magmas

Exposed sections of arc crust are found in a variety of locations worldwide (e.g. Why Worry, Australia (Kemp *et al*., 2005); Tottabetsu, Japan (Kamiyama *et al*., 2007); Northern Victoria Land, Antarctica (Tiepolo & Tribuzio, 2008); Eldorado Mountains, Nevada (Bachl *et al*., 2001; Harper *et al*., 2004); Bonanza Arc, Vancouver (Larocque &

Canil, 2009)). A common feature of these arc-related plutons is the abundance of amphibole-bearing cumulates, which has lead several authors to suggest that amphibole crystallization plays an important role in the compositional diversity observed within many arc suites (Frey et al., 1978; Arculus & Wills, 1980; Carmichael, 2002; Larocque & Canil, 2009), despite a paucity of erupted hornblende-bearing volcanics in arc settings. Carmichael (2002) and Tamura and Tatsumi (2002) suggested that the negative slope of the water-saturated solidus of intermediate magmas would result in rapid crystallization and stalling of these magmas in the lower- to middle-crust. The onset of hornblende crystallization within these 'wet' basaltic magmas would result in a greater increase in crystallinity than would occur in more felsic magmas, and thereby impede the ascent and eruption of hornblende-bearing magmas (Barclay & Carmichael, 2004). Davidson *et al*., (2007) thereby proposed a model for intermediate melt production in arc settings whereby the 'cryptic' fractionation of hornblende at depth controls the trace element variations observed within arc plutons. As Figure 7.1 shows, most arc magmas, including the Halfmoon Pluton, exhibit trends of increasing La/Yb and decreasing Dy/Yb with differentiation (increasing SiO_2), consistent with significant amphibole fractionation (Macpherson *et al*., 2006; Davidson *et al*., 2007).

Figure 7.1. (following page) Graphs for La/Yb and Dy/Yb vs. SiO_2 from Davidson *et al*., (2007) with data for rocks within the Halfmoon Pluton plotted. Red circles represent intermediate-felsic host rocks, green triangles mafic sheets/enclaves, the blue square is a mixed 'hybrid' rock, and the white star is a mafic dike from The Neck (TN#26). Circled green triangles represent mafic sheets from Ackers Point and Evening Cove. Colour coded fields represent volcanoes from a single arc. Insets for each graph show expected fractionation effects. Model fractionation curves are experimental assemblages of Rapp & Watson (1995) (R&W), and a nominal gabbro comprising 20% olivine, 35% clinopyroxene, and 35% plagioclase. Abbreviations: cpx = clinopyroxene; am = amphibole; gt = garnet; plag = plagioclase; opx = orthopyroxene; il = ilmenite. Grey dashed arrows represent vectors for Surigao (Phillipines) and Anatahan (Marianas) which represent suites that have fractionated garnet and gabbro, respectively.

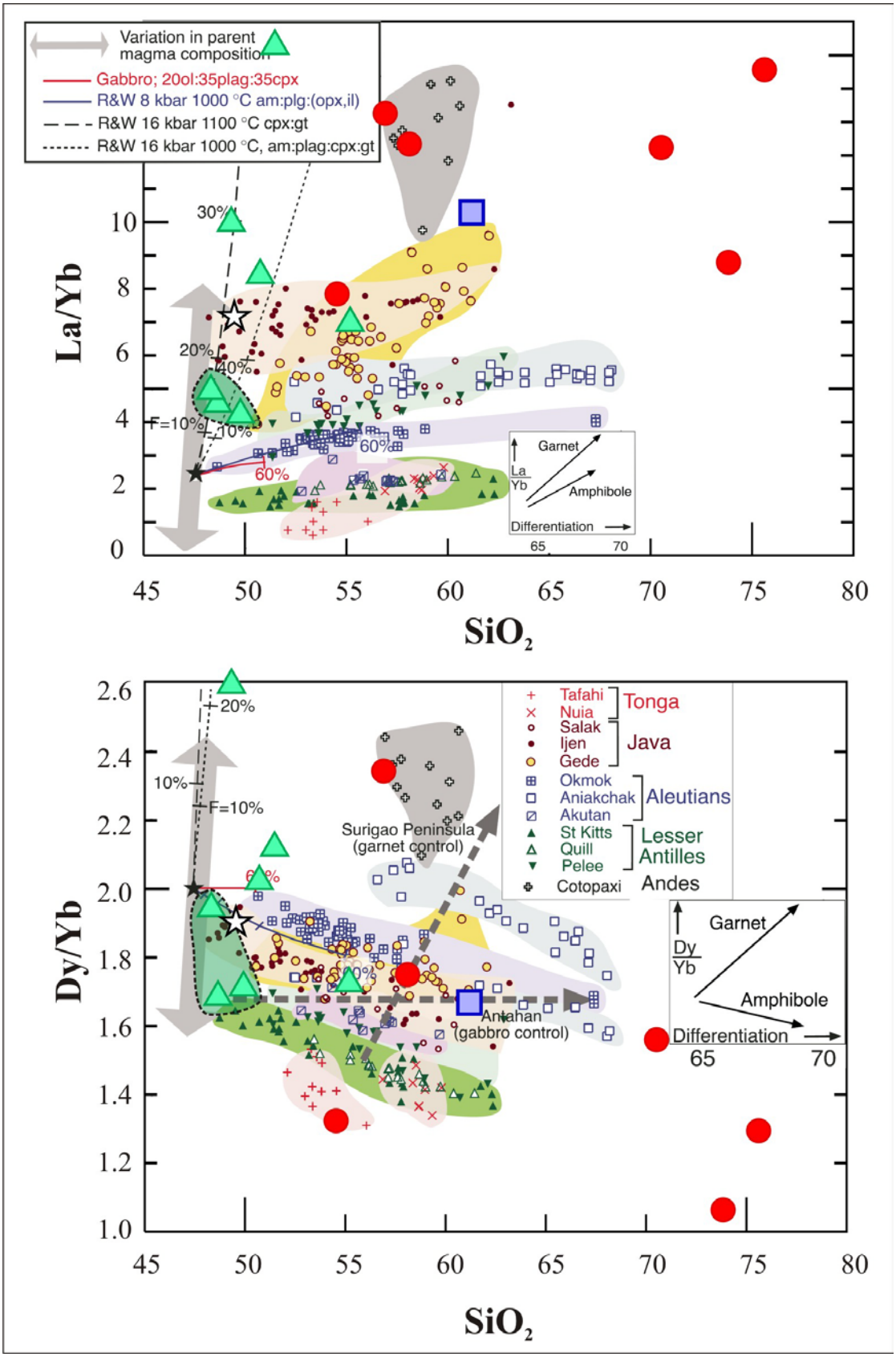
Variation in parent magma composition
Gabbro; 20ol:35plag:35cpx
R&W 8 kbar 1000 °C am:plg:(opx,il)
R&W 16 kbar 1100 °C cpx:gt
R&W 16 kbar 1000 °C, am:plag:cpx:gt
30%
20%
40%
F=10%
10%
60%
60%
Garnet
La/Yb
Amphibole
Differentiation
65
70
La/Yb
SiO2
45
50
55
60
65
70
75
80
0
2
4
6
8
10
20%
10%
F=10%
Surigao Peninsula (garnet control)
Antahan (gabbro control)
Tafahi
Nuia
Salak
Ijen
Gede
Tonga
Java
Okmok
Aniakchak
Akutan
Aleutians
St Kitts
Quill
Pelee
Lesser Antilles
Cotopaxi
Andes
Garnet
Dy/Yb
Amphibole
Differentiation
65
70
Dy/Yb
SiO2
1.0
1.2
1.4
1.6
1.8
2.0
2.2
2.4
2.6

Overall trends of the Halfmoon Pluton rocks are the same as those for the arc-related volcanics displayed in Figure 7.1, with amphibole fractionation indicated by increasing La/Yb and decreasing Dy/Yb with increasing SiO_2 contents. Rocks from the Halfmoon Pluton do however show a much wider amount of scatter, and reach higher SiO_2 contents than the examples displayed in Figure 7.1. This may be due to the Halfmoon Pluton magmas being more compositionally evolved as a result of a larger amount of fractional crystallization, assimilation, and/or magma mixing. Most of the variation within the Halfmoon Pluton intermediate-felsic host samples however can be attributed to the affect of amphibole fractionation. Circled green triangles represent mafic sheets from Ackers Point and Evening Cove, which are inferred to represent the mafic end-member 'parent' from which the rest of the rocks within the Halfmoon Pluton evolved. Variation in Dy/Yb and La/Yb ratios from these samples occurs within the other mafic rocks. This may be as a result of fractionation of these mafic melts from the parent melt, or due to element diffusion between the quenched mafic enclaves and the surrounding host rock. This process was suggested in Chapter 4 to be responsible for the observed enrichment in alkali and mobile trace elements within mafic enclaves.

Barclay and Carmichael (2002) suggested that the geochemical signature within arc rocks may reflect melting of stockpiled basalt magmas that contain amphiboles, rather than just simple amphibole crystallization from an evolving melt. However, Davidson *et al*. (2007), suggested that mafic rocks with high MgO (>6 wt%) and Ni (>50 ppm) would require unrealistically large degrees (~100%) of melting, and that most of these geochemical signatures therefore can be attributed to amphibole fractionation. Mafic sheets at Ackers Point and Evening Cove, and cross-cutting mafic dikes that are inferred to represent the mafic end-members within the Halfmoon Pluton, display MgO contents >6 wt% and Ni contents >55 ppm, indicating that amphibole fractionation is a more probable reason for the observed geochemical trends.

Further evidence for amphibole fractionation controlling the geochemical diversity observed within the Halfmoon Pluton is displayed in Figure 7.2. Major element plots of the different rock types together with averaged biotite and hornblende

compositions show that hornblende compositions fall on a well-defined trend with the whole-rock compositions, indicating that hornblende crystallization had a strong influence on the magmatic differentiation of the Halfmoon Pluton. Biotite compositions show a trend removed from that of the hornblende and whole-rock geochemistry. Other phases that may influence geochemical trends within arc magmas are apatite and zircon, however these serve to increase the LREE and HREE, and have a limited effect on the hornblende signature which affects the MREE.

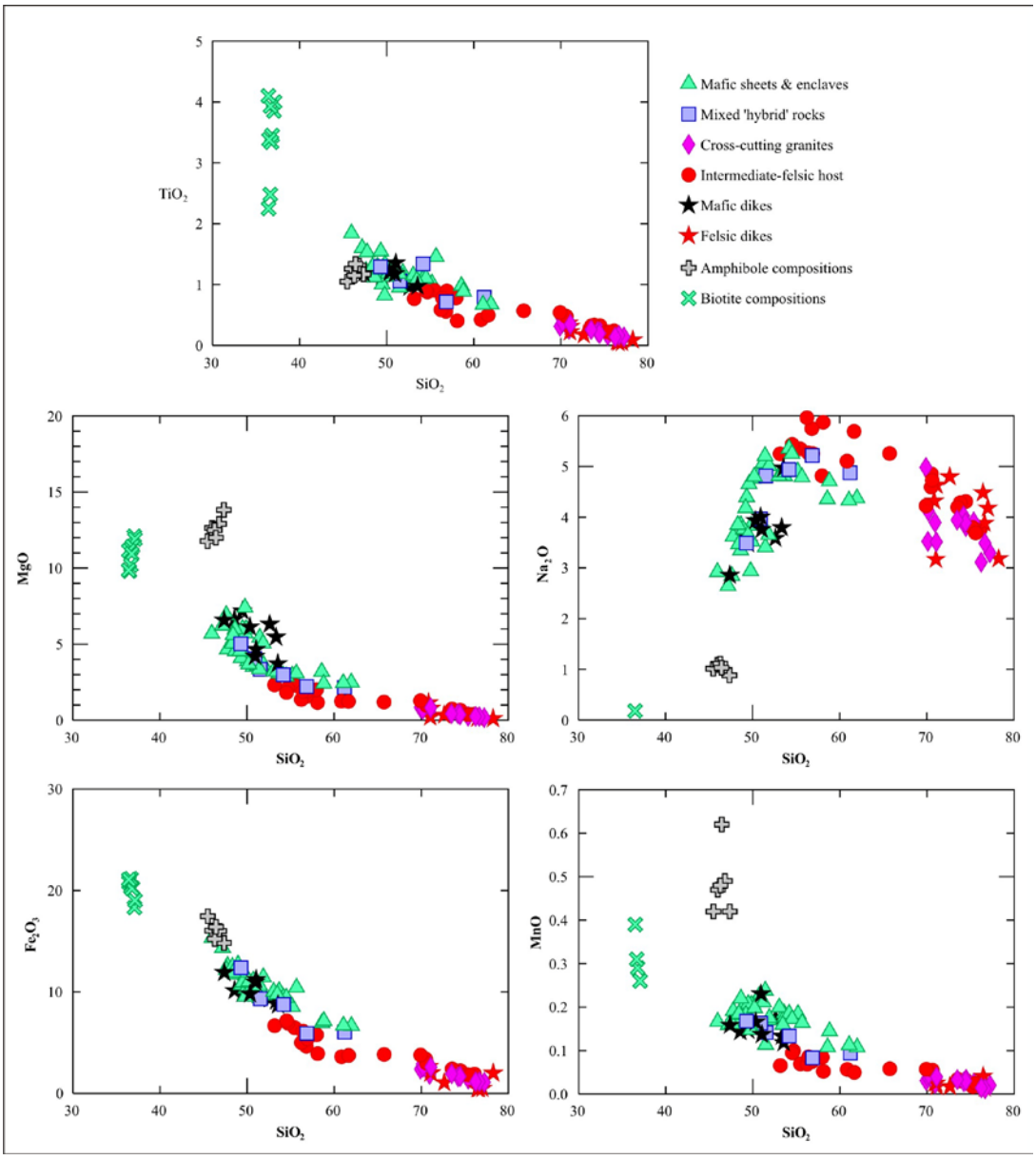

Figure 7.2. Harker diagrams illustrating the relationship between the mafic and felsic rocks within the Halfmoon Pluton, and the hornblende and biotite crystals within them.

The common occurrence of amphibole-rich cumulates within arc settings, and the similarity in their geochemical signatures led Hildreth (2004) and Bachmann and Bergantz (2004) to propose a model in which crystal-poor silicic magmas are generated by extraction from the intermediate amphibole cumulates, a process capable of generating the large volume (>1000km^3 magma) silicic magma reservoirs that sometimes lead to supereruptions. The plutonic rocks of the Halfmoon Pluton therefore probably represent the un-erupted intermediate 'wet' cumulate mush. What is difficult to determine is the proportion of the magma chamber that froze, and the proportion, if any, that was extracted and possibly erupted at the surface. Magma chambers that are crystal-rich, relatively cool (<800°C) and H_2O-rich may crystallize faster than hotter (>800°C), drier magmas, and therefore do not allow significant volumes of liquid to escape (Bachmann *et al*., 2007). This would result in small, or no volcanic activity associated with the active system. Temperature estimates for the Halfmoon Pluton based on the plagioclase-hornblende and Ti-in-zircon geothermometers indicates that these magmas crystallized at temperature between ~650 and 750°C, and the modal abundance of hornblende and biotite within both the host and mafic rocks indicates that both magmas were H_2O-rich. Notwithstanding, the Halfmoon Pluton as a whole appears to have been active for a prolonged period, which would be sufficient for the extraction and accumulation of a crystal-poor silicic cap above the preserved chamber.

Mafic magma replenishment of felsic magma chambers is often cited as a triggering mechanism for large-scale silicic caldera-forming eruptions (Sparks *et al*., 1977; Hildreth et al., 1991; Wiebe, 1993; Leonard et al., 2002). Replenishment of basaltic mafic magmas into a liquid-rich silicic cap may have resulted in eruption and evacuation of the chamber above. Volatile escape into this silicic magma cap may also have triggered an eruption as the result of over-pressurization of the chamber (Huppert *et al*., 1983). Throughout the Halfmoon Pluton there is much evidence for the vertical escape of volatiles, which may have risen vertically into a crystal-poor silicic magma cap that then became unstable and erupted. The volcanic Paterson Group, which consists of basalts, andesites and rhyolites, lies stratigraphically above the Halfmoon Pluton (see Figure 4.8, Chapter 4). The Paterson Group has been postulated by Wiebe and Collins (1998) to be

volcanic equivalents of the Halfmoon Pluton, however it gives an older (~146 Ma; Kimbrough *et al*., 1994) age, and has a more evolved isotopic signature enriched in $^{87/86}Sr_{(i)}$ relative to the rest of the rocks analysed within the Halfmoon Pluton. The repeated replenishment of the Halfmoon Pluton by mafic magmas may also have limited the extent to which crystal-liquid separation occurred. Injecting mafic sheets are more buoyant than the intermediate mush at the base of the chamber, and therefore penetrate into the base of the overlying crystal-poor more felsic magma and spread out along the boundary between the two rheologically distinct magmas. This process can effectively trap the crystal mush, choking off lower sections of the reservoir to further extraction, and limiting the volume of silicic magma that can accumulate. This process has been used to explain the paucity of co-magmatic mush erupted with crystal-poor silicic magmas (Hildreth & Wilson, 2007).

7.4 MODEL OF MAGMA CHAMBER CONSTRUCTION AND EVOLUTION

The Halfmoon Pluton preserves multiple lines of evidence indicating that it was constructed incrementally from the base up, consisting of an aggrading crystal-rich intermediate cumulate mush at the base of the chamber and an overlying crystal-poor evolved felsic magma. Evidence that indicates the Halfmoon Pluton was a single magma chamber constructed from the base up includes;

- intrusive internal contacts are absent (excluding late highly evolved granite dikes and sheets)
- orientations of mafic sheets and enclave swarms within the chamber are consistent with incremental growth from the base up
- U/Pb dates which all overlap within error, indicating that the magmas were all active during the same period
- Al-in-hornblende pressure estimates which overlap within error that indicate that the different rocks crystallized between 8-10km depth

The paleo-floor within the chamber can be defined at any one time by each mafic sheet or enclave horizon which was injected at the boundary between the crystal-rich base and the crystal-poor magma above. The size of the active portion of the magma chamber at any

one time during its crystallization history was likely to have been much smaller than the final overall size of the pluton. Plutons have been conceived by many authors (Glazner *et al*., 2004; Miller & Wooden, 2004; Bachmann *et al*., 2007) to contain portions that are melt-rich and melt poor, and may consist of several adjacent magmatic pods that constitute a single magmatic system. Within the Halfmoon Pluton at least two separate magmatic 'pods' are recognized. The rocks at The Neck display contrasting mingling styles and orientations to the rest of the rocks within the Halfmoon Pluton. These are therefore interpreted to represent a younger adjacent magmatic pod that was part of the same active system, as they have identical chemical and isotopic characteristics.

One of the most salient aspects of the geochemical data is the small amount of isotopic variability across the entire petrologic range within the Halfmoon Pluton, which suggests that all the rocks within the pluton are related petrogenetically. Whole-rock geochemistry, primitive isotopic signatures ($^{87}Sr/^{86}Sr_{(i)}$ range between 0.70379 - 0.70427 and εNd range between +3.5 and +1.9) and a paucity of inherited zircons indicate that the Halfmoon Pluton rocks have suffered very little, if any, crustal contamination. There are two models to explain the generation of intermediate-felsic magmas without the addition of older continental crustal components;

- fractional crystallization of mantle-derived basaltic magmas, or
- partial melting of relatively young primitive lower crustal mafic-intermediate rocks of mantle derivation

Tamura and Tatsumi (2002) suggest that rhyolite magmas within the Izu-Bonin Arc have been produced by dehydration melting of calc-alkaline andesite in the upper- to middle-crust. It is possible that crustal melting of isotopically primitive plutonics could have occurred to produce the Halfmoon Pluton rocks. Subduction along the paleo-Pacific margin of Gondwana was long-lived, and generated large volumes of plutonic bodies which are now exposed in the MTZ. The Halfmoon Pluton itself is incorporated into the composite Bungaree Intrusives, which were active from at least ~175 Ma to ~135 Ma. If Halfmoon Pluton magmas were generated by partial melting of primitive MTZ plutonics they would have to be older material melted at mid-crustal depths as partial melting of

deeper mafic protolith would result in an adakitic signature (Muir *et al*., 1998) which is not observed within the rocks of the Halfmoon Pluton. Rocks with high Sr/Y ratios are interpreted to be the result of plagioclase accumulation and not from remelting a mafic protolith.

Many authors believe it is unlikely that the large volumes of intermediate-felsic magma that are episodically erupted along volcanic arcs can have been formed through fractional crystallization of mantle basalts alone as it would require unrealistic volumes of parental basaltic magma which are not preserved in the rock record. As outlined in Section 7.3.1, recent work by Davidson *et al*., (2007) has however shown that hornblende crystallization plays an important role in magmatic differentiation, and that the involvement of hornblende in the fractionating assemblage significantly reduces the volume of residual cumulate that is required to produce the large volumes of evolved silicic magma commonly erupted from arc-settings (Kuno, 1968; Greene *et al*., 2006). As discussed in Section 7.2.2 and Chapter 4, scattered, curvilinear trends on Harker diagrams indicate that fractional crystallization and crystal accumulation of a plagioclase – hornblende – apatite – zircon mineral assemblage probably played the most important role in generating the observed chemical diversity within the rocks of the Halfmoon Pluton. A system whereby 'wet' amphibole-rich basaltic magmas pond at the crust/mantle interface and episodically rise, inject and mingle with an overlying intermediate-felsic magma chamber that itself represents the fractionated product of these mantle melts, is envisaged for the Halfmoon Pluton.

7.4.1 Petrogenetic and Magmatic Model for the Halfmoon Pluton

A model for the construction and evolution of the Halfmoon Pluton is outlined below, and displayed in simplified and highly schematic diagrams in Figures 7.3 and 7.4A – 7.4C).

1. Partial melting in the mantle wedge due to H_2O-rich fluids or melts released from the subducted slab generates the initial pulse of 'wet' primitive basaltic magmas. These mafic melts ponded at the crust-mantle horizon.

2. Amphibole crystallization within the basaltic magmas fractionates towards intermediate compositions. Extraction and accumulation of these intermediate magmas forms the initial host magma chamber of the Halfmoon Pluton at crustal depths that are likely to have been <12 km and maybe even shallower than 5 km.
3. Underplated amphibole-rich basaltic magmas rise episodically into the crust, inject into the base of the aggrading and fractionating host magma chamber, and mingle to form mafic sheets (Ackers Point and Evening Cove) (Figure 7.4A). Increasing SiO_2 and REE contents and decreasing MgO and CaO contents with "stratigraphic" height in the chamber indicate that the mafic sheets, enclaves and dikes that injected into the Halfmoon Pluton have probably been fractionated themselves from the primitive basaltic melts ponded at the base of the crust.
4. Fractionation of the underplated basaltic magmas has the effect of increasing the H_2O-content of these basalts. Further replenishment of the intermediate-felsic magma chamber by these wet basaltic melts results in the formation of mafic enclave swarms as a result of vesiculation (Ringaringa) (Figure 7.4B). Mafic enclaves are subsequently transported and aligned parallel to mafic sheet orientations via magmatic currents operating within the crystal-poor felsic magma immediately above the cumulate mush.
5. The pluton cooled and sagged as a result of the chamber becoming denser in response to intrusion of dense mafic magmas and possible evacuation of the upper chamber through felsic eruptions
6. Fractionation and extraction of the liquid-rich host magma, and continued mafic magma replenishment forms an adjacent magma 'pod' (The Neck). Episodic injection of wet basaltic magmas into this felsic host magma chamber results in the formation of a thick succession of mafic enclaves (Figure 7.4C). Intruding mafic magmas may have brought up pieces of partially crystallized hybrid mush from the base of the chamber, forming composite enclaves
7. The Halfmoon Pluton cooled substantially and further mafic and felsic magma replenishment resulted in the formation of cross-cutting composite dikes. These are concentrated at the top of the chamber (The Neck) where residual felsic melt is still present.

8. Following complete crystallization of the Halfmoon Pluton, late-stage granitic dikes and sheets with a more evolved whole-rock chemistry and isotopic signature were intruded, coupled with further mafic magma intrusion in the form of cross-cutting mafic dikes. Several mafic dikes intruded into the granite sheets, and disaggregated to form enclaves. Cross-cutting mafic dikes have identical chemistry and isotopic signature to mafic sheets at Ackers Point and Evening Cove, indicating that under-plated basaltic magmas continued to intrude into the Halfmoon Pluton even after it was largely solidified.

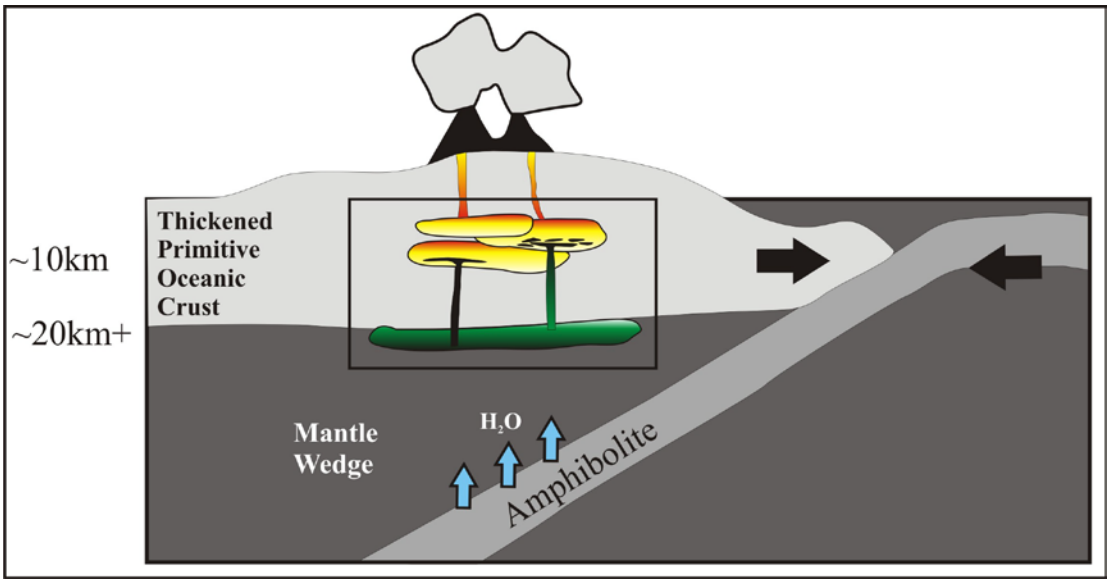

Figure 7.3. Simplified petrogenetic model for the Halfmoon Pluton. Figures 7.4A - 7.4C will focus on the processes operating within the underplated basaltic magmas and the mid-crustal intermediate-felsic host magmas (area is outlined)

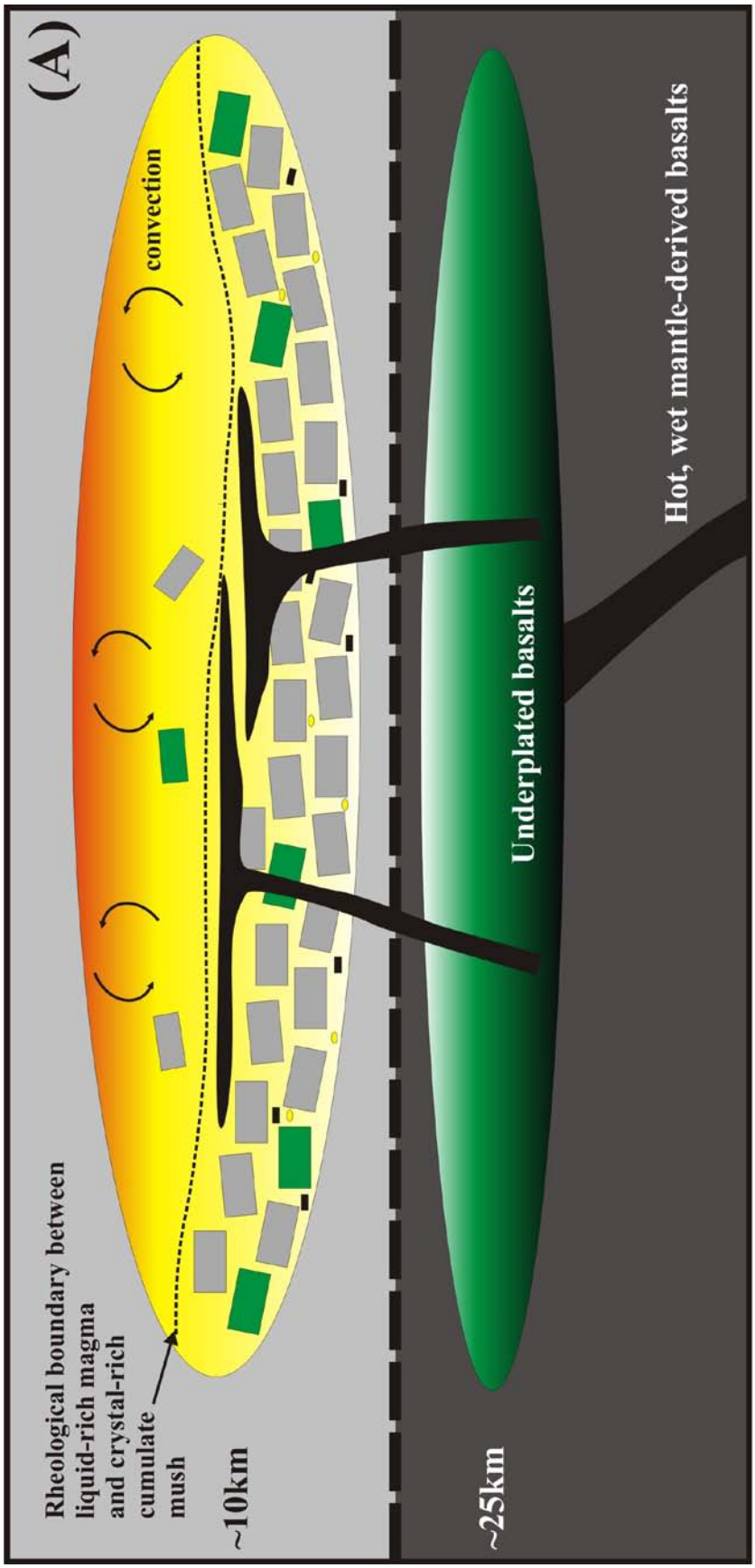

Figure 7.4A. Schematic diagram illustrating some of the processes operating within the Halfmoon Pluton magma chamber. Fractionation and accumulation of a plagioclase (grey crystals) - hornblende (green crystals) - apatite (black crystals) - zircon (yellow crystals) mineral assemblage towards the base of the chamber (Ackers Point and Evening Cove). Crystal settling and compaction accompanied by melt extraction creates a compositional gradient within the mid-upper crustal intermediate-felsic magma chamber. Hot, wet basaltic magmas sourced from the underplated basaltic reservoir intermittently rise and inject vertically into the crystal mush at the base of the magma chamber, spreading laterally at the rheological boundary between crystal mush and overlying liquid-rich magma, and subsequently quench and mingle to form mafic sheets. Note diagram is not to scale.

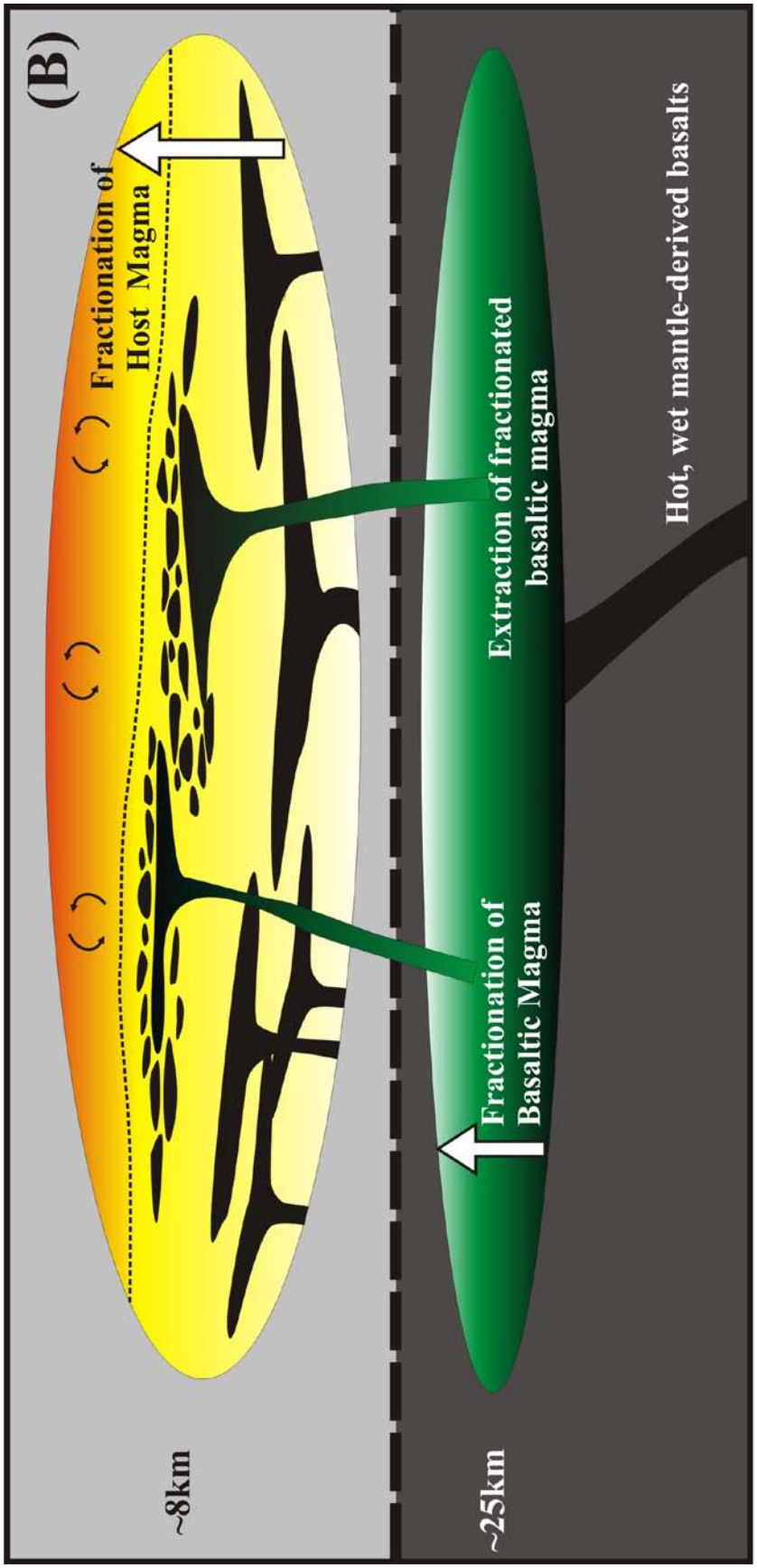

Figure 7.4B. Mid- to upper-crustal felsic magma chamber fractionates towards more evolved compositions. Extraction of magma from the lower crustal basaltic reservoir which has fractionated towards more H_2O-rich compositions. Injected wet basaltic magma vesiculates to form mafic enclaves.

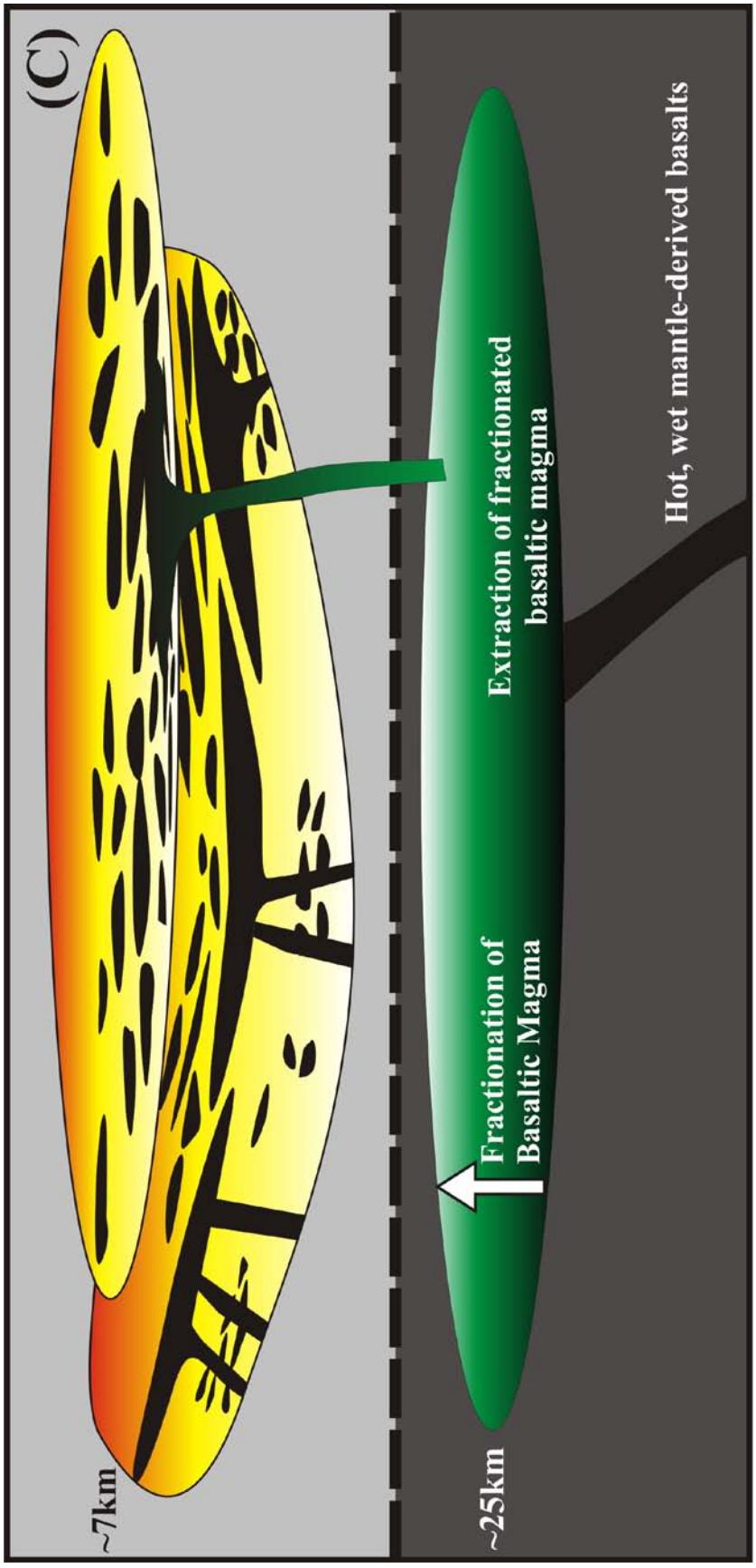

Figure 7.4C. Sagging of the magma chamber due to magma loading and possible eruption above. Extraction of interstitial melt and further injection and fractionation of basaltic magma from the lower crustal reservoir forms an adjacent magmatic 'pod' (i.e. The Neck). Basaltic replenishment into this magma chamber forms large mafic enclave swarms.

7.5 CONCLUSIONS

The exhumed Halfmoon Pluton provides direct evidence for the processes that operate at depth within currently active arc settings. Magmatic processes were identified through a combination of field, petrographic, geochemical and geochronological analyses, and include fractional crystallization, crystal accumulation, episodic mafic magma replenishment, magmatic flow and compaction. Mineral assemblages, chemical characteristics and a lack of isotopic of geochronological evidence for contamination with ancient crustal materials indicates that the amphibole-rich calc-alkaline Halfmoon Pluton was emplaced into a juvenile arc setting, most probably island-arc. The observed change in mingling style from mafic sheet formation at the base of the chamber to mafic enclave formation at the top of the chamber indicates that processes operating within the chamber varied over space and time. Processes attributed to the change in mingling style include fractionation of the mafic magmas towards more H_2O-rich compositions which subsequently resulted in vesiculation of the mafic magma and formation of mafic enclave swarms. Fractionation of amphibole has shown to be an important process controlling the geochemical diversity observed within the Halfmoon Pluton, which provides further evidence to support the conclusions of several authors that amphibole plays an important role in the evolution of many arc suites.

7.6 REFERENCES

Allibone, A.H., Jongens, R., Scott, J.M., Tulloch, A.J., Turnbull, I.M., Cooper, A.F., Powell, N.G., Ladley, E.B., King, R.P. and Rattenbury, M.S. 2009 'Plutonic rocks of the Median Batholith in eastern and central Fiordland: field relations, geochemistry, correlation, and nomenclature' *New Zealand Journal of Geology and Geophysics* 52: 101-148

Arculus, R.J. 1994 'Aspects of magma genesis in arcs' *Lithos* 33:189-208

Arculus, R.J. and Willis, K.J.A. 1980 'The petrology of plutonic blocks and inclusions from the Lesser Antilles Island arc' *Journal of Petrology* 21: 743-799

Bachl, C.A., Miller, C.F., Miller, J.S. and Faulds, J.E. 2001 'Construction of a pluton: Evidence from an exposed cross section of the Searchlight pluton, Eldorado Mountains, Nevada' *GSA Bulletin* 113(9): 1213-1228

Bachmann, O. and Bergantz, G.W. 2004 'On the origin of crystal-poor rhyolites: extracted from batholithic crystal mushes' *Journal of Petrology* 45: 1565-1582

Bachmann, O., Miller, C.F. and de Silva, S.L. 2007 'The volcanic-plutonic connection as a stage for understanding crustal magmatism' *Journal of Volcanology and Geothermal Research* 167: 1-23

Barclay, J. and Carmichael, I.S.E. 2004 'A hornblende basalt from Western Mexico: water-saturated phase relations constrain a pressure-temperature window of eruptability' *Journal of Petrology* 45: 485-506

Blundy, J.D. and Sparks, R.S.J. 1992 'Petrogenesis of mafic inclusions in granitoids of the Adamello Massif, Italy' *Journal of Petrology* 33: 1039-1104

Bonin, B. 1991 'The enclaves of alkaline anorogenic granites: an overview' In: Didier, J. and Barbarin, B. (eds) *Enclaves and Granite Petrology. Developments in Petrology 13* Amsterdam: Elsevier pp 179-189

Carmichael, I.S.E. 2002 'The andesite aqueduct: perspectives on the evolution of intermediate magmatism in west-central (105-99°W) Mexico' *Contributions to Mineralogy and Petrology* 143: 641-663

Collins, W.J., Wiebe, R.A., Healy, B. and Richards, S.W. 2006 'Replenishment, crystal accumulation and floor aggradation in the megacrystic Kameruka Suite, Australia' *Journal of Petrology* 47: 2073-2104

Davidson, J., Turner, S., Handley, H., Macpherson, C. and Dosseto, A. 2007 'Amphibole "sponge" in arc crust?' *Geology* 35: 787-790

Frey, F.A., Green, D.H. and Roy, S.D. 1978 'Integrated models of basalt petrogenesis : a study of quartz tholeiites to olivine melilitites from south eastern Australia utilizing geochemical and experimental petrological data' *Journal of Petrology* 19: 463-513

Frost, T.P. and Mahood, G.A. 1987 'Field, chemical, and physical constraints on mafic-felsic magma interaction in the Lamarck Granodiorite, Sierra Nevada, California' *Geological Society of America Bulletin* 99: 272-291

Glazner, A.F., Bartley, J.M., Coleman, D.S., Gray, W. and Taylor, R.Z. 2004 'Are plutons assembled over millions of years by amalgamation from small magma chambers?' *GSA Today* 14(4): 4-11

Greene, A.R., DeBari, S.M., Kelemen, P.B., Blusztajn, J. and Clift, P.D. 2006 'A detailed geochemical study of island arc crust: the Talkeetna arc section, South-Central Alaska' *Journal of Petrology* 47: 1051-1093

Harper, B.E., Miller, F., Miller, G., Koteas, C., Cates, N.L., Wiebe, R.A., Lazzareschi, D.S. and Cribb, J.W. 2004 'Granites, dynamic magma chamber processes and pluton construction: the Aztec Wash pluton, Eldorado Mountains, Nevada, USA' *Transactions of the Royal Society of Edinburgh: Earth Sciences* 95: 277-295

Hildreth, W. 2004 'Volcanological perspectives on Long Valley, Mammoth Mountain, and Mono Craters: several contiguous but discrete systems' *Journal of Volcanology and Geothermal Research* 136: 169-198

Hildreth, W., Halliday, A.N. and Christiansen, R.L. 1991 'Isotopic and chemical evidence concerning the genesis and contamination of basaltic and rhyolitic magma beneath the Yellowstone Plateau volcanic field' *Journal of Petrology* 32: 63-138

Hildreth, W. and Wilson, C.J.N. 2007 'Compositional zoning of the Bishop Tuff' *Journal of Petrology* 48: 951-999

Huppert, H.E., Sparks, R.S.J. and Turner, J.S. 1983 'Laboratory investigations of viscous effects in replenished magma chambers' *Earth and Planetary Science Letters* 65: 377-381

Johannes, W. and Holtz, F. 1996 *Petrogenesis and experimental petrology of granitic rocks* Springer Verlag, Heidlelburg, pp 165

Kamiyama, H., Nakajima, T. and Kamioka, H. 2007 'Magmatic stratigraphy of the tilted Tottabetsu Plutonic Complex, Hokkaido, North Japan: Magma chamber dynamics and pluton construction' *The Journal of Geology* 115: 296-314

Kemp, A.I.S., Whitehouse, M.J., Hawkesworth, C.J. and Alarcon, M.K. 2005 'A zircon U-Pb study of metaluminous (I-type) granites of the Lachlan Fold Belt, southeastern Australia: implications for the high/low temperature classification and magma differentiation processes' *Contributions to Mineralogy and Petrology* 150: 230-249

Kimbrough, D.L., Tulloch, A.J., Coombs, D.S., Landis, C.A., Johnston, M.R. and Mattinson, J.M 1994 'Uranium-lead zircon ages from the Median Tectonic Zone, New Zealand' *New Zealand Journal of Geology and Geophysics* 37: 393-419

Kuno, H. 1968 'Origin of andesite and its bearing on the island arc structure' *Bullentin of Volcanology* 32: 141-176

Larocque, J. and Canil, D. 2009 'The role of amphibole in the evolution of arc magmas and crust: the case from the Jurassic Bonanza arc section, Vancouver Island, Canada' *Contributions to Mineralogy and Petrology*

Leonard, G.S., Cole, J.W., Nairn, I.A. and Self, S. 2002 'Basalt triggering of the c. AD 1305 Kaharoa rhyolite eruption, Tarawera Volcanic Complex, New Zealand' *Journal of Volcanology and Geothermal Research* 115: 461-486

Macpherson, C.G., Dreher, S.T. and Thirwall, M.F. 2006 'Adakites without slab melting : high pressure differentiation of island arc magma, Mindanao, the Phillipines' *Earth and Planetary Science Letters* 243: 581-593

Miller, C.F. and Miller, J.S. 2002 'Contrasting stratified plutons exposed in tilt blocks, Eldorado Mountains, Colorado River Rift, NV, USA' *Lithos* 61: 209-224

Miller, J.S. and Wooden, J.L. 2004 'Residence, Resorption and Recycling of Zircons in Devils Kitchen Rhyolite, Coso Volcanic Field, California' *Journal of Petrology* 45:2155-2170

Muir, R.J., Ireland, T.R., Weaver, S.D., Bradshaw, J.D., Evans, J.A., Eby, G.N. and Shelley, D. 1998 'Geochronology and geochemistry of a Mesozoic magmatic arc system, Fiordland, New Zealand' *Journal of the Geological Society, London* 155: 1037-1053

Pitcher, W.S. 1991 ‘Synplutonic dikes and mafic enclaves’ In: Didier, J. and Barbarin, B. (eds) *Enclaves and granite petrology. Developments in Petrology 13* Amsterdam: Elsevier pp 383-391

Rapp. R.P. and Watson, E.B. 1995 ‘Dehydration melting of metabasalt at 8-32 kbar: Implications for continental growth and crustal recycling’ *Journal of Petrology* 36: 891-931

Scaillet B., Holtz F., Pichavant M. 1998 ‘Phase equilibrium constraints on the viscosity of silicic magmas. 1. Volcanic-plutonic comparison’ *Journal of Geophysical Research* 103: 27257-27266.

Shukuno, H., Tamura, Y., Tani, K., Chang, Q., Suzuki, T. and Fiske, R.S. 2006 ‘Origin of silicic magmas and the compositional gap at Sumisu submarine caldera, Izu-Bonin arc, Japan’ *Journal of Volcanology and Geothermal Research* 156: 187-216

Smith, I.E.M., Worthington, T.J., Stewart, R.B., Price, R.C. and Gamble, J.A. 2003 ‘Felsic volcanism in the Kermadec arc, southwest Pacific: crustal recycling in an oceanic setting’ In: Larter, R.D. and Leat, P.T. (eds) ‘Intra-oceanic subduction systems: tectonic and magmatic processes’ *Special publication of the Geological Society of London*, 219: 99-118

Smith, I.E.M., Worthington, T.J., Price, R.C., Stewart, R.B. and Maas, R. 2006 ‘Petrogenesis of dacite in an oceanic subduction environment: Raoul Island, Kermadec arc’ *Journal of Volcanology and Geothermal Research* 156: 252-265

Sparks, R.J., Sigurdsson, H. and Wilson, L. 1977 ‘Magma mixing: a mechanism for triggering acid explosive eruptions’ *Nature* 267: 315-318

Tamura, Y. and Tatsumi, Y. 2002 'Remelting of an andesitic crust as a possible origin for rhyolitic magma in oceanic arcs: an example from the Izu-Bonin Arc' *Journal of Petrology* 43: 1029-1047

Tamura, Y., Gill, J.B., Tollstrup, D., Kawabata, H., Shunkuno, H., Chang, Q., Miyazaki, T., Takahashi, T., Hirahara, Y., Kodaira, S., Ishizuka, O., Suzuki, T., Kido, Y., Fiske, R.S. and Tatsumi, Y. 2009 'Silicic magmas in the Izu-Bonin oceanic arc and implicstions for crustal evolution' *Journal of Petrology* 50: 685-723

Tiepolo, M. and Tribuzio, R. 2008 'Petrology and U-Pb geochronology of amphibole-rich cumulates with sanukitic affinity from Husky Ridge (Northern Victoria Land, Antarctica): Insights into the role of amphibole in the petrogenesis of subduction-related magmas' *Journal of Petrology* advance access April 9th

Wandres, A.M., Weaver, S.D., Shelley, D. and Bradshaw, J.D. 1998 'Change from calc-alkaline to adakitic magmatism recorded in the Early Cretaceous Darran Complex, Fiordland, New Zealand' *New Zealand Journal of Geology and Geophysics* 41: 1-14

Wiebe, R.A. 1993 'Basaltic injections into floored silicic magma chambers' *Eos* 74(1): 1-4

Wiebe, R.A. 1994 'Silicic magma chambers as traps for basaltic magmas: the Cadillac Mountain intrusive complex, Mount Desert Island, Maine' *The Journal of Geology* 102: 423-437

Wiebe, R.A., Smith, D., Sturm, M., King, E.M. and Seckler, M.S. 1997 'Enclaves in the Cadillac Mountain Granite (Coastal Maine): samples of hybrid magma from the base of the chamber' *Journal of Petrology* 38: 393-423

Wiebe, R.A. and Collins, W.J. 1998 'Depositional features and stratigraphic sections in granitic plutons: implications for the emplacement and crystallization of granitic magma' *Journal of Structural Geology* 20(9/10): 1273-1289

Wiebe, R.A., Frey, H. and Hawkins, D.P. 2001 'Basaltic pillow mounds in the Vinalhaven intrusion, Maine' *Journal of Volcanology and Geothermal Research* 107: 171-184

Wright, I.C., Worthington, T.J. and Gamble, J.A. 2006 'New multibeam mapping and geochemistry of the 30°-35°S sector, and overview, of southern Kermadec arc volcanism' *Journal of Volcanology and Geothermal Research* 149: 263-296

CHAPTER EIGHT

A COMPARISON OF COMPOSITE PLUTONS FROM DIFFERENT TECTONIC SETTINGS

8.1 INTRODUCTION

Plutons that exhibit mingling structures similar to those within the Halfmoon Pluton occur in different tectonic settings. Interpretations of the magma mingling and mixing textures and structures observed within these plutons have provided much information on magmatic processes, providing insight into the sequence of construction and evolution of magma chambers at different levels within the crust.

Composite plutonic complexes (those that preserve evidence for mingling and mixing of mafic and felsic magmas) of different age, size, and tectonic setting are discussed in this chapter, and comparisons are made with the Halfmoon Pluton. Key similarities and differences between plutons in different tectonic settings are identified in order to determine what fundamental processes control the structures and textures observed. Composite plutonic systems associated with continental extensional tectonic settings discussed include the Cadillac Mountain Intrusive Complex in Maine, and the Aztec Wash Pluton in Nevada. Like the Halfmoon Pluton, the Tottabetsu Igneous Complex in Japan, and the Tuross Head Tonalite in New South Wales are examples from arc-related settings. The author's own field observations from fieldwork undertaken on the Cadillac Mountain Intrusive Complex and the Tuross Head Pluton are supplemented with published information. Interpretations and comparisons with the Tottabetsu Igneous Complex and the Aztec Wash Pluton are drawn solely from published material.

8.2 CONTINENTAL EXTENSIONAL TECTONIC SETTINGS

8.2.1 The Cadillac Mountain Intrusive Complex, Maine, USA

The ~420 Ma Cadillac Mountain intrusive complex (Figure 8.1) belongs to the Coastal Maine Magmatic Province - a suite of bimodal plutons in which magma mingling and mixing structures confirm the coeval intrusion of mafic material into granitic magma chambers (Wiebe, 1994; Wiebe *et al*., 1997a; Wiebe *et al*., 1997b). The Cadillac Mountain intrusive complex (CMIC) was emplaced during a period of transtensional rifting along a continental transcurrent fault system (Hogan & Sinha, 1989; Wiebe, 1994), and is characterized by a large body of granite (the Cadillac Mountain granite) which experienced multiple replenishments of gabbroic and dioritic magma that ponded at its base (Wiebe *et al*., 1997a).

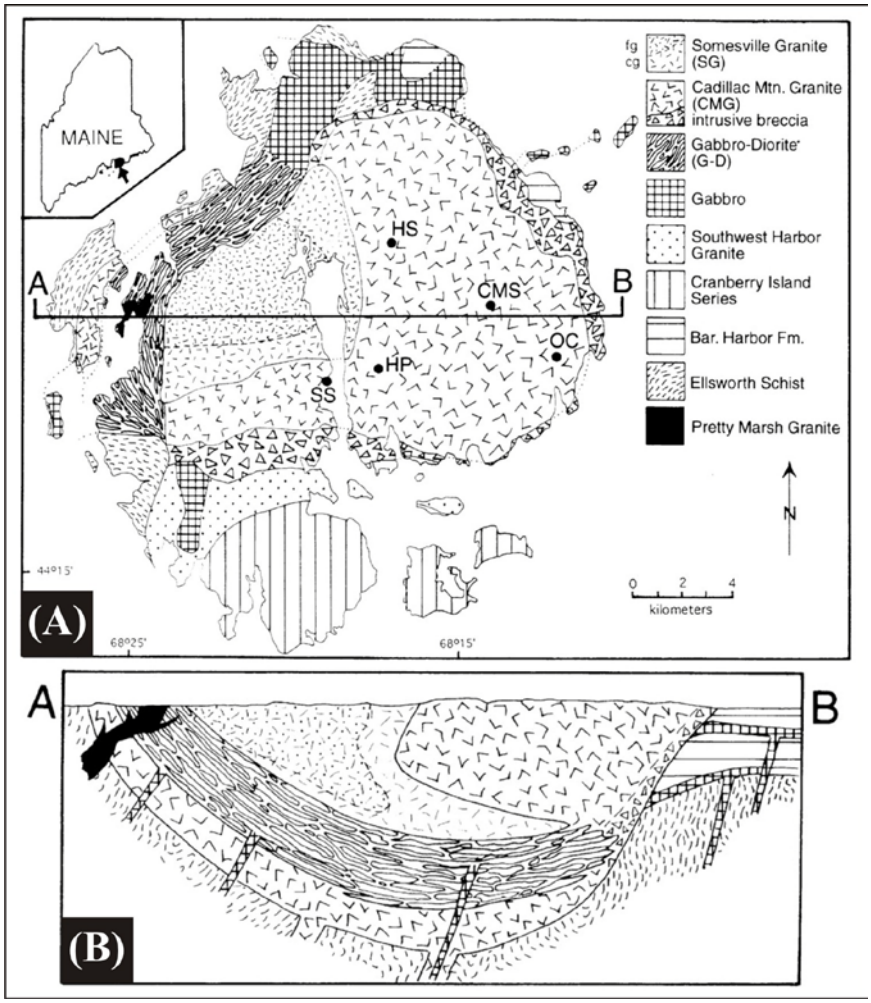

Figure 8.1. (A) Geological map of the Cadillac Mountain intrusive complex (B) schematic cross-section of the CMIC (from Wiebe *et al*., 1997b)

Smaller granitic intrusions that post-date crystallization of the Cadillac Mountain granite include the Somesville granite (SG), the Southwest Harbour granite, and the Pretty Marsh granite (Wiebe, 1994). The lower Cadillac Mountain granite (CMG) is a relatively hydrous, hornblende-bearing I-type granite that crystallized prior to the intrusion of the gabbro-diorite unit (GD). The lower CMG is a two-feldspar granite, with subhedral hornblende, biotite, accessory opaques, zircon, apatite, allanite, titanite and fluorite, and has ~66-73 wt% SiO_2 whole-rock composition (Wiebe *et al*., 1997a). The upper CMG is a relatively homogeneous, medium- to coarse-grained hypersolvus A-type granite with quartz, mesoperthitic alkali-feldspar, interstitial hornblende and biotite, and accessory opaques, zircon, apatite, allanite, titanite and fluorite which crystallized after the intrusion of the GD (Wiebe *et al*., 1997a). It is slightly more evolved than the lower CMG with a composition of 72-75 wt% SiO_2 compared with 45-75 wt% for the GD unit due to fractionation of the mafic magmas. Chilled margins of mafic sheets/pillows probably best represent the original liquid composition of the mafic magmas, which range between 44-56 wt% SiO_2 (Wiebe *et al*., 1997b). Mineral phases within chilled mafic rocks are dominated by plagioclase and hornblende, with subordinate augite, orthopyroxene, opaques and biotite (Wiebe *et al*., 1997a). Textures and compositions of felsic host rocks within the GD indicate that they are probably cumulates (Wiebe *et al*., 1997b). A shallow (5-7 km) emplacement was inferred by Wiebe *et al* (1997b) on the basis of miariolitic cavities, and emplacement of the pluton into comagmatic erupted products.

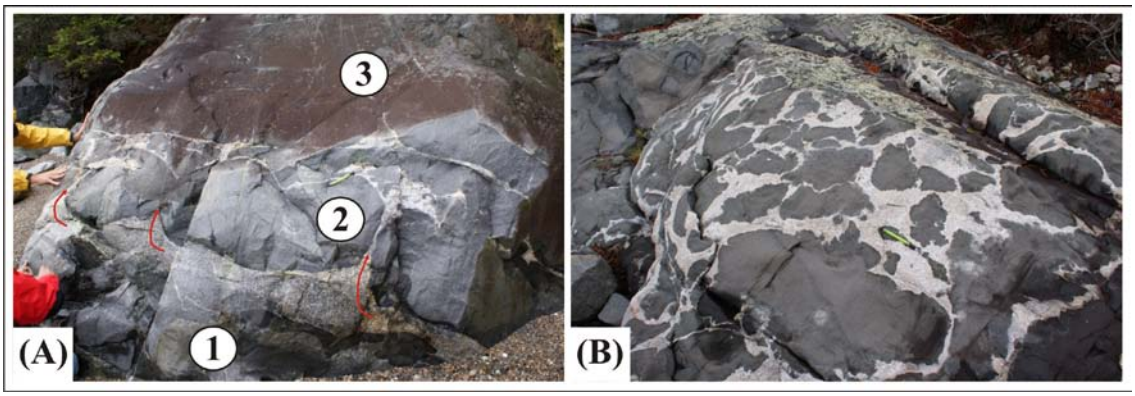

Figure 8.2. (A) Sequence of at least three different injections of mafic magma which quenched within a more felsic host magma to form mafic sheets. Mafic Sheet 1 was the first injected, mafic sheet 3 the last. Red arrows indicate flame structures (B) Composite dike cross-cutting a mafic sheet. Pencil for scale is 14cm long.

Structures and textures within the GD clearly indicate that the gabbroic rocks were intruded as a series of sheet-like intrusions that mingled with dioritic host magma at the base of the CMG (Figure 8.2(A)). These mafic sheets formed macrorhythmic layers that grade upward from basally chilled gabbro, to coarser-grained gabbro, dioritic, or granitic rocks (Wiebe, 1994). The formation of thick (≤50m) macrorhythmic layers suggests that mafic magma injections were voluminous and sufficiently spaced in time to allow for the gabbroic magma to fractionate to granitic compositions. Mafic sheets have fine-grained quenched basal margins that are punctuated by flame structures that often contain amphibole accumulations due to the vertical escape of volatiles. Mafic enclaves are scarce beneath the GD unit, and become more abundant, though scattered, within the CMG. Spectacular silicic pipes that intrude up through the mafic sheets are also present, and represent interstitial melt extracted from the underlying felsic cumulates as a result of compaction. Formation of silicic pipes implies that the silicic material below the gabbroic sheets was not completely solidified, perhaps containing as much as 50% interstitial liquid (Wiebe, 1993). Several composite dikes cross-cut the GD unit, and consist of loosely compacted mafic pillows within a silicic host (Figure 8.2(B)).

8.2.2 Aztec Wash Pluton, Nevada, USA

The ~15.7 Ma Aztec Wash Pluton was emplaced during a period of extension within the northern Colorado River corridor, a region of moderately to highly extended crust along the eastern margin of the Basin and Range province (Faulds *et al*., 2001). The ~3km thick pluton was inferred by Cates *et al*., (2003) to have been active for a period of ~0.2 Ma, and was divided by Falkner *et al*., (1995) into two units based on lithological characteristics (Figure 8.3);

- An upper relatively homogenous zone (GZ) comprising almost entirely granite
- A lower heterogeneous zone (HZ) containing mingled and mixed mafic and felsic magmas

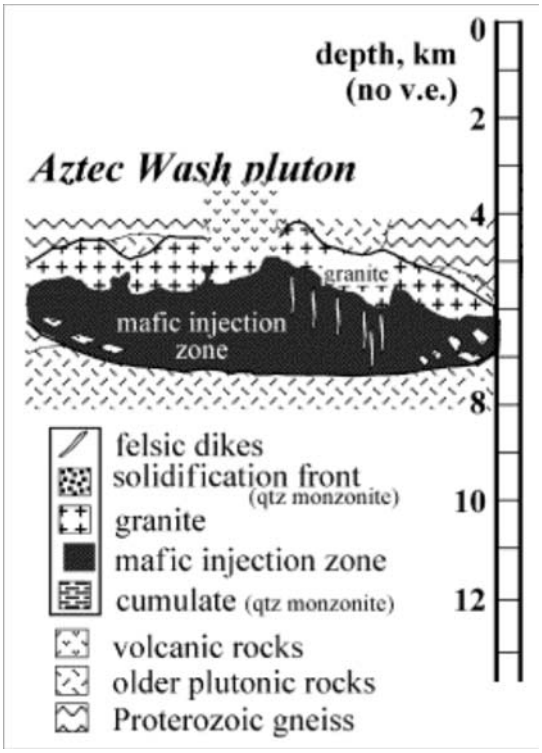

Figure 8.3. Reconstructed cross-section of the Aztec Wash Pluton showing the Heterogeneous Zone (mafic injection zone) and the overlying Homogeneous Granite (from Miller & Miller, 2002)

The lower HZ shows evidence for incremental assembly in the form of multiple injections of mafic magma into a more felsic magma chamber, resulting in the formation of mafic sheets. Like the Halfmoon Pluton, mafic sheets were emplaced at the boundary between the crystal-rich cumulate mush at the base of the chamber, and an overlying melt-rich magma. The HZ felsic cumulates have intermediate SiO_2 compositions between 57 and 65 wt%, are strongly enriched in compatible elements (e.g. Ba, Sr) and contain closely compacted feldspar crystals separated by interstitial quartz, indicating they contained very little trapped liquid. This is consistent with melt extraction from loading by dense overlying mafic sheets (Harper *et al*., 2004). These felsic cumulates are largely classified as quartz monzonites. Intruding mafic rocks vary in size, shape, grain-size (from fine- to medium-grained), and mineralogy (varying quantities of clinopyroxene, hornblende, biotite and olivine). Mafic sheets and enclaves have a restricted range of SiO_2 contents between 45 - 58 wt% (Patrick & Miller, 1997). Coarser-grained mafic rocks are interpreted as cumulates that formed from thicker, slower cooling mafic sheets (Miller & Miller, 2002). Continual input of both mafic and felsic magma into the chamber is evidenced by cross-cutting felsic and composite dikes.

Like the HZ, the GZ consists of granite cumulate at its base which fractionates to finer-grained more evolved rocks towards the top. Whole-rock SiO_2 composition is restricted to 70 - 72 wt% (Harper *et al*., 2004). The GZ represents a thin (~1 km thick) overlying sheet above the denser, more mafic HZ. Evidence for mafic magma input is absent in all but the base of the GZ in the form of mafic enclaves. Shallow emplacement depths (~4-7 km) are inferred from Al-in-hornblende geobarometry (Miller & Miller, 2002), and the presence of miariolitic cavities within a leucogranite at the top of the GZ. Both the GZ and HZ display calc-alkaline chemistry, however they were formed within a rifted continental margin tectonic setting. Melting of a source that formed by arc and collisional processes is inferred by Falkner *et al*. (1995).

8.3 Arc – Back-Arc Tectonic Settings

8.3.1 Tuross Head Tonalite, New South Wales, Australia

The Tuross Head Tonalite (THT) is located on the south coast of New South Wales (NSW), Australia, and belongs to the Moruya Suite within the larger Bega Batholith, a series of I-type plutonic bodies within the Lachlan Fold Belt (Figure 8.4(A)) (Chappell *et al*., 1991). There is no published age for the Tuross Head Tonalite, however as it is part of the Moruya Suite it is probably late Devonian in age (Griffen *et al*., 1978). An extensional arc - back-arc tectonic setting is inferred based on the primitive composition of the intruding mafic rocks (Griffin *et al*., 1978). The Tuross Head Tonalite consists of gabbroic and dioritic sheets and enclaves that have intruded into tonalite host magma (Wiebe & Collins, 1998).

Structures and textures, including load-casts and flame structures at the chilled base of mafic sheets and sporadic felsic pipes, indicate mingling between the mafic and felsic magmas. Way up structures and dips of mafic sheets and enclaves indicate that the chamber sagged inward as accumulation occurred (Wiebe & Collins, 2007) (Figure 8.4(A)). Both mafic and felsic rocks consist dominantly of plagioclase, hornblende and biotite, with accessory magnetite, apatite, titanite and zircon (Griffin *et al*., 1978). Plagioclase crystals within the tonalite host are tabular, defining a foliation parallel to mafic sheet/enclave orientation, which probably developed in response to a combination of crystal accumulation, compaction and magmatic flow.

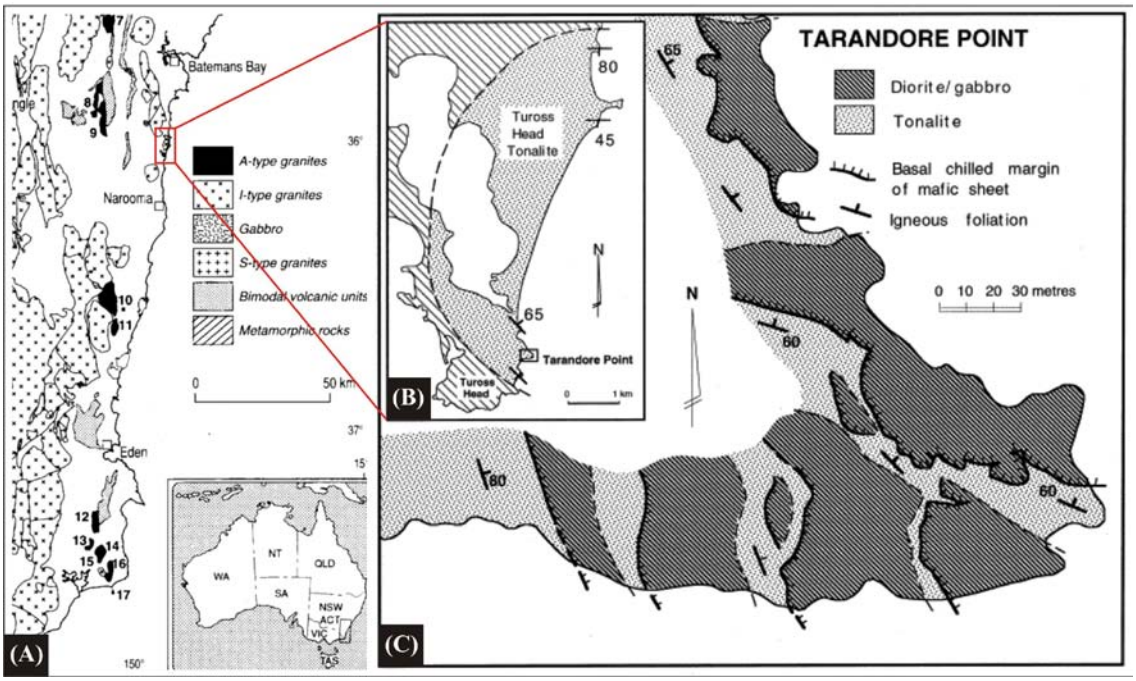

Figure 8.4. (A) Geological Map of southeastern NSW showing the various plutonic bodies that comprise the Lachlan Fold Belt (LFB), highlighting the position of the Tuross Head Pluton within the LFB, New South Wales, Australia (B) Map showing the extent of the Tuross Head Tonalite, with south and north dipping mafic sheets (C) Detailed geological map defining multiple mafic sheets that outcrop at Tarandore Point (adapted from King *et al*., 1996; Wiebe & Collins, 1998)

The tonalitic host magma becomes more mafic and foliated with height in the stratigraphic sequence as a result of mixing with coexisting mafic magma induced by magmatic flow (Collins, 2003). Mafic and intermediate enclaves are abundant within the Tuross Head Tonalite (Figure 8.5), and have textures, modes and mineralogy that are similar to the mafic sheets and cross-cutting mafic dikes. Mafic rocks are interpreted to represent mantle-derived magma that mixed with crustal magmas in the chamber (Wiebe & Collins, 1998). Structural analysis of microgranitoid enclave swarms within the Tuross Head Tonalite by Vernon *et al*. (1988) indicate that magmatic processes are varied quite considerably throughout the active magma chamber, as evidenced by changes in the concentration of enclaves, size and shape of enclaves, amount of elongation, and the nature of the contact between the enclave and the surrounding host. Several mafic enclaves have angular shapes suggesting that they broke up after crystallizing before being moved to their current location by flow (Figure 8.5(A)).

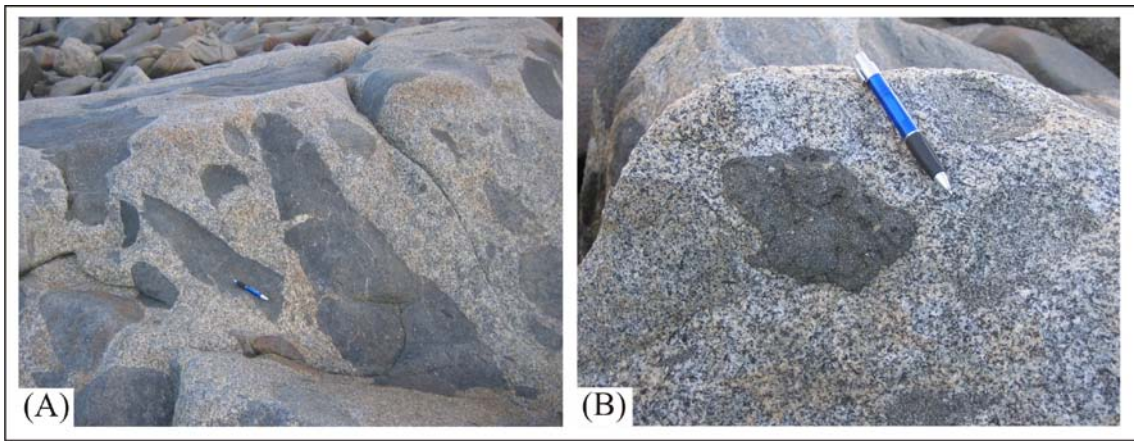

Figure 8.5. (A) Angular mafic enclaves within a more felsic host rock (B) Juxtaposition of mafic and intermediate/hybrid enclaves within a granodiorite host. Pen for scale is 14cm long. Both outcrops located at Tuross Head.

Composite enclaves are also found within the Tuross Head Tonalite (Figure 8.5(A)), and indicate that mixing between felsic and mafic magmas occurred at a location removed from the current site of emplacement, however the location at which this mixing took place cannot be determined. These composite enclaves are very similar both mineralogically and texturally to composite enclaves found within the Halfmoon Pluton (Figure 8.6(B)).

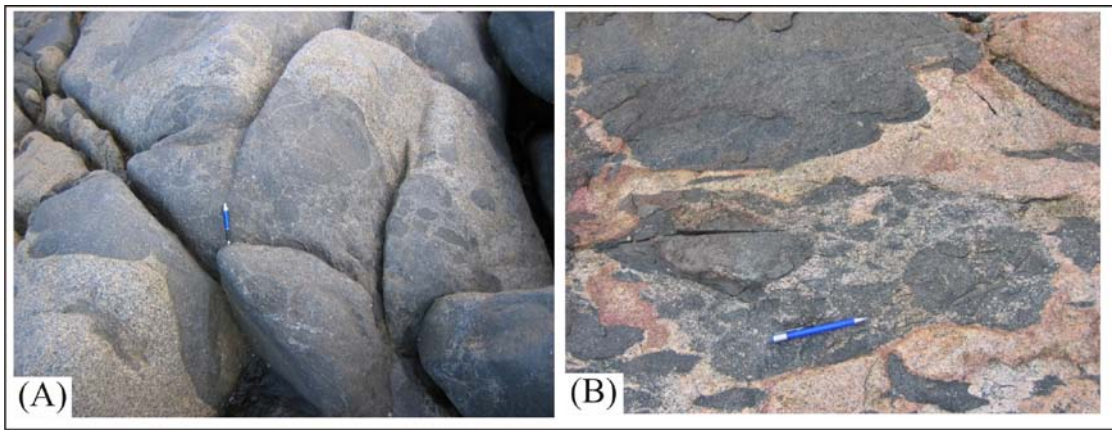

Figure 8.6. (A) Composite enclave within the Tuross Head Tonalite (B) Composite enclave from The Neck, Halfmoon Pluton. Pencil for scale is 14cm in length.

Crenulate margins in response to compaction of composite enclaves indicate that they were not fully crystalline when emplaced in their current location. Composite dikes cross-cut the pluton in places, and consist of fine-grained mafic enclaves within a fine-grained felsic host. Mafic enclaves within the composite dikes have the same mineralogy as mingled mafic enclaves and sheets, and can be compacted or not

compacted within the composite dikes. Mafic dikes that cross-cut the pluton display identical mineralogy and chemistry to the mingled mafic rocks.

8.3.2 Tottabetsu Plutonic Complex, Japan

The 19.8 ± 0.9 Ma Tottabetsu Plutonic Complex was emplaced along a convergent plate boundary, and records a protracted history of pluton construction involving stoping, convection, episodic mafic magma replenishments, fractional crystallization and magma mixing (Kamiyama *et al*., 2007). The plutonic complex, as mapped by Suetake (1997), is subdivided into three zones (Figure 8.7);

- Zone I; ~7km thick lower-most zone of gabbroic sheets separated by thin amounts of host leucodiorite
- Zone II; ~1 – 1.5 km thick middle zone of interlayered mesodiorite within host leucodiorite
- Zone III; ~1 – 1.5km thick upper zone of homogeneous granite containing sporadic mafic and felsic enclaves

The leucodiorites (Zones I and II) represent the resident felsic host magma into which the gabbroic and mesodioritic magmas intruded, and contain high modal abundances of plagioclase (~62-83%), which show a strong preferred alignment parallel to that of mafic sheet orientation. Other mineral phases include orthopyroxene, cummingtonite, hornblende and biotite. Mafic sheets from zones I and II contain high abundances of plagioclase (44 – 67%) and hornblende (6 – 60%), and smaller amounts of clinopyroxene, orthopyroxene and biotite (<1 – 20%). Leucodiorites have SiO_2 contents between 53 and 67 wt%, and geochemical signatures that indicate that they represent the mushy cumulate floor of a chamber, with accumulation of plagioclase and zircon indicated by elevated Al_2O_3, Na_2O, Zr and Hf, positive Eu anomalies, and HREE enrichments (Kamiyama *et al*., 2007). Isotopic signatures vary with rock type. Mafic sheets have low SiO_2 concentrations between 49 and 63 wt%. All mafic and felsic rocks from the upper part of the plutonic complex (Zones II and III), and leucodiorites from the lowermost Zone I have virtually indistinguishable Sr_i, (0.70385 - 0.70423), whereas gabbro sheets from zone I have more primitive Sr_i (0.70271 - 0.70394). Low Sr_i values in the gabbros correlate with low SiO_2 contents, whereas higher Sr_i values correlate with higher SiO_2 contents, indicating open-system evolution of the mafic magma (Kamiyama *et al*.,

2007). Mafic sheets and enclaves within Zones I and II have SiO_2 contents between 48 and 65 wt%. Stoped metasedimentary blocks are present in the lower two zones of the pluton, and may reflect injection of mafic magma within a more felsic magma chamber at shallow crustal levels that induced thermal stresses and subsequent stoping of wall-rock (Oji, 2000).

Figure 8.7. (A) Geological map of the Tottabetsu Plutonic Complex. Zone I represents the more mafic base of the chamber, with the youngest portion of the chamber represented by granites in Zone III (B) (C) Location of Tottabetsu Plutonic Complex (from Kamiyama *et al*., 2007)

A deeper gabbro-diorite unit is inferred from gravity studies to underlie Zone I (Kamiyama *et al.*, 2007), which probably represents the deeper mafic roots that fed the system.

8.4 DISCUSSION

The Halfmoon Pluton and the four composite plutons discussed above are all characterized by coeval mafic-intermediate-felsic magma interaction that resulted in magma mingling, mixing, and the formation of a stratified magma chamber. Magma mingling structures and textures, and geochemical and geochronological data indicate that all these plutons are characterized by a similar magmatic history involving repeated mafic magma replenishments into an evolving more felsic host. Whereas these plutons are all characterized by some identical magmatic processes, there are several significant differences, suggesting that all five composite plutons experienced different histories.

8.4.1 COMMON FEATURES OF COMPOSITE PLUTONS

All five plutonic complexes discussed preserve structures and textures suggesting they were assembled incrementally from the base up as a result of multiple injections of hot mafic magma onto the floor of a cooler, more felsic magma chamber. The evidence of mafic magma injection is preserved in all five plutons in the form of mafic sheets and/or mafic enclaves. Mafic sheets almost always develop similar asymmetric morphologies with fine-grained quenched basal contacts punctuated by flame-structures of upwelling felsic material, coarser-grained centres, and gradational upper contacts. Intruding mafic sheets, and associated enclaves, almost always contain higher abundances of hydrous phases (i.e. hornblende and/or biotite) than their enclosing felsic host. As Figure 8.8 shows, several mingling structures preserved within the Gabbro-Diorite unit within the Cadillac Mountain Intrusive Complex are similar to those observed within the Halfmoon Pluton, including amphibole accumulations at the top of flame structures as a result of the vertical escape of volatiles.

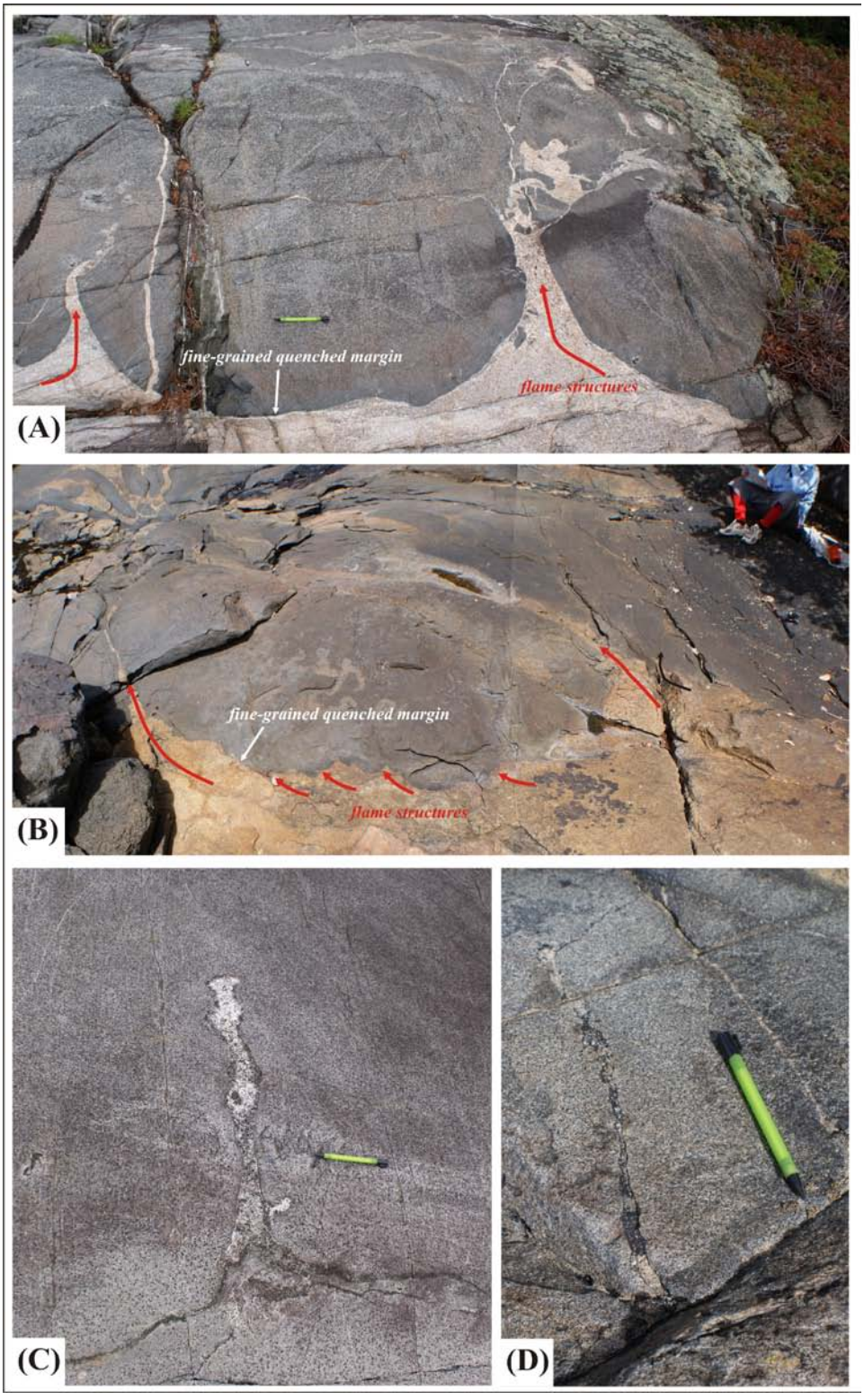

Figure 8.8. (A) Base of a quenched mafic sheet from within the CMIC (B) base of a quenched mafic sheet within the Halfmoon Pluton with person for scale (C) Amphibole seams that feed into an upwelling felsic pipe within a mafic sheet - CMIC (D) Amphibole seam within felsic material upwelling into the base of a mafic sheet – Bungaree Intrusives. Pencil for scale is 14cm in length.

The plutonic complexes are characterized by mafic magma replenishment into a more felsic magma chamber, however there are differences in the compositional gap between the interacting mafic and felsic magmas. Small (>10 wt%) differences in SiO_2 between the interacting mafic and felsic rocks occur within the Halfmoon Pluton, Tottabetsu Plutonic Complex and the Tuross Head Pluton, whereas larger compositional contrasts (12-22 wt% SiO_2) exist between the mafic and felsic rocks within the CMID and the Aztec Wash Pluton. Figure 8.9 shows variation diagrams from CaO and Ba vs. SiO_2 that display the compositional contrast between the interacting mafic and felsic magmas. As shown in Figure 8.8, magma mingling occurred within both plutonic complexes and resulted in several similar structures and textures forming – despite the differences in compositional contrast between the two interacting magmas. This implies that compositional contrasts do not play a significant role in several of the magma mingling structures and textures that result from the coeval interaction of mafic and felsic magmas.

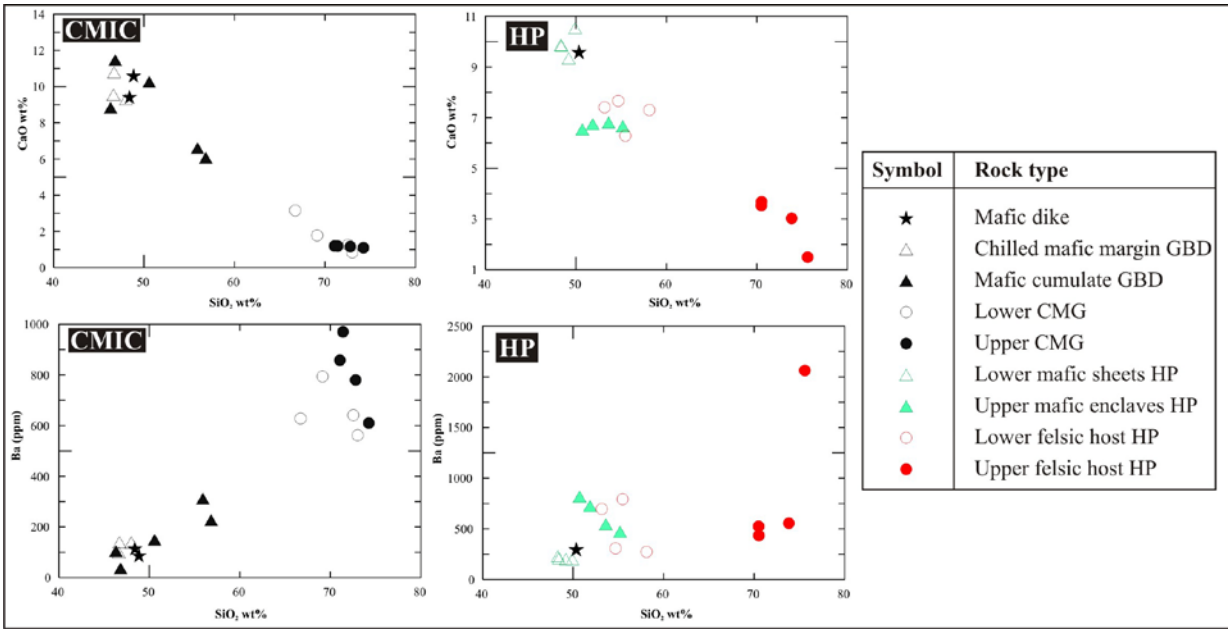

Figure 8.9. CaO and Ba vs. SiO_2 diagrams for the Cadillac Mountain intrusive complex (CMIC) and the Halfmoon Pluton (HP) showing the compositional contrasts between the interacting mafic and felsic rocks. Compositional contrasts are much larger for the CMIC than the HP. Cross-cutting mafic dikes show identical chemistry to the mafic sheets. XRF data for the CMIC sourced from Wiebe (1994), Wiebe *et al*. (1997a) and Wiebe *et al*. (1997b).

Compositional contrasts between the mafic and felsic rocks within the Tuross Head Tonalite are similar to those within the Halfmoon Pluton. Mafic sheets and enclaves have SiO_2 compositions between 50 and 62 wt%, and the intermediate-felsic

host rocks between 58 and 67 wt% SiO_2 (Wiebe, unpublished data). Despite these small compositional contrasts, mingling relationships are still well defined within both the Tuross Head Tonalite and the Halfmoon Pluton in the form of mafic sheets and enclave swarms. Composite dikes that cross-cut the Tuross Head Tonalite are similar to those that cross-cut the Halfmoon Pluton in that they consist of a fine-grained felsic matrix that encloses fine-grained mafic enclaves. Composite dikes from the Halfmoon Pluton however appear to contain more closely compacted mafic enclaves, with very little felsic material separating them (Figure 8.10(B)). Differences in their appearance are probably due to different emplacement processes.

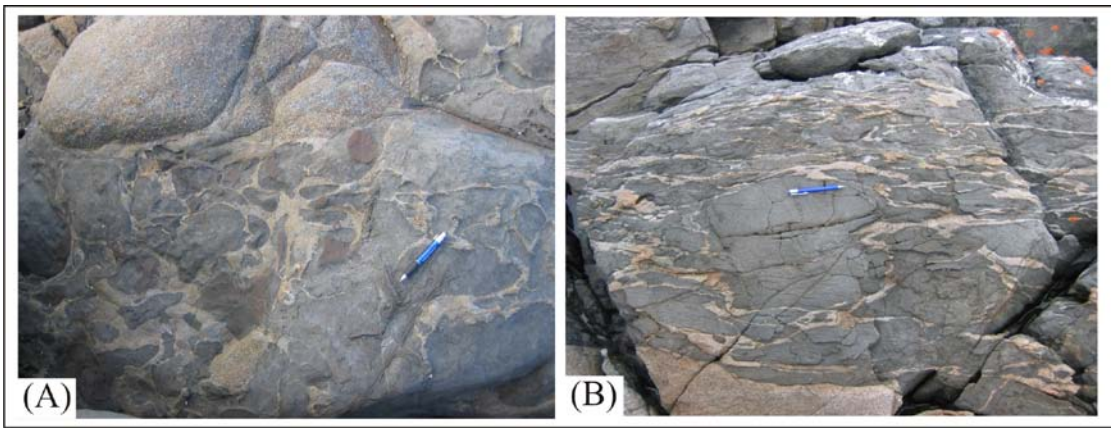

Figure 8.10. (A) Composite dike from the Tuross Head Tonalite (B) Composite dike from The Neck, Halfmoon Pluton. Pencil for scale is 14 cm in length.

It seems probable that the key factor promoting the formation and preservation of mafic sheets within a more felsic host magma is the formation of a rheological boundary between a crystal-rich cumulate mush at the base of the chamber, and and overlying liquid-rich magma into which the mafic magma can inject, and a sufficient temperature contrast between the interacting magmas to allow the mafic magmas to rapidly quench against the cooler more felsic host magma.

Textural and geochemical evidence (Wiebe *et al.*, 1997b; Wiebe & Collins, 1998; Faulds *et al.*, 2001; Kamiyama *et al.*, 2007; Chapters 3 and 4 this thesis) indicates that all five plutons are characterized by the formation of cumulates at the base of the chamber into which the mafic magmas extruded. Fractional crystallization and extraction of interstitial melt from these cumulates results in more evolved felsic rocks in the upper parts of these plutonic complexes. Commonly, an overlying, finer-

grained, highly evolved granitic sheet occurs at the top of the plutonic sequence that is almost devoid of any mafic material. As Figure 8.11 shows, the Tottabetsu Igneous Complex and the Halfmoon Pluton display almost identical geochemical trends in plots of SiO_2 vs. Zr, Al_2O_3 and CaO for both the intermediate-felsic host rocks and the intruding mafic rocks. Both complexes are characterized by accumulation of plagioclase-rich leucodiorites towards the base of the chamber, evidenced largely by large modal abundances of aligned plagioclase, and enrichment in CaO, Al_2O_3 and Sr relative to all other rocks (Figure 8.11). The high concentration of Zr indicates accumulation of zircon within the leucodiorites at the base of the chamber, with decreasing Zr concentrations towards the top of the plutonic complexes probably indicating fractionation.

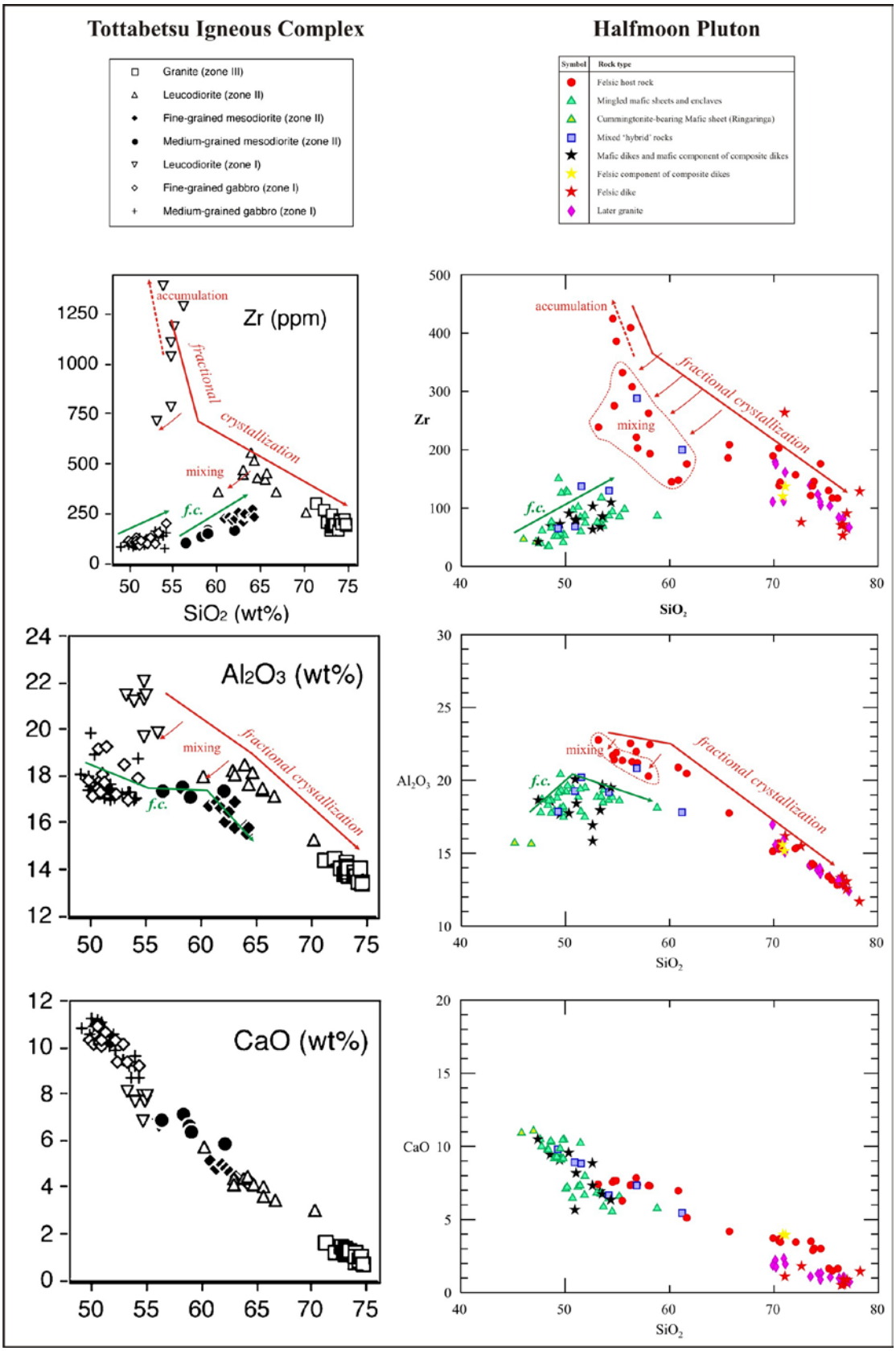

Figure 8.11. SiO_2 vs. Zr, Al_2O_3 and CaO for the Tottabetsu Igneous Complex and the Halfmoon Pluton (Graphs for the TIC from Kamiyama *et al.*, 2007)

8.4.2 Differences Observed between Composite Plutons

Despite the similarities between the five composite plutons discussed in the preceding sections, striking differences in scale, degree of mafic-felsic interaction, mingling structures and textures, mineralogy and geochemistry exist between the plutons. Mafic sheets and enclaves within all five composite plutons contain hydrous mineral phases, however plutons associated with arc-settings typically contain much higher proportions of hydrous minerals. The mineralogy within the intermediate-felsic host rocks they intrude into also varies, with those from the extensional settings containing typically higher abundances of anhydrous minerals (ilmenite, clinopyroxene and olivine), and lower abundances of hydrous minerals (hornblende and biotite), compared to a higher abundance of hydrous mineral phases in the arc-related plutons (hornblende, magnetite and biotite).

Depth estimates for the plutons range from shallow (~3 km) to mid-crustal (<10km). Plutons from extensional tectonic settings (i.e. CMIC, Aztec Wash) were emplaced at shallower depths than the arc-related Halfmoon Pluton, probably as a result of the extensional regime which promoted crustal thinning and allowed magmas to rise and accumulate at shallower levels within the crust. Emplacement depths for the Tuross Head Tonalite and the Tottabetsu Igneous Complex have not been estimated, and therefore links between tectonic setting and depth of emplacement cannot be made. However, most of the discussed composite plutons are upper crustal, which indicates that upper crustal magma chambers regardless of tectonic setting are commonly characterized by replenishments of mafic magma which mix and mingle.

As mentioned in section 8.6.1, despite differences in mineralogy and chemistry, magma mingling structures and textures preserved within all five composite plutons are remarkably similar, with a predominance of mafic sheets. However, mafic enclave swarms appear to be more common within the arc-related magmatic systems. Mafic enclaves do occur within the CMIC and the AWP but are less abundant and are typically scattered throughout the granitic host, as opposed to mafic enclaves within the THT and the HP which appear to be more concentrated and aligned in a similar flow direction (Figure 8.12(A)). Magmatic enclaves, both mafic and felsic, occur within the extension-related rocks, however they are typically smaller, rounded, and more widely dispersed (Figure 8.12(B)). These enclaves may

have been sourced from currents or further replenishment into the chamber bringing up mushy mafic-intermediate-felsic magma from towards the base of the chamber, and then being dispersed throughout the chamber. This suggests a different origin to that of mafic enclave formation within arc-related rocks where mafic enclaves are hypothesized to form by emplacement as more voluminous mafic sheet-like intrusions which subsequently vesiculate/tear apart within the hydrous felsic host magma, and retain an overall orientation. As discussed in Chapter 7, mafic enclave formation within the Bungaree Intrusives is inferred to have been driven by vesiculation of the hydrous mafic magmas. The prevalence of oriented mafic enclave swarms within arc-related magma chambers compared with widely dispersed enclaves within the drier extension-related magmas seems to point towards the importance of water in the formation of mafic enclaves.

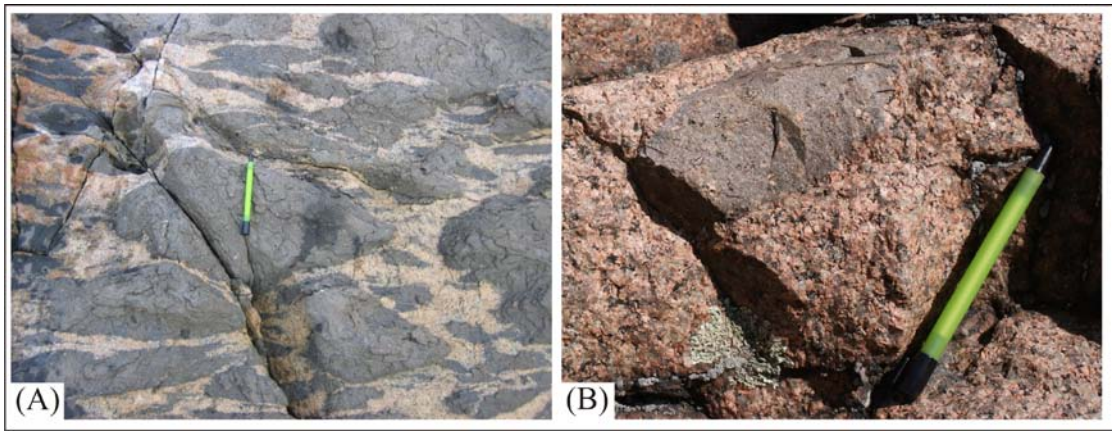

Figure 8.12. (A) Mafic enclave swarm from The Neck, Halfmoon Pluton (B) Mixed mafic-felsic enclave within the Cadillac Mountain Granite, CMIC. Pencil for scale is 14 cm in length.

Sr- and Nd-isotopic compositions are highly variable within the five studied plutons, with no obvious relationship between tectonic setting and isotopic signature observed. Most mafic sheets and enclaves however appear to have more primitive isotopic signatures than the host rocks that enclose them.

The most obvious reason for these observed differences is contrasting tectonic setting. The CMIC and the Aztec Wash Pluton are inferred to have been emplaced within extensional settings, whereas the Tottabetsu Igneous Complex, Tuross Head Tonalite and the Bungaree Intrusives were emplaced within arc-settings. Ease of ascent, cooling rate and water contents of magmas are all influenced by tectonic setting, with

extensional-related magmas typically being more reduced, hotter, and emplaced at shallower depths than the wetter arc-related magmas.

8.5 CONCLUSIONS

Despite emplacement in different tectonic settings, and contrasting histories of magma replenishment and crystallization, the five composite plutons examined in this chapter all preserve evidence for mafic magma replenishment onto the cumulate floor of an aggrading and fractionating intermediate-felsic magma chamber. Similarities in the mingling structures and textures preserved indicate that differences in tectonic setting and composition are not important in controlling whether magma mingling will occur, rather, the key parameter that promotes magma mingling over mixing is probably a sufficient temperature contrast between the intruding mafic magma and the resident felsic magma so that rapid quenching of the mafic magma will occur and mingling will be preserved. All plutons also appear to be characterized by a protracted history of mafic magma injection from a primitive mantle source, with continued mafic magma injection evidenced by cross-cutting mafic and composite dikes with similar chemistry to the mingled mafic rocks. This supports recent publications that hypothesize that magma chambers are indeed long-lived and experience dynamic histories (Glazner *et al*., 2004).

Differences in the style of magma mingling, modal mineralogy and compositional contrasts between the two interacting magmas is probably related to contrasting tectonic settings, with more hydrous magmas being generated in arc-settings, which promotes the formation of large mafic enclave swarms through vesiculation of the hydrous mafic magmas. The primary control on the different styles of mafic-felsic interaction therefore appears to be the H_2O-content, which is largely or most often a function of tectonic setting. These similarities and differences emphasize the potential for magmatic systems within the mid-upper crust to evolve by similar processes of crystal-liquid separation and accumulation, and mafic magma replenishment, though ultimately be preserved in very different ways.

8.6 REFERENCES

Cates, N.L., Miller, J.S., Miller, C.F., Wooden, J.L., Ericksen, S. and Means, M. 2003 'Longevity of plutonic systems: SHRIMP evidence from Aztec Wash and Searchlight Plutons, Nevada' *Geological Society of America, Abstracts with Programs* 35: 63

Chappell, B.W., English, P.M., King, P.L., White, A.J.R. and Wyborn, D. 1991 *Granites and related rocks of the Lachlan Fold belt*. Bureau of Mineral Resources, Geology and Geophysics, Canberra, Australia (1 : 1,250,000 scale map)

Collins, W.J. 2003 'Some modern concepts on Lachlan granite petrogenesis' *The Ishihara Symposium: Granites and associated metallogenesis*

Falkner, C.M., Miller, C.F., Wooden, J.L. and Heizler, M.T. 1995 'Petrogenesis and tectonic significance of the calc-alkaline, bimodal Aztec Wash pluton, Eldorado Mountains, Colorado River extensional corridor' *Journal of Geophysical Research* 100: 10453-10476

Faulds, J.E., Feuerbach, D.L., Miller, C.F. and Smith, E.I. 2001 'Cenezoic evolution of the northern Colorado River extensional corridor, souther Nevada and northwest Arizona *Utah Geological Association Publication 30 – Pacific Section American Association Petroleum Geologists Publication* GB78: 239-271

Glazner, A.F., Bartley, J.M., Coleman, D.S., Gray, W. and Taylor, R.Z. 2004 'Are plutons assembled over millions of years by amalgamation from small magma chambers?' *GSA Today* 14(4): 4-11

Griffin, T. J., White, A. J. R. and Chappell, B. W. 1978 'The Moruya Batholith and geochemical contrasts between the Moruya and Jindabyne suites' *Australian Journal of Earth Sciences* 25: 3235-3247

Harper, B.E., Miller, F., Miller, G., Koteas, C., Cates, N.L., Wiebe, R.A., Lazzareschi, D.S. and Cribb, J.W. 2004 'Granites, dynamic magma chamber processes and pluton

construction: the Aztec Wash pluton, Eldorado Mountains, Nevada, USA' *Transactions of the Royal Society of Edinburgh: Earth Sciences* 95: 277-295

Hogan, J.P. and Sinha, A.K. 1989 ,Compositional variation of plutonism in the coastal Maine magmatic province: mode of origin and tectonic setting' In: Tucker, R.D. and Marvinney, R.G. (eds) *Studies of Maine Geology: Igneous and Metamorphic Geology*, Maine Geological Survery, Department of Conservation, 4: 1-33

Kamiyama, H., Nakajima, T. and Kamioka, H. 2007 'Magmatic stratigraphy of the tilted Tottabetsu Plutonic Complex, Hokkaido, North Japan: Magma chamber dynamics and pluton construction' *The Journal of Geology* 115: 296-314

King, P.L., White, A.J.R., Chappell, B.W. and Allen, C.M. 1996 'Characterization and origin of aluminous A-type granites from the Lachlan Fold Belt, Southeastern Australia' *Journal of Petrology* 38: 371-391

Miller, C.F. and Miller, J.S. 2002 'Contrasting stratified plutons exposed in tilt blocks, Eldorado Mountains, Colorado River Rift, NV, USA' *Lithos* 61: 209-224

Oji, H. 2000 'Stoping and upward migration of a silicic magma chamber by injection of mafic magma: implications from the Tottabetsu Plutonic Complex, North Japan' *Western Pacific Geophysics Meeting*

Patrick, D.W. and Miller, C.F. 1997 'Processes in a composite, recharging magma chamber: evidence from magmatic structures in the Aztec Wash Pluton, Nevada' *Proceedings of the 30th International Geological Congress* 121-135

Suetake, S. 1997 'Heterogeneous structures in a plutonic complex: inferences from the Tottabetsu plutonic complex, the main zone of the Hidaka metamorphic belt, Hokkaido' *Memoirs of the Geological Society of Japan* 47: 57-74

Vernon, R.H., Etheridge, M.A. and Wall, V.J. 1988 'Shape and microstructure of microgranitoid enclaves: indicators of magma mingling and flow' *Lithos* 22: 1-11

Wiebe, R.A. 1993 ‘Basaltic injections into floored silicic magma chambers’ *Eos* 74(1): 1-4

Wiebe, R.A. 1994 ‘Silicic magma chambers as traps for basaltic magmas: the Cadillac Mountain intrusive complex, Mount Desert Island, Maine’ *The Journal of Geology* 102: 423-437

Wiebe, R.A. and Collins, W.J. 1998 ‘Depositional features and stratigraphic sections in granitic plutons: implications for the emplacement and crystallization of granitic magma’ *Journal of Structural Geology* 20(9/10): 1273-1289

Wiebe, R.A. and Collins, W.J. 2007 ‘Construction of the Tuross Head Pluton, Coastal NSW, Australia’ *Eos Transactions AGU* 88(23)

Wiebe, R.A., Holden, J.B., Coombs, M.L., Wobus, R.A., Schuh, K.J. and Plummer, B.P. 1997a ‘The Cadillac Mountain intrusive complex, Maine: The role of shallow-level magma chamber processes in the generation of A-type granites’ *Geological Society of America Memoir* 191: 397-418

Wiebe, R.A., Smith, D., Sturm, M., King, E.M. and Seckler, M.S. 1997b ‘Enclaves in the Cadillac Mountain Granite (Coastal Maine): samples of hybrid magma from the base of the chamber’ *Journal of Petrology* 38: 393-423

CHAPTER NINE

CONCLUSIONS

9.1 CONCLUSIONS

Interpretation of field and petrographic structures, textures and relationships, and extensive geochemical and geochronological data permit the following conclusions to be reached regarding the origin and evolution of the Halfmoon Pluton;

(1) The Halfmoon Pluton represents a magma chamber which preserves evidence for incremental growth as a result of multiple replenishments of mafic magma into an aggrading magma chamber of intermediate-felsic composition

(2) "Way-up" structures and textures within the Halfmoon Pluton are consistent with a younging direction to the south, and allow a magma chamber "stratigraphy" to be constructed

(3) Field and geochemical evidence indicates that the Halfmoon Pluton evolved through a combination of physical and chemical processes including fractional crystallization and accumulation of a plagioclase – hornblende – apatite – zircon mineral assemblage, episodic replenishment by large volumes of mantle-derived 'wet' basaltic magma which mingled and mixed locally and at depth, rejuvenation of the felsic magma to form composite dikes, magmatic flow and compaction

(4) Fine-grained chilled contacts of mafic sheets and enclaves indicate mingling was favoured over mixing largely because of high temperature and viscosity contrasts between the two interacting magmas.

(5) Variation in morphology (i.e. sheets vs. enclaves), texture and chemistry of mafic inclusions according to position within the inferred magmatic "stratigraphy" indicate that processes operating within the chamber varied in space and time. Variables include temperature and viscosity contrasts of the interacting magmas, H_2O-content of the intruding mafic magma, relative magma volumes and compositional contrasts

(6) Fractionation of hornblende within the intermediate-felsic host magmas exerted a strong influence on the whole-rock geochemical concentrations and REE and trace element concentrations in zircon

(7) Variations in mineral zoning and composition, as revealed by detailed transects across plagioclase and hornblende crystals, indicate that the Halfmoon Pluton crystallized within a magma in which melt composition fluctuated in response to repeated mafic magma replenishments, fractionation, crystal settling and convection. Mafic injections increased the temperature, PH_2O and H_2O-content of the resident intermediate-felsic host magma

(8) Core-mid-rim spot analyses within zoned zircons also reveal changes in the chemistry and thermal condition of the Halfmoon plutonic system during crystallization

(9) The mingled mafic and felsic rocks are probably genetically related, as both have very similar modal mineralogy, mineral, chemical and isotopic compositions. Their geochemical similarity and proximity in space and time indicates that the system can be considered as a single composite pluton, with different portions active at different times.

(10) The Halfmoon Pluton consisted of at least two adjacent magma pods that formed incrementally as the result of multiple replenishments of mafic magma into an aggrading magma chamber of evolving intermediate-felsic composition

(11) The calc-alkaline, I-type Halfmoon Pluton was generated within a primitive arc-setting, most probably island-arc as it preserves no evidence for any contamination with old continental crust

(12) All field, petrographic, geochemical and geochronological data and interpretations are consistent with a model whereby ‘wet’ amphibole-rich basaltic magmas pond at the crust-mantle interface and episodically rise, inject and mingle with an overlying intermediate-felsic magma chamber that itself represents the fractionated product of the mantle melts

The implication of this model is that new intermediate-felsic crust is being generated and that processes identified within the Halfmoon Pluton are directly analogous to active arc magma systems. The results of this research therefore

contribute towards understanding the processes that operate within arc-settings and provide perspectives on the origin and evolution of arc magmas, which include;

1) Physico-chemical processes identified within exhumed arc plutons are directly analogous to processes operating within active arc-settings including crystal accumulation, crystal-liquid separation, compaction, magma mingling and mixing and fractional crystallization
2) Mid- to upper-crustal magma chambers are commonly characterized by mafic magma replenishment
3) Amphibole fractionation at mid- to upper-crustal levels plays an important role in controlling the observed chemical diversification of arc magmas
4) Dy/Yb trends observed in arc-volcanics and attributed to “cryptic amphibole fractionation” can be directly observed within plutons that have stalled within the mid- to upper-crust, such as the Halfmoon Pluton
5) Magmas within arc settings can evolve to intermediate and silicic compositions by fractionation and crystal accumulation, and subsequent extraction of evolved melts, without any significant crustal assimilation

9.2 RESEARCH OUTPUTS FROM THIS THESIS

Manuscripts that are currently in review or in advanced states of preparation based on research outcomes within this thesis are presented below, pending additional information and/or interpretation.

FIELD AND GEOCHEMICAL CONSTRAINTS ON MAFIC-FELSIC INTERACTIONS: AND EXAMPLE FROM THE HALFMOON PLUTON, NEW ZEALAND

***Turnbull, R.E*[1]**., Weaver, S.D[1]., Tulloch, A.J[2]., Cole, J.W[1]., Handler, M[3]. and Ireland, T.R[4].

[1]Department of Geological Sciences, University of Canterbury, New Zealand
[2]GNS Science, Dunedin, New Zealand
[3]School of Geography, Environment and Earth Sciences, Victoria University of Wellington, New Zealand
[4]Research School of Earth Sciences, Australian National University, Australia

Under review with the Journal of Petrology

Abstract:

The Halfmoon Pluton of Stewart Island, New Zealand, provides information on the role of coeval mafic magmas in the initiation and evolution of calc-alkaline arc magmas, and the nature of mafic and felsic magma interactions. The Halfmoon Pluton represents a magma chamber of intermediate to felsic composition that was periodically replenished by injection of large volumes of mafic magma. Tilting of ~70° has exposed a cross-section through the pluton that allows processes to be examined at varying stages of the plutons development. A model of pluton construction and evolution is presented that shows that the Bungaree Intrusives consisted of at least two adjacent magma pods that formed incrementally by episodic replenishments of mafic magma into a magma chamber of intermediate-felsic composition. The mingled rocks have a continuum of modal mineralogy's, mineral and chemical compositions, and isotopic characteristics, indicating they are probably genetically related.

Interpretation of magma mingling and mixing structures and textures in the field, combined with detailed geochemical and geochronological analyses, has enabled the identification of several physical and chemical processes operating within the chamber including: (a) incremental assembly as a result of multiple replenishments of mafic magma into a magma chamber of intermediate-felsic composition (b) extensive mingling and mixing of mafic magmas both locally and at depth (c) fractional crystallization and accumulation of a plagioclase – hornblende – apatite – zircon mineral assemblage that was periodically interrupted by mafic magma replenishment (d) limited chemical exchange between the interacting magmas (e) development of fabrics (i.e. plagioclase and mafic enclave alignment) as a result of a combination of processes including magmatic flow, crystal accumulation and shortening of the chamber in response to magmatic loading

Processes identified within the Halfmoon Pluton are directly analogous to those operating within active arc-settings, and provide perspectives on the origin and evolution of arc magmas.

CONTINENTAL ARC MAGMA DYNAMICS: A VOLCANIC-PLUTONIC MARRIAGE IN NEW ZEALAND

Deering, C.D[1]., ***Turnbull, R.E[2].***, and Bachmann, O[1].

[1]Department of Space and Earth Sciences, University of Washington, United States of America
[2]Department of Geological Sciences, University of Canterbury, New Zealand

Target Journal: Geology

Summary:

Despite many attempts during the last half century to bring volcanic and plutonic rocks into a common framework, the volcanic and plutonic environments are still regarded by many as two different realms. Influential researchers claim that the mechanisms responsible for granite generation can not be directly applied to the generation of silicic magma bodies that lead to large, explosive eruptions (Read, 1957; Bachmann *et al*., 2007). Therefore, fundamental questions persist in how these rock types relate to one another. A recent review collection (Large Silicic Systems, *Journal of Volcanology and Geothermal Research*, vol. 167, 2007) emphasizes the importance of these systems in our global understanding of Earth's internal dynamics. In an attempt to bridge the gap between the volcanic and plutonic rock records, we compare the textural, petrological and geochemical variations of recently studied rocks from the Okataina Volcanic Centre (OVC) within the active Taupo Volcanic Zone (TVZ) and the Halfmoon Pluton, both found in New Zealand. We utilize both published and new analyses from these two calc-alkaline magmatic systems in an attempt to provide a link between the plutonic and volcanic realms in arc settings, and suggest that in fact intermediate plutonic sequences in the mid- to upper-crust contain valuable information on the active system, not merely the waning stages of the magmatic cycle.

Our petrologic and geochemical comparison between the Halfmoon Pluton sequence, which represents a frozen magma reservoir, and rare, crystal-rich pumice clasts from the OVC, that represents an active magma reservoir, indicates that: 1) crystal fractionation – including abundant hornblende – drives the production of the felsic magmas in arc settings, 2) processes such as crystal accumulation, mafic intrusion, and dike feeding intrusions captured in mid- to upper-crustal dioritic to

granitic suites are indeed comparable to those in the active volcanic complex as others have suggested (e.g. Wiebe, 1994; Miller & Miller, 2002), and 3) despite the apparent differences in the degree of assimilation between the two systems – Halfmoon Pluton is effectively a closed-system evolution, while the Matahina (OVC) is open-system with up to 25% assimilation – these two calc-alkaline magmatic systems evolved along remarkably similar pathways (TVZ rhyolites have a slightly higher aluminium saturation index than the HP). This emphasizes the dominant control that the crystal fractionation process has on the petrogenetic evolution regardless of the degree of assimilation (Taylor, 1980). The textural, mineralogical, and geochemical data from both plutonic and volcanic systems are equally compatible with a model whereby 'wet' mantle-derived intermediate magmas stall within the mid- to upper-crust and fractionate to form large volumes of silicic magma in arc settings.

References

Bachmann, O., Miller, C.F., and de Silva, S.L. 2007 'The volcanic-plutonic connection as a stage for understanding crustal magmatism' *Journal of Volcanology and Geothermal Research* 167: 1-23

Miller, C.F. and Miller, J.S. 2002 'Contrasting stratified plutons exposed in tilt blocks, Eldorado Mountains, Colorado River Rift, NV, USA' *Lithos* 61: 209-224

Read, H.H. 1957 *The Granite Controversy* Thomas Murby and Co., London. 430pp

Taylor, H.P. 1980 'The effects of assimilation of country rocks by magmas on 18O/16O and 87Sr/86Sr systematics in igneous rocks' *Earth and Planetary Science Letters* 47: 243-254

Wiebe, R.A. 1994 'Silicic magma chambers as traps for basaltic magmas: the Cadillac Mountain Intrusive Complex, Mount Desert Island, Maine' *The Journal of Geology* 102: 423-437

FLUCTUATING MAGMATIC CONDITIONS AND SOURCE CHARACTERISTICS REVEALED BY HORNBLENDE COMPOSITION AND O- AND H-ISOTOPES

***Turnbull, R.E*[1]**., Deering, C.D[2]., Weaver, S.D[1]., Tulloch, A.J[3].

[1]Department of Geological Sciences, University of Canterbury, New Zealand
[2]Department of Space and Earth Sciences, University of Washington, United States of America
[3]GNS Science, Dunedin, New Zealand

Target Journal: Contributions to Mineralogy and Petrology

Summary:

This manuscript includes results presented in Chapter 5. These results are to be supplemented with further EMPA transects across hornblende and plagioclase crystals from the Halfmoon Pluton to provide a more extensive and robust data set. As discussed in Chapter 5, compositional variations within hornblende and plagioclase provide insights into magmatic processes and changing conditions (P-T-PH$_2$O-fO$_2$) within the Halfmoon Pluton that cannot be resolved through fieldwork and whole-rock geochemistry alone. Transects across hornblende and plagioclase crystals reveal that conditions within the chamber fluctuated in response to mafic magma replenishments and the influence of PH$_2$O. Our results indicate that hornblende is an effective tool for assessing the chemical evolution of intermediate magma chambers, however caution is required when applying the Al-in-hornblende geobarometer as sites chosen for analysis (i.e. core vs. rim) have the potential to give pressures that do not reflect actual emplacement/crystallization depths.

O- and H-isotopes on hornblende mineral separates will be undertaken at the University of Canterbury to evaluate source characteristics. Studies have shown that mantle, sediment fluid, and slab-derived fluid contributions to magmas generate distinct hydrogen isotope ratios (Graham et al., 1982; Miyagi & Matsubaya, 1992). Variations in O- and H-isotopes within hornblendes from both mafic and felsic Halfmoon Pluton rocks therefore has the potential to reveal information regarding the amount, source and variation of fluid contribution to the underplated basaltic magmas.

References

Miyagi, I. and Matsubaya, O. (1992) 'Hydrogen isotopic ratios of hydrous minerals from Japanese Quaternary volcanoes' *Report Geological Survey of Japan* 279: 210-211

Graham, A.M., Graham, C.M. and Harmon, R.S. 91982) 'Origin of mantle waters: Stable-isotope evidence from amphibole-bearing plutonic cumulate blocks in calc-alkaline volcanics, Grenada, Lesser Antilles' *Proceedings 5th International Conference of Geochronology and Cosmochronology, Isotope Geology* 119-120

RECHARGE AND HYBRIDIZATION IN A PLUTONIC SYSTEM: EVIDENCE FROM REE'S, O-ISOTOPES AND TI-IN-ZIRCON

***Turnbull, R.E*[1]**., Weaver, S.D[1]., Ireland, T.R[2].

[1]Department of Geological Sciences, University of Canterbury, New Zealand
[2]Research School of Earth Sciences, Australian National University, Australia

Target Journal: American Mineralogist

Summary:

This manuscript will be based largely on results presented in Chapter 6. Recent publications have shown that zircon is an effective tool for unravelling the history of magmatic processes and source characteristics within plutonic bodies (Griffen *et al*., 2002; Belousova *et al*., 2006; Lowry-Claiborne *et al*., 2007; Bolhar *et al*., 2008a). Detailed studies of zircons from the Halfmoon Pluton combining morphologic, zoning, trace and REE profiles from core to rim have shown that fluctuations in magma chemistry and temperature occurred in response to such processes as mafic magma replenishment, magma mixing, fractionation, convection and crystal accumulation.

This manuscript will be submitted once zircons have been analysed for O-isotopes. Analysis of O-isotopes is proving to be a powerful tool for understanding the thermal, magmatic and fluid history of a magma chamber (Valley *et al*., 1994; Hawkesworth & Kemp, 2006; Bolhar et al., 2008b). O-isotope analysis of zircons from the Halfmoon Potential therefore has the potential to reveal information regarding the sources of the mantle melts that produced the Halfmoon Pluton. Arc magmas are thought to represent a combination of mantle, crustal and subducted material (Hildreth & Moorbath, 1988), however their exact contributions have yet to be determined. Whole-rock chemistry, primitive Sr-Nd isotopic signatures and a lack of inherited cores in zircons indicates that the Halfmoon Pluton magmas experienced little, if any crustal contamination. O-isotope analysis will provide further evidence and resolution on magma sources.

References

Belousova, E.A., Griffin, W.L. and O'Reilly, S.Y. 2006 'Zircon crystal morphology, trace element signatures and Hf isotope composition as a tool for petrogenetic modeling: examples from Eastern Australian granitoids' *Journal of Petrology* 47: 329-353

Bolhar, R., Weaver, S.D., Palin, M.J., Cole, J.W. and Paterson, L. 2008a 'Systematics of zircon crystallization in the Cretaceous Separation Point Suite, New Zealand, using U/Pb isotopes, REE and Ti geothermometry' *Contributions to Mineralogy and Petrology* 156:133-160

Bolhar, R., Weaver, S.D., Whitehouse, M.J., Palin, J.M., Woodhead, J.D. and Cole, J.W. 2008b 'Sources and evolution of arc magmas as inferred from coupled O and Hf isotope systematics of plutonic zircons from the Cretaceous Separation Point Suite (New Zealand)' *Earth and Planetary Science Letters* 268: 312-324

Griffin, W.L., Wang, X., Jackson, N.J., Pearson, N.J., O'Reilly. S.Y., Xu, X. and Zhou, X. 2002 'Zircon chemistry and magma mixing, SE China: In-situ analysis of Hf isotopes, Tonglu and Pingtan igneous complexes' *Lithos* 61: 237-269

Hawkesworth, C.J. and Kemp, A.I.S. 2006 'Using hafnium and oxygen isotopes in zircons to unravel the record of crustal evolution' *Chemical Geology* 226: 144-162

Hildreth, W. and Moorbath, S. 1988 'Crustal contributions to arc magmatism in the Andes of Central Chile' *Contributions to Mineralogy and Petrology* 98: 455-489

Lowery-Claiborne, L., Miller, C.F., Walker, B.A., Wooden, J.L., Mazdab, F.K. and Bea, F. 2006 'Tracking magmatic processes through Zr/Hf ratios in rocks and Hf and Ti zoning in zircons: An example from the Spirit Mountain batholith, Nevada' *Mineralogical Magazine* 70: 517-543

Valley, J.W., Chiarenzelli, J.R. and McLelland, J.M. 1994 'Oxygen isotope geochemistry of zircon' *Earth and Planetary Science Letters* 126: 187-206

MIXING AND MINGLING ON STEWART ISLAND: AN EXAMPLE FROM THE COMPOSITE HALFMOON PLUTON, BUNGAREE INTRUSIVES

***Turnbull, R.E*[1]**., Tulloch, A.J[2]. and Weaver, S.D[1].

[1]Department of Geological Sciences, University of Canterbury, New Zealand
[2]GNS Science, Dunedin, New Zealand

Target Journal: New Zealand Journal of Geology and Geophysics

Summary:

This manuscript will be based largely on field, whole-rock and geochemical information, from Chapters 3, 4 and 6. It will also include a more in-depth discussion regarding the implications of the Halfmoon Pluton for the paleo-tectonics of the New Zealand margin of Gondwana ~140 Ma in relation to the Darran Suite and the Median Tectonic Zone.

This paper will present conclusions made in this thesis regarding the construction and evolution of the Halfmoon Pluton, geochemical evidence for the petrogenetic setting, and what these conclusions can contribute towards understanding the tectonics of Cretaceous NZ.

Appendix One: Sample Catalogue

Sample #	Grid Reference	Rock Type/Description	Hand Spec.	Thin Sect.	XRF	REE	Sr/Nd	EPMA	U/Pb SHRIMP	LA-ICP-MS
Ackers Point										
AP #M1	E48/41265711	Mingled mafic sheet	X							
AP #D1	E48/41265711	Cross-cutting felsic dike	X	X			X			
AP #H	E48/41265712	Mingled mafic sheet	X	X	X	X		X		
AP #I	E48/41265713	Bottom of mafic sheet AP#H	X							
AP #M	E48/41265714	Mingled mafic sheet	X		X		X			
AP#G	E48/41265715	Leucodiorite host	X	X	X		X	X	X	X
Evening Cove										
EC 1/1	E48/40085658	Leucodioritic host and microdioritic mafic enclave	X	X						
EC #B4	E48/40085657	Fine-grained base of mingled mafic sheet (see EC#T4)	X	X	X					
EC #T4	E48/40045650	Top of mingled mafic sheet (see EC#B4)	X	X						
EC #B2	E48/40085657	Base of mingled mafic sheet	X	X	X	X				
EC #B5	E48/40045650	Leucodioritic host	X	X	X	X				
EC #8M	E48/40045650	Mingled mafic sheet	X	X	X	X		X		
EC #10D	E48/40045650	Fine-grained mafic dike	X	X	X		X			
EC #10M	E48/40045650	Mingled mafic sheet	X	X	X					
EC #9H	E48/40045650	Leucodiorite host	X	X	X	X		X		
EC #7H	E48/40045650	Leucodiorite host	X	X	X					
EC #6M	E48/40045650	Mingled mafic sheet	X	X	X		X			
EC #6H	E48/40045650	Leucodiorite host	X	X	X					
EC #6	E48/40045650	Contact between mafic sheet and leucodiorite host	X	X	X			X		
EC #6con	E48/40045650	Hble accumulation at top of felsic vein (within host EC#6H)	X	X						
EC 1/3	E48/40085658	Mixed mafic and felsic rock	X	X						
EC 1/4	E48/40085658	Mixed/mingled mafic enclave	X	X	X					
EC 1/5	E48/40085658	Leucodiorite host	X	X	X			X		
EC 1/6	E48/40085658	Contact between mixed mafic enclave and host	X	X	X					
EC 3/2a	E48/40085657	Mixed mafic enclave with plagioclase xenocrysts	X	X	X					
EC 3/2am	E48/40085657	Contact between fg enclave and mixed host	X	X						
EC 3/2b	E48/40085657	Host with mixed mafic enclave	X	X						
EC 3/2c	E48/40085657	Mingled mafic sheet	X	X						
EC 3/2#CX	E48/40085657	Contact between felsic host and mafic sheet	X	X				X		
EC 4/1 4	E48/40085657	Leucodiorite host	X	X	X					
EC 4/1#H	E48/40085657	Mafic enclave in contact with 'mixed' host	X	X						
EC#FD	E48/40085657	Compositionally zoned felsic dike	X	X	X					
EC 4/2 #3	E48/40085657	Contact between host and mafic enclave	X	X						
EC 4/2 #6mix	E48/40085657	Mixed mafic material	X	X	X					
EC#1a	E48/40085657	Contact between mafic enclave & leucodiorite host	X	X	X					

Appendix One: Sample Catalogue Continued

Sample #	Grid Reference	Rock Type/Description	Hand Spec.	Thin Sect.	XRF	REE	Sr/Nd	EPMA	U/Pb SHRIMP	LA-ICP-MS
EC#1b	E48/40085657	Contact between mafic enclave & leucodiorite host	X							
EC#3a	E48/40085657	Mixed (?) host/mafic	X	X						
EC#3b	E48/40085657	Coarser-grained centre of mingled mafic sheet	X	X	X	X				
EC#3c	E48/40085657	Fg-contact of base of mafic sheet with host	X							
EC#3d	E48/40085657	Contact of mixed enclave and host	X							
EC#3e	E48/40085657	Host & mixed enclaves in gradational contact	X							
EC#3f	E48/40085657	Mafic enclave in sharp contact with host	X							
EC#3g	E48/40085657	Host with a few small mafic enclaves	X	X	X					
EC#3h	E48/40085657	Cuspate contact of mafic sheet with host	X		X					
EC#5a	E48/40045650	Leucodiorite host	X							
EC#5b	E48/40045650	Contact of mafic enclave and mixed host/mafic	X							
EC#5d	E48/40045650	Mg-mixed host and fg-mixed enclave	X							
EC#5e	E48/40045650	Mixed top of mafic sheet, mixed host/enclaves	X							
EC#6a	E48/40045650	Mixed lobe at base of unit #6	X		X					
EC#6b	E48/40045650	Contact of mixed host and mafic enclave	X							
EC#7a	E48/40045650	Contact of mixed enclave and host	X							
EC#7b	E48/40045650	Coarser-grained slightly mixed felsic host	X		X					
EC#5f	E48/40045650	Leucodiorite host	X							
EC#6C	E48/40045650	Leucodiorite Host - same sample as EC#6H (see for thin section)	X		X	X	X		X	X
EC#1c	E48/40085657	Leucodiorite host	X							
EC#H	E48/40055656	Leucodiorite host in middle of beach	X							
EC#M1	E48/40055656	Granite from the middle of the beach	X	X						
EC#B1	E48/40205667	Leucodiorite host from the north end of the beach	X	X						
Ringaringa										
RR #M1	E48/39795594	Mingled mafic sheet	X	X						
RR #M2	E48/39825566	Mafic enclave in leucodiorite host	X	X	X					
RR #H1	E48/39795594	Granodiorite with small mafic enclaves	X	X	X					
RR #M3	E48/39795594	Mafic enclave	X	X	X		X			
RR #H2	E48/39855560	Granodiorite host	X	X						
RR #M4	E48/39855561	Contact between mafic sheet and granodiorite host	X	X	X					
RR #M5	E48/39855562	Contact between mafic sheet and granodiorite host	X	X						
RR #G1	E48/39855563	Granitic Host	X	X	X	X				
RR#A1	E48/39815565	Gradation from coarser to finer mixed mafic	X	X						
RR#A2	E48/39815565	Contact between felsic host and mafic enclave	X							
RR#A3	E48/39815565	Contact with top of mafic 'sheet' & felsic host	X							
RR#B1	E48/39815565	Mafic enclave with plagioclase/quartz xenocrysts	X		X					
RR#B1a	E48/39815565	Granitic host material	X	X						

Appendix One: Sample Catalogue Continued

Sample #	Grid Reference	Rock Type/Description	Hand Spec.	Thin Sect.	XRF	REE	Sr/Nd	EPMA	U/Pb SHRIMP	LA-ICP-MS
RR#B2	E48/39815565	Mafic enclave with plagioclase/quartz xenocrysts	X							
RR#B3	E48/39815565	Coarser-grained mafic sheet	X							
RR#B4	E48/39815565	Host material with small mafic enclaves	X							
RR#H2	E48/39815565	Contact of base of mafic sheet with host	X							
RR#H3	E48/39815565	Granitoid host	X		X					
RR#H4	E48/39815565	Granite host with mafic enclaves	X							
RR#J1	E48/39815565	Slightly mixed mafic "sheet"	X							
RR#J2	E48/39815565	Felsic host with small enclaves	X							
RR#J3	E48/39815565	Mafic enclaves in host material	X	X			X			
RR#J4	E48/39815565	Mafic "sheet"	X							
RR#K1m	E48/39815565	Mafic enclave		X		X	X			
RR#K1h	E48/39815565	Felsic host	X	X		X	X			
RR#K2	E48/39815565	Contact between mafic enclave and host	X							
RR#AH	E48/39755598	Contact of granitic host with mafic enclaves	X							
RR#H5	E48/39765598	Felsic host at outcrop beneath road junction	X	X						
RR#M6	E48/39765598	Mafic enclaves within host of RR#H5	X							
RR#M7	E48/39795581	Mafic sheet by seamount (x-cutting?)	X	X	X					
RR#M8	E48/39795581	Mafic sheet by seamount, finer grained sample	X	X	X					
RR#H6	E48/39835562	Granite host	X	X	X					
RR#H7	E48/39835563	Granite host - same sample as RR#G1 (see for thin section & XRF)	X				X		X	X
RR#FD	E48/39765598	Felsic component of composite dike	X	X	X					
RR#SM	E48/39775576	Felsic host from Seamount	X							
RR#D1	E48/39845561	Mafic dike	X							
RR#1a	E48/39855560	Felsic host	X							
RR#1b	E48/39865560	Mafic enclave	X							
RR#1c	E48/39845561	Felsic host	X							
RR#1d	E48/39815565	Felsic host	X	X						
RR#1e	E48/39815565	X-cutting felsic vein (filter-pressed?)	X							
The Neck										
TN#1	E48/43095361	Composite dike	X	X						
TN#2	E48/43095361	Host with mixed enclave & mingled enclave	X	X						
TN#3	E48/43095361	Contact of mafic dike and mafic enclave	X		X					
TN#4	E48/43095361	Tonalite host with small, mixed enclaves	X	X	X			X		
TN#5	E48/43095361	Felsic host with mafic enclaves	X							
TN#6	E48/43095361	Felsic host with mafic enclave (top)	X		X					
TN#7	E48/43095361	Felsic host with mafic enclave (bottom)	X	X				X		
TN#8	E48/43585374	Mafic 'sheet' with plagioclase xenocrysts	X	X	X					

Appendix One: Sample Catalogue Continued

Sample #	Grid Reference	Rock Type/Description	Hand Spec.	Thin Sect.	XRF	REE	Sr/Nd	EPMA	U/Pb SHRIMP	LA-ICP-MS
TN#9	E48/43585374	X-cutting granitic felsic dike	X	X						
TN#10	E48/43585374	Tonalite host	X	X	X					
TN#11	E48/43585374	Mafic enclave	X							
TN#12	E48/43515390	Fine-grained mafic dike	X		X					
TN#13	E48/43675388	Contact with fg-mafic enclave & cg-host	X							
TN#14	E48/43675388	Contact of host with fg-mafic enclaves	X							
TN#15	E48/43675388	Mixed host and non-mixed enclave	X							
TN#16	E48/43675388	Coarse-grained mafic	X	X	X	X				
TN#17	E48/43675392	Mafic enclave from composite dike and host	X	X				X		
TN#18	E48/43865424	Host with mixed and mingled enclaves	X	X						
TN#19	E48/43865424	"mixed" rock between felsic host and mafic enclaves	X	X						
TN#20	E48/43455406	Small mafic enclaves in host	X		X					
TN#21	E48/43455406	Large mafic enclaves in host	X							
TN#22	E48/43305368	Coarse-grained mingled mafic sheet	X	X	X					
TN#23	E48/43575374	Cross-cutting white granite sheet	X	X	X					
TN#24m	E48/43515390	Mafic component of composite dike	X	X	X		X			
TN#24f	E48/43515390	Felsic component of composite dike	X	X	X		X			
TN#25	E48/43865424	Mixed host	X	X	X	X	X	X		
TN#26	E48/43865424	Cross-cutting mafic dike	X		X		X			
TN#27	E48/43445393	Mafic enclaves with amygdules	X	X						
TN#28	E48/43555357	Mingled mafic "feeder" dike	X	X						
TN#29	E48/43095361	Tonalite host - same rock as TN#4 (see for thin section &XRF)	X						X	X
TN#30	E48/42975364	Mafic enclaves with amygdules	X	X	X			X		
TN#31	E48/43295390	Tonalite host	X	X	X					
TN#32	E48/43295390	Mingled mafic sheet	X							
TN#33	E48/43345406	Cross-cutting mafic dike	X		X					
TN#34	E48/43355407	Tonalite host	X							
TN#35	E48/43585374	Tonalite host - same rock as TN#10 (see for XRF)	X	X		X	X			
TN#36	E48/43575374	Cross-cutting granite sheet	X	X	X					
TN#37	E48/43575374	Mingled mafic sheet	X		X	X	X			
TN#38	E48/43325302	Tonalite host	X	X	X		X			
TN#7/3e	E48/43325302	Mafic enclave	X	X	X					
Ulva Island										
UI #G1	E48/38305266	Megacrystic granite	X	X	X					
UI 2/1a	E48/38305266	Foliated granite	X	X						
UI 2/1b	E48/3832652?1	Granite	X	X	X					
UI 2/2a	E48/37765358	Granite host	X	X						
UI 2/2b	E48/37765358	Mixed felsic and mafic contact	X	X						

Appendix One: Sample Catalogue Continued

Sample #	Grid Reference	Rock Type/Description	Hand Spec.	Thin Sect.	XRF	REE	Sr/Nd	EPMA	U/Pb SHRIMP	LA-ICP-MS
UI 2/2c	E48/37765358	Mixed mafic enclave	X							
UI#G1	E48/37715363	Deformed granite	X							
UI#H1	E48/37765357	Granodiorite host	X							
UI#E1	E48/38905375	Mafic Enclave	X	X						
P62077	E48/39055365	Granodiorite host (XRF analyses done by GNS Science)	X	X	X				X	
Horseshoe Bay										
HB #M1	E48/38683595	Coarse-grained mafic rock	X	X	X					
HB #MD1	E48/38683595	Cross-cutting mafic dike	X		X					
HB #F1	E48/39455894	Coarse-grained felsic rock	X							
HB #D1	E48/39425895	Cross-cutting f-g felsic Dike	X		X					
HB #F2	E48/39425895	Felsic host	X							
HB #F3	E48/39275887	Felsic host	X							
HB #E1	E48/39275887	Mafic enclave in felsic host	X							
HB #G1	E48/39455894	Felsic host	X							
HB #M2	E48/39165878	Mixed mafic enclave in felsic host	X	X				X		
HB #M	E48/39165878	Mafic enclave	X		X					
Fisherman Point										
FP #G	E48/40885725	Granitic sheet	X	X	X		X			
FP #MD	E48/40885725	Mafic component of composite dike	X		X					
FP#G1	E48/40885725	Granitic sheet in contact with mafic dike	X	X	X					
FP#D1	E48/40895725	Cross-cutting mafic dike	X	X	X					
FP#C1	E48/40895725	Contact between mafic enclave and felsic host	X							
FP#C2	E48/40935725	Mafic enclave	X	X	X			X		
FP#C3	E48/40935725	Gradaional contact between mafic enclave and felsic host	X							
FP#M1	E48/40895725	Mafic enclave	X		X					
Leask Bay										
LB 3/1a	E48/39835679	Mixed mafic material	X		X					
LB 3/1b	E48/39705678	Granitic host/sheet	X							
LB 3/1c	E48/39725678	Mixed host	X	X	X					
LB 3/1d	E48/39735679	Mafic 'sheet'	X							
LB 3/1e	E48/39735679	Mixed maifc or mixed host?	X							
LB 3/1f	E48/39735679	Less mixed host material	X		X					
LB 3/1g	E48/39755681	Cross-cutting mafic dike	X							
LB 3/1h	E48/39755681	Mixed mafic rock cross-cut by mafic dike	X							
LB 3/3 6	E48/39805680	Cross-cutting felsic dike	X	X	X					

Appendix One: Sample Catalogue Continued

Sample #	Grid Reference	Rock Type/Description	Hand Spec.	Thin Sect.	XRF	REE	Sr/Nd	EPMA	U/Pb SHRIMP	LA-ICP-MS
LB 3/3 7	E48/39705678	Same sample as LB#G1 (see LB#G1 for petrography & XRF)	X						X	X
LB#G1	E48/39705678	Granitic host/sheet	X	X	X		X			
LB#E1	E48/39755681	Mafic enclave and granitic host	X							
LB#E2	E48/39755681	Mixed mafic enclave	X	X	X					
Butterfield Beach										
BB #M1	E48/38805739	Mixed 'hybrid' rock	X	X						
BB #G1	E48/38805739	Granite	X	X	X					
BB #G2	E48/388825757	Granite	X	X	X		X			
Harrold Bay										
HB #D	E48/39325781	Cross-cutting granite dike	X	X	X					
HB #H	E48/39325781	Granite sheet	X	X						
HB #DG	E48/39325781	Granite sheet	X	X	X					
Bragg Bay										
BB#H1	E48/39325778	Mixed 'hybrid' rock	X	X	X					
Little Bay										
LB 1/1	E48/39645668	Granite sheet	X							
LB 1/2	E48/39645668	Granite sheet/dike?	X							
LB 1/5	E48/39645668	Mafic sheet in roadside outcrop	X	X	X					
Lee Bay										
LB#H	E48/38096074	Felsic host	X	X						
LB#D	E48/38096074	Cross-cutting mafic dike	X	X						
Miscellaneous										
TB#1	E48/37565588	Felsic rock, Thule Bay	X							
G#1	E48/38855652	Granite sheet from roadcutting	X		X					
H#1	E48/38476143	Felsic Host from Bob's Point	X	X						
D#1	E48/38476143	Cross-cutting mafic dike at Bob's Point	X	X						
H#2	E48/38856113	Mafic enclaves in contact with felsic host	X							
H#3	E48/38856113	Felsic Host	X	X						
D#2	E48/38856113	Cross-cutting mafic dike	X							
CD#1	E48/40335532	Composite Dike from Native Island (highly weathered)	X							

REE = ICP-MS analyses for rare earth elements Sr/Nd = $^{87}Sr/^{86}Sr$ &/or $^{143}Nd/^{144}Nd$ Isotopes; EPMA = electron microprobe analyses; U/Pb SHRIMP = dated samples;
LA-ICP-MS = trace elements on zircons

Appendix Two: Modal abundances of rocks from the Halfmoon Pluton

Sample #	Rock Type	Rock Name	Grainsize	Plagioclase	Quartz	K-Feldspar	Hornblende	Biotite	Apatite	Titanite	Zircon	Oxides	Comments
Ackers Point													
AP#D1	Felsic dike	Granite	m-g	subhed, 32%	subhed, 28%	subhed, 38%						trc.	
AP #H	Mafic sheet	Melanodiorite	m-g	subhed, 35%			subhed, 63%	blade, 2%		trc.		trc.	Coarse-grained centre of mafic sheet
AP #M	Mafic sheet	Melanodiorite	m-g	subhed, 37			subhed, 61%	2%		trc.		trc.	Coarse-grained centre of mafic sheet
AP#G	Felsic Host	Leucodiorite	m-g	tab, subhed, 84%	int, 6%		subhed, 4%	subhed, 6%	trc.	trc.	trc.	trc.	cumulate text.
Evening Cove													
EC 1/1 (m)	Contact between	Microdiorite	f-g	euhed, 63%			euhed, 32%	euhed, 3%	trc.	trc.	trc.	mag, 2%	flow text., sharp contact
EC 1/1 (f)	host(f) and mafic (m)	Leucodiorite	m-g	tab, euhed, 85%	int, 5%		euhed, 6%	euhed, 4%	1%	trc.	trc.	1%	cumulate text.
EC #B4	Mafic sheet	Microdiorite	f-g	euhed, 51%			subhed, 48%	trc.	trc.			trc.	
EC #T4	Mafic sheet	Microdiorite	f-g to m-g	mos. text, 51%			subhed, 47%	<1%	trc.	trc.		1%	Slighty mixed
EC #B2	Mafic sheet	Microdiorite	f-g	mos. text, 65%			subhed, 33%		trc.	trc.		mag, 2%	
EC #B5	Felsic host	Leucodiorite	m-g	tab, euhed, 85%	int, 5%		euhed, 7%	2%	trc.	trc.	trc.	1%	cumulate text.
EC #8M	Mafic sheet	Mesodiorite	m-g	mos. text, 60%			subhed, 35%		trc.			mag, 5%	plag. xenocrysts
EC #10D	Mafic dike	Microdiorite	f-g	tab, euhed, 42%			euhed, 60%	euhed, 4%	trc.	3%		<1%	xtals flow aligned
EC #10M	Mafic sheet	Mesodiorite	m-g	euhed, 48%			euhed, 51%	trc.	trc.	trc.		mag, 1%	
EC #9H	Felsic host	Leucodiorite	m-g	subhed, 84%			euhed, 12%	3%	trc.	trc.	trc.	mag, 1%	cumulate text.
EC #7H	Felsic host	Leucodiorite	m-g	tab, euhed, 83%	int, 3%		euhed, 8%	euhed, 3%	trc.	trc.	trc.	mag, 2%	cumulate text.
EC #6M	Mafic sheet	Microdiorite	f-g	mos. text , 39%			euhed, 50%		trc.	trc.		mag, 3%	
EC #6H	Felsic host	Leucodiorite	m-g	tab, euhed, 88%	int, 2%		euhed, 8%	trc.	trc.	trc.	trc.	mag, 2%	cumulate text.
EC #6 (m)	Contact between	Microdiorite	f-g	mos. text, 50%			subhed, 44%	subhed, 1%				mag, 5%	plag. xenocrysts/phenocrysts?
EC#6 (f)	host(f) and mafic (m)	Leucodiorite	m-g	tab, euhed, 89%	int, 2%		euhed, 8%	euhed, 2%	trc.	trc.	trc.	mag, 1%	cumulate text., sharp contact
EC #6con	Amphibole accum.	Leucodiorite	m-g	tab, euhed, 84%	int, 2%		euhed, 12%	1%	trc.	trc.	trc.	mag, 2%	~80% hble at accum.
EC 1/3	Mixed mafic	Mesodiorite	m-g	tab, euhed, 61%			euhed, 36%	subhed, 2%	trc.	trc.		mag, 1%	strong magmatic flow alignment
EC 1/4	Mixed enclave	Microdiorite	f-g	subhed, 49%			subhed, 47%	blade, 3%	trc.			1%	strongly aligned plagioclase
EC 1/5	Felsic host	Leucodiorite	c-g	tab, subhed, 90%	int, 4%		euhed, 5%	1%	trc.	trc.	trc.	trc.	cumulate text.
EC 1/6	Mixed mafic enclave	Microdiorite	f-g to m-g	tab, subhed, 64%	int, 1%		subhed, 29%	subhed, 2%	trc.	trc.		mag, 2%	Juxtaposed mineral populations
EC 3/2a	Mixed mafic sheet	Mesodiorite	m-g	tab, euhed, 61%			euhed, 34%	trc.				mag, 5%	
EC 3/2am	Mixed rock	Mesodiorite	m-g	f-g, subhed, 36%			poik, euhed, 62%	trc.				mag, 2%	
EC 3/2b	Felsic host	Leucodiorite	m-g	euhed, 81%	int, 3%		euhed, 6%	euhed, 9%	trc.	trc.	trc.	1%	
EC 3/2c	Mafic sheet	Microdiorite	f-g	subhed, 56%			subhed, 40%	blade, 2%	trc.	trc.		2%	
EC 3/2#CX (m)	Contact between	Microdiorite	f-g	euhed, 65%			subhed, 31%	euhed, 2%	trc.			mag, 2%	aligned plag
EC 3/2#CX (f)	host(f) and mafic (m)	Leucodiorite	m-g	tab, euhed, 90%	int, 5%		euhed, 4%	1%	trc.	trc.		trc.	
EC 4/1 4	Felsic host	Leucodiorite	m-g	tab, euhed, 80%	int, 5%		euhed, 10%	4%	trc.	trc.	trc.	1%	
EC 4/1#H	Mafic enclave	Microdiorite	f-g	tab, euhed, 46%			subhed, 49%	euhed, 2%	trc.	trc.		mag, 3%	irregular contact with host
EC#FD	Felsic Dike	Aplite	m-g	subhed, 38%	anhed, 40%	subhed, 21%		trc.	trc.			1%	+ trc. Muscovite + trc. Myrmekite
EC 4/2 #3 (m)	Contact between	Microdiorite	f-g	mos. text, 55%			euhed, 40%	2%	trc.	trc.		mag, 3%	
EC 4/2 #3 (f)	host(f) and mafic (m)	Leucodiorite	m-g		int, 5%		euhed, 8%	2%	trc.	trc.	trc.	<1%	Sharp contact
EC 4/2 #6mix	Mixed mafic sheet	Microdiorite	f-g to m-g	tab, euhed, 68%			subhed, int, 28%	blade, 1%		trc.	trc.	mag, 2%	
EC#1a	Felsic host	Leucodiorite	m-g	subhed, 68%	int, 3%		euhed, 7%	blade, 19%	2%			2%	Slightly mixed
EC#3a	Mixed 'hyrbid'	Mesodiorite	f-g to m-g	euhed, 48%			euhed, 46%	3%	trc.	trc.		3%	Juxtaposed mineral populations
EC#3b	Mafic enclave	Microdiorite	f-g	mos. text, 54%			subhed, 40%	blade, 2%	trc.	trc.		mag, 4%	
EC#3g (m)	Contact between	Microdiorite	f-g	tab, subhed, 54%			subhed, 44%	trc.	trc.			2%	
EC#3g (f)	host(f) and mafic (m)	Leucodiorite	m-g	subhed, 78%	int, 2%		euhed, 16%	1%	trc.	trc.	trc.	3%	
EC#M1	X-cutting felsic sheet	Granite	m-g	anhed, 29%	anhed, 26%	anhed, 44%		int, 1%			trc.	trc.	Slightly weathered
EC#B1	Felsic host	Leucodiorite	m-g	tab, subhed, 80%	int, 2%		euhed, 16%	trc.	trc.	trc.	trc.	trc.	cumulate text.
Ringaringa													
RR #M1	Mafic sheet	Microdiorite	f-g	tab, subhed, 58%			int, subhed, 37%	blade, trc.	acic. trc.			mag, 5%	Strong mineral alignment, flow?
RR #M2	Mafic enclave	Microdiorite	f-g	euhed, 65%			subhed, 17%	euhed, 15%	1%			ilm(?), trc.	Qtz xenocrysts rimmed by biotite
RR #H1	Felsic Host	Tonalite	m-g	euhed, 59%	anhed, 31%	trc.		euhed, 10%	trc.		trc.	ilm(?), trc.	Moderate crystal alignment
RR #M3	Mafic enclave	Microdiorite	f-g	tab, subhed, 72%			subhed, 18%	subhed, 7%	1%			2%	Possible skeletal text. in hble
RR #H2	Felsic Host	Tonalite	m-g	subhed, 66%	anhed, 23%	trc.		int, 11%	trc.		trc.	trc.	
RR #M4	Mafic sheet	Microdiorite	f-g	mos. text, 64%			subhed, 26%	blade, 5%	acic. trc.			5%	Moderate crystal alignment
RR #M5 (m)	Contact between	Microdiorite	f-g	mos. text. 69%			euhed, 15%	euhed, 11%	trc.	trc.		4%	Moderate crystal alignment
RR #M5 (f)	host(f) and mafic (m)	Qtz Monzonite	m-g	euhed, 70%	anhed, 9%	euhed, 11%	rounded, 2%	euhed, 8%	trc.		trc.	ilm(?), trc.	Hble cores altered to cummingtonite
RR #G1	Felsic Host	Monzogranite	m-g	subhed, 21%	anhed, 46%	subhed, 28%		int, 5%	trc.		trc.	trc.	+ trc. Muscovite
RR#A1	Mafic sheet	Microdiorite	f-g	tab, euhed, 67%			rounded, 23%	5%	trc.			5%	Hble cores altered to cummingtonite

Appendix Two: Modal abundances continued

Sample #	Rock Type	Rock Name	Grainsize	Plagioclase	Quartz	K-Feldspar	Hornblende	Biotite	Apatite	Titanite	Zircon	Oxides	Comments
RR#B1a	Felsic Host	Tonalite	m-g	subhed, 52%	anhed, 42%			int, 5%	trc.	trc.	trc.	mag, 1%	
RR#J3	Mafic enclave	Microdiorite	f-g	subhed, 62%			sub, 41%	5%	trc.			2%	
RR#K1m	Mafic enclave	Microdiorite	f-g	subhed, 53%			subhed, 6%	subhed, 38%	trc.			3%	
RR#K1h	Felsic Host	Granodiorite	m-g	euhed, 50%	anhed, 47%			3%	trc.				
RR#H5	Felsic Host	Granite	m-g	subhed, 70%	anhed, 20%	subhed, 4%		int, 6%			trc.	trc.	
RR#M7	Mafic sheet	Melanodiorite	m-g	tab, euhed, 34%			poik, 64%		trc.	trc.		mag, 2%	Hble cores altered to cummingtonite
RR#M8	Mafic sheet	Melanodiorite	f-g	mos. text, 47%			subhed, 52%		trc.	trc.		mag, 1%	Hble cores altered to cummingtonite
RR#H6	Felsic Host	Granite	m-g	subhed, 14%	anhed, 46%	subhed, 37%		int, trc.	trc.		trc.		+ trc. Myrmekite
RR#FD (m)	Composite Dike with	Microdiorite	f-g	mos. text, 41%			subhed, 48%	tab, subhed, 11%	trc.			trc.	Biotite-rich at contact, mafic clots
RR#FD (f)	mafic (m) and felsic (f)	Microtonalite	f-g	subhed, 50%	anhed, 41%			tab, subhed, 8%	trc.			1%	Meta. overprint?
RR#1D	Felsic Host	Quartz Diorite	m-g	subhed, 74%	int, 6%	subhed, 2%	subhed, 11%	subhed, 5%	trc.	trc.	trc.	mag, 2%	
The Neck													
TN#1 (m)	Composite Dike with	Microdiorite	f-g	mos. text, 50%			subhed, 43%	euhed, 7%	trc.	trc.		trc.	Strong xtal alignment
TN#1 (f)	mafic (m) and felsic (f)	Leucodiorite	f-g	tab, euhed, 87%	anhed, 9%		subhed, 4%			trc.		trc.	Sharp contact with enclaves
TN#2	Felsic Host	Tonalite	m-g	tab, subhed, 62%	int, 31%			int, 6%	trc.			1%	Sharp cuspate contact with mafic enclave
TN#4	Felsic Host	Tonalite	m-g	tab, euhed, 74%	int, 21%			subhed, 5%	trc.		trc.	trc.	+ trc. Clinozoisite
TN#7 (m)	Contact between	Microdiorite	f-g	tab, euhed, 60%			subhed, 14%	euhed, 21%	trc.	trc.		trc.	Sharp f-g contact with host
TN#7 (f)	host(f) and mafic (m)	Tonalite	m-g	euhed, 63%	int, 22%	subhed, 10%		subhed, 5%	acic. trc.	trc.	trc.	trc.	Plagioclase aligned
TN#8	Mafic sheet	Microdiorite	f-g	tab, euhed, 78%			subhed, 17%	euhed, 5%	trc.	trc.		trc.	Plagiolcase xenocrysts
TN#9	Felsic Dike	Microtonalite	f-g	subhed, 56%	anhed, 43%			1%	trc.				+ trc. Myrmekite
TN#10	Felsic Host	Tonalite	m-g	subhed, 71%	int, 33%			int, 5%	trc.	trc.	trc.	1%	
TN#16	Mafic sheet	Microdiorite	f-g	tab, euhed, 54%			poik, subhed, 46%			trc.		trc.	
TN#17 (m)	Composite Dike with	Microdiorite	f-g	mos. text, 51%			euhed, 19%	tab, euhed, 20%	trc.			trc.	Sharp contact between m + f, pervasive
TN#17 (f)	mafic (m) and felsic (f)	Tonalite	f-g	euhed, 55%	anhed, 39%		trc.	tab, euhed, 6%	trc.			trc.	crystal alignment in both m + f
TN#18	Felsic Host	Tonalite	m-g	tab, euhed, 87%	int, 12%		trc.	1%	trc.			trc.	
TN#19	Mixed 'hybrid'	Mesodiorite	m-g	tab, subhed, 71%	int, 3%		subhed, 15%	subhed, 9%		0.50%		1.50%	Crystal alignment
TN#22	Mafic sheet	Melanodiorite	m-g	subhed, 41%	int, 1%		subhed, 33%	subhed, 24%	acic. trc.	trc.	trc. (inherit?)	mag, 1%	Biotite replacing the hornblende
TN#23	X-cutting felsic sheet	can't determine	f-g	X	X	X		X		X			+ myrmekite + epidote, highly weathered
TN#24m	Composite Dike with	Microdiorite	f-g	mos. text, 50%			subhed, 22%	euhed, 28%	trc.			trc.	Sharp contact + crystal alignment
TN#24f	mafic (m) and felsic (f)	Tonalite	f-g	euhed, 40%	anhed, 58%			subhed, 2%	trc.	trc.		trc.	
TN#25	Mixed 'hybrid'	Quartz Diorite	m-g	subhed, 76%	int, 11%		subhed, 3%	subhed, 7%		2%		mag, 1%	Biotite replacing the hornblende
TN#27	Mafic enclave	Microdiorite	f-g	tab, euhed, 64%			subhed, 10%	euhed, 21%	trc.	trc.		trc.	Contains qtz. amygdules rimmed by hble
TN#28	Mafic sheet	Microdiorite	f-g to m-g	tab, subhed, 73%	int, 2%		subhed, 17%	subhed, 6%	0.50%	trc.		1.50%	
TN#30	Mafic enclave	Microdiorite	f-g	mos. text. 57%			subhed, 23%	euhed, 18%	trc.			2%	Contains qtz. amygdules rimmed by hble
TN#31	Felsic host	Tonalite	m-g	subhed, 69%	int, 19%			int, 12%	trc.	trc.	trc.	trc.	
TN#35	Felsic Host	Tonalite	m-g	subhed, 54%	anhed, 42%			int, 3%		trc.	trc.	trc.	
TN#36	X-cutting felsic sheet	Granodiorite	f-g	anhed, 62%	anhed, 31%	anhed, 6%		int, 1%					+ trc. muscovite, moderately weathered
TN#38	Felsic Host	Tonalite	m-g	subhed, 60%	anhed, 36%			int, 3%		trc.	trc.	1%	Slight meta. overprint(?)
Ulva Island													
UI #G1	X-cutting felsic sheet	Quartz Monzonite	c-g	subhed, 9%	anhed, 32%	subhed, 58%		int, 1%			trc.		Meta. overprint(?), + myrmekite
UI 2/1a	X-cutting felsic sheet	Quartz Monzonite	c-g	subhed, 15%	anhed, 41%	subhed, 43%		int, 1%			trc.	trc.	Meta. overprint(?), + myrmekite
UI 2/1b	X-cutting felsic sheet	Quartz Monzonite	m-g	subhed, 21%	anhed, 19%	subhed, 59%		int, 1%		trc.	trc.	trc.	Meta. overprint(?), + myrmekite
UI 2/2a	Felsic host	Quartz Diorite	m-g	subhed, 77%	int, 7%		subhed, 7%	subhed, 8%	trc.	trc.	trc.	mag, 1%	
UI 2/2b	Felsic host	Quartz Diorite	m-g	subhed, 83%	int, 10%		int, subhed, 5%	int, 1%	trc.	trc.	trc.	mag, 1%	
UI#E1	Mafic enclave	Microdiorite	f-g	subhed, 58%			subhed, 19%	euhed, 22%	trc.	trc.		1%	
P62077	Felsic host	Tonalite	m-g	tab, subhed, 53%	anhed, 42%	3%	trc.	2%	trc.	trc.	trc.		+ trc. Muscovite, slight meta. text.
Horseshoe Bay													
HB #M1	Mafic enclave	Microdiorite	f-g	tab, subhed, 52%			poik, subhed, 40%	lath, euhed, 7%	trc.	1%		trc.	Mafic minerals form in clots
HB #M2	Mixed mafic enclave	Microdiorite	f-g to m-g	tab-mos. text, 68%			int, subhed, 29%	int, 2%	trc.			mag, 1%	juxtaposed zoned plag. population
Fisherman Point													
FP #G	X-cutting felsic sheet	Granite	m-g	subhed, 26%	anhed, 32%	subhed, 40%		int, 2%		trc.	trc.	trc.	+ trc. Myrmekite
FP#G1	X-cutting felsic sheet	Granite	c-g	subhed, 19%	anhed, 41%	perth, euhed, 39%		int, 1%					
FP#D1	Mafic dike	Microdiorite	f-g	tab, euhed, 44%			tab, euhed, 38%	tab, euhed, 13%	acic, 1%	trc.		mag, 4%	Strong mineral alignment - flow?
FP#C2	Mafic enclave	Microdiorite	f-g	tab, euhed, 70%			euhed, 29%	1%		trc.		trc.	

Appendix Two: Modal abundances continued

Sample #	Rock Type	Rock Name	Grainsize	Plagioclase	Quartz	K-Feldspar	Hornblende	Biotite	Apatite	Titanite	Zircon	Oxides	Comments
Leask Bay													
LB 3/3#6	Felsic dike	Granodiorite	f-g to m-g	subhed, 49%	anhed, 35%	subhed, 16%		trc.					+ trc. Muscovite
LB#G1	X-cutting felsic sheet	Granite	m-g	subhed, 31%	int, 25%	perth, subhed, 42%		int, euhed, 2%			trc.	trc.	+ trc. Myrmekite
LB#E2	Mafic enclave	Microdiorite	f-g	mos. text, 60%			int, subhed, 37%	blade, 1%	trc.	trc.		2%	moderately weathered
Butterfield Beach													
BB #M1	Mixed 'hybrid'	Mesodiorite	f-g	subhed, 63%			subhed, 13%	euhed, 22%	trc.	trc.		2%	
BB #G1	X-cutting felsic sheet	Granite	m-g	subhed, 32%	anhed, 38%	subhed, 28%	anhed, 0.5%	euhed, 1.5%				trc.	
BB #G2	Felsic sheet	Monzogranite	m-g	euhed, 35%	int, 38%	euhed, 22%	euhed, 1%	euhed, 4%	trc.	trc.	trc.	trc.	Mafic minerals form in clots
Harrold Bay													
HB #H	X-cutting felsic sheet	Monzogranite	m-g	tab, subhed, 35%	int, 29%	subhed, 27%	subhed, 2%	subhed, 7%	trc.	trc.	trc.	trc.	
HB #DG	X-cutting felsic sheet	Granodiorite	m-g	tab, euhed, 38%	anhed, 41%	euhed, 20%	trc.	euhed, 1%			trc.	trc.	
Bragg Bay													
BB #H1	Mixed 'hybrid'	Mesodiorite	m-g	euhed, 71%	int, 6%		subhed, 8%	subhed, 13%	trc.	trc.		2%	
Little Bay													
LB 1/5	Mafic rock	Mesodiorite	f-g to m-g	subhed, 51%			euhed, 46%	trc.	trc.	trc.		3%	
Lee Bay													
LB#H	Felsic host	Tonalite	m-g	tab, euhed, 66%	int, 18%		int, subhed, 4%	int, subhed, 9%	trc.	euhed, 2%	trc.	mag, 1%	
LB#D	Mafic dike	Microdiorite	f-g	euhed, 48%			euhed, 47%	euhed, 5%	trc.	trc.		trc.	Strong mineral alignment
Miscellaneous													
H#1	Felsic host	Quartz Diorite	m-g	tab, subhed, 65%	int, 9%	int, 6%	int, subhed, 11%	int, subhed, 6%	trc.	int, 1%		mag, 2%	
D#1	Mafic dike	Microdiorite	f-g	tab, euhed, 60%			subhed, 35%		trc.			mag, 5%	15% zoned m-g plag phenocrysts
H#3	Felsic host	Quartz Diorite	m-g	tab, euhed, 58%	int, 7%	int, 8%	subhed, 12%	subhed, 11%	trc.	euhed, 2%	trc.	mag, 2%	

f-g = fine grained; m-g = medium grained, c-g = coarse grained; euhed = euhedral; subhed = subhedral; anhed = anhedral; int = interstitial; trc. = trace; acic. = acicular; poik. = poikilitic; accum. = accumulation; tab. = tabular; mos. = mosaic; perth = perthitic; m = mafic; f = felsic; xtal = crystal; hble = hornblende, qtz = quartz; mag = magnetite; meta. = metamorphic